In-silico guided design, synthesis and bio-evaluation of potential chemotherapeutic agents against malaria, cancer and disease-causing pathogens

by

OLUWATOSIN YEMISI AUDU

Submitted in partial fulfilment of the requirements for the

Ph.D Degree in Chemistry

in the Faculty of Natural & Agricultural Sciences

University of Pretoria

Pretoria

February, 2022

Declaration

I, Oluwatosin Yemisi Audu, declare that the thesis titled "*In-silico* guided design, synthesis and bio-evaluation of potential biological agents against malaria, cancer and disease-causing pathogens" which I hereby submit for the award of PhD (Chemistry) degree at the University of Pretoria is my own work and has not previously been submitted by me for a degree at this or any other tertiary institution.

Signature 

Date 02/10/2021

Acknowledgements

First and foremost, I want to express my gratitude to God, the Almighty, for His mercies in allowing me to complete my research work successfully.

I would like to express my deep and sincere appreciation to my research supervisors, Dr. N. October, Prof. O.O. Ajani, and Dr. S A. Egieyeh for giving me the opportunity to do this research. Thank you for allowing me to learn under your tutelage. Thank you, for your priceless guidance and support, throughout the course of this research. My completion of this research could not have been accomplished without the support of my husband, Dr Dele Peter Fapojuwo and son, Isaac Fapojuwo. You deserve special thanks for your love, patience, prayers, and unwavering support during this research. I owe my parents, Elder and Deaconess Audu, a debt of gratitude for their love, prayers, care, and encouragement throughout the research work. I am tremendously grateful to Pastor David Adebayo and Paul Adebayo for their untiring encouragement and prayers. I also want to thank my brothers, and sisters-in-law, for their love and prayers. Also, I would like to appreciate my friend Chidinma Ezeofor for her love and encouragement.

Finally, I am grateful to the World Academy of Science – National Research Foundation TWAS-NRF and University of Pretoria for their financial assistance throughout this programme. I shall be forever grateful. I am also grateful to the entire member of staffs of the Department of Chemistry, University of Pretoria; especially, Dr M. Selepe, Dr Frederick Malan, Mrs R. Swart, and Mrs N. Steenkamp, for their contributions to this research. I would like to offer my appreciation to the everyone on the organic chemistry research floor.

Plagiarism Declaration

1. I understand what plagiarism is and I am aware of the University's policy in this regard.

2. I declare that this thesis is my own original work. Where other people's work has been used (either from a printed source, internet, or any other source), this has been properly acknowledged and referenced in accordance with departmental requirements.

3. I have not used work previously produced by another student or any other person to hand in as my own.

4. I have not allowed, and will not allow anyone to copy my work with the intention of passing it off as his or her own work

Signature 

Table of Contents

Declaration……...ii

Acknowledgements……. iii

Plagiarism Declaration……...…...iv

Table of Contents……. .v

List of Figures……x

List of Schemes……. xiv

List of Tables……...…xvi

List of Abbreviations…….xvii

Summary……... xix

1 Chapter One

Introduction……1

1.1 Introduction to Computational Methods in Drug Discovery……..1

1.2 Molecular Docking and its Discovery……1

1.2.1 Importance of *in silico* in Drug Discovery……3

1.3 Reverse Molecular Docking as an Alternative Strategy in Drug Discovery…….....4

1.4 The Concept of Molecular Hybridization……..6

1.5 Study Rationale……..7

1.6 Aim……8

1.6.1 Specific Objectives……8

1.6.1.1 Objective (i)Molecular Docking and *in silico* Guided Design, Synthesis and Antimalarial Activities of Novel 4(*1H*)-pyridone Derivatives…….....8

1.6.1.2 Objective (ii) Investigation of 2-substitued Benzimidazoles Derived Anticancer Compounds……9

1.6.1.3 Objective (iii) Synthesis of Quinoxaline-6-carboxamidine-urea based. Antimicrobial Compounds……9

2 Chapter Two

An Investigation of 4(1*H*)-Pyridone-Derived Compounds as Antimalarials……...….10

2.1 Global Malaria Burden.……10

2.2 Malaria Life Cycle……11

2.3 Malaria Chemotherapy ……...…….12

2.4 Mechanism of Action of Recent Synthetic Antimalarial Drug-like Candidates……14

2.5 Antimalarial Drug Resistance……...15

2.6 Discovery of 4(1*H*)-Pyridone as Antimalarial Scaffolds……...…...16

2.7 Structure Activity Relationship (SAR) Studies of 4-(1*H*)Pyridone Derivatives…….18

2.8 Pharmacokinetic Profile of 4 (1*H*)-Pyridones as Antimalarial Compounds ……19

2.9 Reported Syntheses of 4(1*H*)-pyridones as Antimalarial Compounds……21

2.10 *In-Silico* Studies and Binding of 4(1*H*)-Pyridones to Cytochrome bc_1……22

2.11 Synthesis of Derivatives of 2,6-dimethylpyridin-4(1*H*)-ones……..26

2.11.1 Synthesis of 2,6-dimethylpyridin-4(1*H*)-one Derivatives *via* a Reported Method…..26

2.11.2 Synthesis of 2,6-Dimethylpyridin-4(1*H*)-one Derivatives *via* 4-Bromophenylacetone. ……..28

2.11.2.1 Proposed mechanism for the Darkin-West synthesis of β-Aryl Ketone, 4-bromophenylaceton.……..…….30

2.11.3 Cyclization of 4-Bromoacetophenone **2.3** *via* Oxidative Cyclization Reaction……...31

2.11.3.1 Crystallographic analysis of compounds **2.4a** and **2.4b**…….33

2.11.4 Amination of the 4(1*H*)-Pyranone……36

2.11.5 Synthesis of *Tert*-butyl 3-(4-bromophenyl)-2,6-dimethyl-4-oxopyridine-1(4*H*)-carboxylate, **2.6**……37

2.12 Altered Synthesis Towards the Target Compounds **2.9a**-b using Palladium Catalyzed Cross Coupling Reactions as a Key Reaction…….…….38

2.12.1 Formation of Methylsulphane (CH_2S) Linker for Hybrid Compounds (**2.10-2.12, 2.9a,b**) …….41

2.12.2 Description of Crystal Structure of Compound **2.12b**…….46

2.13 Modified Synthesis of Target Molecules **2.27-2.31** *via* Suzuki Miyaura Coupling reaction ……...51

2.13.1 Suzuki Miyaura Coupling Reaction…….51

2.13.2 Impact of Cross-Coupling Reaction in Drug Discovery……51

2.13.2.1Synthetic Applications of Miyaura Suzuki Coupling Reaction in Drug Discovery….52

2.13.3 Synthesis of Target Molecules **2.27-2.31**…….…….54

2.13.4 The Mechanism of the Miyaura Suzuki Coupling Reaction…….57

2.13.5 Alternative synthesis of target compound **2.16**…….58

2.13.6 An Investigation into the possible reasons for the failed formation of target compounds **2.16, 2.25-2.28**…….62

2.14 Density Functional Theory (DFT) analysis……..….63

2.15 Molecular Modelling (Molecular Docking and Prime MM-GBSA) of Pyridones……..68

2.16 Antiplasmodial Activity and Structure Activity Relationships (SAR)……72

2.17 Conclusion……...77

3 Chapter Three

Investigation Of 2-substituted Benzimidazole Anticancer Based Compounds……79

3.1 Introduction…….….79

3.2 Chemotherapy…….….80

3.3 Anticancer Derivatives of Benzimidazole ……...81

3.4 Reported Synthesis of Benzimidazoles as Anticancer Agents…….84

3.5 Reported *In-silico* Docking of Some Benzimidazole Anticancer Agents…….87

3.6 ADMET Properties in Drug Discovery……90

3.6.1 ADMET Properties of Benzimidazole Derivatives……...91

3.7 Designed Target Compounds Based on Previous Literature Reports……...92

3.8 Reverse Docking and Molecular Similarity as Computational Molecular Docking Strategies……..93

3.8.1 Molecular Similarity Searching of Target Compounds for Target Prediction……..95

3.8.2 Molecular Docking for Ligand-Target Binding of Target Benzimidazoles, **3.4a-3.6f,** using Estrogen Receptor Alpha (ER) in Breast Cancer as a Suitable Target……95

3. 9 Synthesis of Derivatives of 2, 5-Disubstituted Benzimidazoles……102

3.9.1 Synthesis of 2-(4-Substituted phenyl) Benzimidazoles via a Cyclo-condensation Reaction……..103

3.9.1.1 Mechanism for the Cyclo-condensation of Benzimidazole……...103

3.9.2 Williamson Ether Synthesis of 4-(2-Bromoethoxy)-3-Methoxybenzaldehyde (Vanillin Linker) ……...105

3.9.3 Synthesis of the N-alkylated benzimidazoles **3.4a-e**……106

3.9.4 Synthesis of Target Compounds **3.6a-e**……..109

3.9.4.1 Synthesis of Aldimines or Schiff base via Nucleophilic Catalysis of Pyrrolidine……110

3.10 Cytotoxicity……115

3.11 Conclusion……..116

4 **Chapter Four**

Synthesis of Quinoxaline-6-Carboxamidine-Urea Based Antimicrobial Compounds…….....**118**

4.1 The Pathogenic Nature of Microbes……118

4.1.2 General Characteristics and Classification of Bacteria……...118

4.2 Classification of Antimicrobials and Multi-drug Resistance thereof…….119

4.3 Chemical Properties and Synthesis of Quinoxalines and their Biological Significance……120

4.3.1 Some Synthetic Approaches used in the Synthesis of Quinoxaline and its Derivatives……122

4.4 Synthesis of Quinoxaline-6-carboxamidine-urea based Compounds **4.5a-f**……...125

4.4.1 Synthesis of 6-Isocyanoquinoxaline-2,3(1*H*,4*H*)-dione, **4.2**……126

4.4.2 Synthesis of Amidoxime Derivative, **4.3** of the Quinoxaline-2,3-dione……128

4.4.3 Synthesis of the Target Molecules **4.5a-f** *via* Reductive Amination…….132

4.5 Reported synthesis and molecular docking studies on quinoxaline as antimicrobials.135

4.6 Molecular Docking of Target Molecules **4.5a-f**……139

4.7 Conclusion……142

5 **Chapter Five**

Conclusion And Future Work……143

5.1 Summary and Conclusion……..143

5.2 Future Work……147

6 Chapter Six

Experimental……148

6.1 General Experiment……148
6.2 X-ray Crystallography……149
6.3 Procedures for Biological Activities……..174
6.4 Molecular Modelling Procedure……176
7 Reference……...178
8 Appendix……...215

List of Figures

Figure 1.1: Docking performed by (A) simulation strategy (B) shape complementary strategy ……..…...2

Figure 1.2: Discovery of novel hit and lead compounds through *in silico* docking [13]……..3

Figure 1.3: Image illustrating the difference between a virtual screening and a reverse docking……...5

Figure 1.4: A schematic representation of a reverse docking.……..…6

Figure 1.5: Molecular hybridization of compounds…...……...7

Figure 2.1: Malaria Transmission Worldwide……11

Figure 2.2: Life Cycle of the Malaria Parasite…...……12

Figure 2.3: Structural Classes of Antimalarial Drugs[39]……..13

Figure 2.4: Quinoline derived compounds…… 14

Figure 2.5: Tautomeric forms of 4-pyridone…...……17

Figure 2.6: Structures of Atovaquone, Clopidol and some Novel 4-(1*H*)Pyridone Motifs…17

Figure 2.7: Structures illustrating transformation of 4-pyridones at the position C6 and modification of lipophilic phenolate moiety of 4-(1*H*)pyridone with a pyridine ring…….20

Figure 2.8: The binding of GW84452 and GSK932121 Figure 2.6, to cytochrome bc1 Qi binding site……...……22

Figure 2.9: Modification of **GSK932121** to give to the target molecule and the binding poses of a specific target molecule into the Qi-site of cytochrome bc1 of *P. falciparum*……..…25

Figure 2.10: The binding of 3-(4-(benzylthio)phenyl)-2,6-dimethylpyridin-4(1*H*)-one onto malaria cytochrome bc1 in the Qi binding site with binding energy of -10.3 kcal/mol……25

Figure 2.11: ^{1}HNMR Spectrum of **2.3** (400 MHz, DMSO-d_6)……...…29

Figure 2.12: 1H NMR Spectrum of **2.4** (300 MHz, DMSO-d_6)…….33

Figure 2.13: Crystal Structures of Compounds **2.4a** and **2.4b**……..…….34

Figure 2.14: SCXRD Packing diagrams of **2.4a** when viewed along the a-axis and b-axis, respectively…….....35

Figure 2.15: Packing Diagrams of **2.4b** when viewed along the a-axis and b-axis, respectively ……..…….35

Figure 2.16: ^{1}H NMR Spectrum of **2.5** (300 MHz, $CDCl_3$)……36

Figure 2.17: ^{1}H NMR of tert-butyl 3-(4-bromophenyl)-2,6-dimethyl-4-oxopyridine-1(4H)-carboxylate **2.6** (400 MHz, $CDCl_3$)……..38

Figure 2.18: 1H NMR Spectrum of **2.10d** (400 MHz, $CDCl_3$)……...42

Figure 2.19: ^{1}H NMR Spectrum of **2.11c** (300 MHz, $CDCl_3$)……43

Figure 2.20: ^{1}H NMR Spectrum of **2.11a** (300 MHz, $CDCl_3$)……45

Figure 2.21: ^{1}H NMR Spectrum of **2.12a** (300 MHz, $CDCl_3$)……46

Figure 2.22: Molecular Structure of Compound **2.12b**…….....46

Figure 2.23: IR of compound **2.9a**…… 49

Figure 2.24: ^{1}H NMR of Target Compound **2.8** (400 MHz, CD_3OD)……50

Figure 2.25: ^{1}H NMR Spectrum of **2.3** (400 MHz, $CDCl_3$) ……...56

Figure 2.26: Catalytic Cycle for Suzuki-Miyaura Cross-coupling Illustrating the Formation of**2.21**.[78],[84],[85]……57

Figure 2.27: ^{1}H NMR Spectrum of **2.14** (400 MHz, $CDCl_3$)……..59

Figure 2.28: ^{13}C NMR Spectrum of **2.14** (400 MHz, $CDCl_3$)……60

Figure 2.29: ^{1}H NMR Spectrum of **2.15** (400 MHz, $CDCl_3$) ……61

Figure 2.30: ^{13}C NMR Spectrum of **2.15** (101 MHz, $CDCl_3$) ……...61

Figure 2.31: Thermogravimetric Analysis (TGA) of Selected Compounds **2.4a, 2.15, 2.22**, and **2.25**……63

Figure 2.32: B3LYP Functional DFT Calculated HOMOs and LUMOs of the indicated Neutral Compounds from this Study. A Contour of 0.03 e/Å3 was used for the MO plots…65

Figure 2.33 Three-dimensional Crystalized Structure of Atovaquone-inhibited Cytochrome BC1 Complex……...69

Figure 2.34: Hydrogen bonds (yellow dotted line) and Van der Waals (VDW) (green dotted line) interactions as well as the MM-GBSA free binding energies of the three docked compounds with cytochrome bc1 complex Q_o active site……...70

Figure 2.35: Electrostatic Distribution [- 0.3eV (red) to + 0.3eV (blue)] on the surface of compound **2.9a**, compound **2.9b**, and Atovaquone as well as the Q_0 site of the Cytochrome bc1……....71

Figure 2.36: Structures of Seven newly synthesized compounds, namely **2.9a, 2.9b, 2.10c, 2.11b, 2.11c, 2.12a, 2.12b**……72

Figure 2.37: *In vitro* Antiplasmodial Activity of the newly Synthesized Compounds **2.9a, 2.9b, 2.10c, 2.11b, 2.11c, 2.12a, 2.12b** at 1 and 5 µM against asexual *P. falciparum*……...73

Figure 2.38: Antimalarial Activities of previously Synthesized GSK Compound **I,** [93] G844520,[93] GSK932121,[75] and newly synthesized target compounds **2.9a** and **2.9b**…… 76

Figure 3.1: Cancer Distribution Across the Globe…..…….. 80

Figure 3.2: Chemical Structure of 5,6-dimethyl-1-(α-D-ribofuranosyl) benzimidazole (VitaminB12)……..…….……..82

Figure 3.3: Some Benzimidazole-based Active Drugs……...83

Figure 3.4: The Binding Mode and Ligand Interaction of the Synthesized 3-(1*H*-benzo[d]imidazol-2-yl)-5-phenyl-1-(pyridin-4-yl)-1*H*-pyrrol-2-amine with CYS 191, SER 195 and HIS 57, using urokinase-type plasminogen activator (uPA) as the receptor……..…..85

Figure 3.5: 2-Arylbenzimidazole and 2-Heteroarylbenzimidazole Derivatives…….86

Figure 3.6: Binding Mode and Ligand Interaction of 2-Substituted-benzimidazoles in the CDK-8 protein 2 Binding Site…….…….…….....88

Figure 3.7: Docking of 2,6-Disubstituted Benzimidazole against DNA Topoisomerase **I** enzyme complex…….……89

Figure 3.8: The Binding Mode 1-(1*H*-Benzimidazol-2-yl)-3-phenylprop-2-en-1-one, **I**, ring unto EGFR-TK complex……...……..90

Figure 3.9: 2-Aryl benzimidazole, **I**…..……..90

Figure 3.10: 2- And 5-Substituted Benzimidazole Analogues Identified as Angiotensin II–AT1 Receptor Antagonist……..…….……91

Figure 3.11: 2-substituted benzimidazole derivatives…….92

Figure 3.12: The Binding Mode of Estradiol unto the Active Site of Estrogen Receptor (ER) Alpha……..……....97

Figure 3.13: The Binding Mode of the Target Compound **3.4a** unto the Active Site Of Estrogen Receptor (ER)Alpha…….……..98

Figure 3.14: The Binding Mode of the Most Probable Target Compound **3.4b** With Dock Score Of -9.16 unto the Active Site of Estrogen Receptor (ER) Alpha ....……98

Figure 3.15: The Binding Mode of the Target Compound **3.4c** unto the Active Site Of Estrogen Receptor (ER) Alpha……..99

Figure 3.16: The Binding Mode of the Target Compound **3.4e** unto the Active Site Of Estrogen Receptor (ER) Alpha……..……..…99

Figure 3.17: The Binding Mode of the Target Compound **3.4f** unto the Active Site Of Estrogen Receptor (ER) Alpha……..……...100

Figure 3.18: The binding mode of other target benzimidazoles **3.4d, 3.6a-3.6f,** unto the active site of estrogen receptor (ER) alpha……..……101

Figure 3.19: ^{1}H NMR (DMSO-d_6, 400 MHz) of compound **3.2b** ……...…105

Figure 3.20: ^{1}H NMR (DMSO-d_6, 300 MHz) of Compound **3.3**…….106

Figure 3.21: ^{1}H NMR (DMSO-d_6, 400 MHz) of Compound **3.4a**……...108

Figure 3.22: ^{13}C NMR (DMSO-d_6, 400 MHz) of Compound **3.4a**……...109

Figure 3.23: Infra-red Spectrum of Compound **3.6d**……...…….112

Figure 3.24: ^{1}H NMR (DMSO-d_6, 400 MHz) of Compound **3.6a**……....112

Figure 3.25: ^{13}C NMR (DMSO-d_6, 400 MHz) of Compound **3.6a**…….……..115

Figure 3.26: Cytotoxicity Screening Of Target Compounds……116

Figure 4.1: Isomeric Chemical Structures of Quinoxalines……..120

Figure 4.2: Chemical Structures of Some Quinoxaline-based Drugs[201],[202],[188]…...122

Figure 4.3: ^{1}H NMR of **4.2** (400 MHz, DMSO-d_6)……... 127

Figure 4.4: ^{13}C NMR of **4.2** (100 MHz, DMSO d_6) …….128

Figure 4.5: Infra-red Spectrum of Compound **4.3**……130

Figure 4.6: ^{1}H NMR of **4.3** (400 MHz, DMSO-d_6)…… 131

Figure 4.7: Infra-red Spectrum of Compound **4.5a**……..133

Figure 4.8: 1H NMR of **4.5a** (400 MHz, DMSO d_6) ……..... 134

Figure 4.9: ^{13}C NMR of **4.5a** (100 MHz, DMSO-d_6) …….....135

Figure 4.10: Docking Of Novel Di-Substituted Sulfonylquinoxaline **I** Unto DNA Gyrase Binding Site……..……136

Figure 4.11: Binding Of Compounds **I** And **II** To Badhps In The Active Site……137

Figure 4.12: Quinoxaline Moieties with the Substituted Electron-withdrawing Group at the Positions 6……..…….....138

Figure 4.13: Thiazolidine–Quinoxaline Derivative……..138

Figure 4.14: The Binding Mode of **4.5b** unto the Active Site Of *Escherichia Coli* Lytic Transglycosylase (PDB Code: 2PIC)…….……141

Figure 4.15: The Binding Mode of **4.5f** unto the Active Site of Beta-Lactamase (PDB Code: 2NZE)…….141

List of Schemes

Scheme 2.1: Synthesis of 4-(1*H*)Pyridones from Isoxazole……..21

Scheme 2.2: General Reaction Scheme for Unsuccessful Synthetic Approaches to 3-(4-substituted(benzylthio)phenyl)-2,6-dimethylpyridin-4(1*H*)-one…….27

Scheme 2.3: Synthesis of 4-bromophenylacetone……28

Scheme 2.4: Suggested Mechanism for Synthesis of the aryl 4-bromophenylacetone, **2.3**….31

Scheme 2.5: Synthesis of 3-(4-bromophenyl)-2,6-dimethyl-4H-pyran-4-one **2.4a**……32

Scheme 2.6: Synthesis of 3-(4-bromophenyl)-2,6-dimethylpyridin-4(1H)-one, **2.5**……....36

Scheme 2.7: Synthesis of *tert*-butyl 3-(4-bromophenyl)-2,6-dimethyl-4-oxopyridine-1(4*H*)-carboxylate 2.6…….37

Scheme 2.8: Successful synthetic approaches to 3-(4-(substitutedbenzylthio)phenyl)-2,6-dimethylpyridin-4(1*H*)-one……..40

Scheme 2.9: Synthesis of 2-(4-(4-substitutedbenzylthio)phenyl)acetic acids, **2.10a-d**……41

Scheme 2.10: Synthesis of 1-(4-(4-*tert*-butylbenzylthio)phenyl)propan-2-one, **2.11a-d**…….43

Scheme 2.11: Synthesis of 4(1*H*)pyranone derivatives……..44

Scheme 2.12: Synthesis of target compound **2.9a** ……48

Scheme 2.13: General reaction scheme of Suzuki cross-coupling reaction…….51

Scheme 2.14: Synthesis of Losartan through cross coupling reaction…….52

Scheme 2.15: Synthesis of GSK, SB-245570 through biaryl Suzuki coupling reaction……...52

Scheme 2.16: Total synthesis of Camptothecin, by the means of Miyaura Suzuki Coupling reaction…….53

Scheme 2.17: Synthesis of intermediates products **2.27-2.31** *via* Boronic Acids **2.17-2.21**….54

Scheme 2.18: Synthesis of target compound **2.16**……58

Scheme 2.19: Nucleophilic substitution mechanism for the conversion of 4-pyrone to 4-pyridone……65

Scheme 3.1: Benzo-fused Imidazole Ring Tautomerism…….. 82

Scheme 3.2: Synthesis of 3-(1*H*-benzo[d]imidazol-2-yl)-5-phenyl-1-(pyridin-4-yl)-1*H*-pyrrol-2-amine…….84

Scheme 3.3: Synthesis of Benzimidazole Schiff Base and its Complex…….86

Scheme 3.4: Retrosynthesis of the proposed Figure benzimidazole derivative…….93

Scheme 3.5: General synthetic pathway towards the target compounds **(3.4)** and **(3.5)** ….103

Scheme 3.6: Mechanism for the cyclo-condensation of benzimidazole……104

Scheme 3.7: Nucleophilic Catalysis used by Pyrrolidine…….……111

Scheme 4.1: Synthesis of 2,3-diphenylquinoxaline **III,** by means of recyclable alumina-supported molybdophosphovanadates catalysts…….……123

Scheme 4.2: Synthesis of 2-phenyl-3-(2-phenylethynyl)quinoxaline, **III** *via* oxidative coupling……..123

Scheme 4.3: Cascade synthesis of ethyl 3-methylquinoxaline-2-carboxylate, **III**……124

Scheme 4.4: A three component reaction synthesis of *N*-cyclohexyl-3-phenylquinoxalin-2-amine, **IV**……124

Scheme 4.5: Synthesis of 2,3-diphenylquinoxaline, **III** *via* nanoparticle…….…125

Scheme 4.6: Solvent-free synthesis of quinoxaline**, III**…….125

Scheme 4.7: Synthetic path towards target Compounds……126

Scheme 4.8: Synthesis of 6-isocyanoquinoxaline-2,3(1*H*, 4*H*)-dione, compound **4.2**…..…127

Scheme 4.9: Reaction Mechanism for the formation of 1,2,3,4-tetrahydro-N-hydroxy-2,3-dioxoquinoxaline-6-carboxamidine**, 4.3**……...……129

Scheme:4.10: Synthesis of 1,2,3,4-tetrahydro-*N*-hydroxy-2,3- dioxoquinoxaline-6-carboxamidine, compound **4.3**…….……129

Scheme4.11: Synthesis of 1,2,3,4-tetrahydro-*N*-hydroxy-2,3-dioxoquinoxaline-6-carboxamidine, `compound **4.4**…….…….131

Scheme 4.12: General reaction mechanism for the synthesis of target compounds **4.5a-f...**132

List of Tables

Table 2.1: Crystal data and structure refinement for **2.12b**……47

Table 2.2: Selected bond length (Å) and angles (°) for the compound **2.12b**……47

Table 2.3: Molecular parameters and reactivity descriptors of compounds **2.15, 2.22-2.26** and **2.16, 2.27-2.31**……67

Table 2.4*: In vitro* activity of the newly synthesized compounds **2.9a, 2.9b, 2.10c, 2.11b, 2.11c, 2.12a, and 2.12b** at 1 and 5 µM against asexual *P. falciparum*……...….74

Table 2.5: Antimalarial activities of target compounds **2.9a** and **2.9b**……...……75

Table 3.1: Docking scores of targets, 2-substituted benzimidazoles…….….96

Table 4.1: Docking scores of quinoxaline-6-carboximidine target molecules **4.5a-f**……140

List of Abbreviations

AcOH	acetic acid
Ac_2O	acetic anhydride
Å	angstrom
Ar	aromatic
°C	degrees Celsius
^{13}C NMR	carbon-13 nuclear magnetic resonance spectroscopy
^{1}H NMR	proton nuclear magnetic resonance spectroscopy
$(Boc)_2O$	di-tert.butyldicarbonate
$CDCl_3$	deuterated chloroform
CD_3OD	deuteromethanol
CQ	Chloroquine
d	doublet
dd	doublets of doublets
DCM	dichloromethane
DFT	density functional theory
DIPEA	*N*,*N*-Diisopropylethylamine
DMAP	4-Dimethylaminopyridine
DMF	dimethylformamide
DMSO	dimethyl sulfoxide
DMSO-d_6	deuterated dimethyl sulfoxide
EtOH	Ethanol
FTIR	Fourier transform infrared
GSK	GlaxoSmithKline
h	hour
IR	Infrared
IC_{50}	50% Inhibitory Concentration
IR	Infrared
LDA	Lithium diisopropylamide
µM	micromolar
m	multiplet
MeOH	methanol
MIM	1-Methylimidazole
min	minutes
mL	millilitres
mmol	millimole
m.p	melting point
NMR	nuclear magnetic resonance
$Pd_2(dba)_3$	tris(dibenzylideneacetone)dipalladium(0)
$Pd(OAc)_2$	palladium(II)acetate
$Pd(PPh_3)_4$	tetrakis(triphenylphosphine)palladium(0)
ppm	parts per million
Rf	retention factor
r.t.	room temperature
s	singlet
SCXRD	Single Crystal X-Ray Diffractometry

S_N2	substitution nucleophilic bimolecular
t	triplet
TCCA	Trichloroisocyanuric acid
TFA	Trifluoroacetic acid
THF	Tetrahydrofuran
TLC	thin layer chromatography
TMS	tetramethylsilane
ν	frequency of light
WHO	World Health Organization

Summary

Title:
In-silico guided design, synthesis and bio-evaluation of potential biological agents against malaria, cancer and disease-causing pathogen

By:

Oluwatosin Yemisi Audu

Supervisor:
Dr Natasha October

Co-supervisor:
Prof. O.O. Ajani

Co-supervisor:
Dr Samuel Egieyeh

Department:
Department of Chemistry

Degree:
PhD

My Contribution:
Design, syntheses, crystals growth and characterization of compounds and writing of the thesis.

Abstract

Computational-based strategies have become of great significance in drug discovery, owing to their key contributions towards the development of new therapeutics.

In various diseases, the overall lack of response to existing therapeutic treatments, primarily associated with gene mutations, is the major driver of drug resistance. Therefore, this work focuses on addressing this challenge, by designing and identifying new potential bioactive hybrids, using molecular and reverse docking as prediction studies, targeting three diseases; malaria, cancer, and microbial related infections.

4(1*H*)-pyridone-based antimalarial, 2,5-disubstituted benzimidazole-based anticancer, and quinoxaline-6-carboxamidine-urea-based antimicrobial compounds were designed *via* molecular hybridization and molecular docking, synthesized through multi-step synthetic routes. Their potential inhibitors as were predicted using biological screening.

A library of new 4(1*H*)-pyridone-containing intermediates, and target molecules were successfully synthesized. Seven of the newly synthesized compounds **2.9a, 2.9b, 2.10c, 2.11b, 2.11c, 2.12a, 2.12b** screened for antimalarial activities, only target compounds **2.9a** and **2.9b** displayed excellent inhibitory activities (96% and 97% at 1 μM, 99% and 98% at 5 μM**)** against K1 CQ resistant strain (CQR) and CQ-sensitive (CQS) NF54, (Table 2.4), compared to that of CQ reference drug with an inhibitory activity of 100, both at 1 and 5 μM respectively. Other newly synthesized intermediates **2.10c, 2.11b, 2.11c, 2.12a, 2.12b** gave moderate to low inhibitory *P*. *falciparum* activities**.**

The IC_{50} of these target compounds **2.9a** and **2.9b** displayed notable anti-plasmodial activities against K1 CQ resistant strain (CQR) at 0.10 and 0.04, while at 0.13 and 0.05 against *P.*

falciparum CQ-sensitive (CQS) NF54. Single crystal structures of intermediate compounds **2.4a** and **2.4b** were also determined using X-ray diffraction.

Molecular modelling of target compounds **2.9a** and **2.9b** showed binding potential of these compounds **2.9a** and **2.9b,** unto the Q_0 binding site of the cytochrome bc1 complex and the disruption of the electron transport chain of the mitochondrial.

In the second aspect of the work, as a result of remarkable anticancer activities of 2-disubstituted benzimidazole derivatives, series of 2-disubstituted benzimidazole derivatives **3.4a-e**, and **3.6a-f**, **Scheme 3.5,** were designed, using literature reports as a guide. The target molecules **3.6a-f** were successfully synthesized when pyrrolidine was employed as the catalyst, ensuring the formation of final products. The synthesized compounds were tested for cytotoxicity activity against MCF-7 cell lines, but none of the target compounds, even at all concentrations (0.195-100 μg/mL), demonstrated cytotoxicity comparable to the standard drug, camptothecin, which induces cell death at 57% (at 0.08 μg/mL). As a result, the target structures were docked using reverse docking, and the most likely target compound **3.4b,** gave a docking score of -9.16.

Finally, in the third aspect of the work, quinoxaline-6-carboximidine target molecules **4.5a-f** were successfully designed and synthesized. Out of twelve envisaged target structures, only six were successfully synthesized, which may be due to the presence of an electron-withdrawing substituent on the phenyl ring of the isocyanate. This discovery emphasizes the importance of the presence of an electron withdrawing group in the isocyanate derivatives towards the reactivity with the amidine **4.4**. Successfully synthesized target compounds **4.5a-f** were docked unto *Escherichia coli* lytic transglycosylase (PDB code: 2PIC) and beta-lactamase (PDB code: 2NZE). The molecular docking results indicated that these target structures could be important targets for the discovery and development of novel antibacterial medicinal agents.

Chapter One
Introduction

1.1 Introduction to Computational Methods in Drug Discovery

The first synthetic drug, chloral hydrate known as a sedative-hypnotic was discovered in 1869.[1] Drug discovery involves the use of computational, experimental, translational, and clinical modelling to identify novel drug candidates.[2] Drug discovery primarily underpins the design of new therapeutics that can bind to a known enzyme or target responsible for a particular disease. This step could further progress into the identification of "lead compounds" that can be synthesized for potential candidate drug development.[3] The tedious long drug development process has stirred researchers to consider alternative options to hasten the process. [4] Amongst these, is the use of computational modelling, by means of computer aided drug design (CADD) and structure-based drug design (SBDD), through molecular docking and synthesis of the novel compounds. Computational methods have played a key role in rationalizing the path to drug discovery, it has proven to be a time-saving and therefore, a cost effective method.[5]

1.2 Molecular Docking and its Discovery

Molecular docking is a powerful, *in silico* structure-based computational drug discovery technique, used to model and study the interaction of ligands (chemical structure) with their molecular targets (protein) and was first used in the middle of the 1970s.[6] The ligand-protein interaction enables one to depict the activities of a specific ligand in the binding site of the target protein, thereby elucidating the vital biochemical processes.[7] Molecular docking also performs vital functions in the prediction of ligand binding onto nucleic acids. It also predicts an adjusted orientation on its target, as well as different binding modes, which is used in the design and development of active drug agents.[8] Two fundamental strategies are employed in

performing molecular docking, which are; simulation and shape complementary strategies.[8] In the simulation strategy, interaction takes place through H-bonding between the ligand and the target in a distance, while in shape complementary strategy, interaction takes place by characteristic surface structure of the ligand and the target, Figure 1.1.[9] Docking can be attained through two interconnected steps which include ligand conformation in the protein active site, subsequently the conformations are ranked through the means scoring function.[10]

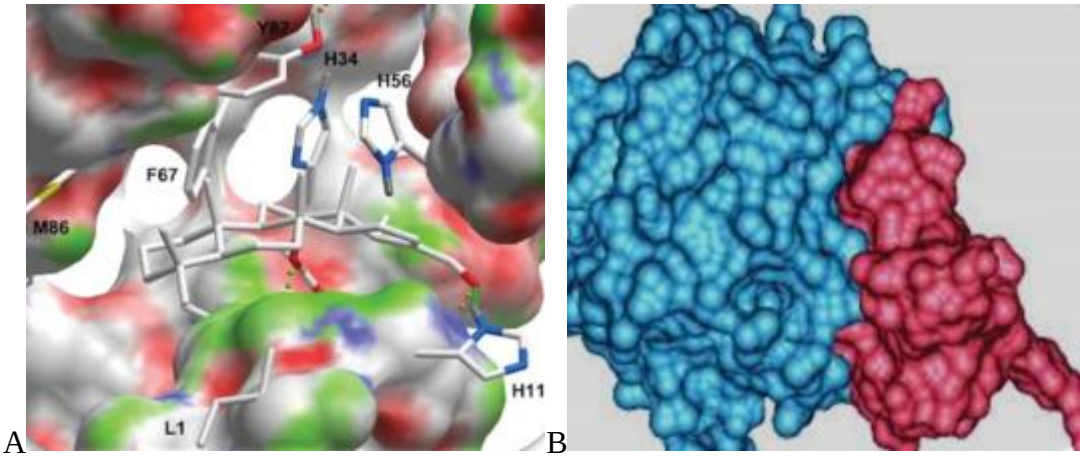

A B

Figure 1.1: Docking performed by (A) simulation strategy (B) shape complementary strategy[8]

The docking software include Autodock, FlexX, Surflex, Glide and Gold[11] Auto dock is a leading software used by researchers due to its program accessibility, while other software like Gold, Glide, Surflex, and Flex, are mostly used commercially due to their speed and efficiency.[12]

During an *in-silico* docking experiment, new ligands are discovered by the means of a template created by the target structure. Docking is initiated via a database of compounds with a known protein receptor, then the probable ligand binds onto the receptor (protein) in the binding site.[13] Considering hit identification and lead optimization, libraries of small molecular structures are docked into macromolecular targets (protein) and their potential is scored to their binding

sites,[14] Figure 1.2. Procedures during docking are arranged in such a way that the binding modes and all interractions are evaluated by the docking scores which shows that binding has taken place.[12] *In vitro* or *in vivo* assays such as minimum inhibitory concentration MIC, inhibition of enzymes and cytotoxicity assays are done in order to validate the obtained *in silico* testing of virtual hit compounds before drug development.[15]

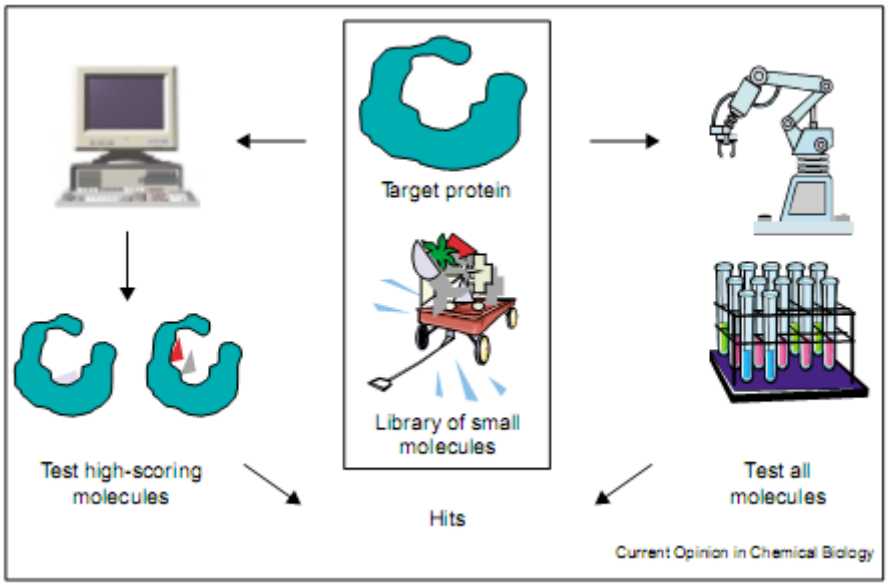

Figure 1.2: Discovery of novel hit and lead compounds through *in silico* docking [13]

However, one must be aware of the limitations associated with molecular docking, since it is only helpful in determining and distinguishing between good and poor inhibitors. As a result, in practice, molecular docking results are not accurate enough to determine the potency of compounds conclusively, as IC_{50}-values are.

1.2.1 Importance of *in silico* Docking in Drug Discovery

In silico docking or rational drug design has a tremendous role in structure-based drug discovery.[7] Molecular docking, in general, helps to identify novel ligand that binds to a specific

protein in a binding site through a virtual screening.[16] Drug development may take several years, is costly and be cumbersome for researchers.[17] Most pharmaceutical companies have engaged *in silico* applications in the areas of pharmacokinetics (ADMET: absorption, distribution, metabolism, excretion and toxicity) and pharmacodynamics (potency, affinity, efficacy, selectivity), before exploring a particular lead compound as a drugs.[10] Also, rational drug design through *in silico* has been considered an effective way of drug discovery compared to the traditional way. *In silico* application, figures out the rationale behind the molecular basis of a particular disease by the means of the three-dimensional structure of the biological target.[16] Consequently, the use of molecular docking via *in silico* testing by *in vitro* has been found useful in validation of research work before chemical synthesis and *in vivo* screening of novel compounds.[15]

1.3 Reverse Molecular Docking as an Alternative Strategy in Drug Discovery

Reverse molecular docking is a new and alternate strategy used in drug discovery, which helps in the repositioning of drug and drug rescue. [18] In reverse docking, the ability of one or a few compounds to bind a large dataset of proteins is evaluated *in silico*. In contrast to conventional virtual screening, which identifies the ligands of a targeted protein from a compound database, reverse screening is used to identify the potential targets of a given compound from a large number of receptors by examining their known ligands or crystal structures, Figure 1.3. [19] Reverse docking helps in discovering new targets for existing drugs and natural compounds, thereby, describing their polypharmacology and molecular mechanism.[20] In reverse docking, the goal is to discover protein targets that can bind to a certain ligand. The important component of reverse docking is comparable to forward docking which involves; preparation of data sets, searching for ligand poses, and scoring and rating the complicated structures. [21] This strategy

is useful for identifying molecular targets of orphan bioactive compounds, proposing new molecular mechanisms, finding alternative indications of drugs, or predicting drug toxicity.

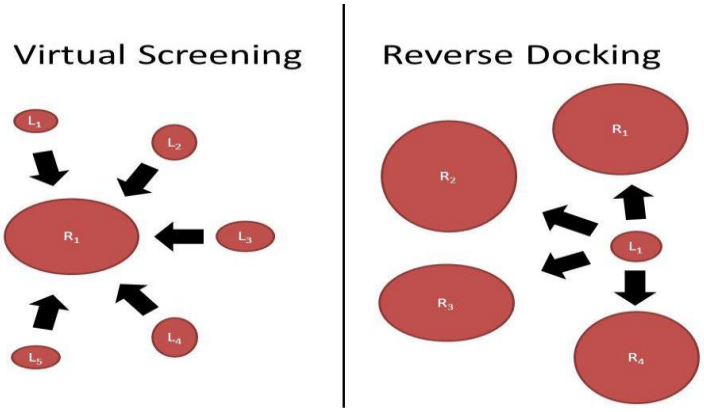

*L represents Ligand; *R represents receptor

Figure 1.3: Image illustrating the difference between virtual screening and reverse docking[22]

The fundamental premise of reverse docking is that the interaction energy of a small-molecule ligand and a putative protein target determines their binding strength (docking energy).[23] Many researcher have used reverse docking as a main or secondary strategy to investigate a broad range of targets of a small molecule.[20]

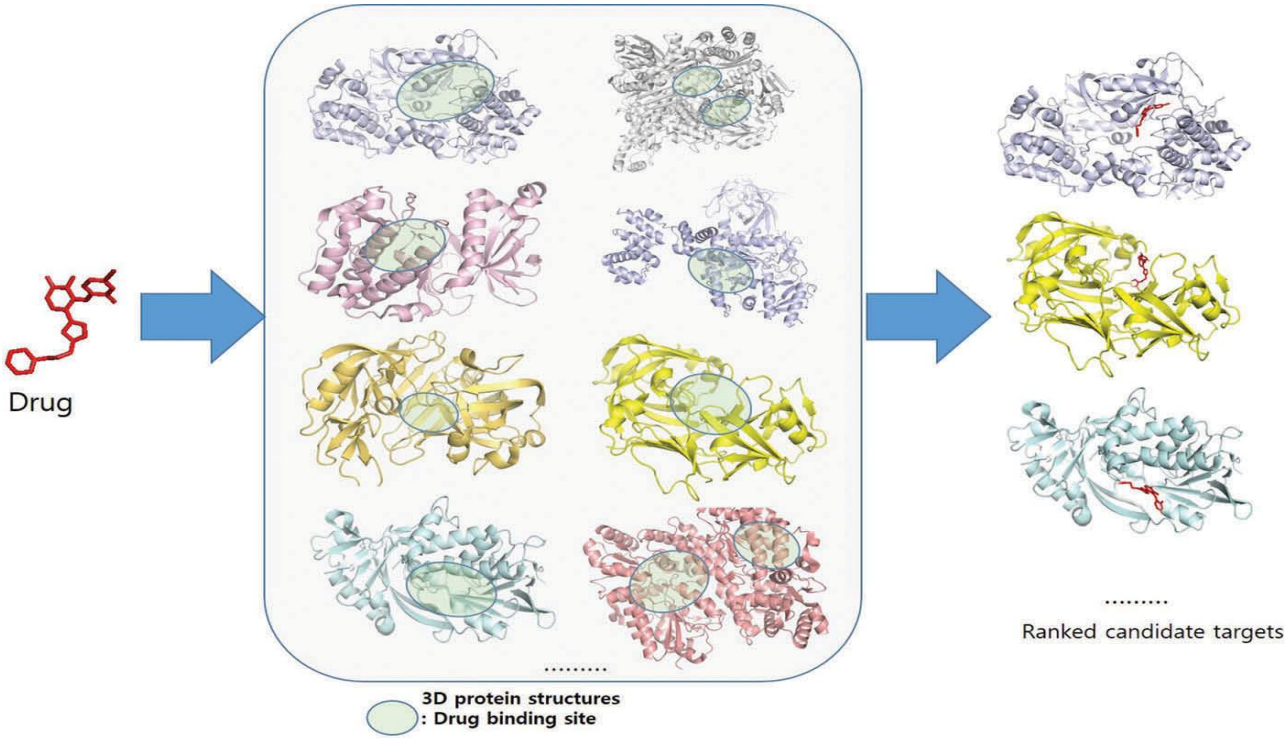

Figure 1.4: A schematic representation of reverse docking.[20]

1.4 The Concept of Molecular Hybridization

Molecular hybridization is a novel approach in drug development that involves combining pharmacophoric moieties from various bioactive substances to create a new hybrid product with better affinity and efficacy over the parent medications.[24] It is a useful tool for developing new drug prototypes. The pharmacophores address the active sites of various targets and have the potential to overcome drug resistance. Molecular hybridization includes, drug-drug molecular hybridization which occurs when two or more drugs hybridize, Figure 1.5. [25]

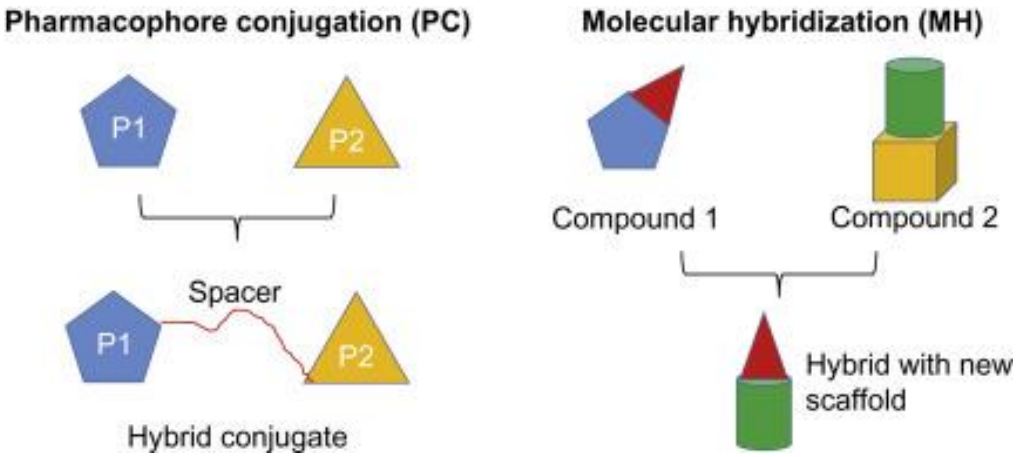

Figure 1.5: Molecular hybridization of compounds.[26]

1.5 Study Rationale

In various diseases, the overall lack of response to existing therapeutic treatments, primarily associated with gene mutations, is the major driver of drug resistance. Drug resistance has been on the increase over the years and has posed a major threat to public health across the globe. Also, infectious agents including fungi, bacteria, viruses other parasites have further shown a rise in multidrug resistance with an increase in morbidity and mortality.[27]. Irrespective of the extensive advances in the development of effective drugs, the overwhelming need for new drugs remains a priority. Therefore, this work focuses on addressing this challenge, by designing and identifying new potential bioactive hybrids, using molecular and reverse docking as prediction studies, with the hope of finding potential new lead therapeutics which can be developed into drug candidates.

Molecular docking analysis was solely used as a complementary study, to identify the best fit ligands to give optimum binding at the active sites. Molecular docking has been found useful in the design of active lead compounds. With the aid of molecular docking tools, antimalarial,

anticancer and antimicrobial molecules were designed, synthesized, characterized and virtually screened for their biological activities.

1.6 Aim

The overall aim of this research was to design, and identify new potential bioactive hybrids using molecular docking as prediction studies, and to evaluate the biological activities against three target diseases; malaria, cancer and microbial related infections.

1.6.1 Specific Objectives

More specifically, this research work is divided into three aspects which are:

In silico guided design, synthesis and antimalarial activities of novel 4(1*H*)-pyridone derivatives; investigation of 2-substituted benzimidazole derived compounds anticancer agent; and synthesis of quinoxaline-6-carboxamidine-urea based antimicrobial compounds.

1.6.1.1 Objective (i) Molecular docking and *in-silico* guided design, synthesis and antimalarial activities of novel 4(1*H*)-pyridone derivatives

(a) To design a series of novel 4(1*H*)-pyridone derivatives based on the best prediction docking scores from *in-silico* analysis;

(b) To synthesize the identified compounds and investigate their structure activity relationship;

(c) To evaluate the *in vitro* antiplasmodial activity of the synthesized compounds against CQ-sensitive (CQS) NF54 and chloroquine-resistance (CQR) K1 *P. falciparum* strains.

1.6.1.2 Objective (ii) Investigation of 2-substituted benzimidazole derived anticancer compounds

(a) To synthesize and characterize a library of novel 2-substituted benzimidazole derived anticancer compounds and investigate their structural-activity relationship profile;

(b) To use reverse docking and molecular similarity searching to establish the *in-silico* breast cancer target profiles for a set of benzimidazole analogues;

(c) To evaluate their anti-cancer activity against a selection of cancer cell-lines.

1.6.1.3 Objective (iii) Synthesis of quinoxaline-6-carboxamidine-urea based antimicrobial compounds

(a) To synthesize and characterize a library of novel quinoxaline-6-carboxamidine-urea based antimicrobial compounds and investigate their structural-activity relationship profile;

(b) To use reverse docking and molecular similarity searching of a selected series of derivatives against six different bacterial proteins;

(c) To evaluate their inhibitory activity against various microbes, selected from previous literature reports that displayed antimicrobial activity against this class of compounds.

Chapter Two

An Investigation of 4(1*H*)-Pyridone-Derived Compounds as Antimalarials

2.1 Global Malaria Burden

Over the years, malaria has been a major global life-threatening disease in which 228 million cases were reported with 405,000 number of deaths in 2018, Figure 2.1.[28] Malaria is a parasitic disease caused by a protozoan of which five species: *Plasmodium falciparum, P. ovale, P. malariae, P. knowlesi, P. vivax, and P. falciparum* are known to infect humans. *Plasmodium vivax and P. falciparum* are the most predominant. It accounts for more than 95% percent of malaria cases globally[29] Figure 2.1; particularly among children under the age of five and pregnant women in Sub-Saharan Africa.[30]

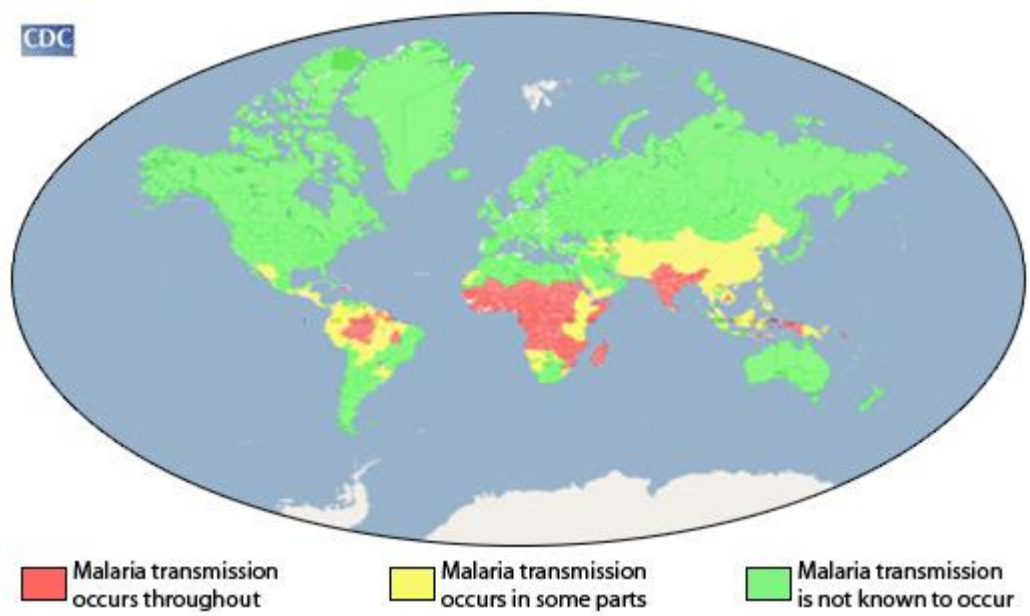

Figure 2.1: Malaria Transmission Worldwide.[31]

The parasite is transmitted to the human through the bites of an infected female anopheles mosquito.[32] In malaria prevalent regions of the world such as the tropical and sub-tropical regions, major challenges in health care have been associated with drug resistance caused by the *Plasmodium* parasite.[33] Factors contributing to the increase in malaria include: (i) resistance of parasites to commonly used antimalarial drugs; (ii) breakdown of control programmes; (iii) complex emergencies such as insecurity and mass population movements.; (iv) collapse of local primary health services; and (v) resistance of mosquito vectors to insecticides.[32- 34]

2.2 Malaria Life Cycle

The dual host life cycle of malaria parasite is complex, and it is divided into four stages which are liver stage, blood stage, transmission stage and the mosquito stage, Figure 2.2. At these different stages, there is a need to develop drugs that target each stage.[35], [36] Infection begins with the liver stage, when the sporozoites from the salivary gland of the anopheles mosquito and are injected into the skin of the human during the blood sucking after which the parasites invade the liver cell (hepatocytes) in about 30 minutes during the blood meal.[34], [37] After 10 days, the liver cells burst, and merozoites invade into the red blood cells, where replication of these parasites and invasion of new red blood cells occur, and malarial symptoms are developed at this erythrocytic stage.[36] These parasites later undergo asexual reproduction in which they differentiate into female and male gametocytes. When this happens, new sporozoites are formed, which later invade the liver cell of the human host. The aforementioned stages are referred to as the transmission and the mosquito stages.[38] Although, drug resistance has been

attributed only to *P. falciparum* and *P. vivax* [39], studies showed that in order to eradicate malaria and the spread of *P. falciparum* at the sexual stage to mosquito vectors, it is essential to combine treatments that inhibit the growth of gametocytes.[40]

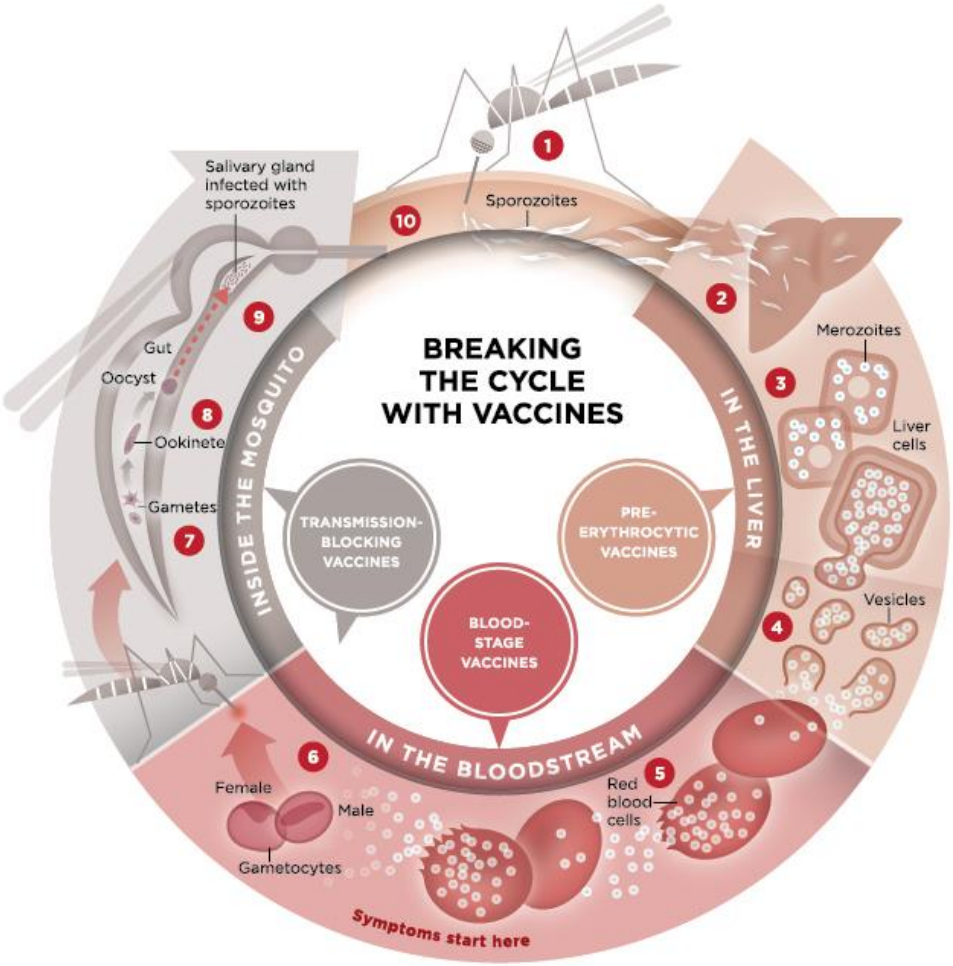

Figure 2.2: Life Cycle of the Malaria Parasite.[36]

2.3 Malaria Chemotherapy

Presently, structural classes of antimalarial drug derivatives are in use which include; 4-aminoquinolines (chloroquine (CQ), and amodiaquine), 8-aminoquinolines (primaquine), atovaquone and artemisinin, Figure 2.3.[41]

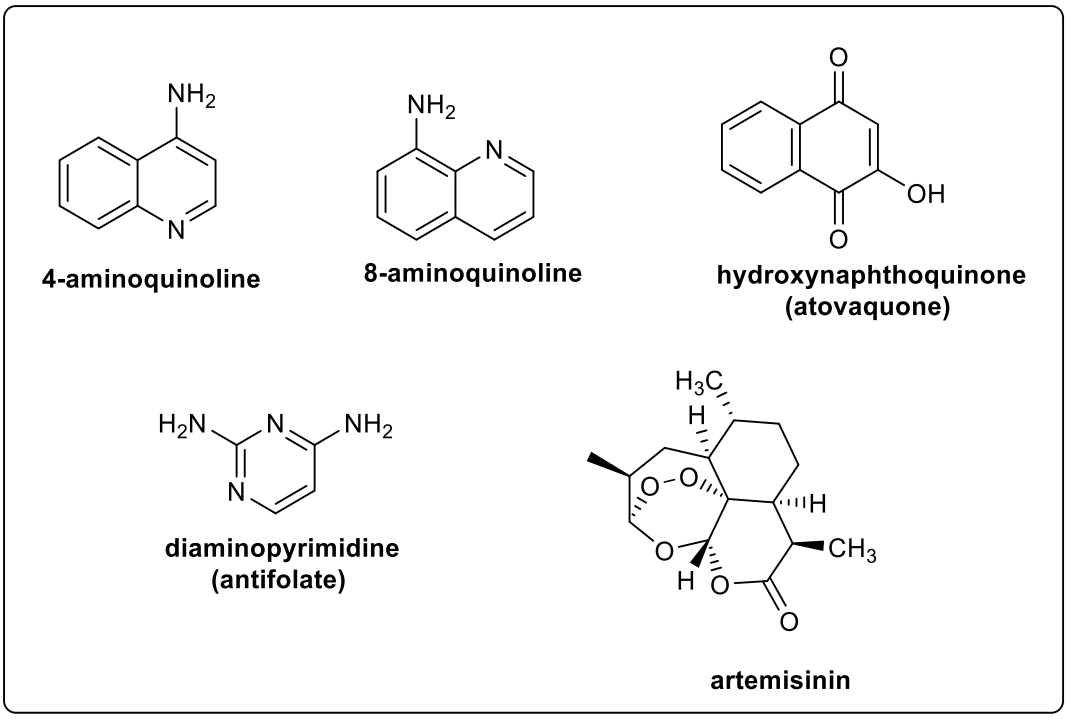

Figure 2.3: Structural Classes of Antimalarial Drugs.[42]

In order to treat malaria, the following have to be considered:(i) the pattern of local resistance where the disease was acquired; (ii) the age of patient; (iii) the parasite species; (iv) the pregnancy status of the patient; and (v) the disease severity.[43] In 2018, the Department of Health in South Africa highlighted important reasons for treating malaria which included; prevention of growth, prevention of death, severe malaria growth, morbidity reduction, eradication of parasitemia and its further spread, and reduction of the emergence of drug resistance.[44] In order to prevent severe malaria, prompt treatment can help to reduce its effect.[43] In the 1940s, there was an introduction of an individual drug, the 4-aminoquinoline chloroquine,[45] Figure 2.4. Later, in 1952, additional drugs such as primaquine were approved by the Food and Drug Administration (FDA).[46] In spite of the positive achievement of these individual drugs in the treatment of malaria, with chloroquine as the most widely used drug, *Plasmodium falciparum* developed resistance and these individual drugs became ineffective.[47]

Artemisinin(and its derivatives) is an antimalarial drug which has short-life and can be removed in the blood in a duration of 1- 3 h. It is used for treatment of symptomatic patients. It acts on young ring and more mature trophozoite; thus, eliminating biomass of the parasites.[48] Due to longer half-life of combination therapy with artemisinin, WHO introduced artemisinin-based combination treatments (ACT) in 2005, which help to mitigate against individual drug resistance; thus, increasing cure rate for malaria case. [49], [50] In order to avert and reduce malarial infections, general public preventive measures must be established to reduce risks and infections.[51]

2.4 Mechanism of Action of Recent Synthetic Antimalarial Drug-like Candidates

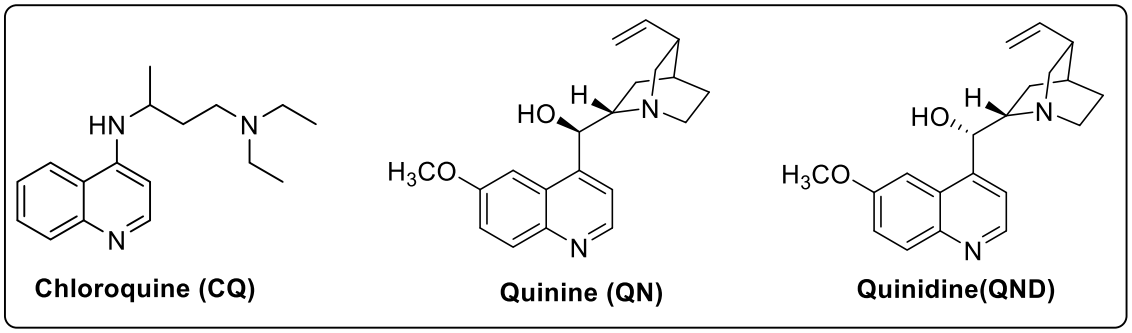

Figure 2.4: Quinoline derived compounds

Heme detoxification in the digestive vacuole, folate and pyrimidine production in the cytosol, and electron transport in the mitochondrion are all often targeted biological processes.[52] Binding of antimalarial agents to heme (in heamoglobin) has been recognized as a possible mode of action of 4-aminoquinoline compounds. Basically, it has been reported that heme is an amphiphilic molecule which consists of water soluble component i.e. polar hydrophilic attached to water insoluble hydrocarbon chain i.e. fat soluble chain and performs a major biological functions such as detoxification of drugs and cellular respiration.[53] In the cell when

heme is in its free state it is crystallized, into a brown pigment referred to as hemozoin, and into mitochondrial cytochromes upon the cell's invasion by the parasite.[54] In the red blood cell the parasite survive when these parasites damage the hemoglobin which leads to hemozoin formation via crystallization of the heme, this leads to detoxification of the heme. In the plasmodium parasite, the formation of hemozoin is responsible for malaria disease.[55] Therefore, studies showed the importance of the possible use of heme crystallization inhibitors which could serve as anti-parasitic agents in the *Plasmodium* parasite.[56] Over the years, 4-aminoquinoline Figure 2.4, compounds have shown promising action against the blood stages of *Plasmodium* in a way by which hemozoin formation is hindered.[53] Therefore, in the *Plasmodium* parasite using 4-aminoquinoline compounds, the major target is the free heme in which complexes are formed, thereby hindering formation of hemozoin. In order to detect heme crystallization inhibitor, high-throughput colorimetric assay can be used.[57]

2.5 Antimalarial Drug Resistance

Antimalarial drug resistance can be referred to as multiplication or survival of a parasite strain, in spite of drug administration and absorption in an equal or higher dose recommended within the tolerance of the subject.[58] The mode of resistance in chloroquine is through gene mutation that occurs in the gene encoding a transporter protein (PfCRT).[59]

In order to clinically evaluate antimalarial drug resistance, the following factors has to be compared: (i) the effectiveness of the antimalarial drug agent, (ii) assessment of *ex vivo/in vitro* cultured sensitivities of cultured *P. falciparum* and (iii) evaluation of the subsequent infection through selective pressure of antimalarial treatment.[60]

It was reported that in the South East Asia, malaria parasites have begun to display resistance to new clinically tested artemisinin class of drugs.[61] Studies also showed that resistance parasites have become resistant to artemisinin-based combination therapy (ACT) partner in the Greater Mekong Sub region. Due to this emergence of resistance to existing drugs, there is a pressing call for the development of new inhibitor. [62] with specific structures and new mechanisms of action different from present therapies, capable of selectively killing the parasite. Hence, many researchers have come up with various approaches for the synthesis of drug-like candidates which could help to eliminate or reduce the transmission of this deadly parasite. Antimalarial drug resistance has raised concerns among researchers worldwide and encouraged them to discover new promising antimalarial pharmacophores which may display different modes of action for drug formulations.[63] Also, extensive efforts had been made by major pharmaceutical companies to eradicate or reduce malaria cases, primarily by improving and enhancing the pharmacokinetic properties through structural modification of existing antimalarial drugs which may ultimately boost their malaria inhibitory activity.[34]

2.6 Discovery of 4(1*H*)-Pyridone as Antimalarial Scaffolds

Researchers have reported the various substituted pyridones as antimalarial agents. Pyridones are isomers of hydroxypyridines, which are formed through carbonyl tautomerism Figure 2.5. The oxygen can be located at any of the carbon atoms; C-2, C-3, or and C-4 of the pyridine ring.[64]

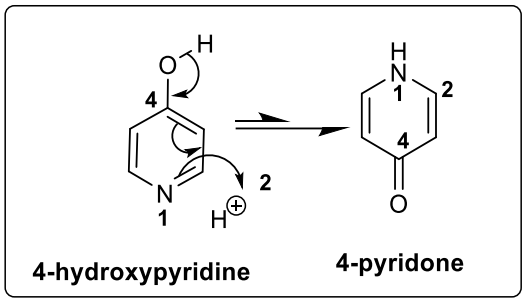

Figure 2.5: Tautomeric forms of 4-pyridone

As far back as 1960s, studies done by the Walter Reed Army Institute of Research demonstrated that clopidol, Figure 2.6, a derivative of 4(1*H*)-pyridone, was active against *Plasmodium sp*., as well as chloroquine-resistant strains, in which clopidol inhibits the electron transport chain in mitochondrial.[65] Pyridones then became motifs of interest in antimalarial drug research.[66] Studies have shown since 4(1*H*)-pyridone derivatives to be a class of inhibitors targeting the Qi-site of cytochrome bc (complex III) in the mitochondrial electron transport chain, which is a validated target for the selectively elimination of *P. falciparum* parasites.[67]

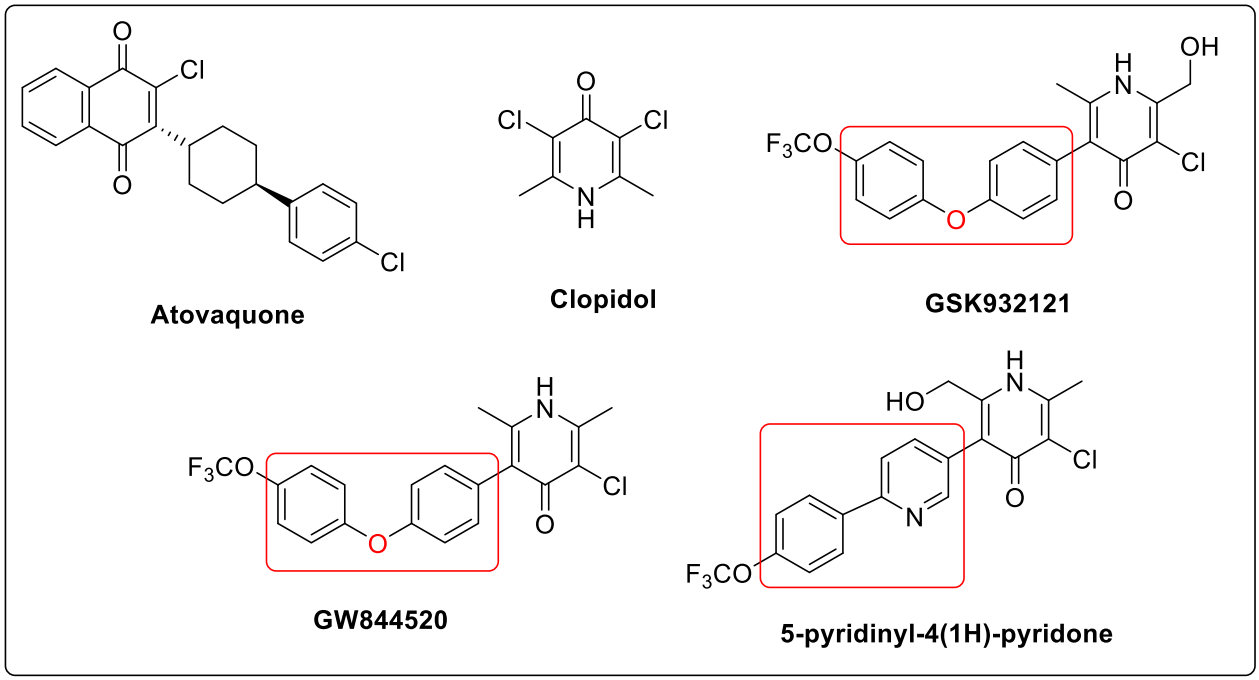

Figure 2.6: Structures of atovaquone, clopidol and some 4-(1*H*)Pyridone motifs

2.7 Structure Activity Relationship (SAR) Studies of 4-(1*H*)Pyridone Derivatives

In order to design a new series of antimalarial drug agents, researchers have used SAR modelling methods to establish the antimalarial activity of 4-(1*H*)pyridone derivatives by comparing the biological activities or physicochemical properties.[67] of such compounds with those of the modelled molecular characteristics.[68] Thus, SAR modelling could help in the discoveries and design of series of antimalarial drug candidates.

SAR studies conducted by GSK on clopidol *via* the optimization of the different substituent on clopidol, Figure 2.6, the 4(1*H*)-pyridone motif, revealed that the presence of a substituent on position 5, exhibited the greatest effects towards antimalarial activity and physicochemical properties. They observed a marked increase in *in-vivo* antimalarial activity, primarily attributed to the replacement of one of the chloro substituents on clopidol with a diarylether side chain. This significant finding led to the synthesis of **GW844520**, Figure 2.6, which has been shown to exhibit remarkable *in vitro* and *in-vivo* inhibitory activities with ED_{50} values in the lower nanomolar range.[69]

However, the unexpected cardiotoxicity side effects displayed by **GW844520**, resulted in Yeast *et al*. [65], partnering with GSK. Their main objective was to further explore the antimalarial potential of this class of compounds by modifying and synthesizing various derivatives of disubstituted clopidol. All their efforts finally gave rise to the synthesis of 4-pyridone derivative, **GSK932121**, Figure 2.6. Using SAR studies, they synthesized a series of diaryl ether containing-4-pyridones which were tested against *Plasmodium falciparum (in vitro)* and murine *Plasmodium yoelii (in vivo).* The result from this study demonstrated that diaryl ether substituted 4-pyridones displayed superior antimalarial activity compared to their corresponding chloro-containing derivatives, clopidol. Further structural modification at

carbon 5 of the pyridone framework, led to the synthesis of 5-pyridinyl-4(1H)-pyridones, Figure 2.6, which have shown a superior pharmacokinetic characteristic when compared to the lipophilic phenoxyphenyl pyridone derivatives previously reported.[70] This improved pharmacokinetic profiles observed of this compound may be a result of its derivation from anticoccidial drug clopidol. [65]

2.8 Pharmacokinetic Profile of 4 (1*H*)-Pyridones as Antimalarial Compounds

Pharmacokinetics is referred to as a reaction of the body to a particular medication through its absorption, distribution, metabolism, and excretion (ADME) processes.[71] The antimalarial drug activity in the blood depends on the profiles of its fundamental pharmacokinetic and pharmacodynamic processes, the vulnerability of the malarial parasites to the medication(s), the sum of asexual malaria parasites present in the blood and mechanism of action of the host-defence.[72]

Therefore, the pharmacokinetic profile of 4-pyridone clinical candidates was investigated as a possible means to further enhance their antimalarial activity. [67] These studies showed that the structural modification of 4-pyridones at the different carbon positions, namely positions 5 and 6, could improve their solubility properties. Incorporation of a CH_2OH group at position C6 of the 4-pyridone increased the *in vitro* antimalarial activity, compound **I (GSK932121)**, Figure 2.7, displaying a *P. falciparum* IC_{50} value of 0.002 µM, compared to the presence of a methyl group at position 6 of compound **II (GW844520)**, Figure 2.7, which displayed an IC_{50} value of 0.007 µM. This marked enhanced antimalarial activity was ascribed to the presence of the CH_2OH group, which improved solubility and pharmacokinetic properties of compound **I**, Figure 2.7.[67]

Also, substituting the lipophilic phenolate moiety (in red), compound **III**, Figure 2.7 with a pyridine ring in compound **IV,**[73]has shown to have a noteworthy effect on its pharmacokinetic profile and thus antimalarial activity. As a result, the *in vitro* and *in vivo* bioassays on the newly synthesized 4(1*H*)-pyridone-based compounds revealed promising malarial inhibitory activity.[65] The development of the pharmacokinetic profiles of these compounds became significantly important due the presence of the pyridine ring and a polar hydroxymethyl group linked at the C6 position of the 4(1*H*)-pyridone ring, compound **IV**. This led to a prominent increase in the solubility and oral bioavailability in mice, while still maintaining their antimalarial properties.[70]

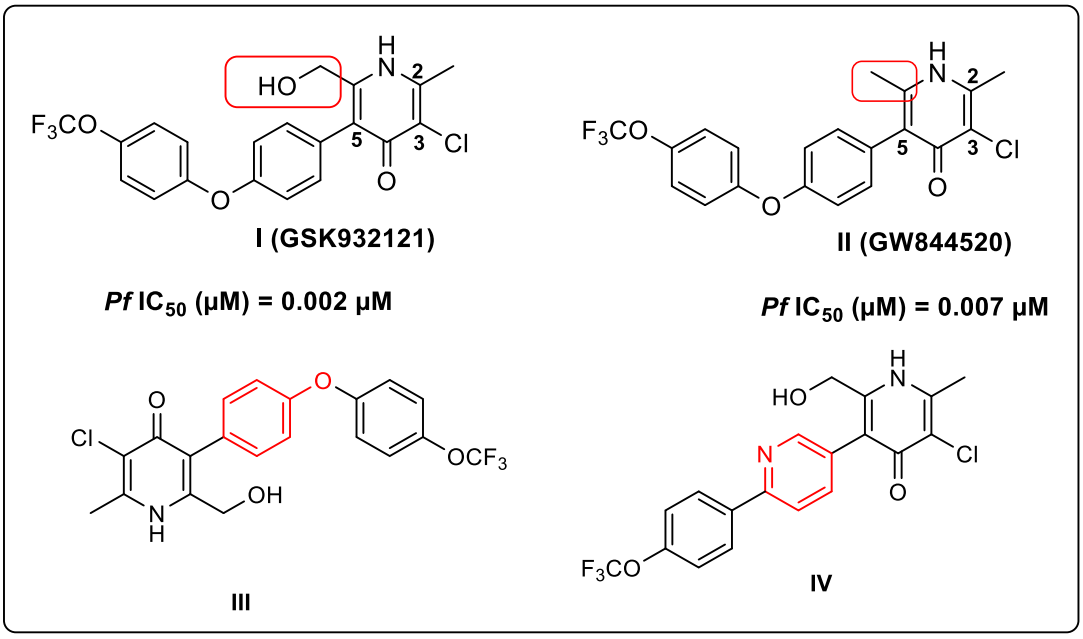

Figure 2.7: Structures illustrating transformation of 4-pyridones at the position C6 and modification of lipophilic phenolate moiety of 4-(1*H*)pyridone with a pyridine ring. [67],[73]

2.9 Reported Syntheses of 4(1*H*)-pyridones as Antimalarial Compounds

As an improved alternative synthesis to the 10 step procedure reported by Yeast *et al.* [67], Fernandez *et al.*,[68] developed a 5-step synthesis which afforded **GSK932121** in a good yield, Scheme 2.1.

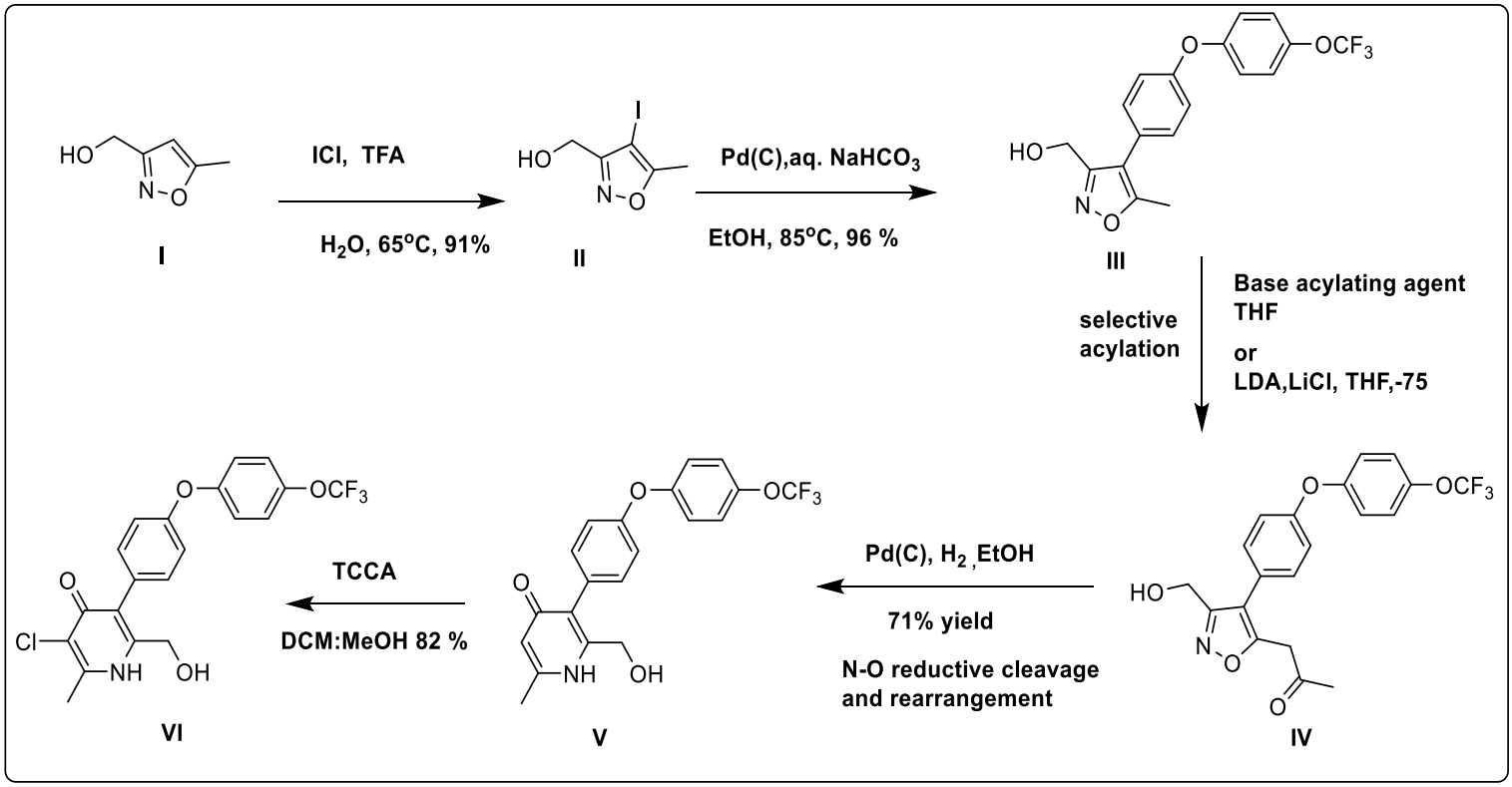

Scheme 2.1: Synthesis of 4(1*H*)-Pyridones from Isoxazole

4(1*H*)-pyridone **GSK932121** antimalarial clinical drug candidates were synthesized in good yields through a 5-step synthetic approach, Scheme 2.1. The notable progress was due to the key action of the isoxazole **I**, which was employed as the precursor. The two major reactions which were conducted included the selective acylation of the unprotected 3-hydroxymethyl-5-methyl isoxazole derivative **III** to yield the intermediate compound **IV** and the reductive cleavage of the nitrogen-oxygen bond of this intermediate to afford the intermediate pyridone **V**, Scheme 2.1.[68]

2.10 *In-Silico* Studies and Binding of 4(1*H*)-Pyridones to Cytochrome bc_1

New 4(1*H*)-pyridones motif or analogues could as well be designed since it has been proven that **GSK932121** and **GW844520**, Figure 2.6, could bind at Qi site which could overcome the atovaquone Qo resistance.[74], [75] This class of inhibitors were reported to have shown potent antimalarial activity in *in-vivo* screening as a result of a complex which formed with the co-crystallization structure of the cytochrome bc_1. In 2015, Capperin and his team studied the binding modes of the 4(1*H*)-pyridones at Qi site complex III (cytochrome bc_1), Figure 2.8. Docking studies conducted on the binding of 4(1*H*)-pyridones class of inhibitor onto cytochrome bc_1 revealed that both the 4(1*H*)-pyridones and the co-crystallized bovine cytochrome bc_1 complex exhibit the same binding modes at the Qi sites.[49] This was made possible by a strong hydrogen bond between most of the residues and these pyridones. The amide head of these pyridones was separated by a short distance less than 3.3 Å, and also from the carbonyl group. [49]

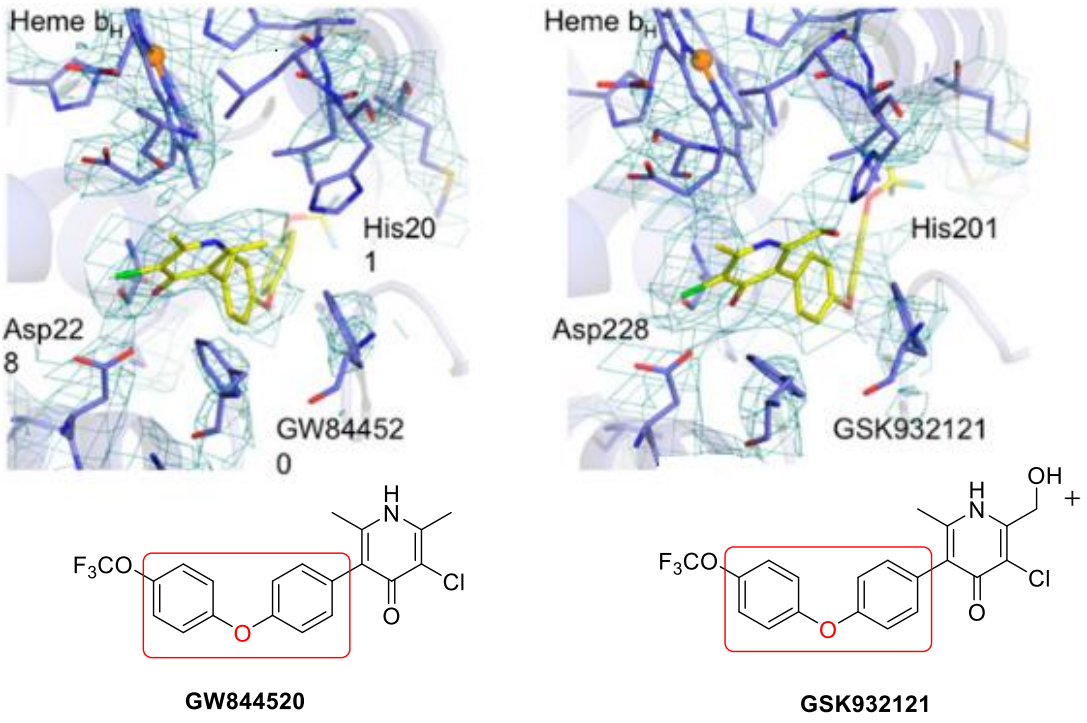

GW844520 **GSK932121**

Figure 2.8: The binding of **GW844520** and **GSK932121**, to cytochrome bc1 Qi binding site[49]

GSK932121 and **GW84450** are 4-(1*H*)-pyridones with a single heavy atom (oxygen) between the benzene rings. Gamo *et al.* identified potent and selective 4-(1*H*)-pyridone-based antimalarial agents (clusters 87 and 143) where the benzene/pyridine rings are separated by two heavy atoms [76]. Compounds with the sulphur and oxygen heavy atoms between the benzene/pyridine rings performed better more with ethene. In this research, guided by *in-silico* screening, a series of new cytochrome bc1 (Qi site) inhibitors, containing the 4(1*H*)-pyridone scaffolds, Figure 2.9, were designed and docked to investigate their binding potency against this active site. The results emanating from this study showed an enhanced binding energy of -10.3 kcal/mol, Figure 2.10, which may be as a result of the sulfur linker *via* ligand binding.[77] Docking of the specific target compound placed the sulphur close to PHE30, and this was interesting for two reasons. Firstly, crystallographic evidence suggests that strong interactions exist between divalent sulphur atoms and aromatic rings, and the sulphur of the target molecule Figure 2.9 is within range (<5 Å) of PHE30[78]. Secondly, in human cytochrome bc_1 there is a Serine amino acid instead of Phenylalanine which provides a good opportunity to design species-specific inhibitors.[79] The docked pose of the of the target compound in Figure 2.9 showed a hydrogen bond interaction between the nitrogen of the pyridone and histidine 12. A water bridge is observed between the oxygen of the pyridone and ASP218. The pyridone also forms two pi-stacking interactions between HIS192 and PHE210. Additional hydrophobic interactions were observed between the ligand and PHE30, VAL34, VAL184 and PHE185.

This finding thus supports the viability of this class of compounds as potential antimalarials, owing to their observed binding at the Qi site which could make them possible candidates to overcome the resurgent effects of resistance.

Thus, based on our findings through these *in-silico* studies and previous work recently carried out on 2,6-dimethyl-4-(1*H*)pyridones, [80], [70], [65] we have successfully designed and synthesized a new series of antimalarial agents which may selectively inhibit the Qi site of the complex III the electron transport chain of mitochondria, Figure 2.9. The synthesis of these antimalarials was further enhanced by using the formerly synthesized **GSK932121** and **GW844520** as precedented support, owing to their remarkable *in-vivo* inhibitory malarial activity. Moreover, the design of the new 4-(1*H*)pyridone-based antimalarial target molecules primarily stemmed from the structural modification of **GSK932121**, Figure 2.9. This modification was accomplished by the incorporation of the lipophilic benzyl(phenyl) sulfide using palladium catalyzed cross coupling reactions (i.e the sulfur linker as compared to oxygen linker) as the major step, after the use of the reported method to introduce 1-phenoxybenzene moiety into the molecule posed great challenges. These changes in the synthesis of these compounds were moderately successful.

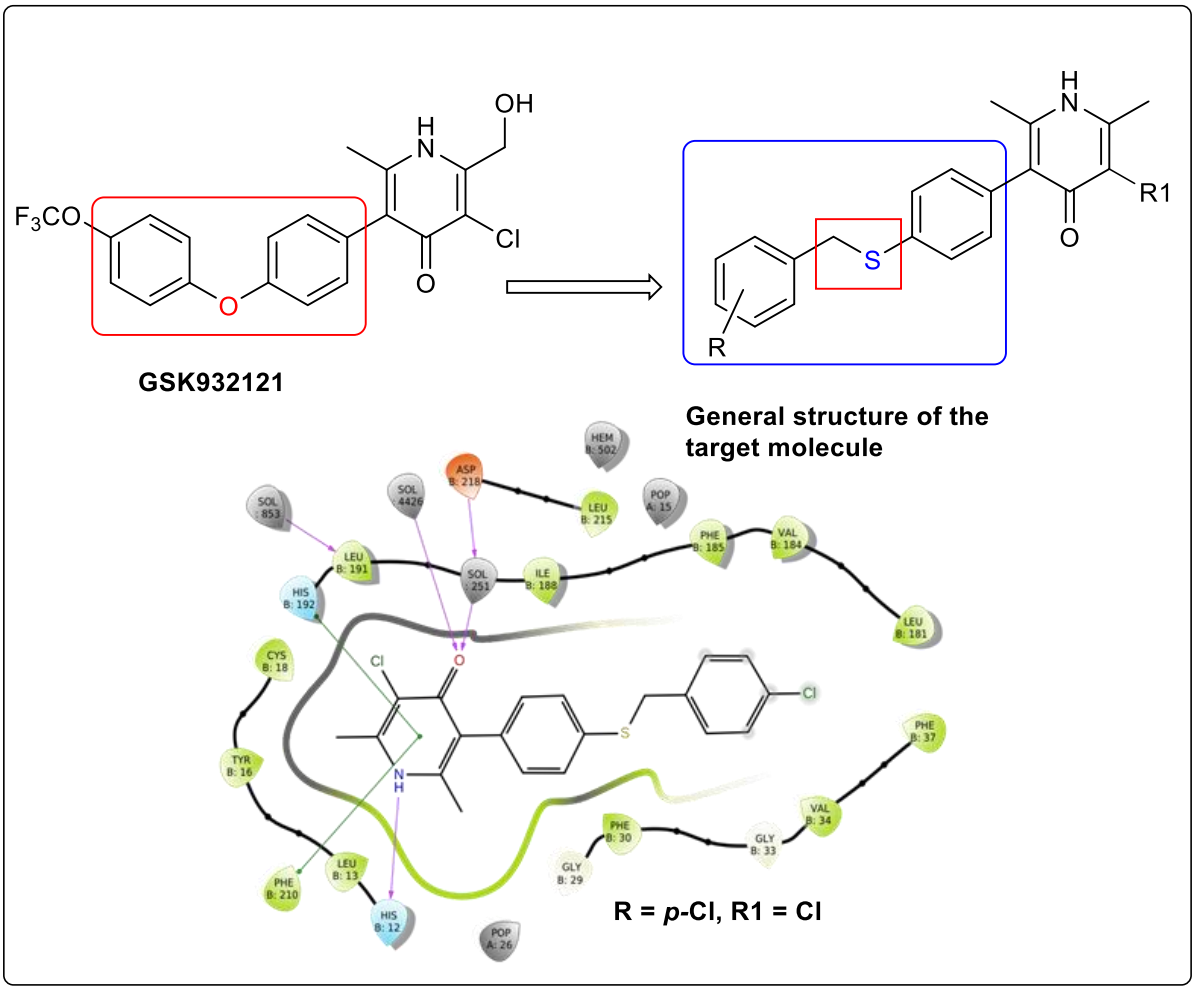

Figure 2.9: Modification of **GSK932121** to afford the target molecules and the binding pose of a specific target molecule into the Qi-site of cytochrome bc1 of *P. falciparum*.

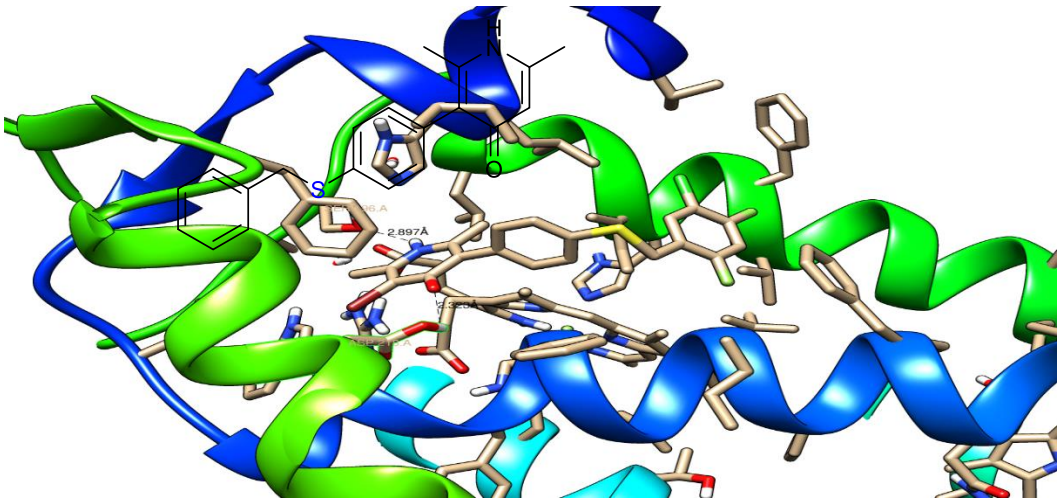

Figure 2.10: The binding of 3-(4-(benzylthio)phenyl)-2,6-dimethylpyridin-4(1*H*)-one onto malaria cytochrome bc1 in the Qi binding site with binding energy of -10.3 kcal/mol

2.11 Synthesis of Derivatives of 2,6-dimethylpyridin-4(1*H*)-ones

Guided by the findings from our molecular docking studies, we designed and screened libraries of 4(1*H*)-pyridone based compounds using molecular docking tools. We used Autodock Vina to identify 4(1*H*)-pyridone-benzylthiophenyl derivatives as novel targets with potential Qi-site inhibitory activity. The target molecules were synthesized according to previous reports.[81 - 82]

2.11.1 Synthesis of 2,6-dimethylpyridin-4(1*H*)-one derivatives *via* a reported method

In an attempt to synthesize the envisaged target compounds **2.9a-b**, we proceeded by way of a well-developed method[65], Scheme 2.2, which included; (a) a Dakin West reaction of β-aryl ketone *via* reductive methylation; [81,83] (b) an oxidative cyclization reaction with acetic anhydride; (c) an amination reaction; [73] and (d) a benzylation and a thiolation reaction.[84] However, all efforts to synthesize the target compounds were futile and an alternative synthesis route was explored.

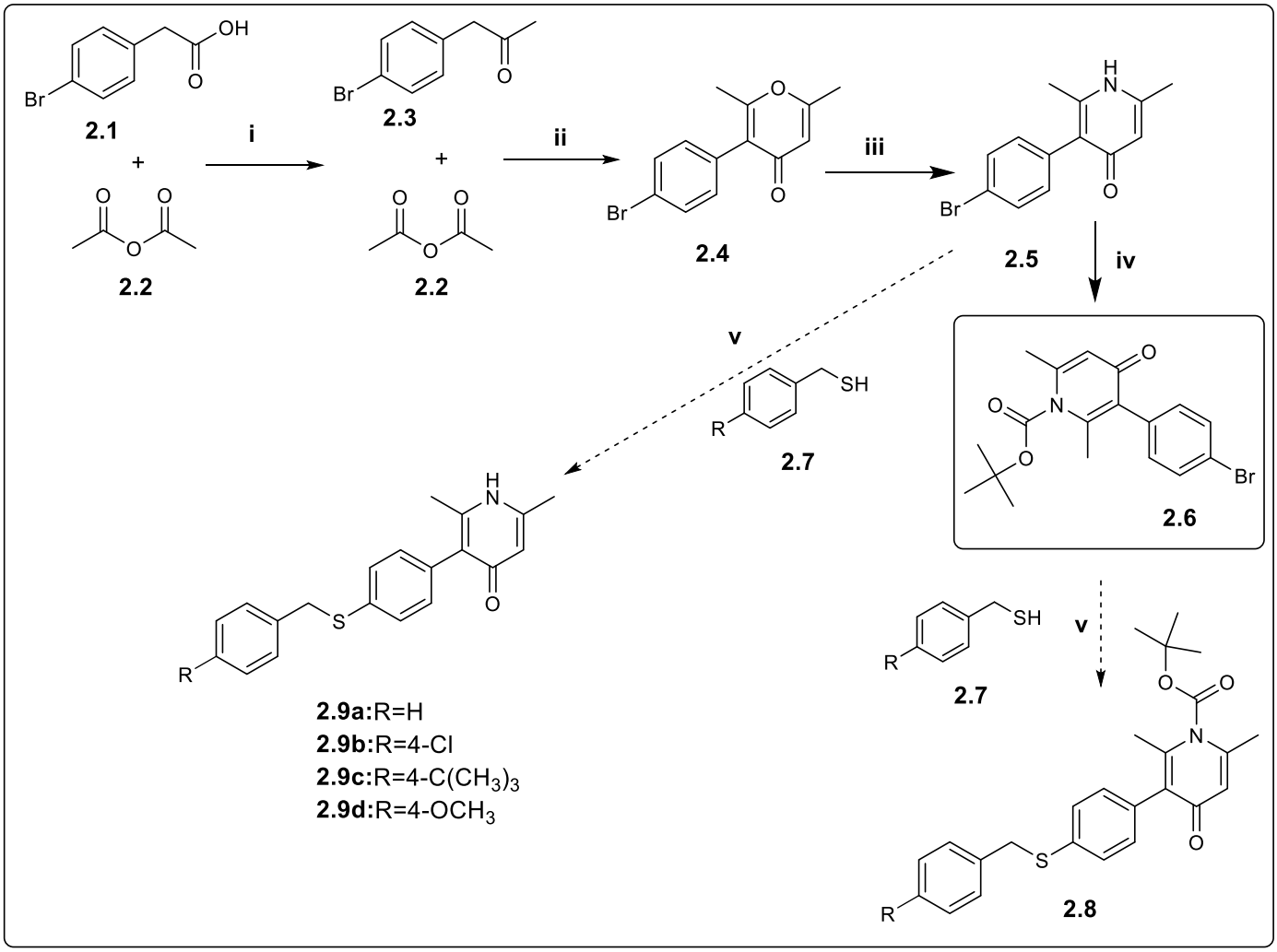

Scheme 2.2: General Reaction Scheme for Unsuccessful Synthetic Approaches to 3-(4-substituted(benzylthio)phenyl)-2,6-dimethylpyridin-4(1*H*)-one. Reagents and conditions: (i) 1-methylimidazole, rt, N_2, 15 h; (ii) Eaton's reagent, 95 ^oC, N_2, 2 h; (iii) NH_3, EtOH, 140 ^oC, 50 h; (iv) $(Boc)_2O$, DMAP, acetonitrile, 40 ^oC, 14 h; (v) Dry 1.4-dioxane, DIPEA, $Pd(dba)_3$, Xantphos, 90 ^oC, 4 h.

2.11.2 Synthesis of 2,6-Dimethylpyridin-4(1*H*)-one Derivatives *via* 4-Bromophenylacetone

The second attempt to synthesize the target compounds **2.9a-b** entailed the use of a reductive methylation reaction whereby commercially available 4-bromophenylacetic acid **2.1** was converted to the ketone **2.3** by treatment with acetic anhydride **2.2** using *N*-methylimidazole as the catalyst, Scheme 2.3. The intermediate compound **2.3** revealed the characteristics peaks in the ^{1}H and ^{13}C NMR spectra. The ^{1}H NMR revealed absence of 1H of carboxylic OH and appearance of a highly intense singlet, integrating for three alkyl protons of 4-bromophenylacetone at 2.14 ppm.

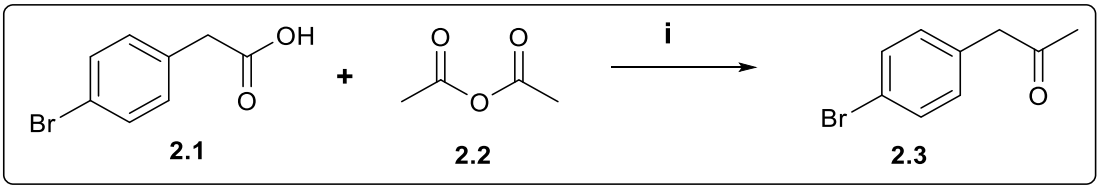

Scheme 2.3: Synthesis of 4-bromophenylacetone **2.3**. Reagents and conditions: (i) 1-methylimidazole, Ac_2O, rt, N_2, 15 h.

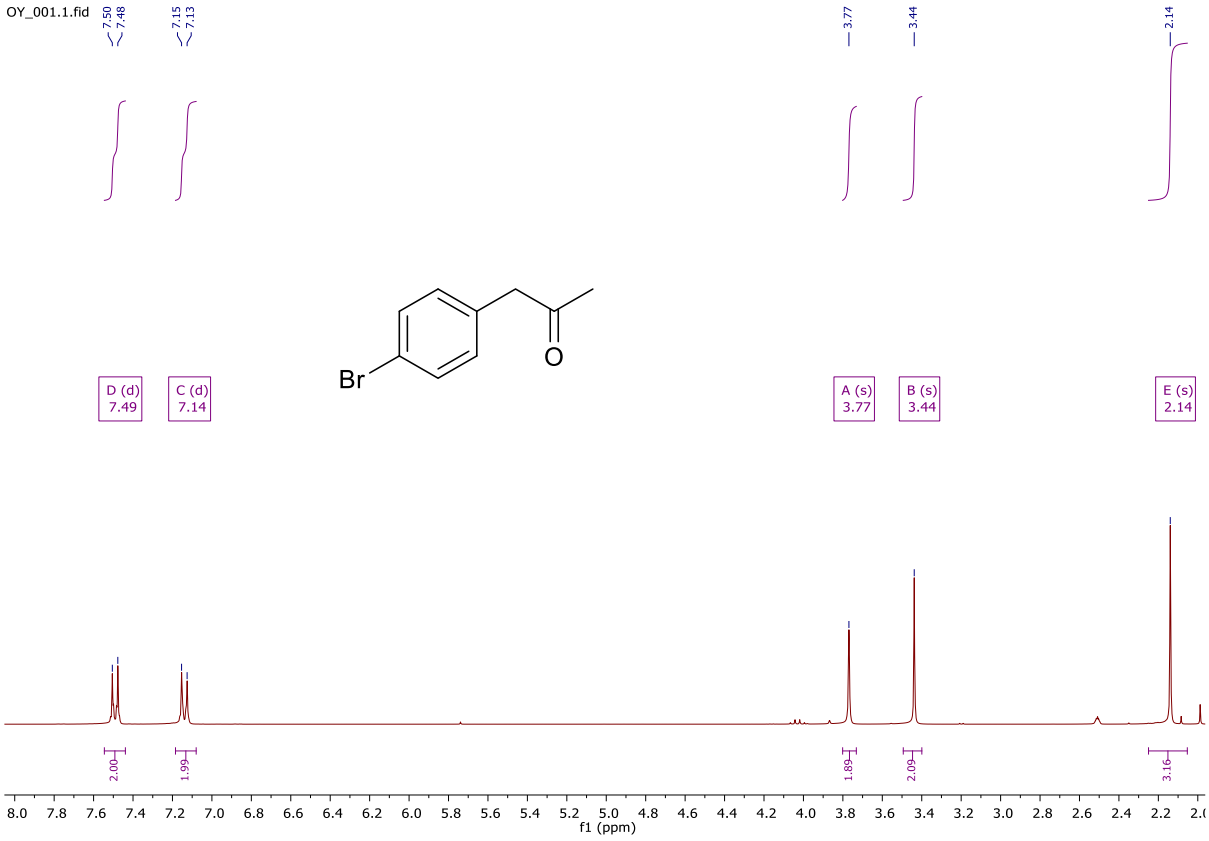

Figure 2.11: ^{1}H NMR Spectrum of **2.3** (400 MHz, DMSO- d_6)

2.11.2.1 Proposed mechanism for the Darkin-West synthesis of β-Aryl Ketone, 4-bromophenylacetone

The mechanism involves; (a) acyl-imidazolium and carboxylate anion formation; (b) acid-anhydride acetyl transfer; (c) formation of enolate ion *via* acid from the anhydride; (d) formation of tetrahedral intermediate *via* nucleophillic attack; (e) breakdown of the tetrahedral intermediate and loss of imidazole; (f) attack on acetyl carbonyl; (g) transfer of acetyl group; (h) decarboxylation to release CO_2 and formation of enolate ion; and (i) protonation of enolate ion to form 4-bromo phenyl-2-propanone, Scheme 2.4.

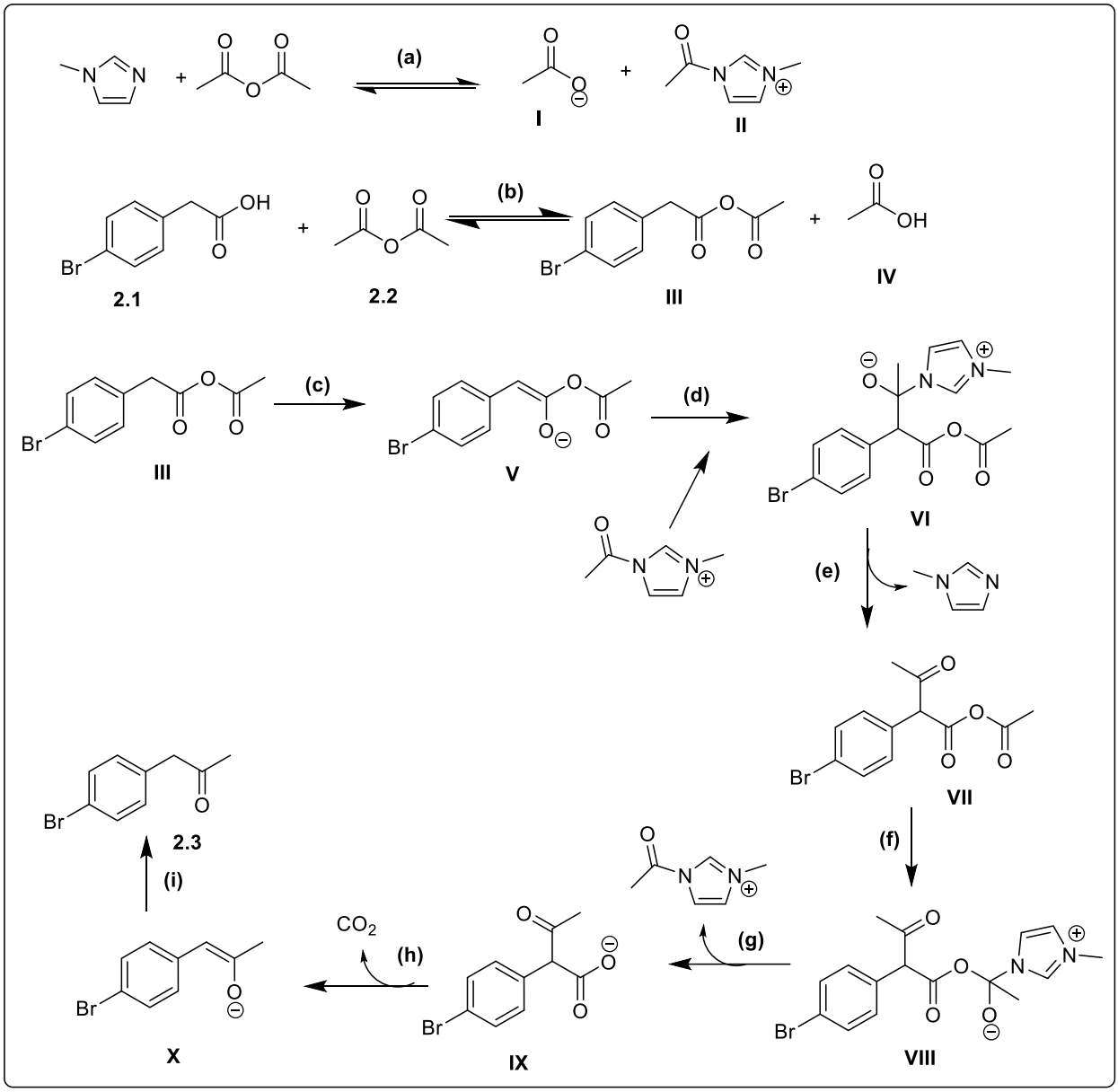

Scheme 2.4: Suggested Mechanism for Synthesis of the aryl 4-bromophenylacetone **2.3**

2.11.3 Cyclization of 4-Bromoaphenylmethyl ketone 2.3 *via* Oxidative Cyclization Reaction Intermediate benzylmethyl ketone, **2.3** was further treated with acetic anhydride **2.2**, Scheme 2.5, under inert conditions, in the presence of Eaton's reagent to give aryl 4(1*H*)-pyranone, **2.4a** in a moderate yield (48%). Cyclization of **2.4a** was confirmed with the appearance of a vinylic proton, which resonated downfield as a singlet at δ_H 6.22 ppm, also

characteristic peaks were found in the ^{1}H NMR with two sharp singlets found at δ_H 2.15 and 2.28 ppm, which suggested the presence of six protons of the two -CH_3 substituents attached to positions 2 and 6 of the 4(1*H*)-pyranone ring. It was also worthy to note that the two doublets seen in the aromatic region of the 4(1*H*)-pyranone ring gave the same coupling constant of 8.4 Hz, and consistent with the neighbouring effect of these aromatic protons on one another.

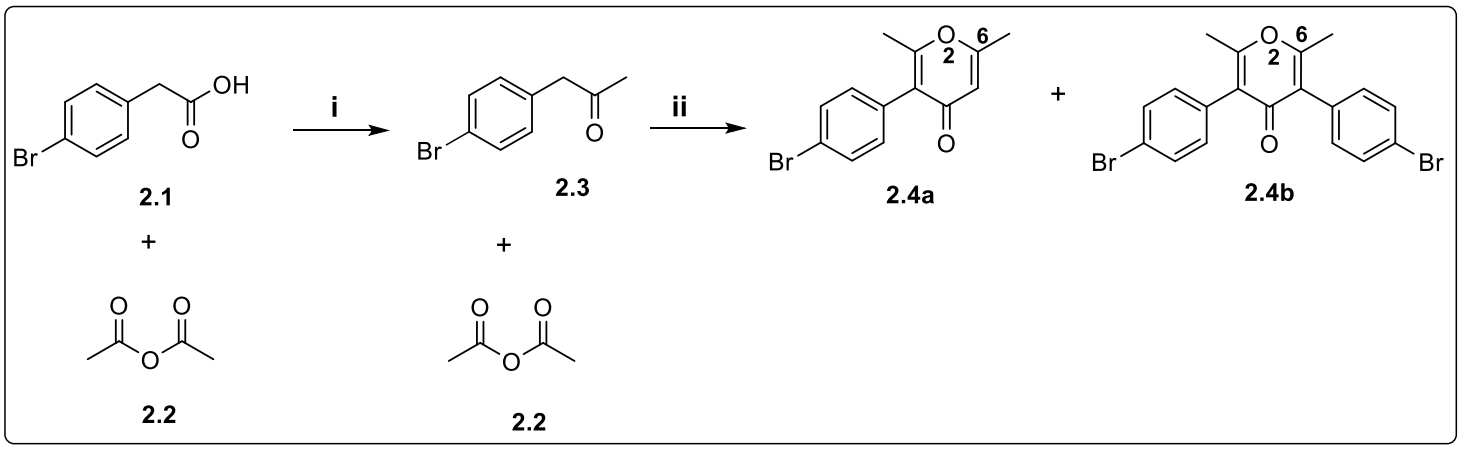

Scheme 2.5: Synthesis of 3-(4-bromophenyl)-2,6-dimethyl-4H-pyran-4-one **2.4a**. Reagents and conditions: (i) Acetic anhydride, 1-Methylimidazole, rt, N_2, 15 h; (ii) Acetic anhydride, Eaton's reagent ($CH_4O_8P_2S$), 95 ^{o}C, 2 h.

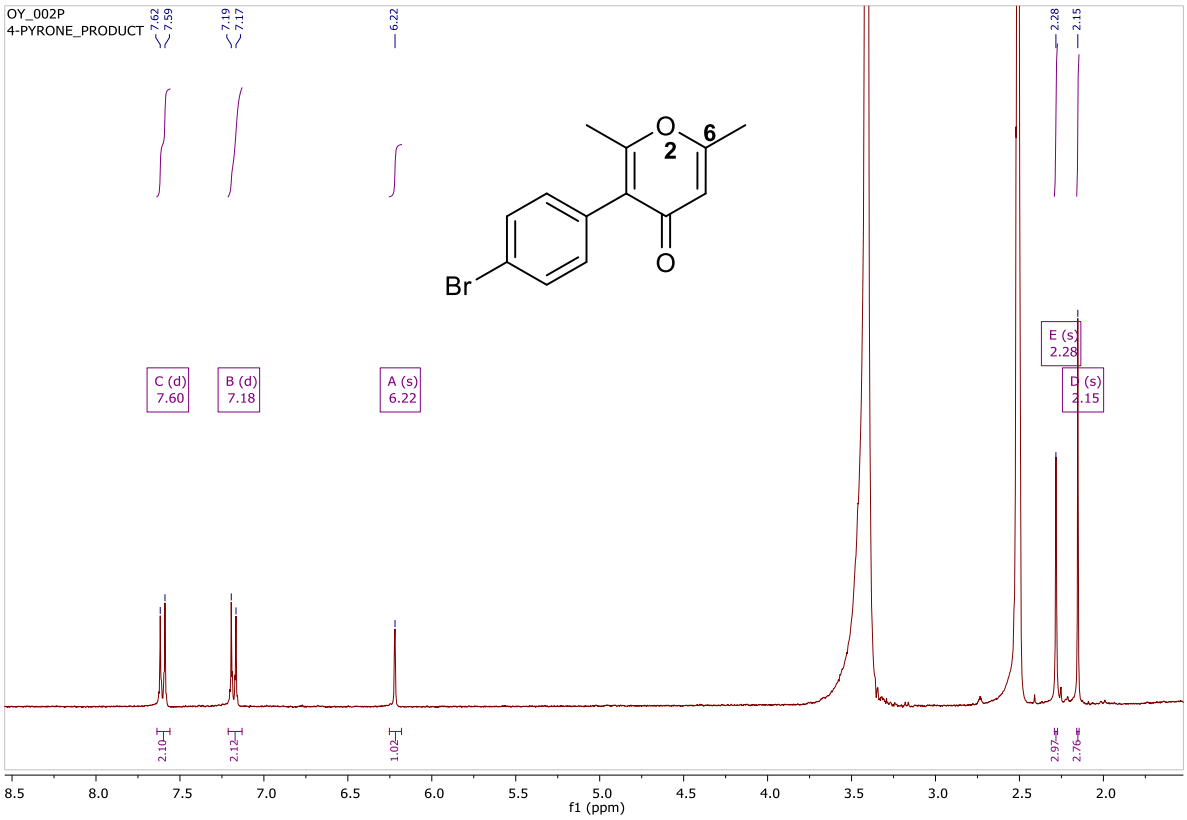

Figure 2.12: ^{1}H NMR Spectrum of **2.4** (300 MHz, DMSO-d_6)

2.11.3.1 Crystallographic analysis of compounds 2.4a and 2.4b

Compound **2.4a** was further confirmed with single-crystal X-ray diffractometry (SC-XRD), Figure 2.13. Interestingly, further analysis of the crystal structure of compound **2.4a** revealed the formation of an additional crystal structure, compound **2.4b** Figure 2.13, which was not detected through other standard means. The formation of this compound could explain the observed low yields and the relatively increased reactivity of compound **2.4a**.

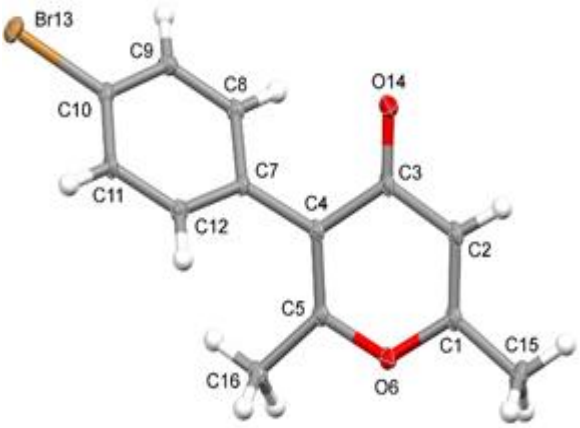

2.4a

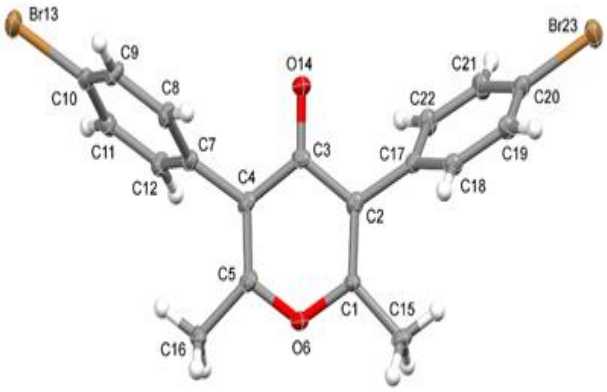

2.4b

Figure 2.13: Crystal structures of Compounds **2.4a** and **2.4b**

Single crystals of **2.4a** and **2.4b** suitable for X-ray diffraction were grown from saturated Hex:EtOAc (3:1) solutions. Crystals of **2.4a** crystallized in the monoclinic P21/c space group with Z = 4, Figure 2.14, whereas crystals of **2.4b**, Figure 2.15, crystallized in the orthorhombic space group P212121 also with Z = 4. A slight bend of the 4-BrPh group connected to the pyridone ring structure in **2.4a** is seen with a O14-C3-C4-C7 torsion angle of -5.1(5)°. The corresponding angle in **2.4b** is a near-linear 2.0(12) ° with the remaining 4-Br-Ph group only slightly twisted (O14-C3-C2-C17 = -7.0(12)°). Each of the arene groups twist with respect to the pyridine ring with torsion angles of C3-C4-C7-C8 = 49.1(5) ° (4), C3-C4-C7-C8 = -67.9(11)° (5), and C3-C2-C17-C18 = 119.7(8)° (5). Molecules in the structure of **2.4a** pack in three dimensions, Figure 2.14, as a ribbon with the pyridone moieties of adjacent molecules linking by weak intermolecular forces, and then overlays with the arene rings to other adjacent molecules. A similar pattern is also seen with the packing of molecules in the structure of **2.4b**, Figure 2.15, except those adjacent molecules are connected via weak intermolecular forces from adjacent arene rings on either side of each molecule. No other notable hydrogen bonding

or pi-pi stacking interactions were observed in either of the structures of **2.4a** and **2.4b**. Typical bond distances and angles observed in **2.4a** and **2.4b** compare well with each other as well as with other closely related structures.[85]

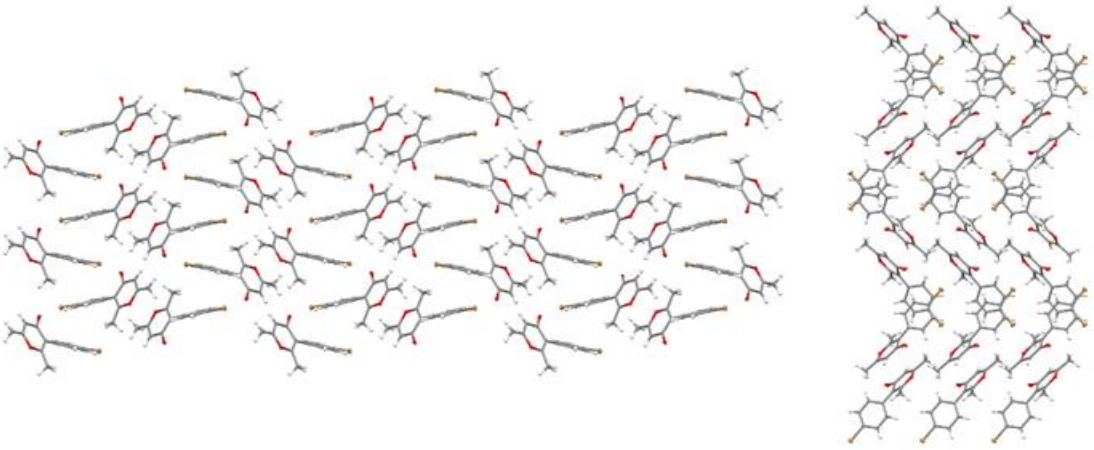

Figure 2.14: SCXRD Packing diagrams of **2.4a** when viewed along the a-axis and b-axis, respectively.

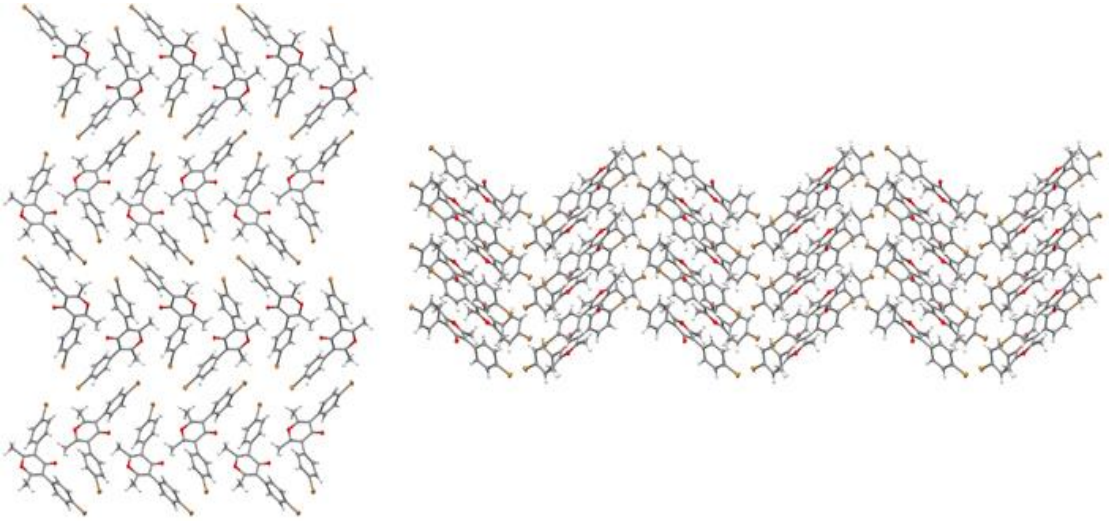

Figure 2.15: Packing diagrams of **2.4b** when viewed along the a-axis and b-axis, respectively.

2.11.4 Amination of the 4(1*H*)-Pyranone

Amination of the 4(1*H*)-pyranone ring portion of compound **2.4a**, Scheme 2.6 was achieved with NH_4OH in ethanol. Interestingly, the formation of 4(1*H*)-pyridone was unequivocally confirmed with ^1H NMR spectroscopy which revealed a singlet in line with the resonance of N-H of pyridone at δ_H 2.06 ppm upfield of the TMS, as earlier reported that the NH signal could appear anywhere in the NMR spectrum.[86]

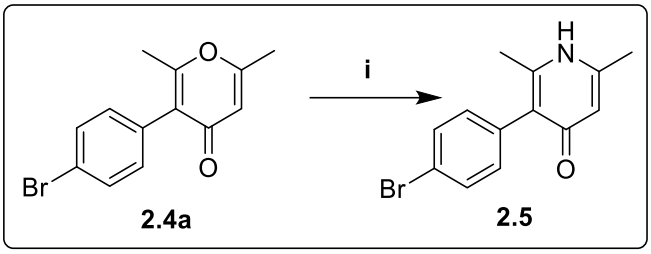

Scheme 2.6: Synthesis of 3-(4-bromophenyl)-2,6-dimethylpyridin-4(1*H*)-one, **2.5**. Reagents and conditions: (i) NH_4OH, EtOH, 140 ^oC, 50 h.

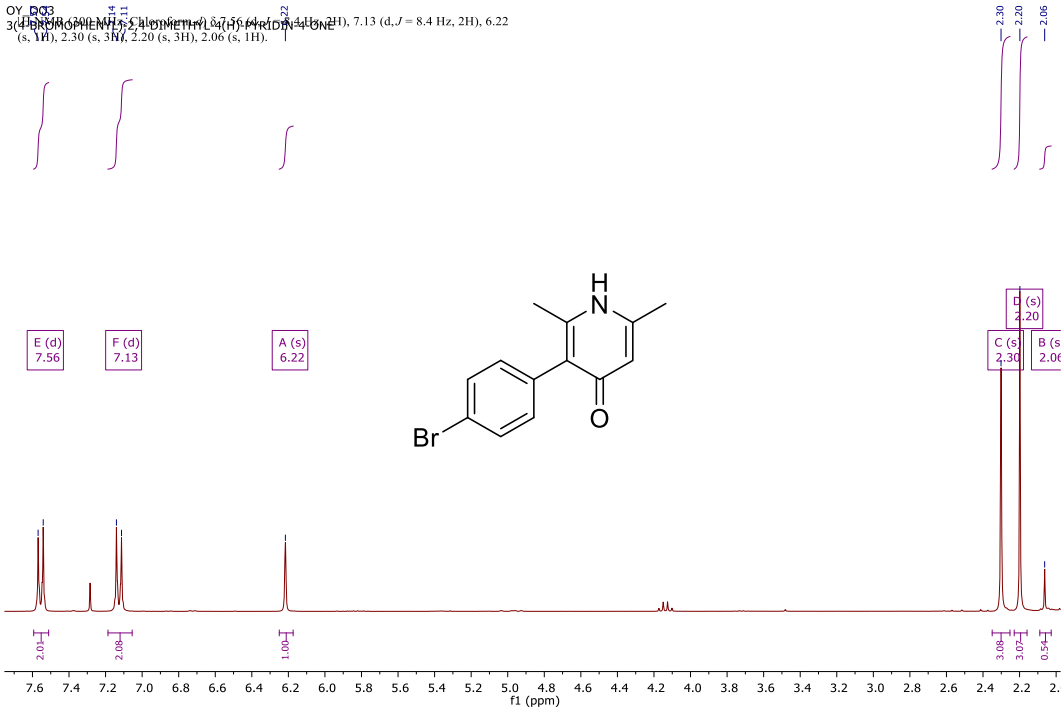

Figure 2.16: ^1H NMR Spectrum of **2.5** (300 MHz, $CDCl_3$)

2.11.5 Synthesis of *Tert*-butyl 3-(4-bromophenyl)-2,6-dimethyl-4-oxopyridine-1(4*H*)-carboxylate, 2.6

At this point, various attempts were made to couple 4-substituted phenyl methanethiols with the synthesized 4(1*H*)-pyridone scaffold to afford the target compounds **2.9a-b**. Therefore, we protected the free N-H on the pyridone ring with *tert*-butoxycarbonyl (Boc)-anhydride, using 4-dimethylaminopyridine (DMAP) as a catalyst and in acetonitrile as the solvent. The reaction was conducted at a carefully controlled temperature of 40°C for a period of 14 h to afford compound **2.6** in excellent yield (97%),[87] Scheme 2.7. The formation of *tert*-butyl3-(4-bromophenyl)-2,6-dimethyl-4-oxopyridine-1(4*H*)-carboxylate, **2.6** was confirmed with ^{1}H NMR spectroscopy with the presence of a distinct singlet of tert butyl which resonate upfield at 9.24 ppm of the TMS.

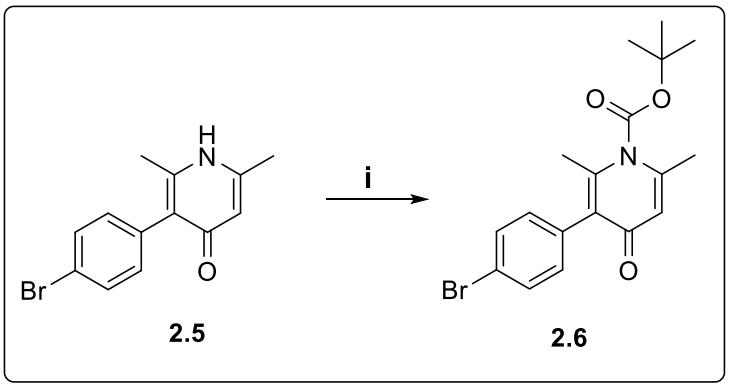

2.5 **2.6**

Scheme 2.7: Synthesis of *tert*-butyl 3-(4-bromophenyl)-2,6-dimethyl-4-oxopyridine-1(4*H*)-carboxylate **2.6**. Reagents and conditions: (i) $(Boc)_2O$, DMAP, acetonitrile, 40 ^{o}C, 14 h.

The protected N-H pyridone was then treated with 4-substituted phenyl methanethiols but unfortunately the reaction was unsuccessful. However, all our efforts to synthesize the target

compounds **2.9a-d** from the 4(1*H*)-pyridone scaffold were in vain, prompting us to proceed *via* a different route to obtain the envisaged target compounds **2.9a-b**, (Scheme 2.8).

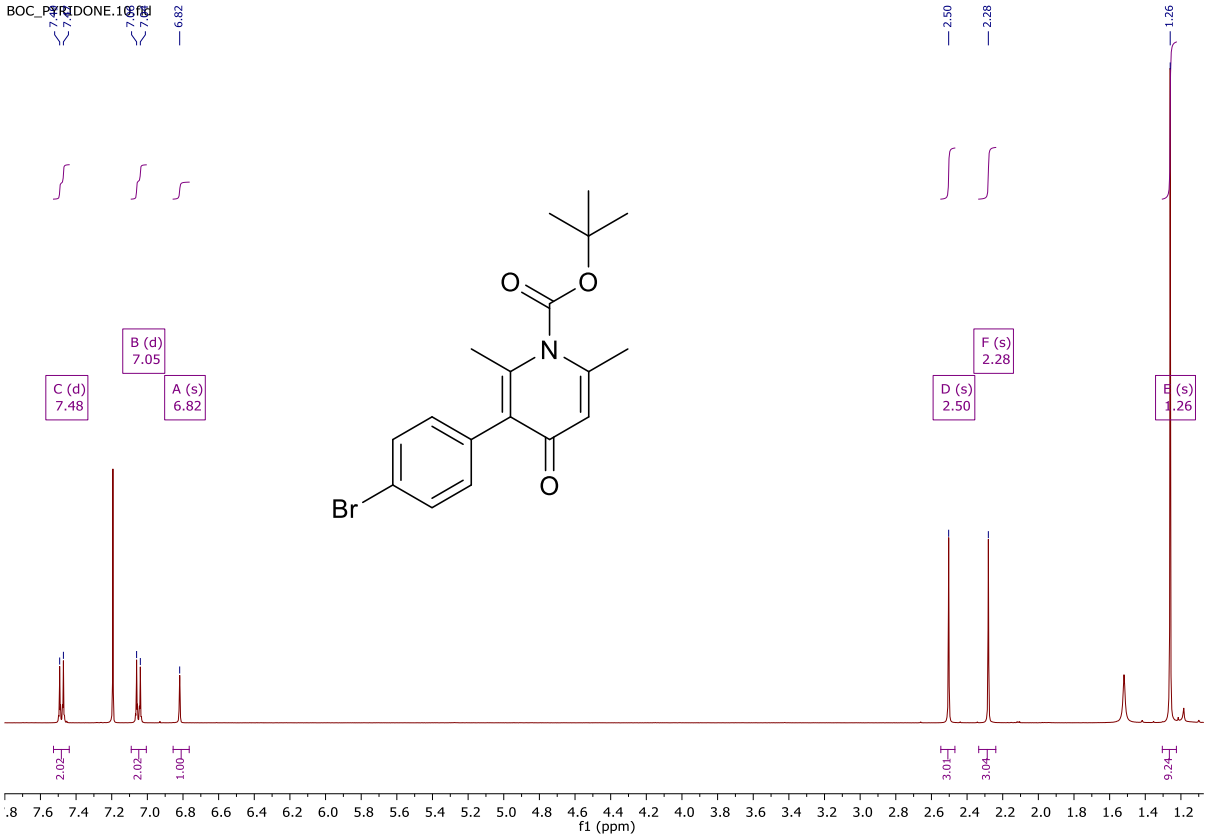

Figure 2.17: ^{1}H NMR of *tert*-butyl 3-(4-bromophenyl)-2,6-dimethyl-4-oxopyridine-1(4*H*)-carboxylate **2.6** (400 MHz, $CDCl_3$)

2.12 Altered Synthesis Towards the Target Compounds 2.9a-b using Palladium Catalyzed Cross Coupling Reactions as a Key Reaction

As an alternative approach to successfully synthesize the target compounds **2.9a-d**, Scheme 2.8, a literature search revealed a synthetic pathway which entails the incorporation of a palladium catalysed cross coupling reaction as a key reaction. In Organic Chemistry, the use

of palladium as a catalyst is highly recognized due to the mild conditions associated with coupling reactions and ability to tolerate a range of functional groups.[88] Apart from the well-known hydrogenation and oxidation processes, it also plays crucial role as a catalyst for various major C—C, C—S and C-N bond forming reactions. An extensive variety of palladium (0) catalysts are applied in organic synthesis for cross coupling reaction. These include $PdCl_2(PPh_3)_2$, $Pd(OAc)_2$ with PPh_3 and other phosphine ligands, while $Pd(PPh_3)_4$, is the most frequently used.[89] These catalysts are stable to air and can be reduced to the active Pd (0) complexes with organometallics or phosphines used for the cross coupling.[90] As a result of the complete formation of the coordinatively unsaturated palladium species, palladium complexes which generally have less than four phosphines are highly reactive for the additive oxidation reaction.[91] Oxidative addition reaction is otherwise referred to as rate determining step reaction. The role of palladium-catalyzed cross couplings is that two molecules are assembled on the metal through the metal-carbon bonds formation.[88]

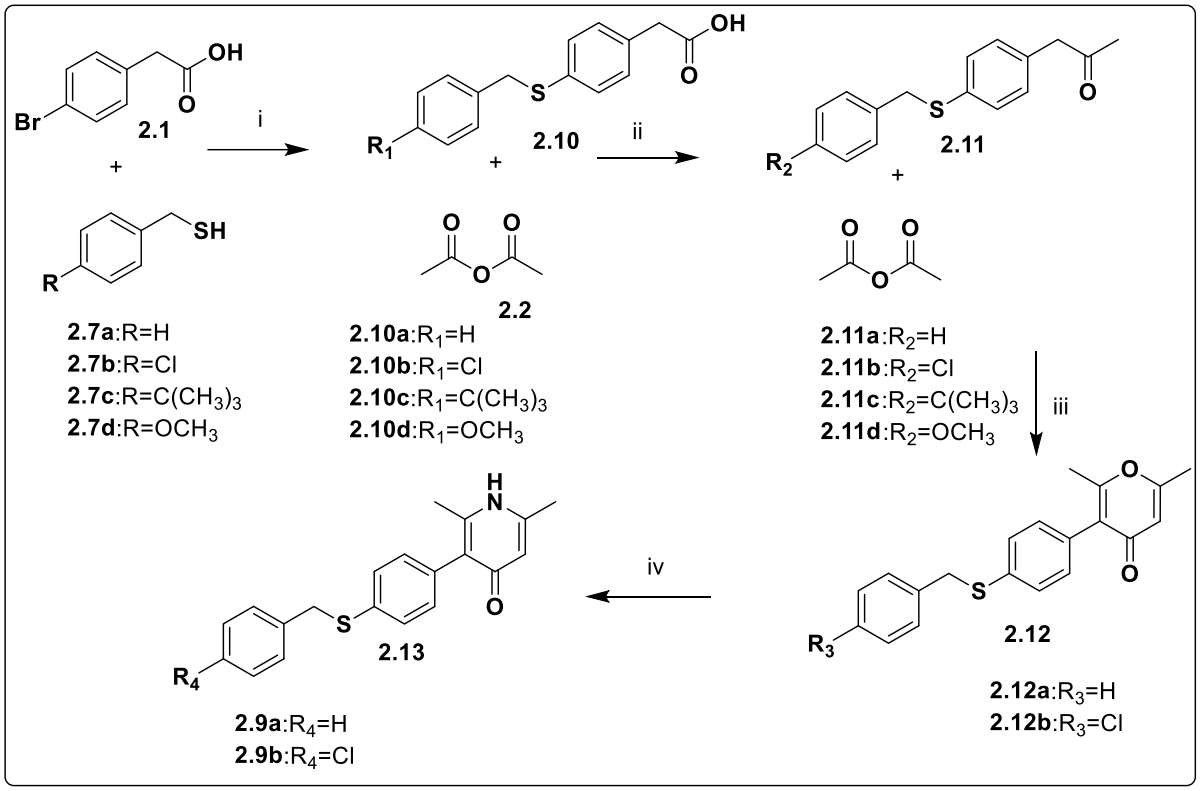

Scheme 2.8: Successful synthetic approaches to 3-(4-(substitutedbenzylthio)phenyl)-2,6-dimethylpyridin-4(1*H*)-one. Reagents and conditions: (i) Dry 1.4-dioxane, DIPEA, $Pd(dba)_3$, Xantphos, 90 ^oC, 4 h.; (ii) 1-Methylimidazole, rt, N_2, 15 h.; (iii) Eaton's reagent, 95 ^oC, 2 h; (iv) NH_4OH, EtOH, 150 ^oC, 50 h

2.12.1 Formation of Methylsulphane (CH_2S) Linker for Hybrid Compounds 2.10-2.12, 2.9a, b

Using palladium catalyst $Pd_2(dba)_3$, the synthesis of only two target molecules **2.9a** and **2.9b** was successfully achieved, Scheme 2.8. The reaction pathway commenced with an aromatic nucleophilic reaction by adding phenyl methanethiol to 4-bromophenylacetic, under basic conditions (DIPEA), in the presence of the coupling catalyst $Pd_2(dba)_3$ and the ligand (Xantphos), Scheme 2.9.[92] This reaction worked successful for all the derivatives **2.10a-d** in a moderate yield of 41%, 43%, 39%, and 35% respectively.

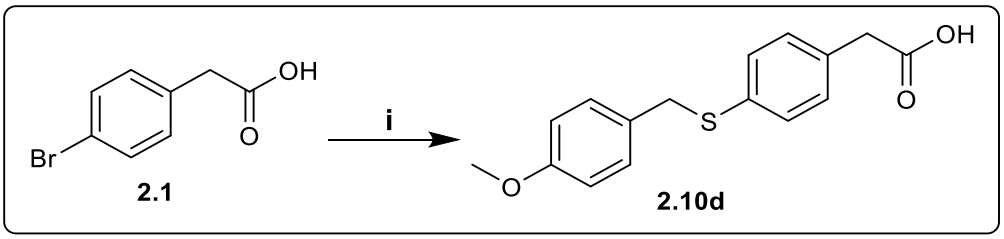

Scheme 2.9: Synthesis of 2-(4-(4-substituted benzylthio)phenyl)acetic acids, **2.10a-d**. Reagents and conditions: (i) Substituted phenylmethanethiol, dry 1.4-dioxane, DIPEA, $Pd(dba)_3$, Xantphos, 90 ^oC, 4 h.

Using compound **2.10d** as the representative in discussing NMR data, the presence of methyl sulfide (CH_2S) linker of **2.10d** was confirmed by ^1H NMR, revealing the presence of a new intense singlet integrating for 2H and resonating downfield at a chemical shift of 4.08 ppm. It is clearly seen from the spectrum in Figure 2.18 that CH_2S protons tends to be more downfield than CH_2COOH protons. The reason for this is that electronegative components additionally attached to carbon change the resonance position of the protons, causing these protons to be more down field. Thus, the higher the electronegativity of the directly bonded atom, the more the down field shift.[93]

The OH peak of the carboxylic acid functional group was observed as a broad singlet at 12.36 ppm which confirmed the formation of **2.10d** unambiguously, Figure 2.18.

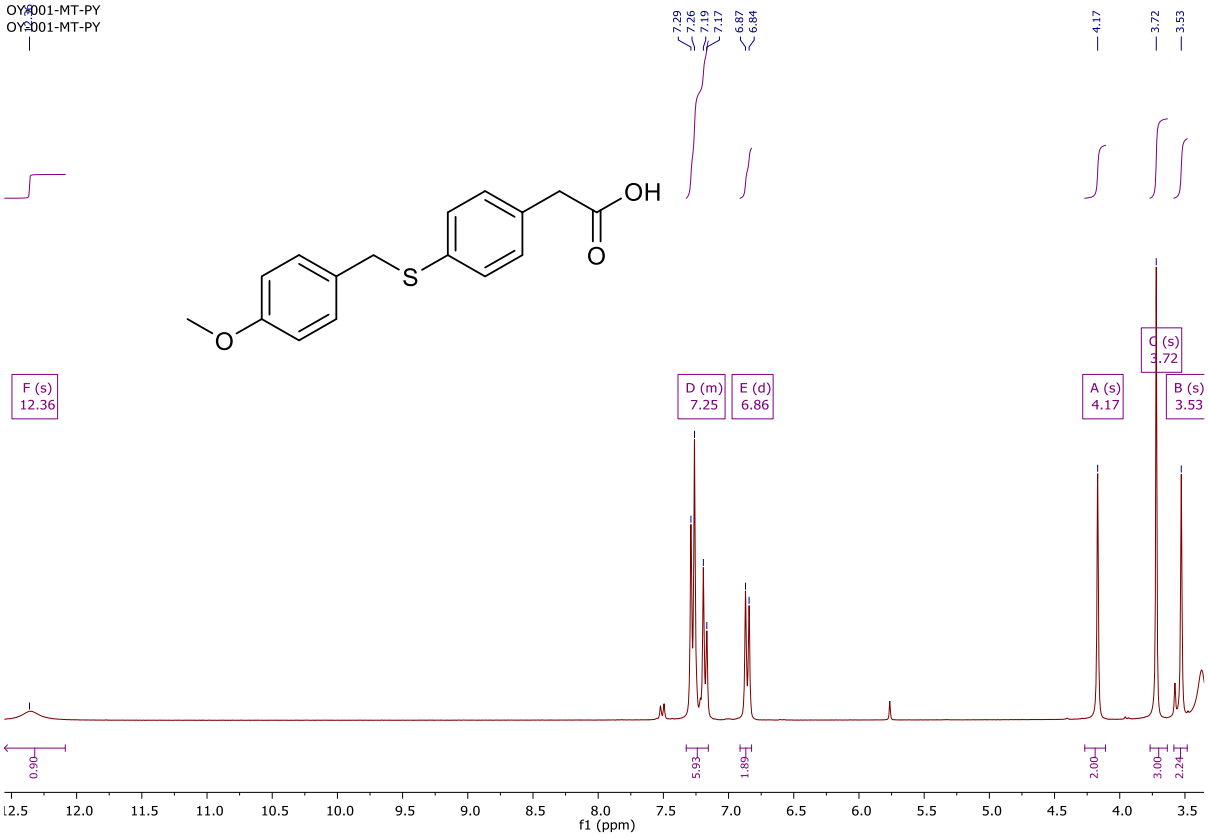

Figure 2.18: ^{1}H NMR Spectrum of **2.10d** (400 MHz, $CDCl_3$)

The reaction conditions as displayed in Scheme 2.10 were followed for the subsequent reactions. Therefore, acetic acid derivatives **2.10a-d** were transformed to their corresponding ketones **2.11a-d** by treatment with acetic anhydride **2.2**, Scheme 2.8 and 1-methylimidazole.

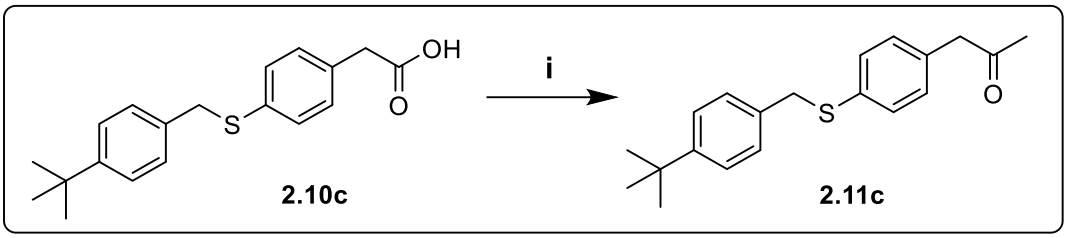

Scheme 2.10: Synthesis of 1-(4-(4-*tert*-butylbenzylthio)phenyl)propan-2-one, **2.11c.** Reagents and conditions: (i) Ac_2O, 1-Methylimidazole, rt, N_2, 15 h.

The ^1H NMR spectrum confirmed the product with the disappearance of the OH group of the acetic acids, **2.10a-d** and appearance of methyl group of the ketones **2.11a-d** which resonated upfield as 3H singlet at 2.17 ppm as seen in compound **2.11c**, Figure 2.19.

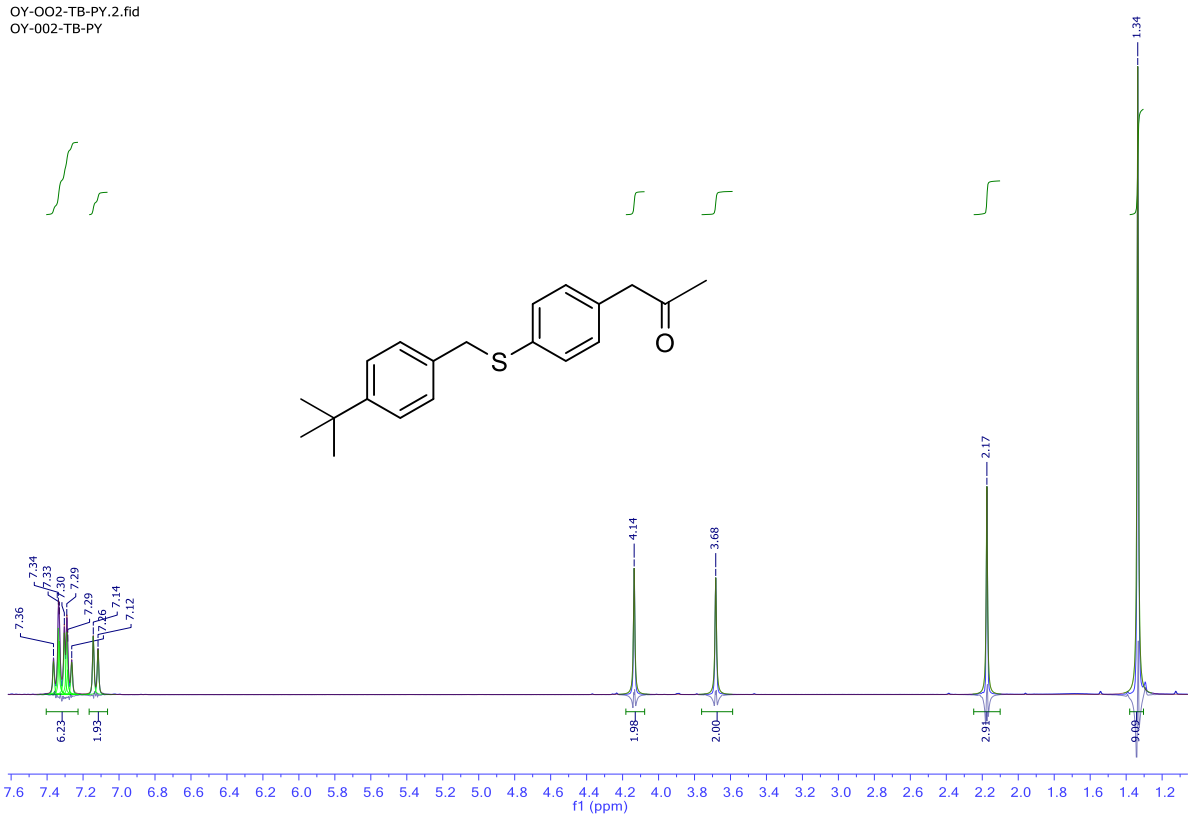

Figure 2.19: ^1H NMR of **2.11c** (300 MHz, $CDCl_3$).

In the following step, only two ketones, **2.11a-b,** were successfully cyclized under acidic conditions to afford the 4(1*H*)-pyranones, **2.12a-b,** Scheme 2.11. The ^{1}H NMR spectrum of **2.11a** also confirmed the formation of the product showing all the characteristic peaks associated with it, Figure 2.20. The conversion of compounds **2.11c** and **2.11d** to their corresponding 4-pyrone derivatives **2.12c** and **2.12d**, was unsuccessful. This observed trend could be due to the electronic profiles of the -C(CH_3)$_3$ and -OCH_3 substituents since their presence led to a lack of reactivity. Both substituents are electron donating groups, however -C(CH_3)$_3$ exert its effect *via* an inductive effect, whilst the -OCH_3 may mesomerically donates its electrons. Although the mesomeric effect is stronger in this case, both of these groups have an overall unfavourable outcome, which may result from the destabilization of intermediates formed during the reaction mechanism.

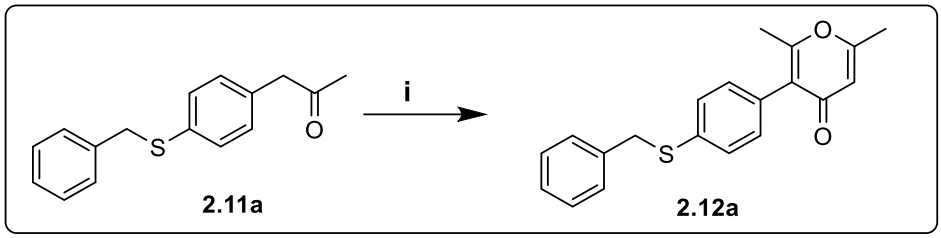

Scheme 2.11: Synthesis of 4(1*H*)pyranone derivatives. Reagents and conditions: (i) Eaton's reagent, 95 ^{o}C, 2 h.

^{1}H NMR spectroscopy confirmed formation of compound **2.12a** by showing a noticeable appearance of an additional singlet assigned to one of the two CH_3 groups on the 4(1*H*)-pyranone ring at δ_H 2.30 ppm. The other singlet which resonated at δ_H 2.19 ppm was ascribed to the second CH_3 group. The CH_3 group at position 6 appeared more downfield due to the deshielding effect exerted by the O atom at position 1, the double bonds at position 6 and the phenyl group at position 5 as seen in Figure 2.21.

Figure 2.20: ^{1}H NMR of **2.11a** (300 MHz, $CDCl_3$)

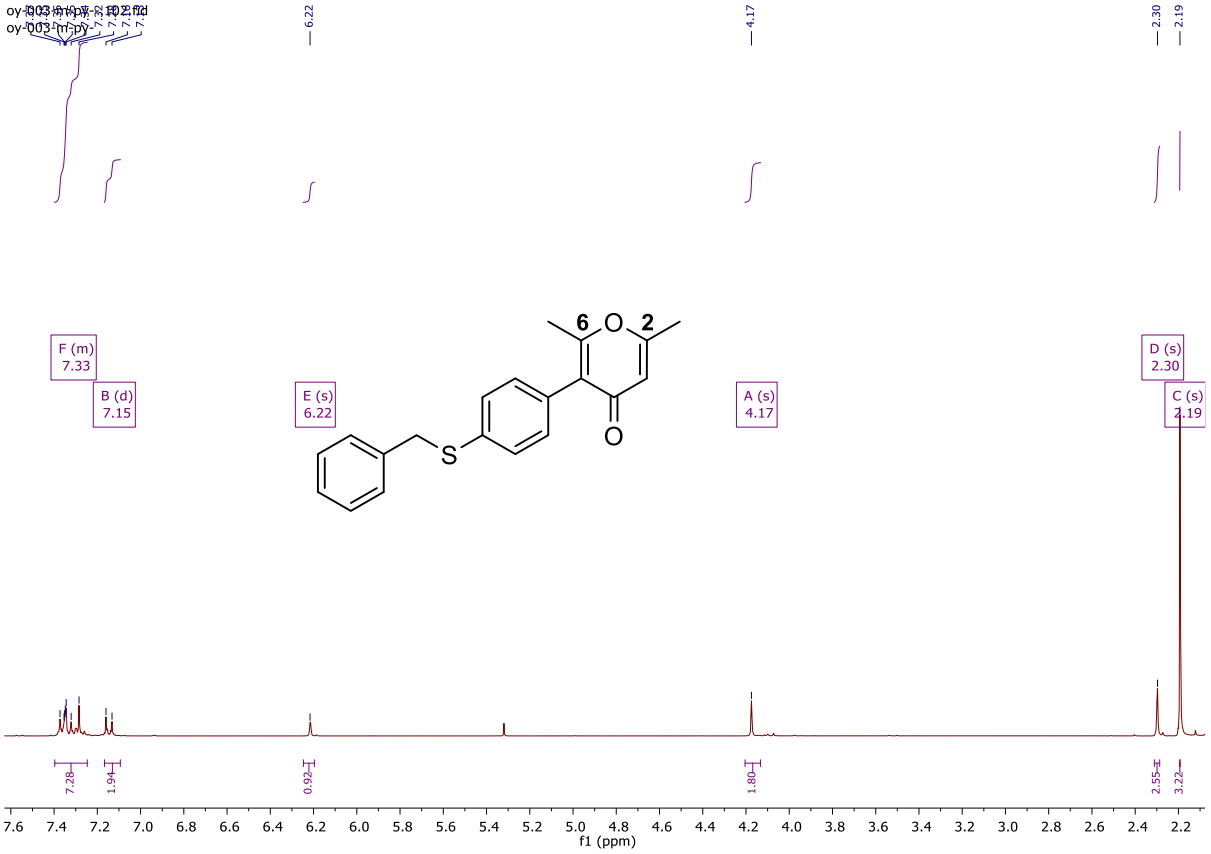

Figure 2.21: ^{1}H NMR Spectrum of **2.12a** (300 MHz, $CDCl_3$)

2.12.2 Description of the Crystal Structure of Compound 2.12b

Furthermore, the structure of compound **2.12b** was unambiguously assigned based on the crystal structure as seen in Figure 2.22, which crystallized as a brown crystal. The Ortep representation of the structure of **2.12b**, indicating atom numbering scheme, is shown in Figure 2.21, and the selected bond length and bond angles are given in Table 2.1. The complex crystallizes in a triclinic space group P-1 in which the Sulphur (II) ion is linearly coordinated to two Carbon (C) atoms of 1-chloro-4-methylbenzene and 2,6-dimethyl-3-phenyl-4*H*-pyran-4-one respectively. The 3-(4-((4-chlorobenzyl)thiophenyl)-2,6-dimetyl-4*H*-pyran-4-one compound was formed by the reaction between 1-(4-(4-chlorobenzylthio)phenyl) propan-2-one **2.11b** and Eaton's reagent **2.2**, Figure 2.22.

Table 2.1. Crystal data and structure refinement for **2.12b**

Empirical formula	$C_2H_{17}ClO_2S$
Formula weight	358.0794
Temperature/K	293.0
Crystal system	triclinic
Space group	P-1
a/Å	8.0458(8)
b/Å	10.1481(1)
c/Å	11.4805(1)
α/°	73.584(3)
β/°	73.767(3)
γ/°	87.535(3)
Volume/Å3	862.659
Z	4

Table 2.2 Selected bond length (Å) and angles (°) for compound **2.12b**

Bond Lengths (Å)		**Bond Angles (°)**	
S1- C7	1.744(2)	C7-S1-C8	104.54(7)
S1-C8	1.820(2)	C15-O2-C17	119.7(1)
O1-C20	1.234(2)		
O2-C15	1.371(2)		
O2-C17	1.362(2)		

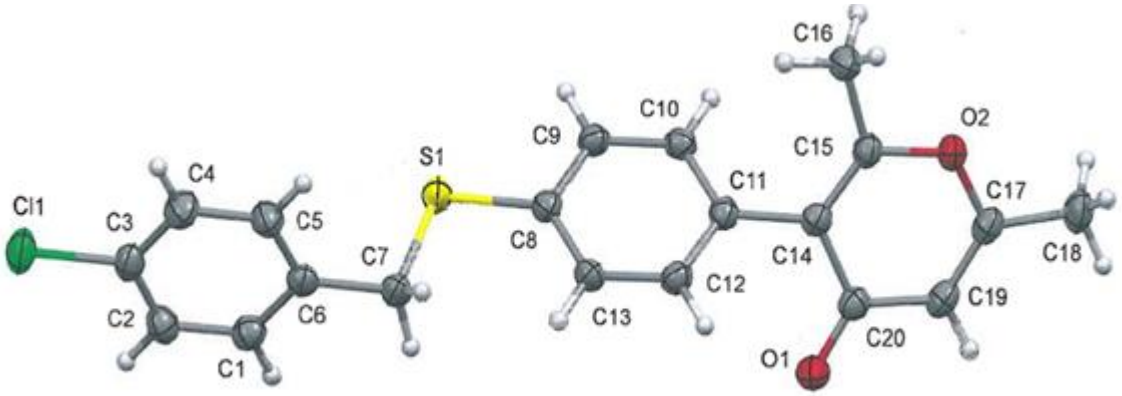

Figure 2.22: Molecular Structure of Compound **2.12b.**

Compounds **2.12a and 2.12b** were in turn, converted to 4(1*H*)-pyridones **2.9a, b** under reflux using ethanol as solvent in the presence of NH_4OH, Scheme 2.12.

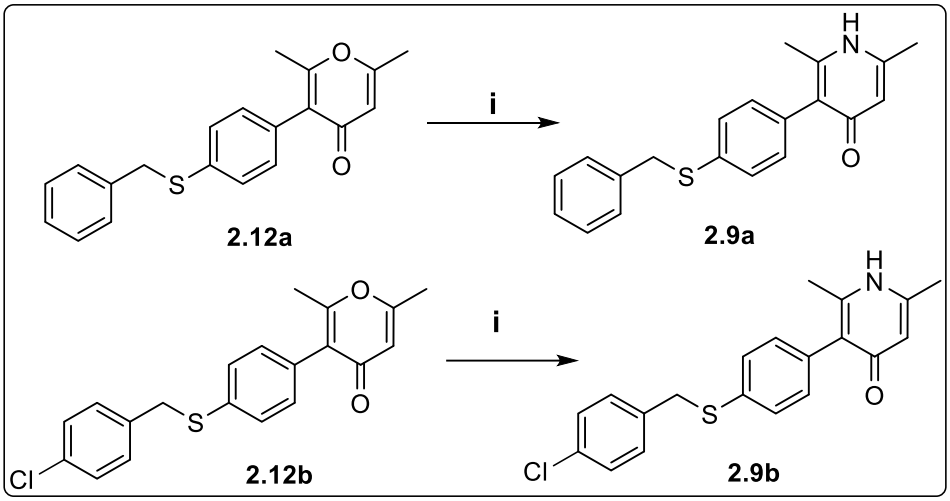

Scheme 2.12: Synthesis of target compound **2.9a** and **2.9b**. Reagents and conditions: (i) NH_4OH, EtOH, 150 ^oC, 50 h.

Compound **2.9a** was used as the representative in analysis of spectra study for the target structural validation of 4(1*H*)-pyridone molecules. Therefore, in the infrared spectrum of **2.9a,** Figure 2.23, the absorption band of NH, C=O were seen at 3288 cm^{-1} and 1708 cm^{-1} stretching vibrational frequency while the CH aliphatic of the dimethyl group appeared at 2850 cm^{-1} and

2918 cm^{-1} respectively. Also, absorption band of C=C of the 4(1*H*)-pyridone was found at 1618 cm^{-1}. This was in agreement with earlier assignment in a previous study.[94]

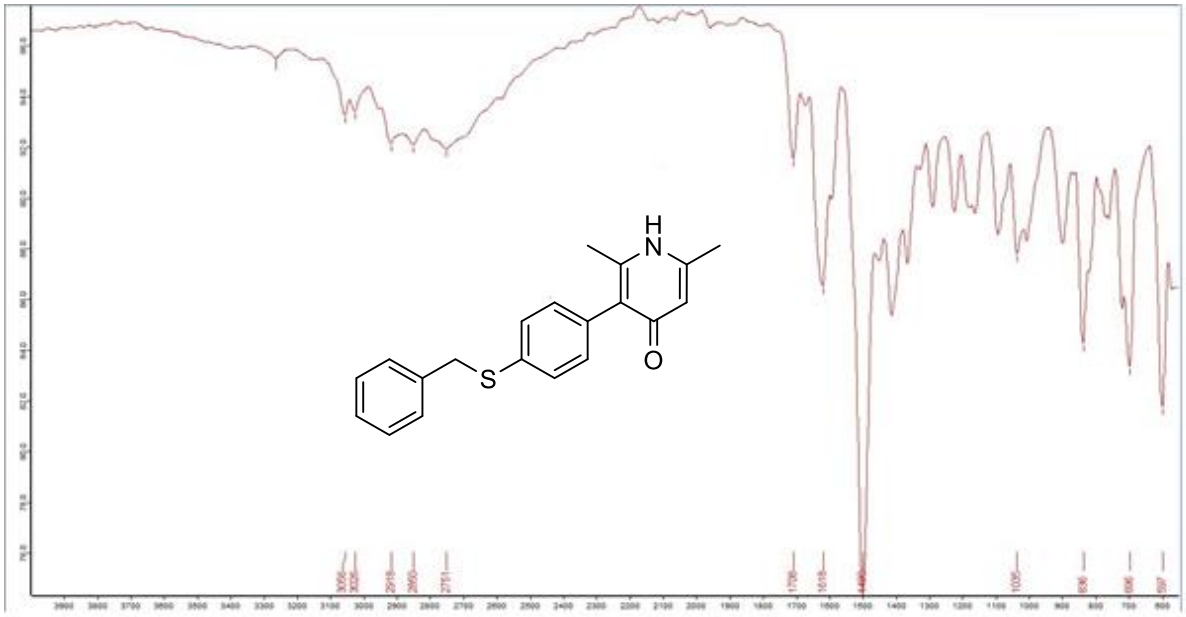

Figure 2.23: IR of compound **2.9a**

Furthermore, the chemical shift and multiplicity patterns are in alignment with the anticipated structures. The ^{1}H NMR of **2.9a** was recorded in DMSO-d_6 and displayed a singlet conforming to N–H resonance at 11.13 ppm downfield of TMS scale, and this is in agreement with an earlier reported literature with a different scaffold but with a similar functional group.[73] However, when **2.9a** was run in CD_3OD, N-H peaks disappeared completely due to exchange of the labile N-H with the deuterium of the CD_3OD solvent, Figure 2.17. The multiplet at 7.11 - 7.39 ppm confirmed the presence of nine aromatic protons. A low intense H peak at 6.30 ppm observed as a singlet, confirmed the presence of the vinylic proton at position 3 of 4(1*H*)-pyridone ring. As seen in Figure 2.24, a singlet at 4.19 ppm integrating for two methylene protons confirmed the presence of the CH_2S linker in the proposed structure, which is consistent with previously reported data, with a comparable functionality but a distinct moiety[95]. The presence of six alkyl protons of the two -CH_3 substituents attached to the 4(1*H*)-

pyridone ring on positions 2 and 6 was confirmed with the appearance of sharp, intense singlets seen at 2.05 and 2.20 ppm respectively. The ^{13}C NMR of **2.9a** displayed twenty carbon atoms with C=O having the highest signal at 178.73 ppm while $–CH_2$ linker carbon atom was seen at 37.98 ppm. The two $–CH_3$ carbon atoms signals appeared at 16.72 ppm and 17.38 ppm, upfield of the TMS scale. Finally, the remaining 16 carbon atoms are the sp^2 hybridized carbon atoms with signals ranging from 78.08 -147.80 ppm. The mass spectroscopic data of **2.9a** revealed the molecular ion peak at m/z (m+1) 322 which is in correlation with the molecular mass of compound **2.9a** ($C_{20}H_{19}NOS$).

Figure 2.24: ^1H NMR Spectrum of Target Compound **2.9a** (400 MHz, CD_3OD-d_4)

2.13 Modified Synthesis of Target Molecules 2.27-2.31 via Suzuki Miyaura Coupling Reaction

2.13.1 Suzuki Miyaura Coupling Reaction

The well-studied Suzuki Miyaura coupling reaction is used to create carbon-carbon bonds to produce conjugated systems of alkenes, styrenes, or biaryl compounds, and primarily involves the use of metal catalysts, such as Pd metal.[96] Boronic acids are used as reagents in this type of reactions due to their versatile transformations in organic synthesis.[97] They are organoborons with three valence electrons, made up of a carbon-based substituent and two hydroxyl groups.[98] The Coupling reaction occurs in the presence of a metallic catalyst and a base, between an aryl, or alkene or boronic acid or its ester and aryl, alkenyl and alkynyl halide or triflate yielding linked alkenes, styrenes, or biaryl compounds, Scheme 2.13.[91]

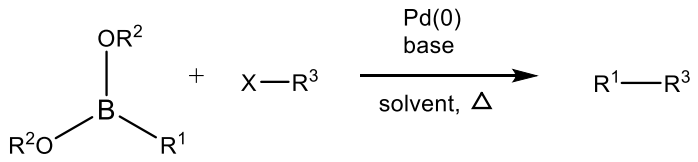

R1 = aryl, alkene (vinyl), alkyne **R2** = H (boronic acid), alkyl (boronic ester) **R3** = aryl, alkene (vinyl), alkyne
X = halide (I, Br, Cl*) triflate ($^{-}$OTf) *Cl requires special conditions for activation

Scheme 2.13: General reaction scheme of Suzuki cross-coupling reaction

2.13.2 Impact of Cross-Coupling Reaction in Drug Discovery

In identifying potential drug candidates, cross coupling reactions have shown to be of significant value in the process of drug development and discovery.[99] Cross-coupling reactions are a versatile, cost -effective and reliable approach and enable rapid expansion of structure-activity relationships (SAR) to give rise to new libraries of promising drug candidates, a strategy which is not feasible *via* the multi-step synthetic pathways.[100,101] Cross-coupling

reactions have been found useful in the parallel synthesis of drug-like and drug fragment-like compounds.[102]

2.13.2.1 Synthetic Applications of Suzuki Miyaura Coupling Reaction in Drug Discovery

This section highlights the impactful applications of cross-coupling reactions in medicinal chemistry with a few recent examples in the field, with emphasis on the Suzuki–Miyaura. One of the most renowned and prescribed medications, losartan, an angiotensin II receptor antagonist, was synthesized *via* cross-coupling reaction to afford this product at an excellent yield (93%), Scheme 2.14.[100]-[103]

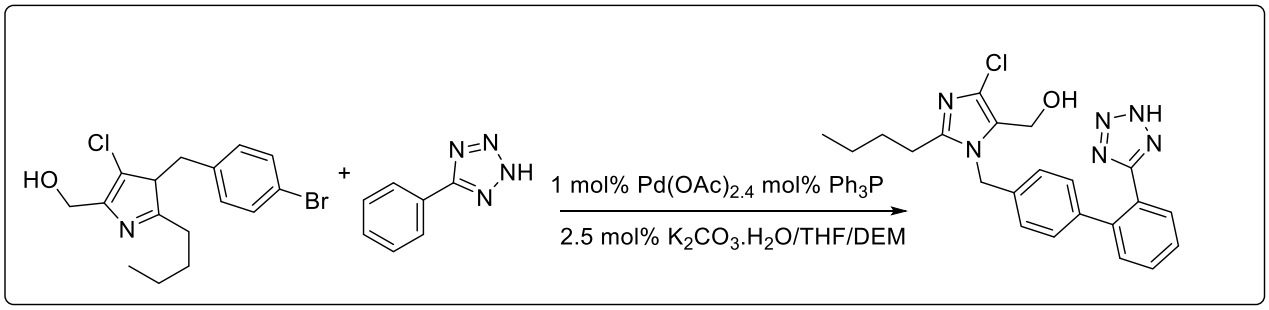

Scheme 2.14: Synthesis of Losartan through cross coupling reaction

An antidepressant medication was also synthesized by GlaxoSmithKline using biaryl Suzuki coupling reaction with the aid of cost-effective palladized charcoal (Pd/C) to give a good yield (64%), (Scheme 2.15).[104]

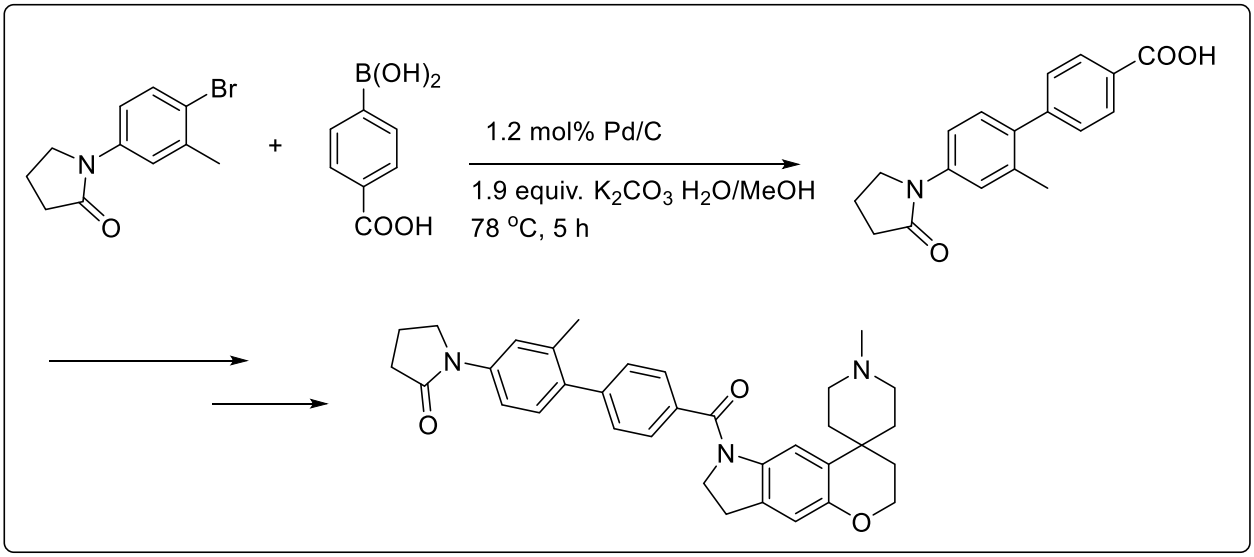

Scheme 2.15: Synthesis of GSK, SB-245570 through biaryl Suzuki coupling reaction

The Suzuki Miyaura Coupling reaction has been extensively used in the total synthesis of natural products such as Camptothecin.[105] Camptothecin was synthesized from readily available fused pyridine, which was coupled to bis(pinacolato)diboron in the presence of a palladium catalyst and potassium acetate to form a boronic ester. The boronated product was further coupled to an arylhalide in the presence of a palladium catalyst, dimethoxyethane and sodium carbonate to form an aldehyde product in an excellent yield (94%). Camptothecin, was subsequently formed after several synthetic steps of the reaction, Scheme 2.16.[106]

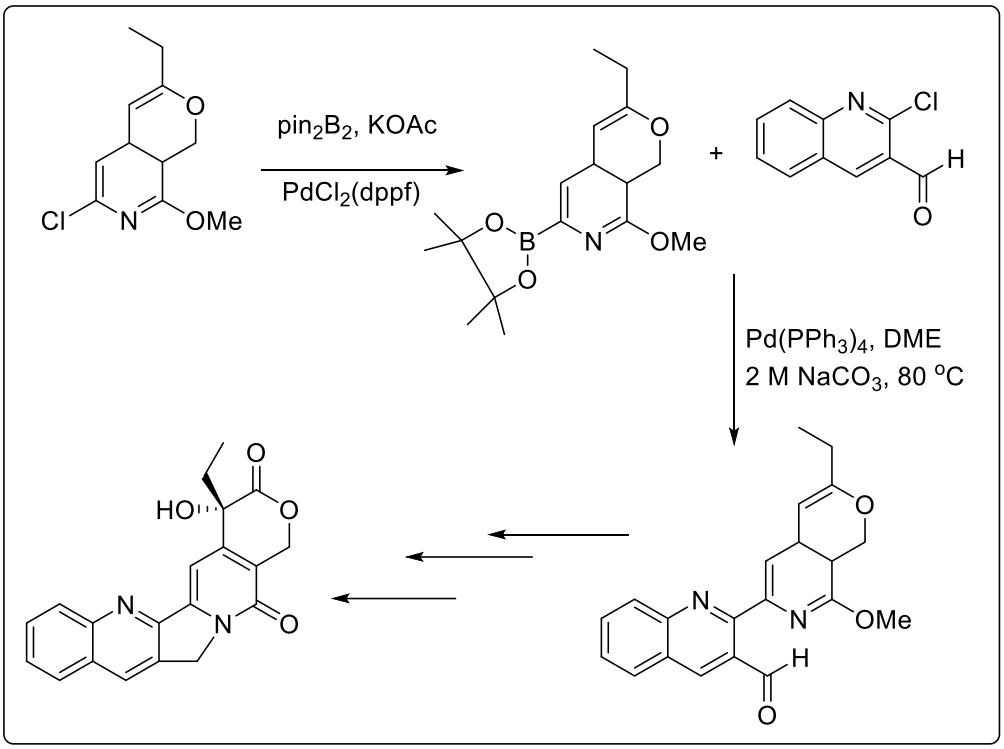

Scheme 2.16: Total synthesis of Camptothecin, by the means of the Suzuki-Miyaura Coupling reaction

2.13.3 Synthesis of Target Molecules 2.27-2.31

In an attempt to optimize the overall yield and to simplify the methodology towards the synthesis of our previously designed (3-(4-(4-subtituted-benzylthio)phenyl)-2,6-dimethyl pyridin-4(1*H*)-one) **2.9a**, Scheme 2.8, we devised a modified design which led to the extension of the library by an additional five (5) compounds **2.27-2.31**, Scheme 2.17. Various 2-substituted-phenylboronic acids **2.17-2.20** underwent a Suzuki-Miyaura coupling reaction in the presence of $PdCl_2(PPh_3)_2$ (10 mol%), and K_2CO_3 to afford the intermediate products **2.22-2.26** in low to excellent yields (39 – 75%), Scheme 2.17.

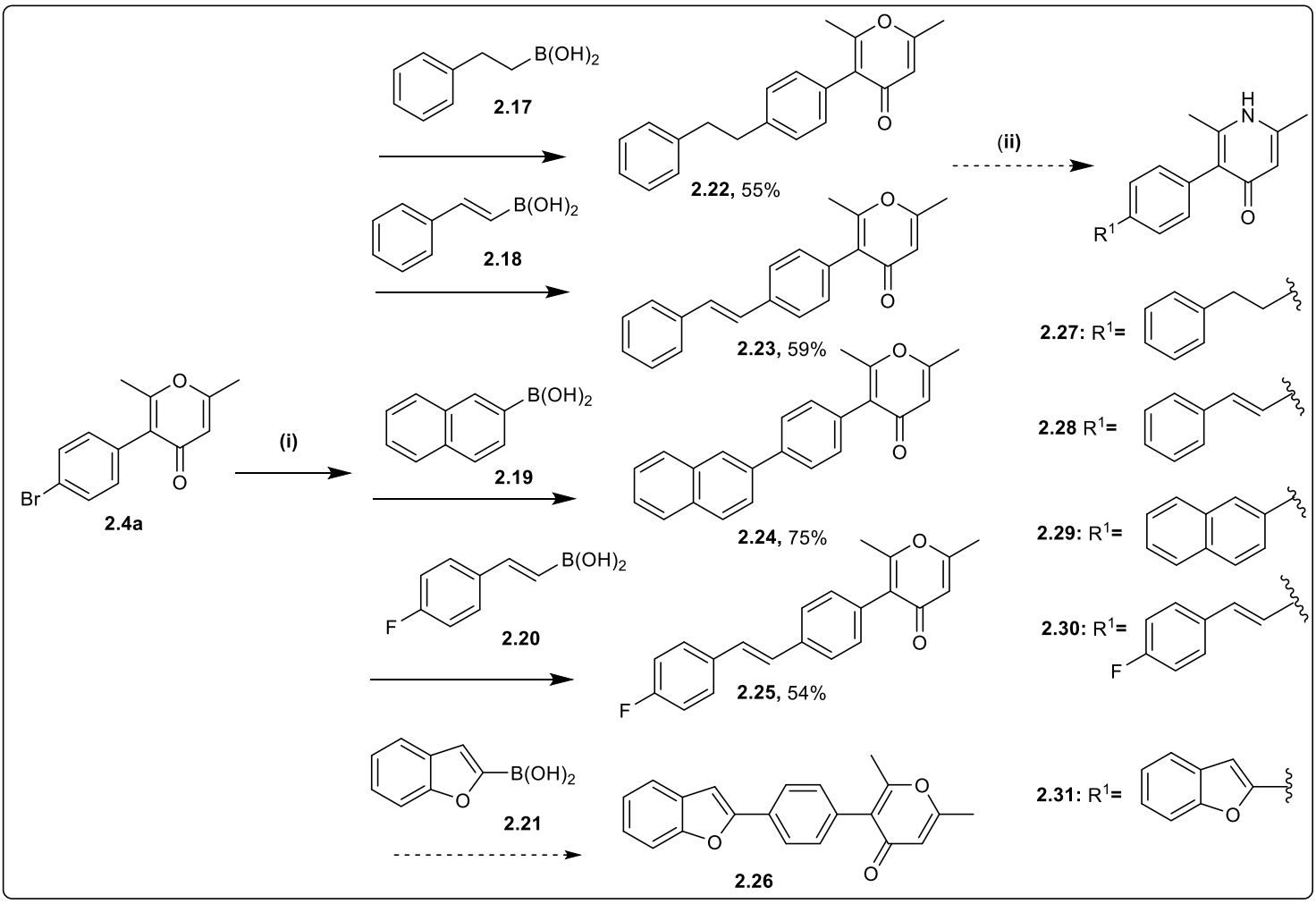

Scheme 2.17: Synthesis of intermediates products **2.22-2.26**- *via* Boronic Acids **2.17-2.21**. Reagents and conditions: (i) $PdCl_2(PPh_3)_2$, K_2CO_3, distilled H_2O, 80 ^oC, 3 h; (ii) NH_4OH, EtOH, 150 ^oC, 50 h.

The precursor 3-(4-bromophenyl)-2,6-dimethyl-4*H*-pyran-4-one) **2.4a** Scheme 2.17, was prepared by using a well-established procedure.[73,74] Several attempts were made to synthesize the desired target 4(1*H*)-pyridone derivatives **2.27-2.31**, but the reactions were all unsuccessful. In the intermediate series, **2.23-2.26**, compound **2.23** was used as a representative in the spectroscopic studies. The ^1H NMR analysis of this compound displayed a total of 18 protons,

revealing the following key signals; nine aromatic protons which appeared as multiplets between 7.62-7.20 ppm; two alkene (H-C=C-H) protons which appeared as a singlet at 7.16 ppm. A singlet proton of a vinyl of the 4*H*-pyran-4-one ring was also observed downfield at 6.26 ppm, while the remaining two $–CH_3$ protons at the position 2 and 6 of the 4H-pyran-4-one ring were observed downfield TMS at 2.3 and 2.2 ppm, respectively Figure 2.25. The result of the ^{13}C NMR of 2.23 presented twenty-one carbon atoms with 15 peaks, with the δ_C value ranging from 178.5 ppm to 18.7 ppm. A carbonyl carbon on the position 4 of the 4H-pyran-4-one is seen at 178.5 ppm while other twelve carbon atoms are aromatic carbons, displayed around 164.8 ppm to 113.8 ppm and the remaining two carbon atoms are ascribed to two $–CH_3$ groups at the position 2 and 6 of the 4*H*-pyran-4-one ring, seen at 18.7 and 19.8 ppm respectively.

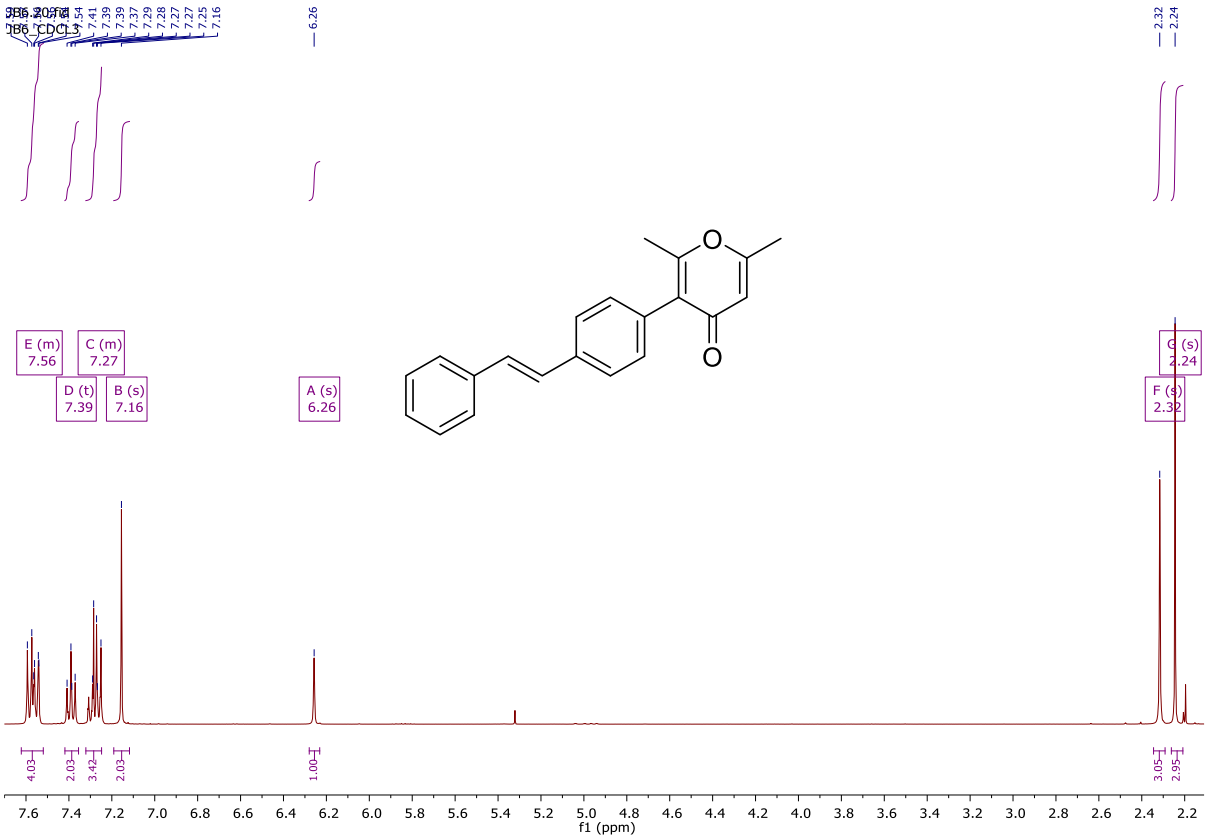

Figure 2.25: ^1H NMR Spectrum of **2.23** (400 MHz, $CDCl_3$)).

2.13.4 The Mechanism of the Miyaura Suzuki Coupling Reaction

The mechanism involves the oxidative additive of the aryl bromide **2.4a** to the palladium catalyst to give **II**. The transmetalation reaction step leads to the formation of organoboron compound $ArB(OH)_2$ in the presence of a base K_2CO_3. The final step involves a reductive elimination to give the **2.22** and to regenerate the palladium catalyst [77], Figure 2.26.

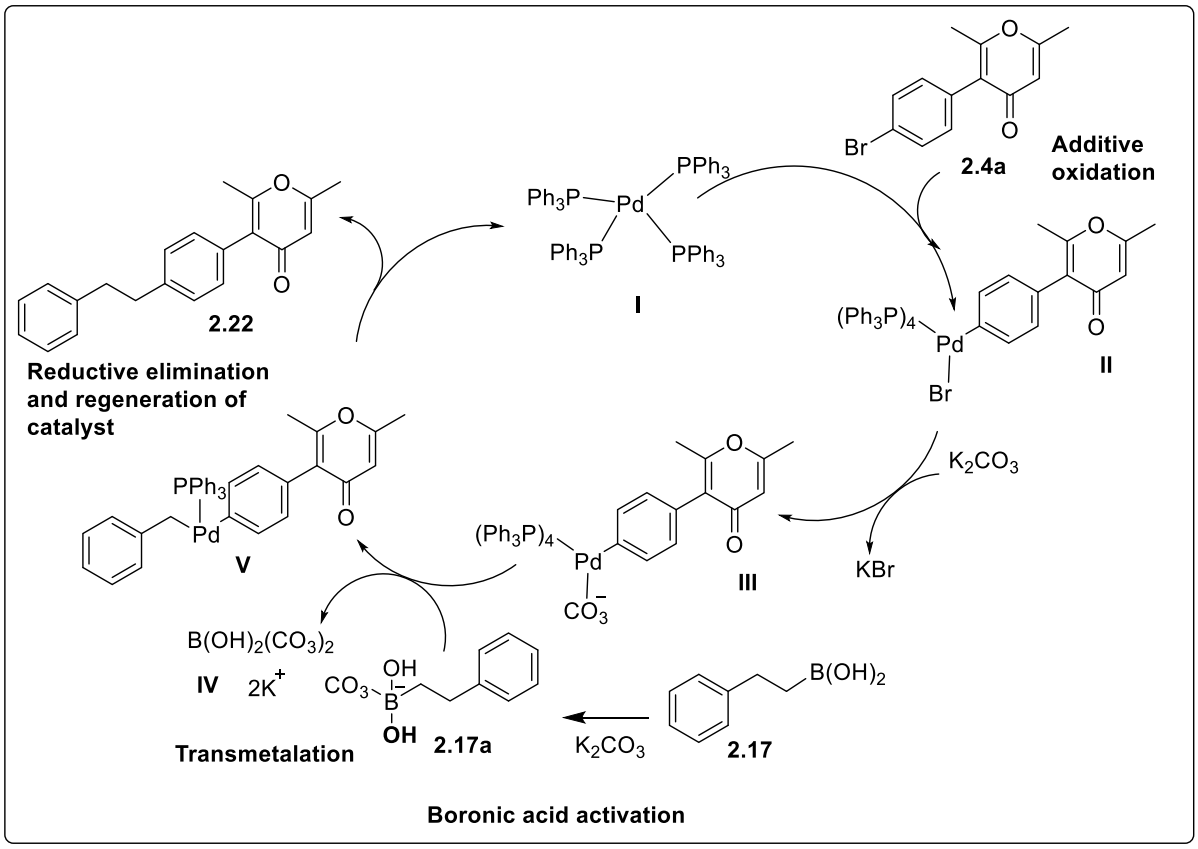

Figure 2.26: Catalytic cycle for Suzuki-Miyaura cross-coupling illustrating the formation of **2.21**.[88,99,100,107]

2.13.5 Alternative synthesis of target compound 2.16

As a result of limited commercial availability of specific alkylated boronic acids in our laboratory and prompted by the failed formation of target compounds **2.27-2.31**, through the use of 2-substituted phenylboronic acids **2.17-2.20**, Scheme 2.17, we opted to synthesize one of the desired target compounds, compound **2.16** *via* the styrylphenylboronic acid pinacol ester **2.14**, Scheme 2.18. In this method, the styrylphenylboronic acid pinacol ester **2.14** was synthesized in a moderate yield (62%) from 1-bromo-4-phenethylbenzene in the presence 10% mol of $PdCl_2$(dppf) and potassium acetate. Further heating of compound **2.14** with the catalyst, $PdCl_2(PPh_3)_2$ (10 mol%) and base, K_2CO_3 gave the compound **2.15** in a low yield of 39%. Unfortunately, this adapted route towards the synthesis of compound **2.16** has also been shown to be futile.

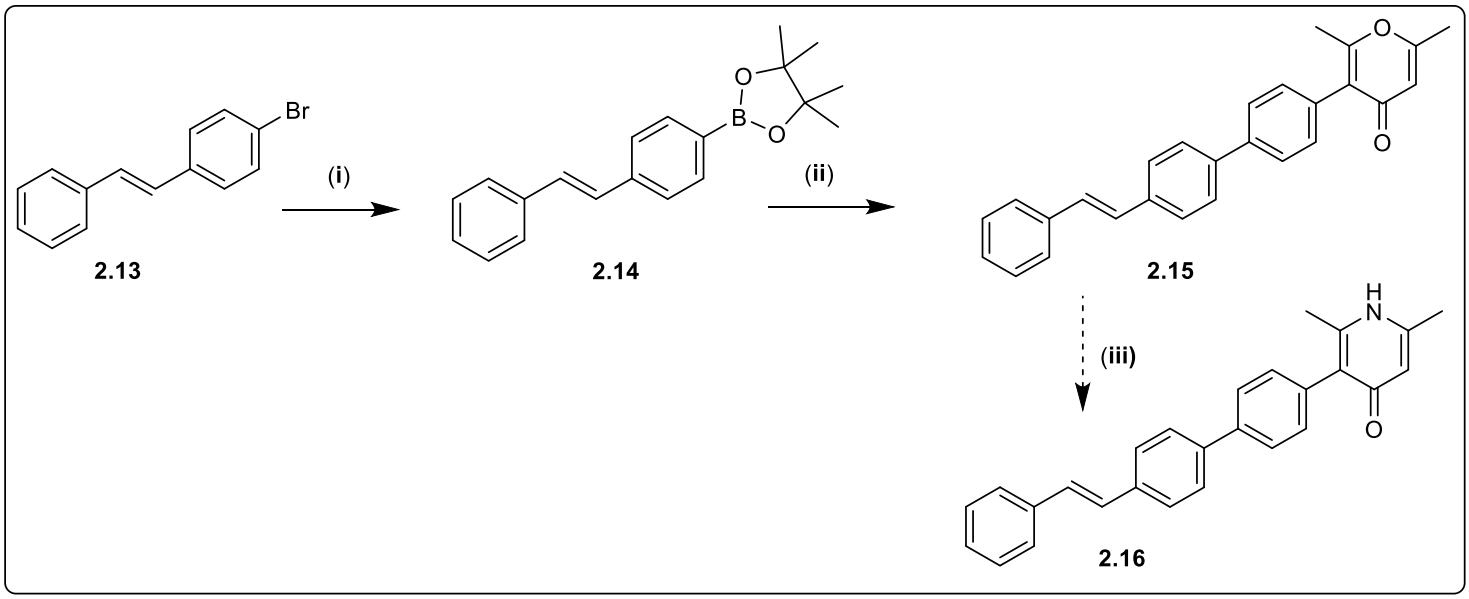

Scheme 2.18: Synthesis of target compound **2.16**, Reagents and conditions: (i) Bis(pinacolate)diboron, dry 1,4-dioxane, $PdCl_2$(dppf) (10 mol%), KOAc, 120 ^oC, 5 h; (ii) $PdCl_2(PPh_3)_2$ (10 mol%), K_2CO_3, distilled H_2O, 80°C, 3 h; (iii) NH4OH, EtOH, 150°C, 50 h

The ^{1}H NMR spectrum of **2.14** showed tetramethyl dioxaborolane at position 1 of the styrlbenzene, **2.14**, Figure 2.27. The characteristic 12 protons of the four –CH_3 groups gave a sharp, intense singlet were seen upfield at 1.28 ppm, while in the aromatic region there were 11 protons around 7.05-7.73 ppm respectively, which were attributed to 9 protons of the two benzene rings and 2 protons of the vinyl linker. Also, as Figure 2.28 seen in the ^{13}C NMR spectrum of **2.14** (Figure 2.28) there were twenty carbon atoms with seven peaks, with the δ_C value ranging from 135.2 ppm to 24.9 ppm. The two tertiary carbon atoms of the tetramethyl dioxaborolane moiety were seen as a single peak at 135.2 ppm, while the two ethylenic carbon atoms are seen as a single peak at 126.6 ppm. The other ten carbon atoms are aromatic carbons, which were displayed between 129.6 ppm and 125.8 ppm. The remaining four carbon atoms are attributed to four –CH_3 groups of the tetramethyl dioxaborolane, appearing at 24.9 ppm.

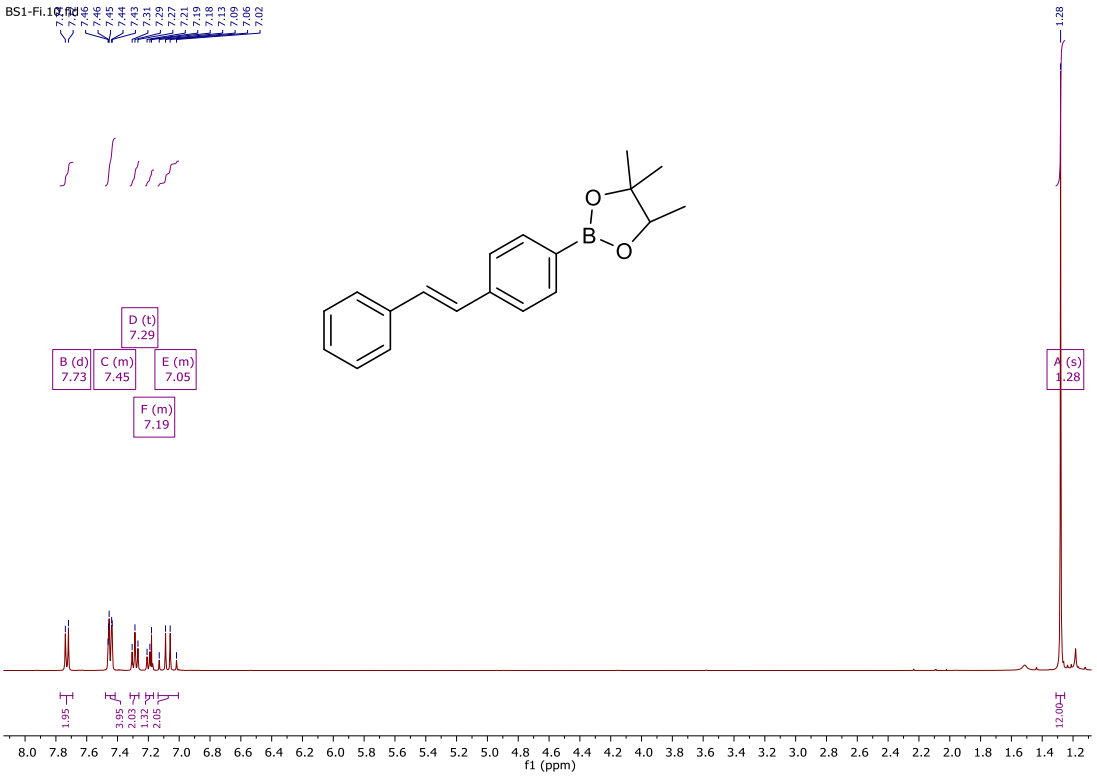

Figure 2.27: ^{1}H NMR Spectrum of **2.14** (400 MHz, $CDCl_3$)

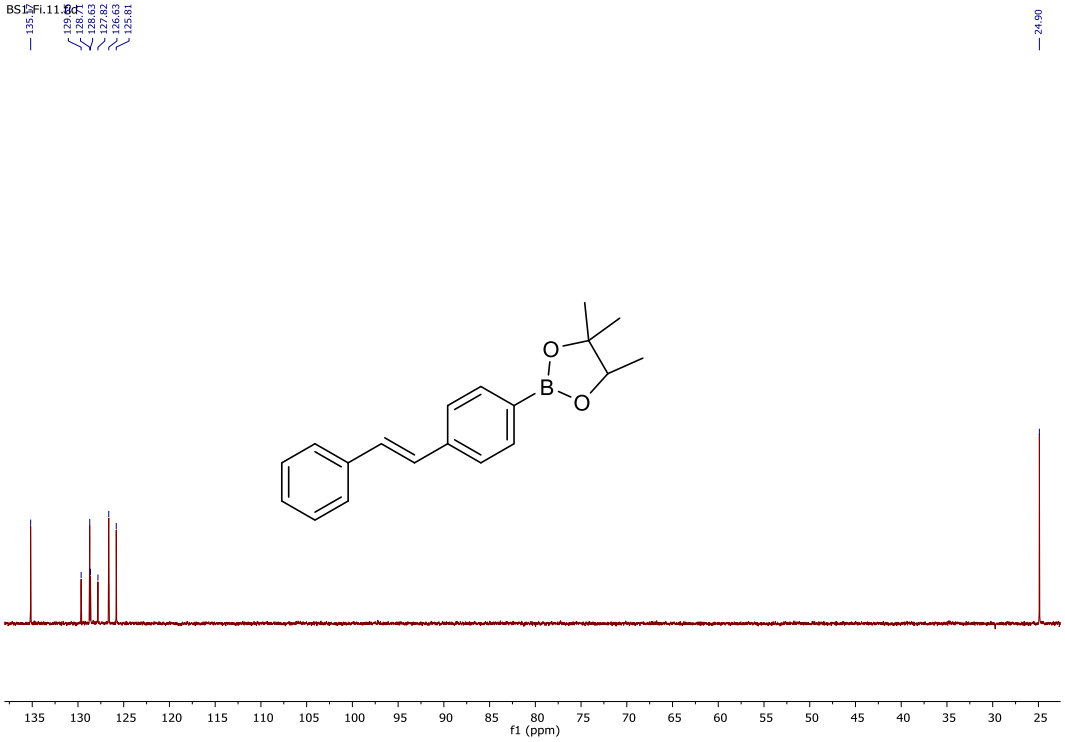

Figure 2.28: ^{13}C NMR Spectrum of **2.14** (100 MHz, $CDCl_3$)

^{1}H NMR analysis in Figure 2.29 of compound **2.15** displayed additional four aromatic proton signals, which appeared at 7.24, 7.26, 7,58, and 7.60 ppm, shifted downfield compared to compound **2.14**. The additional four aromatic protons are as a result of coupling of (*E*)-4,4,5,5-tetramethyl-2-(4-styrylphenyl)-1,3,2-dioxaborolane, **2.14**, to the 3-(4-bromophenyl)-2,6-dimethyl-4*H*-pyran-4-one **2.4a**. The result of the ^{13}C NMR spectrum of **2.15** presented twenty-seven carbon atoms with 15 peaks, with the δ_C values ranging from 186.8 ppm to 18.8 ppm. A carbonyl carbon substituent on the position 4 of the 4*H*-pyran-4-one is seen at 186.8 ppm while other twenty-one carbon atoms are aromatic carbons, displayed around 178.6 ppm to 113.8 ppm and the remaining two carbon atoms are ascribed to two $-CH_3$ groups at the position 2 and 6 of the 4*H*-pyran-4-one ring, seen at 18.8 and 19.8 ppm respectively, Figure 2.30.

Figure 2.29: ^{1}H NMR Spectrum of **2.15** (400 MHz, $CDCl_3$).

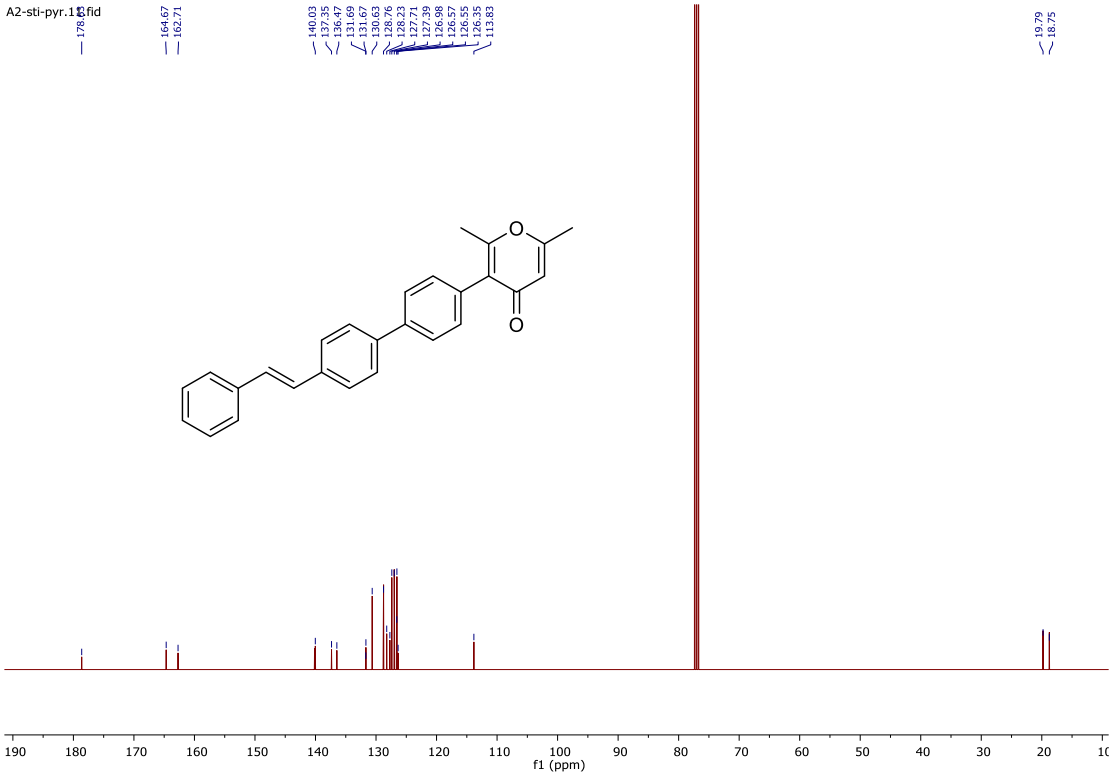

Figure 2.30: ^{13}C NMR Spectrum of **2.15** (101 MHz, $CDCl_3$).

2.13.6 An Investigation into the possible reasons for the failed formation of target compounds 2.16, 2.25-2.28

The unsuccessful synthesis of the target compounds **2.16, 2.25-2.28** could be due to the initial introduction of the electron-donating group in the substituted phenylboronic acids, **2.14, 2.17-2.21,** which led to a reduction in the reactivity of the pyrone ring. This alternatively could have also led to an unfavourable S_N2 nucleophilic substitution of amino group on position 1 of the 4(1*H*)-pyran-4-one ring. Another reason for unsuccessful reaction could be the occurrence of steric hindrance, as a result of the bulkiness of the 4(1*H*)-pyran-4-one substrate which led to an increase in the energy of the substrate that slows down the rate of reaction.[108] As a result of increased energy of the substrate and lack of reactivity displayed by the 4(1*H*)-pyran-4-ones, the thermogravimetric analysis TGA Figure 2.31 was conducted on the series of selected 4*H*-pyran-4-ones **2.4a, 2.15, 2.22,** and **2.25**. Compounds **2.15, 2.22**, and **2.25** displayed a high rate of thermal decomposition and instability even at a temperature of 37 ^{o}C, 73 ℃, and 104 $^{\circ C}$respectively, lower than the temperature (140°C)[67] at which the reaction would have taken place, using ammonium hydroxide (NH_4OH) as the reactant.[67] Compound **2.4a** (starting material to compounds **2.14, 2.17-2.21**), was relatively stable as compared to compounds **2.15, 2.22,** and **2.25,** as seen in Figure 2.31.

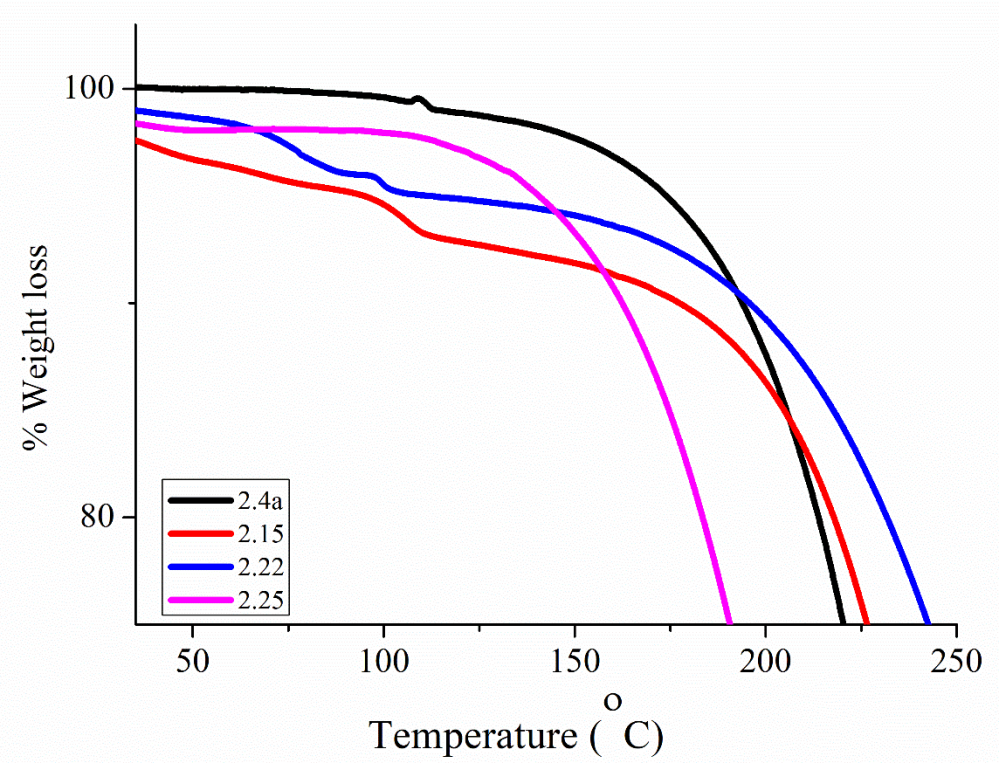

Figure 2.31: Thermogravimetric Analysis (TGA) of Selected Compounds **2.4a, 2.15, 2.22**, and **2.25**

2.14 Density Functional Theory (DFT) analysis

A Density Functional Theory (DFT) computation study was performed to gain more insight into the substituent effect(s) of boron-containing compounds on (by-)product formation, as well as the lack of reactivity of compounds **2.15, 2.22-2.25** to form **2.16, 2.27-2.31**, Scheme 2.17. In general, input structures were derived from crystallographic information files (CIFs) for the relevant compounds (or derivations thereof) and optimized in the gas phase until conversion with zero imaginary frequencies was achieved. Considering the C-C coupled compounds **2.15, 2.22-2.25**, their corresponding frontier molecular orbitals and associated properties may be analyzed to help explain the difference in-stability, as well as their lack of reactivity with NH_4OH to form the corresponding compounds **2.16, 2.27-2.31**. The highest

occupied molecular orbital (HOMO) may be visualized as providing the source of electrons in an oxidizing reaction and therefore be correlated to the ionization potential of the compound. In contrast, the lowest unoccupied molecular orbital (LUMO), may in turn be visualized as the electron sink in a reduction reaction and hence be correlated to the electron affinity of the compound. The HOMOs and LUMOs of compounds **2.15** and corresponding **2.16** (theoretical), as well as **2.23** and corresponding **2.28** (theoretical) were chosen as representative examples and are depicted in Figure 2.32. In general, the HOMOs of compounds **2.15, 2.22-2.26** are primarily distributed over the biphenyl group (at the site where C-C coupling took place). Electron diffusion *via* resonance is inhibited in the case of aliphatic linkers (e.g., **2.22**), but electron diffusion to include the remaining arene groups is present in case of unsaturated linkers (e.g., **2.23**). The LUMOs of both examples are comparable with one another, with the LUMOs being delocalized mainly over the biphenyl groups as well as the pyranone ring structure Figure 2.32. The nucleophilic attack of the ammonia molecule on a partially electron-poor carbon atom adjacent to the oxygen atom is accepted as the first step towards the formation of pyridone, as part of the general Baeyer pyridine synthesis mechanism Scheme 2.19.[109] In this case, electron transfer between both the ether-like oxygen (in the pyranone ring) and the carbonyl oxygen is vital for the formation of an anionic oxygen intermediate specie in the pyranone ring moiety Scheme 2.19. In general, the LUMO of the reactant and the HOMO of the corresponding product molecule should be correlated so that electron transfer can be observed. Collectively, the reactivity (reduction/oxidation) of the compounds **2.15, 2.22-2.26** is suggested to lie within the biphenyl moiety and only slightly populated within the pyrone ring system (containing the oxygen-containing functional groups) where electron transfer is expected. It is thus interesting to note that the corresponding HOMO of the product molecules (compounds **2.16, 2.27-2.31**) is only slightly populated on either of the two oxygen atoms

which may also indicate the molecule's lack of reactivity towards the ammonium cation. This observation remains unchanged when the implicit solvent model (EtOH) is included in an attempt to more closely mimic the reaction conditions. For example, after fully optimizing compound **2.15** (including the implicit solvent model of EtOH), the HOMO and LUMO is practically identical to 2.15 (gas phase optimized), Figure 2.32.

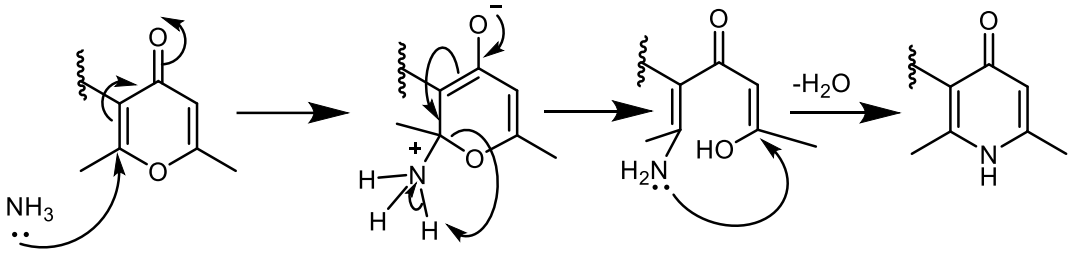

Scheme 2.19: Conjugate addition mechanism for the conversion of 4-pyrone to 4-pyridone

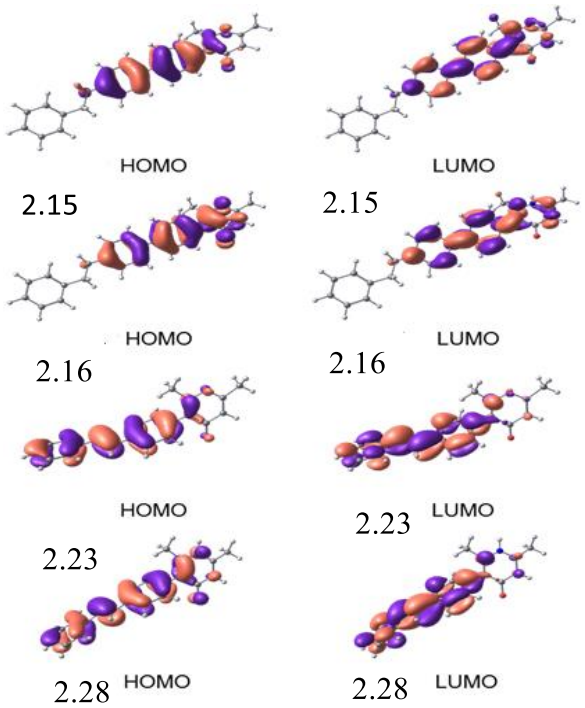

Figure 2.32: B3LYP functional DFT calculated HOMOs and LUMOs of the indicated neutral compounds from this study. A contour of 0.03 e/Å3 was used for the MO plots.

Each compound's energy gap (ΔE, energy difference between the HOMO and LUMO) may directly be compared to provide information on its respective molecular reactivity and stability. As a result, a molecule with a small energy gap is thought to be more polarizable, softer, more reactive, and kinetically less stable. Table 2.3 shows the energy gap (ΔE), ionization potential (I), electron affinity (A), electronegativity (χ), chemical potential (μ), chemical hardness (η), chemical softness (S), and electrophilicity index (ω) of compounds **2.14, 2.17-2.21and 2.16, 2.27-2.31**. It is clear from the data that the energy gap of the pyranone-based compounds (**2.15, 2.22-2.26**) is generally slightly larger than the energy gap of the corresponding pyridone compounds (**2.16, 2.27-2.31**), implying higher stability and thus lowered reactivity. Incorporating the solvent effect (EtOH as an implicit solvent model) further increases both ΔE and the ionization potential slightly by ca. 0.02 and 0.1 eV, respectively, suggesting lower reactivity when compared to the corresponding isolated molecule in the gas state. Comparing the effect of the functional groups in **2.14, 2.17-2.21**, the energy gap varies between 3.91 and 5.17 eV, where the C_2H_2-linked (ethene bridge) functional groups **(2.23** and **2.26**) are the least stable (3.91 and 3.94 eV, respectively), and the C_2H_4-linked (ethylene bridge) functional groups (**2.15** and **2.22**) are the most stable (4.55 and 5.17 eV, respectively). This trend is also reflected in their corresponding electron affinity (A), chemical softness (S) and electrophilicity indices (ω), where compounds having the lowest electron affinity would be the compounds most likely to act as Lewis's acids in the reactions converting pyranones to pyridones. The remainder of the computed reactivity descriptors compares relatively well among the two series of compounds (**2.14, 2.17-2.21** and **2.16, 2.27-2.31**) and functional-group related compounds between the two series of compounds.

Table 2.3: Molecular parameters and reactivity descriptors of compounds **2.15, 2.22-2.26,** and **2.16, 2.27-2.31.**

Parameter	**Compound**											
	2.15	**2.22**	**2.23**	**2.24**	**2.25**	**2.26**	**2.16**	**2.27**	**2.28**	**2.29**	**2.30**	**2.31**
Energy gapa (ΔE) (eV)	4.55	5.17	3.91	4.42	3.94	4.08	4.44	5.09	3.95	4.37	3.88	4.05
Ionization potential[b] (I) (eV)	5.84	6.23	5.63	5.82	5.67	5.63	5.60	5.78	5.46	5.68	5.46	5.46
Electron affinityc (A) (eV)	1.29	1.06	1.72	1.41	1.73	1.55	1.16	0.69	1.51	1.31	1.58	1.41
Chemical potentiald (μ) (eV)	-3.56	-3.64	-3.68	-3.61	-3.70	-3.59	-3.38	-3.23	-3.49	-3.50	-3.52	-3.44
Electronegativitye (χ) (eV)	3.56	3.64	3.68	3.61	3.70	3.59	3.38	3.23	3.49	3.50	3.52	3.44
Chemical hardnessf (η) (eV)	4.55	5.17	3.91	4.42	3.94	4.08	4.44	5.09	3.95	4.37	3.88	4.05
Chemical softnessg (S) (eV)	0.22	0.19	0.26	0.23	0.25	0.25	0.23	0.20	0.25	0.23	0.26	0.25
Electrophilicity indexh (ω) (eV)	1.39	1.28	1.73	1.48	1.74	1.58	1.28	1.03	1.54	1.40	1.60	1.46

a ΔE = EHOMO - ELUMO. b I = -EHOMO. c A = -ELUMO. d μ = -(I + A)/2. e χ = -μ. f η = I - A. g S = 1/η. h ω = μ2/2η.

2.15 Molecular Modelling (Molecular Docking and Prime MM-GBSA) of Pyridones

Schrodinger Maestro was used to simulate the interaction and binding affinity of compounds **2.9a, 2.9b,** and atovaquone with the Q_o site of the C chain, Figure 2.33, of the cytochrome bc_1 complex (RSCB PDB ID: 4PD4). Figure 2.34 describes the interaction of the three docked compounds with cytochrome bc_1 complex Q_o active site. The molecular lipophilicity potential (MLP) maps for the active site of cytochrome bc1 complex Q_o are shown. The molecular surface coloration ranges from dark cyan (the most hydrophilic) to white to dark goldenrod (most lipophilic). Figure 2.34 also shows the number of hydrogen bond interactions and Van der Waals (VDW) interactions. Atovaquone formed two hydrogen bond interaction with glutamic acid 1055 whereas compound **2.9a** and **2.9b** formed one hydrogen bond interaction each with the same residue. Compound **2.9b** had 69 VDW interactions, compound **2.9a** had 84, and atovaquone had 86 VDW interactions with the cytochrome bc_1 complex Q_o active site.

The Prime MM-GBSA was used to calculate ligand binding energies and ligand strain energies for compound **2.9a**, compound **2.9b** and atovaquone in complex with C chain of the cytochrome bc1. Figure 2.34 depicts MM-GBSA_ΔGBind and its components energy.

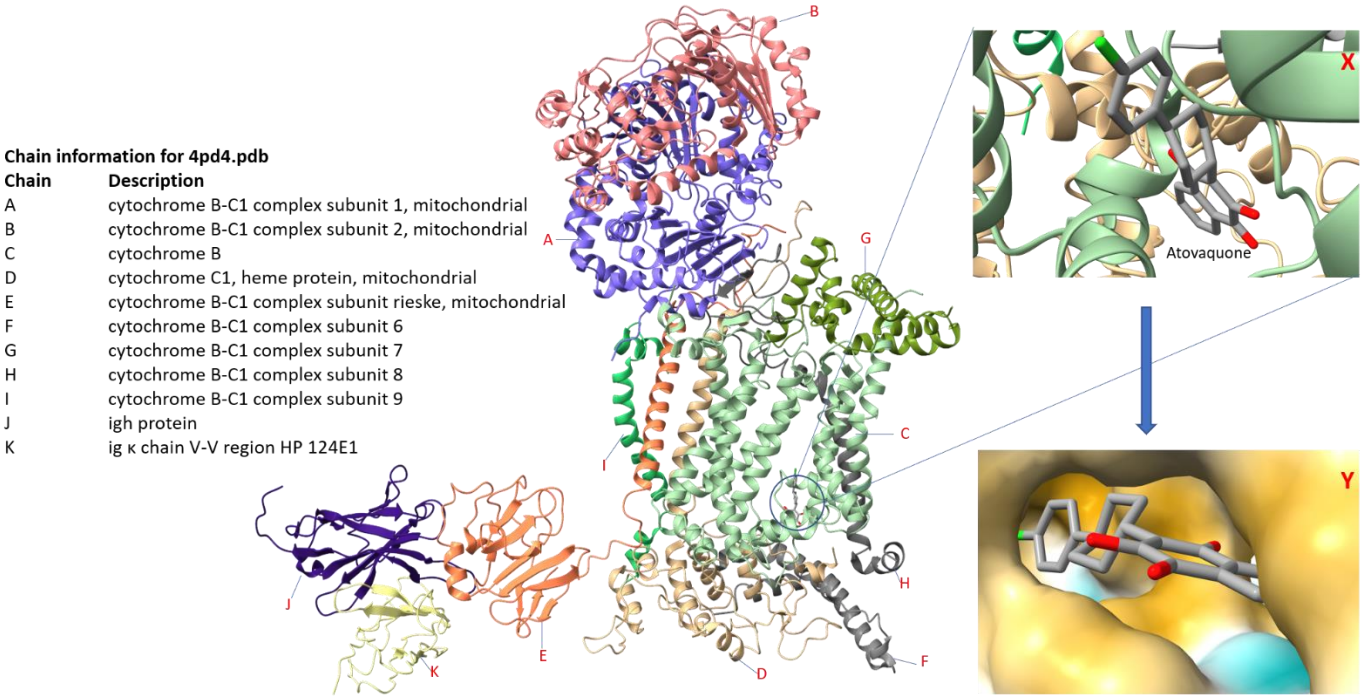

Figure 2.33: Three-dimensional crystalized structure of atovaquone-inhibited cytochrome BC1 complex.The inserted table displays the chain information for the 11 units that make up the complex. The inserted image X is a closer look at atovaquone in the Q_o site while Y shows the molecular lipophilicity potential (MLP) surface for then Q_o active site. The colouring on the molecular surface ranges from dark cyan (most hydrophilic) to white to dark goldenrod (most lipophilic). The Q_o site is essentially lipophilic except the entrance part that is hydrophilic (caused by the glycine residue in that position).

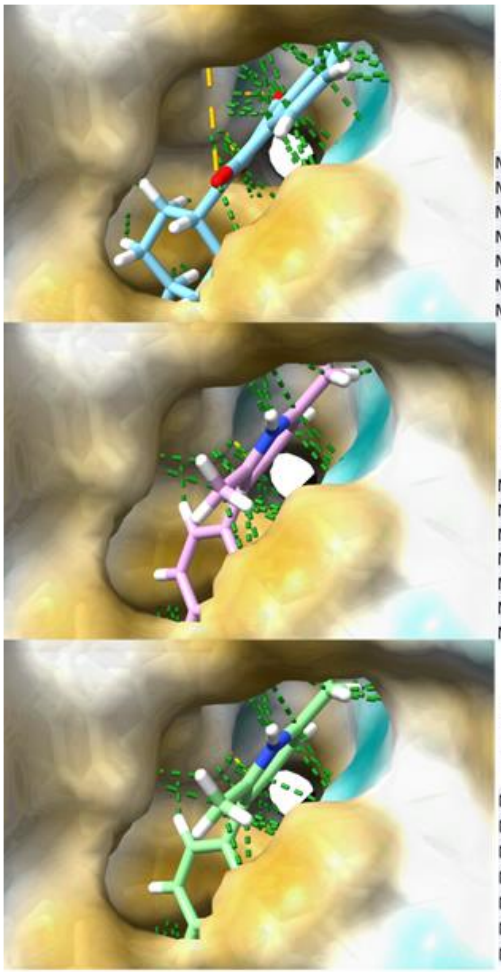

Atovaquone:

2 hydrogen bonds to Glutamic acid 1055 (Yellow dotted lines)
86 VDW contacts (Green dotted lines)
MMGBSA_ΔG_Bind: -50,34 kJ/mol

MM-GBSA energy components (kJ/mol)	Atovaquone
MMGBSA_ΔG_Bind_Coulomb	6,5715
MMGBSA_ΔG_Bind_Covalent	7,2413
MMGBSA_ΔG_Bind_Lipo	-35,7238
MMGBSA_ΔG_Bind_Packing	-0,4194
MMGBSA_ΔG_Bind_Solv_GB	22,3544
MMGBSA_ΔG_Bind_vdW	-50,3511

Compound 2.9b:

1 hydrogen bonds to Glutamic acid 1055 (Yellow dotted lines)
69 VDW contacts (Green dotted lines)
MMGBSA_ΔG_Bind: -58,43 kJ/mol

MM-GBSA energy components (kJ/mol)	Compound 2.9b
MMGBSA_ΔG_Bind_Coulomb	-3,0447
MMGBSA_ΔG_Bind_Covalent	3,2891
MMGBSA_ΔG_Bind_Lipo	-32,3356
MMGBSA_ΔG_Bind_Packing	-1,6116
MMGBSA_ΔG_Bind_Solv_GB	24,1517
MMGBSA_ΔG_Bind_vdW	-48,8526

Compound 2.9a:

1 hydrogen bonds to Glutamic acid 1055 (Yellow dotted lines)
84 VDW contacts (Green dotted lines)
MMGBSA_ΔG_Bind: -65,56 kJ/mol

MM-GBSA energy components (kJ/mol)	Compound 2.9a
MMGBSA_ΔG_Bind_Coulomb	-2,8380
MMGBSA_ΔG_Bind_Covalent	3,1713
MMGBSA_ΔG_Bind_Lipo	-35,4920
MMGBSA_ΔG_Bind_Packing	-1,9495
MMGBSA_ΔG_Bind_Solv_GB	22,5015
MMGBSA_ΔG_Bind_vdW	-50,9348

Figure 2.34: Hydrogen bonds (yellow dotted line) and Van der Waals (VDW) (green dotted line) interactions as well as the MM-GBSA free binding energies of the three docked compounds with cytochrome bc_1 complex Q_o active site. The molecular surface colouration ranges from dark cyan (most hydrophilic) to white to dark goldenrod (most lipophilic). MMGBSA_ΔGBind energy and the component energies are outlined for each compound.

From Figure 2.34, we observed that atovaquone has a MM-GBSA_ΔGBind of - 50,34 kJ/mol, whereas compound **2.9b** showed a better free energy of binding of − 58,43 kJ/mol. The best-docked compound is compound **2.9a** with MM-GBSA_ΔGBind of −65.56 kJ/mol. The components of the MM-GBSA_ΔGBind for each compound was compared with the other two. With regards to the coulombic free energy, it was observed that atovaquone had a positive value while compound **2.9b** and compound **2.9b** had negative values. A positive coulombic energy suggests potential repulsive force between atovaquone and cytochrome bc_1. A look at the electrostatic distribution on atovaquone, Figure 2.35, shows the preponderance of negative

charges which might repel the electron density at the Q_o site of cytochrome bc_1. Conversely, compound **2.9a** and compound **2.9b** have negative coulombic energies suggesting an attraction between these compounds and the electron density at the Q_o site of cytochrome bc_1. The electrostatic distribution on compound **2.9a** and compound **2.9b** revealed a greater distribution of positive electrostatic potential that might attract the electron density at the Q_o site of cytochrome bc_1.Overall, the energy components of the MM-GBSA GBind suggest that compound **2.9a** and compound **2.9b** have good antimalarial potency. This antimalarial potency could be attributed to a significant increase in favourable electrostatic interactions between these compounds and cytochrome bc_1, which was aided by the improved pi-pi packing energy, Figure 2.35.

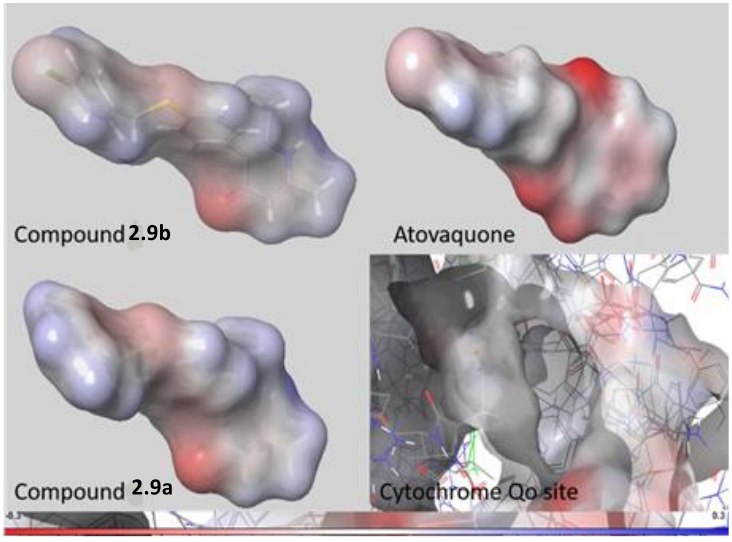

Figure 2.35: Electrostatic distribution [- 0.3eV (red) to + 0.3eV (blue)] on the surface of compound **2.9a**, compound **2.9b**, and atovaquone as well as the Q_o site of the cytochrome bc_1.

Overall, compound **2.9a** and compound **2.9b** were predicted to have greater propensity to bind to and interfere with the electron density and transport at the Q_o site of cytochrome bc_1. MM-GBSA calculation for the three docked compounds was able to correctly rank the compounds in the following order regarding their ability to bind to and probably inhibit cytochrome bc_1: compound **2.9a**, compound **2.9b** and atovaquone. The breakdown into components of MM-

GBSA_ΔGBind energy provided the opportunity to gain some additional insights into the differences in binding affinity.

2.16 Antiplasmodial Activity and Structure Activity Relationships (SAR)

Atovaquone based drugs have shown to be highly effective against drug-resistant strains of *P. falciparum*, and cross-resistance has not been observed between atovaquone and other antimalarial agents.[110] Based on this finding, the synthesized intermediate and target molecules were only screened against the asexual stages of CQ-sensitive (CQS) NF54 and chloroquine-resistant (CQR) K1 *P. falciparum* strains, using CQ as a control.

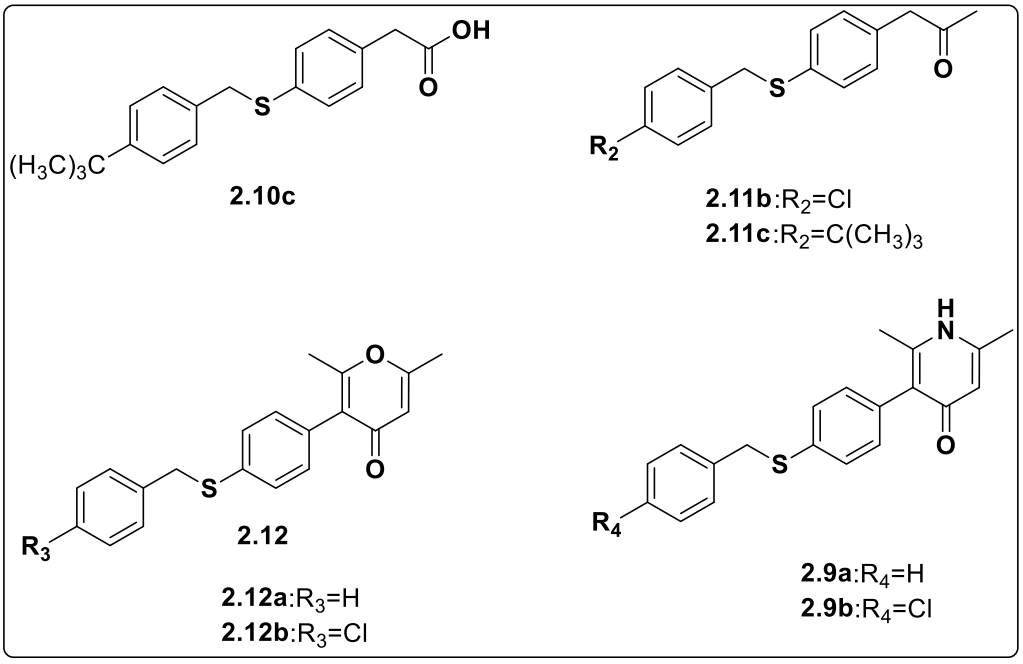

Figure 2.36: Structures of Seven newly synthesized compounds, namely **2.9a, 2.9b, 2.10c, 2.11b, 2.11c, 2.12a, 2.12b**

Seven newly synthesized compounds, namely **2.9a, 2.9b, 2.10c, 2.11b, 2.11c, 2.12a, 2.12b**, Figure 2.36, were screened by *in vitro* by Dr. Dina Coertzen and Dr. Phanakosi Moyo, for their activity against the asexual stage of CQ-sensitive (CQS) NF54 *P. falciparum* parasites using

the SYBR Green assay 1 µM and 5 µM, alongside CQ as the control. Of the compounds screened, **2.9a** and **2.9b** inhibited *P. falciparum* asexual growth by 96% and 97% at 1 µM, 99% and 98% at 5 µM, (Table 2.4), respectively, which was comparable to the activity of CQ, Figure 2.37.

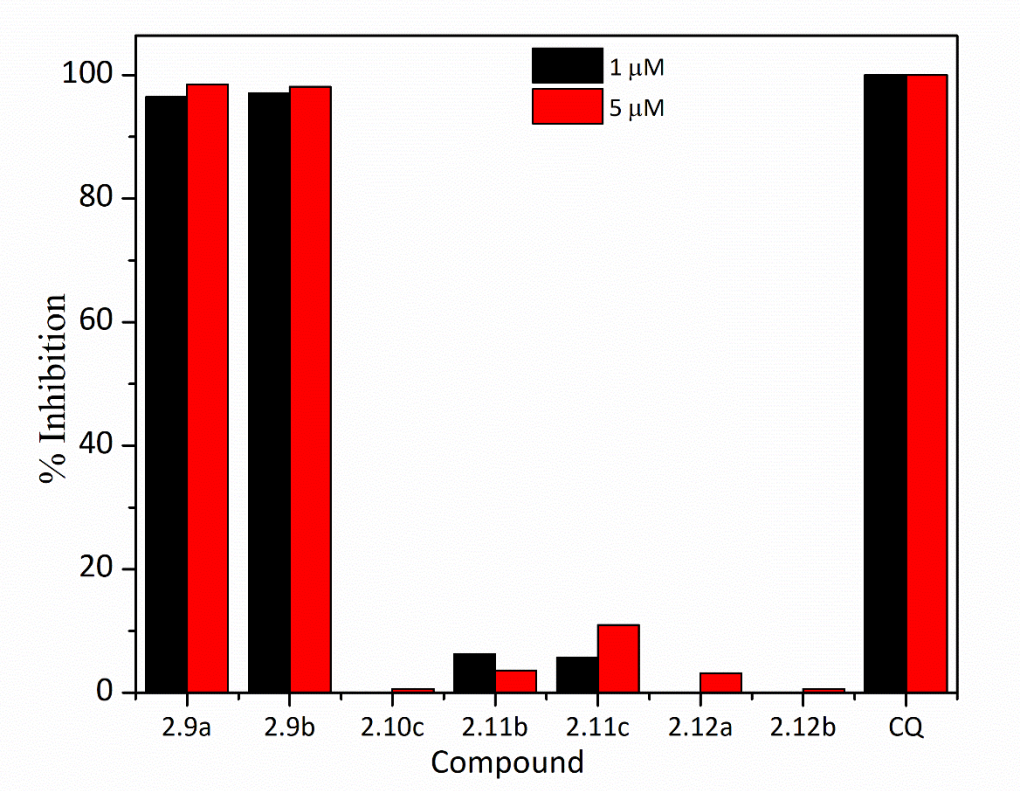

Control: Chloroquine, CQ

Figure 2.37: *In vitro* antiplasmodial activity of the newly synthesized compounds **2.9a, 2.9b, 2.10c, 2.11b, 2.11c, 2.12a, 2.12b** at 1 and 5 µM against CQ-sensitive strain.

The enhanced activity of **2.9a** and **2.9b** can be attributed to the presence of the 4(1*H*)-pyridone pharmacophore, which is absent in **2.10c, 2.11b, 2.11c, 2.12a, 2.12b,**. Notably, replacing O in

the 4(1*H*)-pyranone ring of compounds **2.12a** and **2.12b** with NH shown to be beneficial for antiplasmodial activity as observed for compounds **2.9a** and **2.9b**.

Table 2.4*: In vitro* activity of the newly synthesized compounds **2.9a, 2.9b, 2.10c, 2.11b, 2.11c, 2.12a,** and **2.12b** at 1 and 5 µM against asexual *P. falciparum*

Compound	**% Inhibition**		**% Inhibition**	
	Average	**±SEM**	**Average**	**±SEM**
2.9a	96.5	0.3	98.5	0.2
2.9b	97.1	0.3	98.1	0.2
2.10c	0	3.4	0.6	2.5
2.11b	6.2	3.2	3.6	2.5
2.11c	5.7	3.8	11.0	4.6
2.12a	0	1.5	3.2	2.7
2.12b	0	3.1	0.6	2.5
CQ	100	-	100	-

*n=3, three biological assays with technical triplicates

The 50% inhibitory concentrations (IC_{50}) were subsequently determined for the two most potent compounds, compounds **2.9a** and **2.9b**, against CQS NF54 and chloroquine-resistant (CQR) K1 *P. falciparum* strains. Compound **2.9a** exhibited IC_{50} values of 0.13±0.008 µM (NF54) and 0.10±0.010 µM (K1), while compound **2.9b** exhibited IC_{50} values of 0.05±0.003 µM (NF54) and 0.04±0.003 µM (K1). In the same assay, CQ displayed IC_{50} of 0.04±0.04 µM (NF54) and 0.004±0.002 µM (K1). There was a notable decrease in the Resistance Index (RI) factor for the target compounds **2.9a** and **2.9b**, which were 0.8 and 0.7, respectively, compared to that of the RI of CQ, which displayed a RI factor of 8.5. This observation signifies the importance of the 4(1*H*)-pyridone pharmacophore and the incorporated structural features in altering the observed K1 strain sensitivity, Table 2.5.[73]

Table 2.5: Antimalarial activities of target compounds **2.9a** and **2.9b**

Compound	**NF54**		**K1**		
	IC_{50}(µM)	**±SEM**	**IC_{50}(µM)**	**±SEM**	**RI**
2.9a	0.13	0.008	0.10	0.010	0.8
2.9b	0.05	0.003	0.04	0.003	0.7
CQ	0.04	0.04	0.004	0.002	8.5

***Resistance Index (RI)** = IC_{50} K1/ IC_{50} NF54, CQ = Chloroquine

This also suggests that the target compounds **2.9a** and **2.9b** displayed no cross-resistance, thereby suppressing resistance in the CQR K1 of *P. falciparum*, Figure 2.38. Similarly, as demonstrated with the reported GSK compounds, Figure 2.38.[73] The structure activity relationship of the synthesized 4(1*H*)-pyridone analogs seemed to be more channelled towards the lipophilic side chain C5 of the 4(1*H*)-pyridone scaffold. As shown in Figure 2.38,

replacement of the oxygen linker in the previously synthesized GSK compound **I** with the CH_2S linker in the newly synthesized target compounds **2.9a,** and **2.9b** gave rise to a marked increase in their inhibitory activity, exhibiting IC_{50} values of 0.13 and 0.05 against NF54, whilst compound **I** showed from IC_{50} values of 0.16 However, **GSK932121** and **GW844520** were ten-fold more active than the newly synthesized target compound **2.9b** and more than 20 fold more active than compound **2.9a,** which may be ascribed to the absence of halogen or CH_2OH at the carbon position 3 of the 4(1*H*)-pyridone.

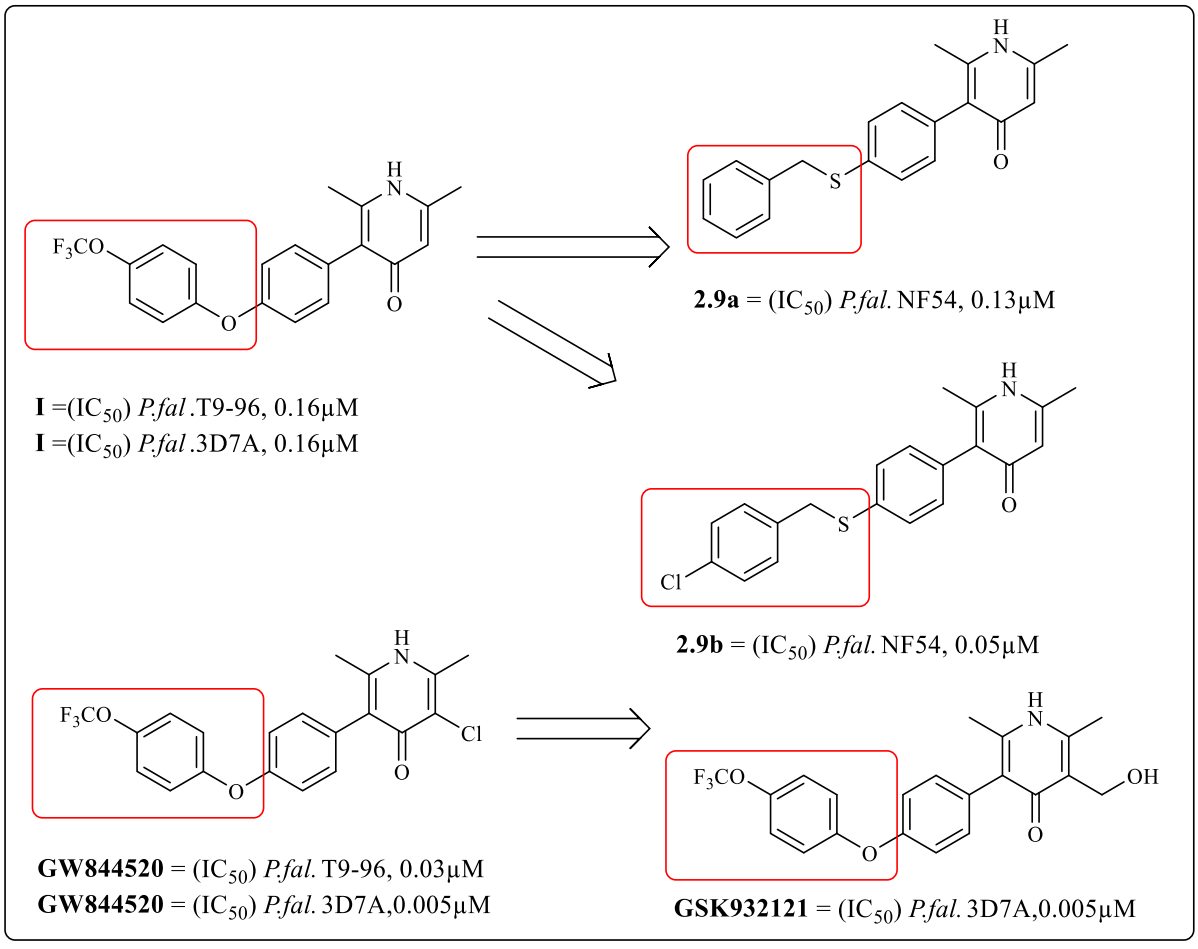

Figure 2.38: Antimalarial activities of previously synthesized GSK compounds **I**,[111] **G844520**,[111] **GSK932121**,[73] and newly synthesized target compounds **2.9a** and **2.9b**.

2.17 Conclusion

Based on preliminary findings through the *in-silico* studies and previous reports carried out on 2,6-dimethyl-4-(1*H*)pyridones, we have successfully synthesized a series of new 4(1*H*)-pyridone-containing target molecules, as antimalarial agents. However, after many failed attempts, only target molecules **2.9a** and **2.9b** were successfully synthesized from the envisaged series.

In the search to find a viable synthetic procedure to afford the target molecules, the palladium-catalyzed coupling reaction was employed as the key reaction in the synthesis of intermediate compounds and target molecules. Single crystal structures of intermediate compounds **2.4a** and **2.4b** were also determined using X-ray diffraction; their unique identities were revealed upon which the side reactions were identified.

Hence, to synthesize a target, four synthetic steps, as stated in Scheme 2.2 were followed for each target. Also, new derivatives of 2,6-dimethyl-4*H*-pyran-4-one compounds **2.15,** in Scheme 2.12, and **2.22-2.26** in Scheme 2.17 were successfully synthesized and obtained in moderate to good yields using palladium catalyzed Suzuki-Miyaura coupling reactions apart from compound **2.26**, whose yield was not determined due to its decomposition.

SC-XRD analysis of the by-products of the reactions forming compounds **2.23 (2.23')** and **2.26 (2.26')** showed that the homocoupling of boronic acids remains to be one of the significant side-reactions occurring that lower the yield of the main products.

DFT analysis showed that electron density in the HOMO of compounds **2.15, 2.22-2.26** is mainly distributed over the substituted R-groups (resulting biphenyl moiety after C-C coupling) and hence suggests a lack of reactivity via either of the oxygen-atoms in the pyranone ring. TGA analysis confirmed the high rate of instability and thermal decomposition of the

selected 2,6-dimethyl-4*H*-pyran-4-one compounds **2.15, 2.22,** and **2.25,** and as result we were unable to synthesize the target compounds **2.16, 2.27-2.31**.

Overall, compound **2.9a** and **2.9b** showed a higher proclivity for binding to the Q_o site of cytochrome bc_1 and interfering with electron density and transit than atovaquone.

Furthermore, the IC_{50}s of the most potent compounds **2.9a** and **2.9b** were determined. Compounds **2.9a** and **2.9b** exhibited remarkable anti-plasmodial activities against K1 CQ resistant strain (CQR) at 0.10 µM and 0.04 µM, while at 0.13 µM and 0.05 µM against *P. falciparum* CQ-sensitive (CQS) NF54.

Moreover, the notable superior molecular docking outcome observed for compounds **2.9a** and **2.9b** was evidenced by their strong growth inhibitory activity against the K1 and NF54 strains of *P. falciparum*, even though compound **2.9b** was found more potent than compound **2.9a**, a result contrary to that shown in the molecular docking studies. Holistically in this study, there is a reasonable correlation between the molecular docking and the biological activity of the envisaged target compounds. Therefore, in this case molecular docking can be used as a guide to design and synthesize promising drug candidates in a rapid and cost-effective manner.

Chapter Three

Investigation of 2-substituted Benzimidazole Anticancer Based Compounds

3. Introduction

3.1 Cancer

Cancer is described as a type of disease that occurs due to uncontrolled development and spread of abnormal cells.[112] In recent years, cancer has been reported to be a universal problem and a primary cause of untimely death. It is a major global health challenge that is escalating in the low- and middle-income countries (LMICs), mainly in developing countries, which account for about 70% of deaths.[113],[114],[21] Estimated number of cancer cases has risen to 17 million new cases in 2018, Figure 3.1. Evident from the ongoing alarming rise in cancer deaths, cancer still poses significant health challenges, even though many marked advances in medical research have been accomplished. According to the World Health Organization (WHO), 9.6 million cancer deaths were recorded in 2018 and it is classified as the second leading cause of death globally.[115] As a result of demographic change, the global cancer burden is expected to increase to 21.7 million cases and 13 million deaths by 2030.[115]

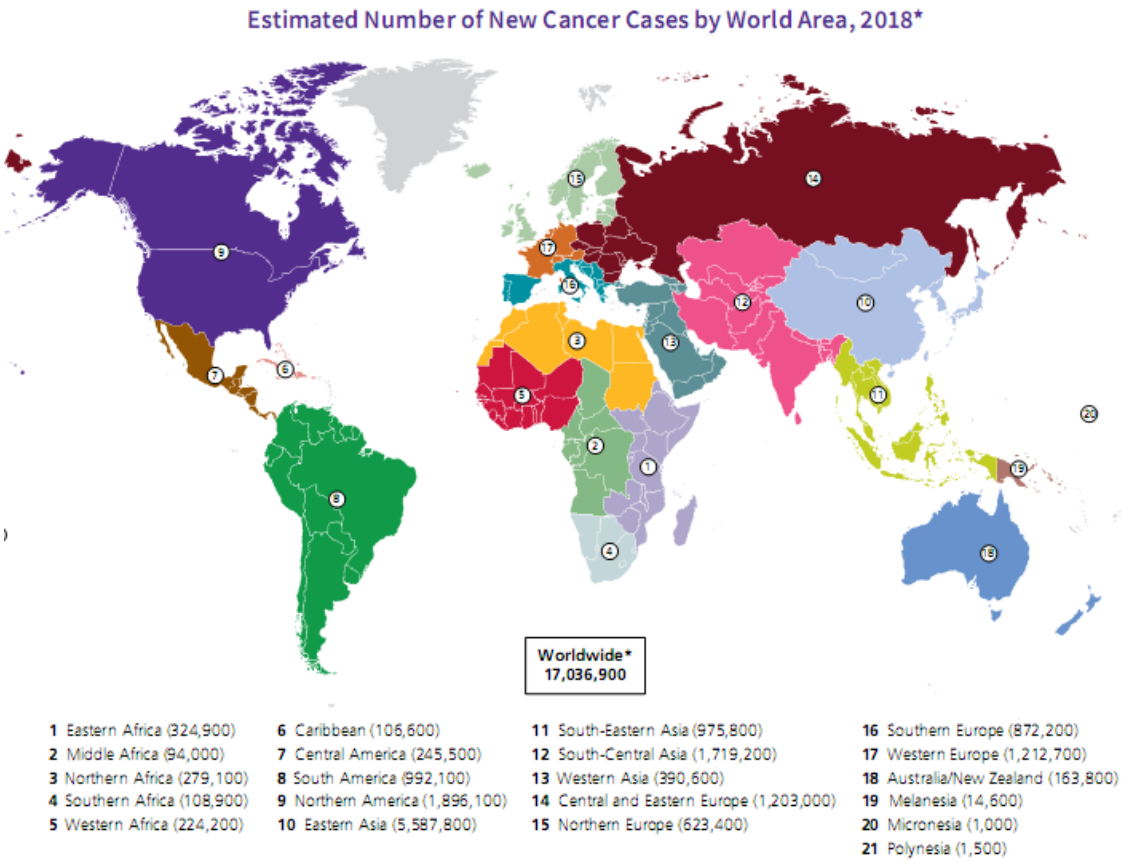

Figure 3.1: Cancer Distribution Across the Globe[116]

3.2 Chemotherapy

The most common clinical cancer treatment approaches are radiotherapy, surgery and chemotherapy. Chemotherapy is described as the application of a drug that contains powerful chemicals in the treatment and killing of fast-growing cancer cells in the body.[117] The use of chemotherapy in cancer treatment was initiated in 1940 when nitrogen mustard and antifolate drugs were administered.[118]

Chemotherapy has been proven to be the first-choice strategy in these treatments due to its ability to suppress cancer cells.[117] The majority of chemotherapeutic drugs act by inhibiting cell division by targeting vital cellular processes and consequently prevent cancer cell multiplication. Existing clinical anticancer drugs typically act on fast replicating cells and

present shortcomings such as poor selectivity between cancer cells and healthy cells.[119] Cancer cells usually disrupt the cell signaling mechanisms and tissue morphogenesis for the neoplastic spread of tumors.[119] The use of chemotherapeutic agents has been demonstrated to be a viable approach to slow down tumor growth and disease progression by targeting these cell mechanisms. Unfortunately, most cytotoxic drugs cause side effects due to the poor selectivity and specificity toward cancer cells. Therefore, the potent harmful profiles and poor tolerance of the existing chemotherapeutic medicines are major hindrances to the effective treatment of cancer.[120] Moreover, the lack of selectivity of current drugs between cancerous and normal cells has strengthened the need for new, safe, and cost-effective therapeutics. Most of the synthesized anticancer agents comprise heterocyclic compounds; amongst these are benzimidazole derivatives [121–125] which have shown promise as potential candidates, and thus, are ideal scaffolds for our anticancer drug discovery program.

3.3 Anticancer Derivatives of Benzimidazole

Benzimidazole is a heterocyclic bicyclic compound, which contains benzene ring fused to an imidazole ring.[126] Benzimidazoles are generally synthesized by the condensation of *o*-phenylenediamine and different aldehydes or carboxylic acids.[127] These compounds can also be easily made through various heterogeneous catalysts using, [4+1]-cycloaddition of *o*-phenylenediamine with one carbon donor source.[128] The benzimidazole scaffold has captured the interest of many medicinal chemists since vitamin B12, contains a benzimidazole nucleus, Figure 3.2. This vitamin B12, is essential for the development of red blood cells in humans.[129]

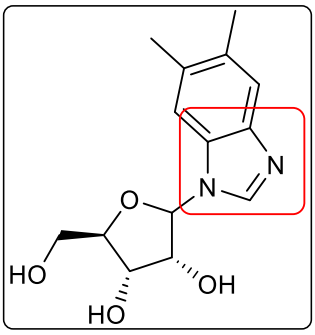

Figure 3.2: Chemical Structure of 5,6-dimethyl-1-(α-D-ribofuranosyl) benzimidazole found in (Vitamin B12)

Therefore, benzimidazole derivatives have attracted significant considerations in the preparation of active drugs by combining the modified positions 1, C2, and C5 of the benzo-fused ring as shown in Scheme 3.1, owing to their extensive valuable pharmaceutical benefits.[130] Benzimidazole undergoes tautomerism. Tautomerism occurs when hydrogen is bound to either of the two nitrogen atoms present in the imidazole ring, existing as two equal tautomers.[131]

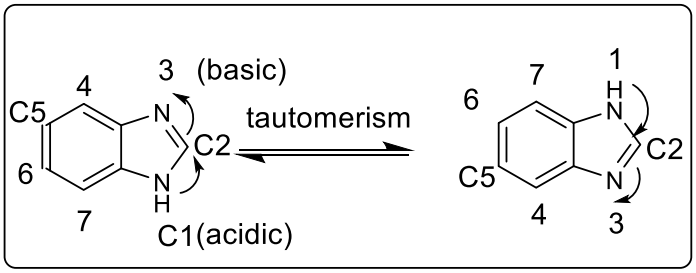

Scheme 3.1: Benzo-fused Imidazole Ring Tautomerism[132]

Benzimidazoles are vital bioactive molecules and one of the major nitrogen-containing heterocyclic compounds. Benzimidazoles have a wide range of biological activities, used as building blocks for the design of drug agents. They play key roles in medicinal applications such as anti-microbial[133],[134], anti-tubercular,[135] anti-parasitic[136],[137] anti-viral,[138],[139] anti-

inflammatory,[140] antidepressant,[141] anti-leukemic,[142] and anti-cancer.[143,123,144] anti-diabetic, numerous anti-oxidant, anthelmintics, antiproliferative, anti-convulsant, anti-hypertensive, anti-neoplastic, proton pump inhibitors, and anti-trichinellosis.[133,145] Benzimidazole derivatives have been reported to display anticancer activities against several cancer cell lines,[146] such as; MCF-7 (breast adenocarcinoma),[147] HeLa (cervical carcinoma), SW620 (cervical carcinoma),[148] HL60 (peripheral blood acute promyelocytic leukemia), K52 (bone marrow chronic myelogenous leukemia), HT29 (colon carcinoma).[149] Some of the recognized benzimidazole-based drugs are seen in Figure 3.3.

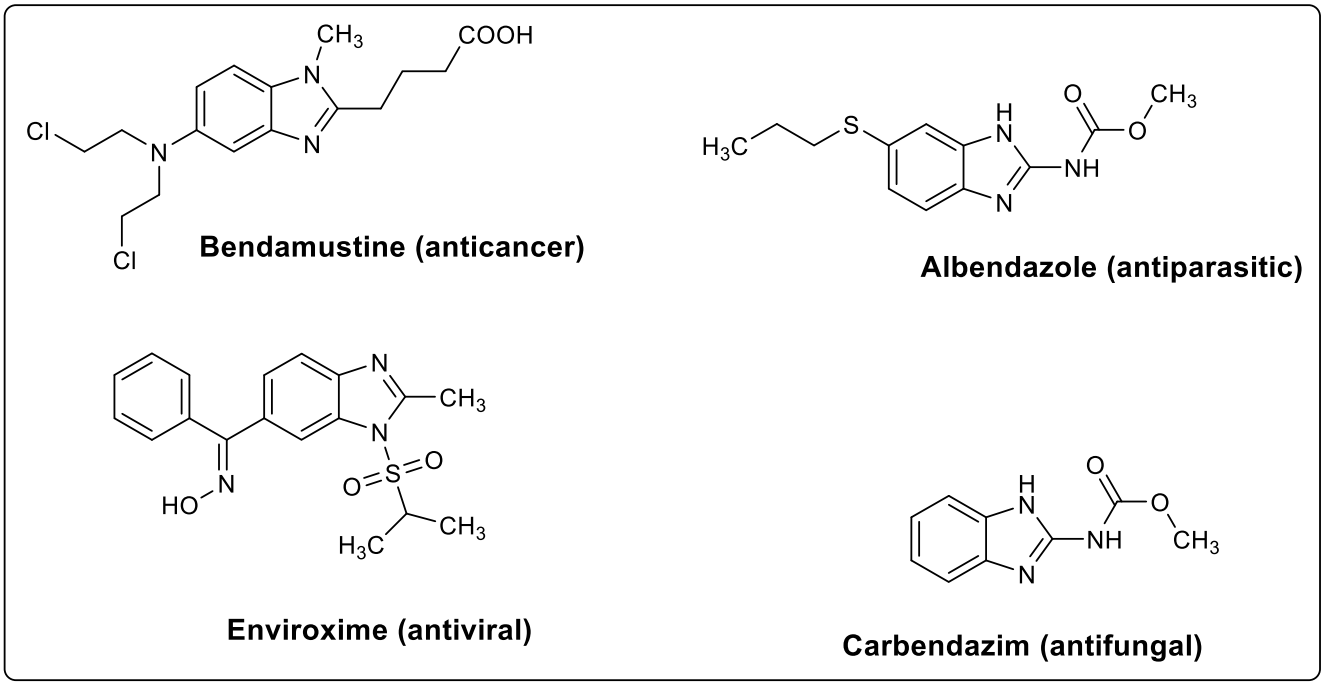

Figure 3.3: Some Benzimidazole-based Active Drugs[132]

3.4 Reported Synthesis of Benzimidazoles as Anticancer Agents

Reports in the literature have presented 2-substituted benzimidazoles as exhibiting notable anticancer activities. Omar and co-workers docked and synthesized numerous series of 2-substituted benzimidazoles.[150] Interestingly, their findings have shown a clear correlation between the docked benzimidazoles, Figure 3.4, and their antitumor activity. Both results gave excellent anticancer activity, better than the bis-benzoxazole natural product (UK-1), used as the standard against lung cancer (A549) cell line cell, Scheme 3.2.[150]

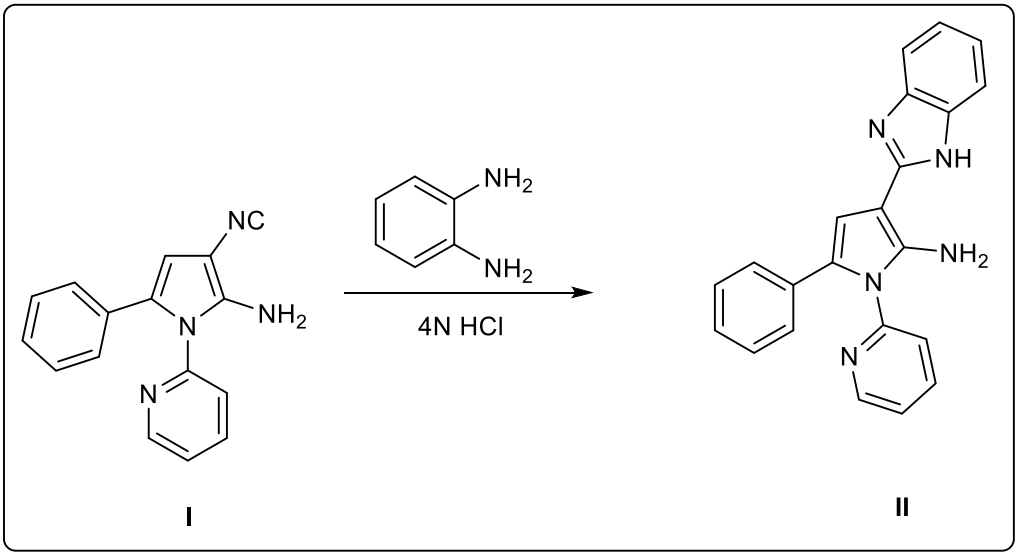

Scheme 3.2: Synthesis of 3-(1*H*-benzo[d]imidazol-2-yl)-5-phenyl-1-(pyridin-4-yl)-1H-pyrrol-2-amine

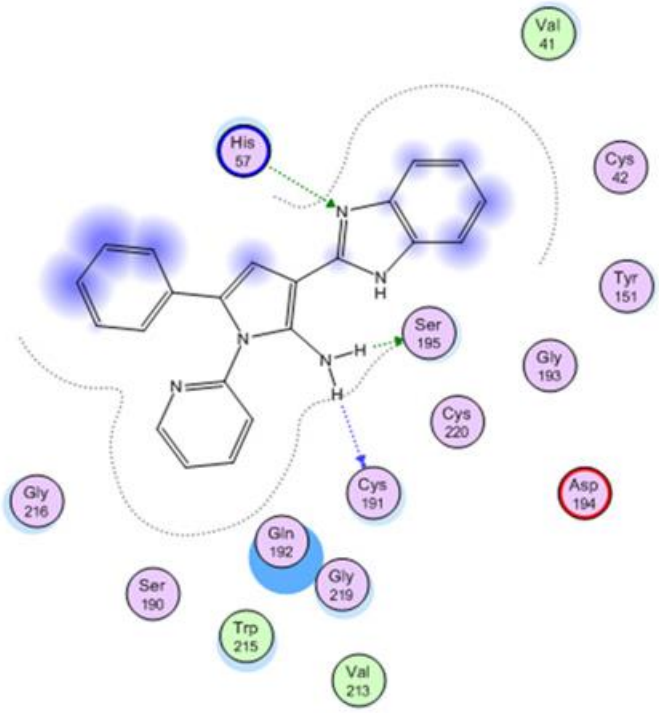

Figure 3.4: The binding mode and ligand interaction of the synthesized 3-(1*H*-benzo[d]imidazol-2-yl)-5-phenyl-1-(pyridin-4-yl)-1H-pyrrol-2-amine with CYS 191, SER 195 and HIS 57, using urokinase-type plasminogen activator (uPA) as the receptor.[150]

Another paper reported the synthesis of a series of novel benzimidazole Schiff bases and their complexes.[151] These compounds were synthesized using both conventional heating and microwave irradiation approaches. The synthesized targets were screened against breast, liver, and lung cancer cell lines for their antitumor activity. Notably, this series of compounds displayed good anticancer activity compared to the drug doxorubicin, used as the control, Scheme 3.3.

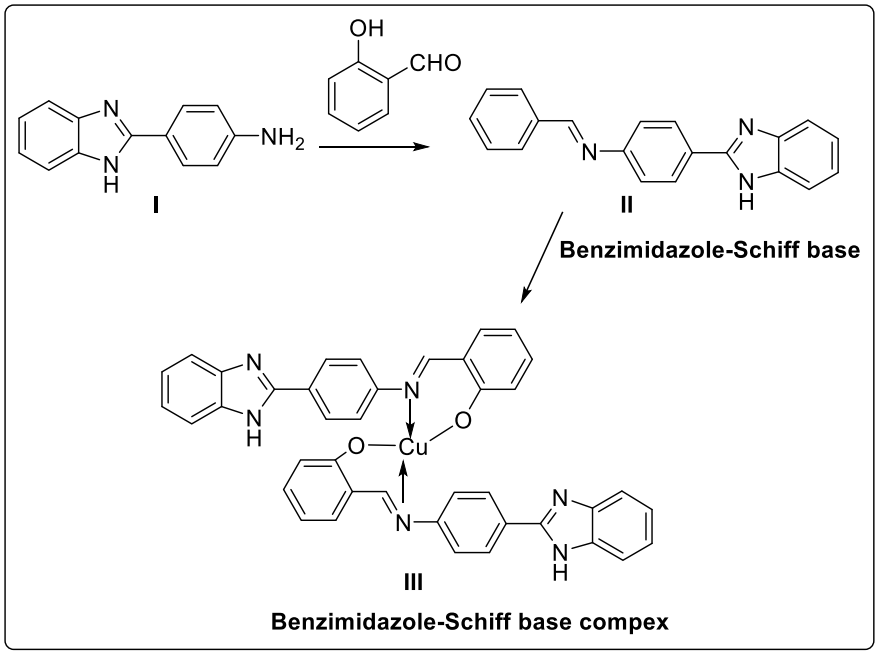

Scheme 3.3: Synthesis of Benzimidazole Schiff Base and its copper Complex

Another study showed the multistep synthesis, anticancer activities, and specific kinases assessment of 2-arylbenzimidazole derivatives.[152] These compounds were reported to show excellent anticancer activities when tested against a tumor cell line HepG-2 and their specific kinases were assessed. Two of the synthesized compounds which were I (2-aryl-) and II (2-heteroaryl)benzimidazoles possessed great cytotoxicity against HepG-2 cells with IC_{50} value 2µM, (Figure 3.5).

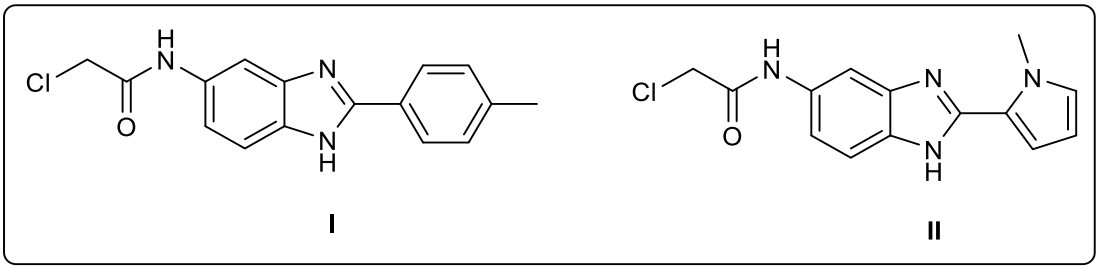

Figure 3.5: 2-Arylbenzimidazole and 2-Heteroarylbenzimidazole Derivatives

The prominent role and the contribution of vanillin in the treatment and prevention of cancer have been well-documented in literature.[153] Additionally, reports have further shown that vanillin and its derivatives, such as benzimidazole derivatives, are significant pharmacophores in drug discovery, especially used in the treatment of breast cancer. [142],[154] It was also reported that benzimidazoles bearing a vanillin nucleus exhibit anti-proliferative activity in HL60 leukemia cancer cells, resulting in cell cycle progression at G2/M phase.[142]

3.5 Reported *In-silico* Docking of Some Benzimidazole Anticancer Agents

As a result of the remarkable cancer inhibitory activity displayed by benzimidazole derivatives, extensive attention and efforts have been invested in designing more efficacious benzimidazole-based anticancer agents by focusing primarily on how to modify their chemical structures.[155] These strategies include molecular in-silico docking, which involves using ligand-protein and structure-based design of drugs (SBDD) *via* computational modeling. This technique is a powerful tool to aid in fast-tracking the design of potential lead compounds.[156] Also, the in-silico technique is a cost-effective approach, guiding researchers into the rapid synthesis of potential biologically active libraries as alluded to earlier, in chapter one. [157]

Recent reports have demonstrated 2-substituted benzimidazole derivatives as promising anticancer agents employing in-silico molecular docking as the key approach.[158,144,125]. Docking studies conducted by Talan and his group,[155] employing human cyclin-dependent kinase CDK-8 protein 2 as the active site, revealed the binding mode of 2-substituted benzimidazoles with various important amino acids such as Thr347, Asp351, and Cys530. A bond with the oxygen of the amino acid and the nitrogen atoms of the 2-substituted benzimidazoles was clearly observed as seen in Figure 3.6., exhibiting high negative score,[159]

a significant docking score of -7.69, which shows that there is a strong binding interaction between the ligand and the receptor CDK-8 protein 2, Figure 3.6.

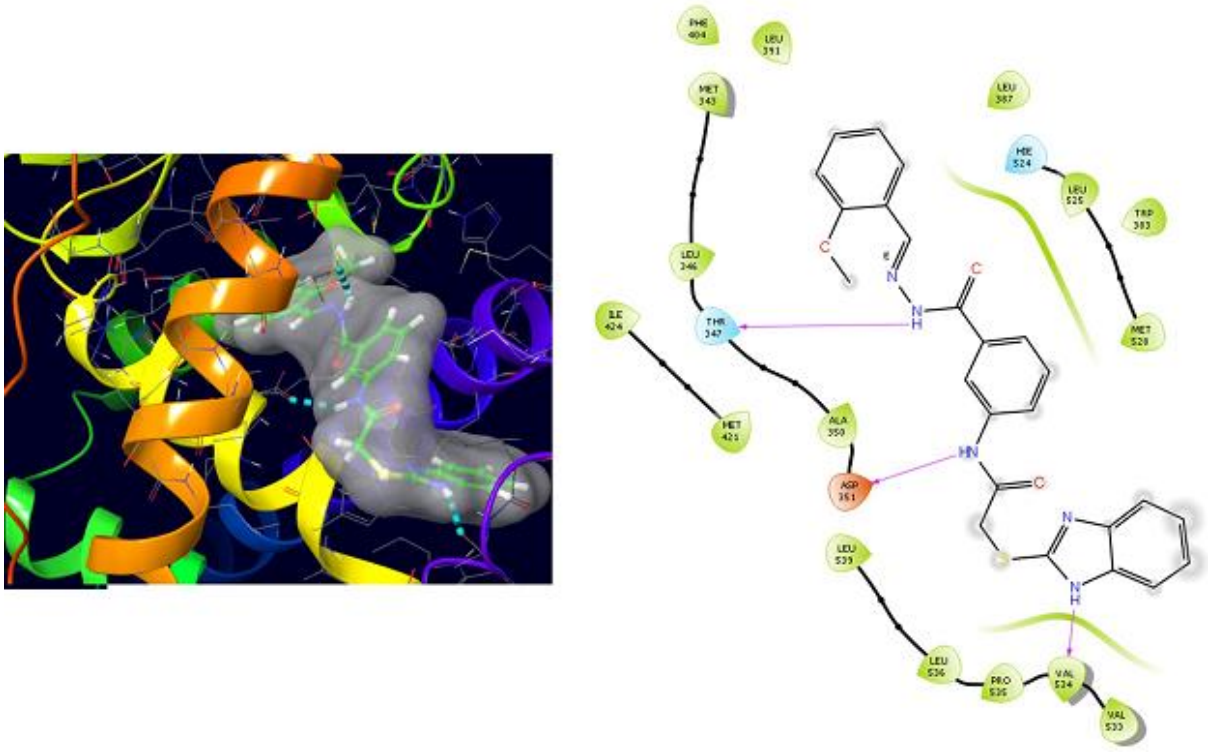

Figure 3.6: Binding mode and ligand interaction of 2-substituted-benzimidazoles in the CDK-8 protein 2 binding site

Moreover, a series of 2,6-disubstituted benzimidazoles were synthesized and screened against various five cancer cell lines, including HeLa, MCF7, A549, HepG2 and C6.

Two of the series of the compounds displayed excellent antiproliferative activity, more than doxorubicin with IC_{50} of 0.224 ± 0.011 µM and 0.205 ± 0.010 µM, respectively. These two compounds were further docked against DNA topoisomerase **1** enzyme complex, Figure 3.7 and they were shown to displayed probable interaction and inhibited topoisomerase **1** enzyme complex.

A π- π interaction was observed between the amino acid, Arg364, and the phenyl ring of the benzimidazole while the nitrogen atom of the benzimidazole ring was involved in strong polar interactions.

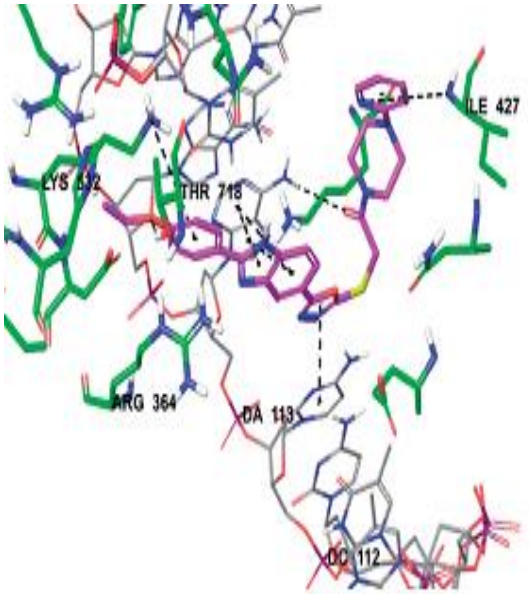

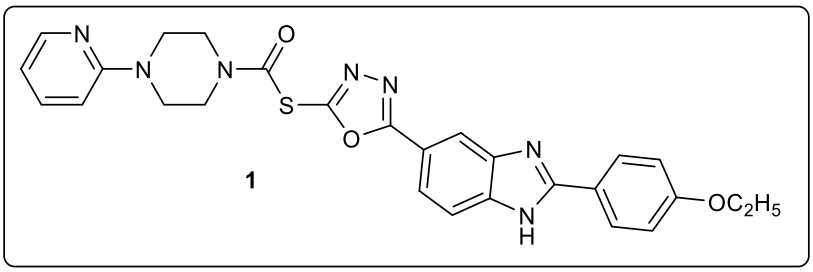

Figure 3.7: Docking of 2,6-disubstituted benzimidazole against DNA topoisomerase **I** enzyme complex[144]

Due to the favorable antiproliferative activities of 1-(1*H*-benzimidazol-2-yl)-3-substituted prop-2-en-1-one, **2**, Figure 3.8, against breast cancer cells, Mohamed *et al* [158] carried out molecular docking on a series of novel benzimidazoles. The docking study demonstrated the binding of 1-(1*H*-benzimidazol-2-yl)-3-phenylprop-2-en-1-one ring to a narrow hydrophobic pocket in the N-terminal domain of epidermal growth factor receptor-tyrosine kinase EGFR-TK, which is similar to that of Erlotinib inhibitor, Figure 3.8.[158]

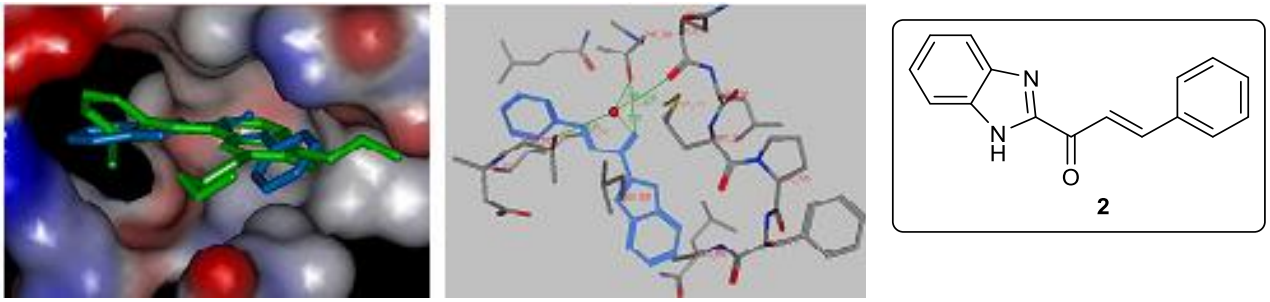

Figure 3.8: The binding mode 1-(1*H*-Benzimidazol-2-yl)-3-phenylprop-2-en-1-one, **I**, ring unto EGFR-TK complex.[158]

A report by Chu *et al*, showed the activities of 2-aryl benzimidazole **3,** Figure 3.9 and its derivatives against breast cancer both *in-vitro* and *in-vivo*.[160] These derivatives exhibited anti breast cancer activities against epidermal growth factor receptor (EGFR) and human epidermal growth factor receptor 2 (HER2) through tyrosine phosphorylation reduction. Downstream activation of PI3K/Akt and MEK/ Erk pathways were also prevented in an *in vitro* bioassay.[160]

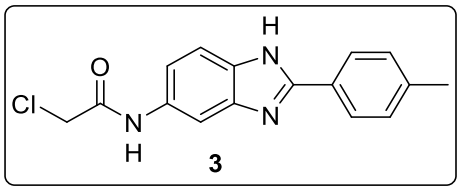

Figure 3.9: 2-Aryl benzimidazole I

3.6 ADMET Properties in Drug Discovery

The study involving drug metabolism and pharmacokinetics is mostly referred to as ADMET properties in drug discovery and development.[161] Chemical absorption, distribution, metabolism, excretion, and toxicity (ADMET), are vital at every stage in the drug discovery and development.[162] ADME deals with the pharmacokinetic properties of a drug molecule which determine if it will get to the target protein in the body and how long it will stay in the bloodstream.

3.6.1 ADMET Properties of Benzimidazole Derivatives

Reports have shown some fundamental ADMET properties of benzimidazole derivatives. The lipophilicity and H-bonding of the 2- and 5-substituted benzimidazole analogues, Figure 3.10, were investigated *in vitro*. These 2- and 5- disubstituted benzimidazole analogues were identified as vital substituents responsible for the angiotensin II– AT1 receptor antagonistic activity.[163]

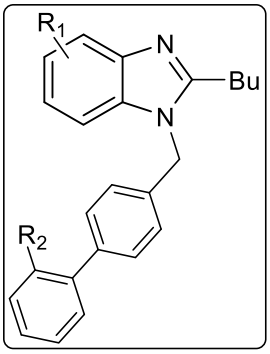

Figure 3.10: 2- and 5-substituted benzimidazole analogues identified as angiotensin II–AT1 receptor antagonist.[163]

Another series of 2-substituted benzimidazole derivatives, Figure 3.11, were analyzed for their ADMET properties. The key ADME and drug-likeness properties predicted on the series of 2-substituted benzimidazoles displayed no violations in all drug-likeness rules (Veber, Lipinski, Ghose, Muegge, and Egan). Also, these series of benzimidazoles revealed no PAINS (pan assay interference structures) alerts nor structural alerts (Brenks).This series of benzimidazoles also displayed promising *in vitro* anticancer activities. [164]

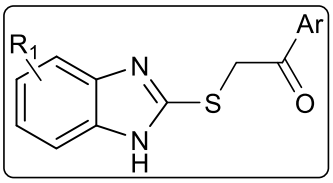

R_1= H; **R_1**= -$(CH)_4$

Figure 3.11: 2-substituted benzimidazole derivatives. [164]

3.7 Designed Target Compounds Based on Previous Literature Reports

At this point, we sought to design a library of highly functionalized benzimidazole scaffolds based on previous literature reports and that were simple, and effortless to synthesize in a short period of time. Scheme 3.4 shows the retrosynthesis of the target compounds. Previous studies reported azomethine (imine) linkage (dashed rectangle in green), Scheme 3.4, incorporated with heterocyclic system to exhibit a higher affinity and lipophilic properties thus, reducing the toxicity of a proposed drug, this could as well increase the anticancer properties of the proposed drug.[165] Also, benzimidazole moiety (red cycle), Scheme 3.4, has been reported to exhibit antitumor activity through the versatile mechanism of action, including DNA alkylation, DNA binding, disturbing tubulin polymerization or depolymerization, enzyme inhibition, anti-angiogeneic, and signal transduction inhibitors.[166] Also, previous literature reported molecular docking of these benzimidazole derivatives confirmed by its importance as anticancer with the π- π interaction observed between the amino acids, and the phenyl ring of the benzimidazole, while the nitrogen atom of the benzimidazole ring was involved in strong polar interactions. Furthermore, it was worthy to note that the introduction of more phenyl rings (circled in blue) could increase the π- π interaction, which might in turn enhanced the number of interactions and consequently increase the potency. Also, more interaction allows the ligand to be more tightly bound into the active site, thereby increasing the compound's activity. Also, the ethylene linker in the compounds, **3.6a-f** may extend the functional groups near the active site. Finally,

fluorine has previously been described as a small but highly electronegative atom that performs a vital role in medicinal chemistry.[167] Substitution of fluorine (light blue dashed circle) in a drug candidate increases its ADME and physicochemical properties, including improved metabolic stability and enhanced membrane permeation.[168]

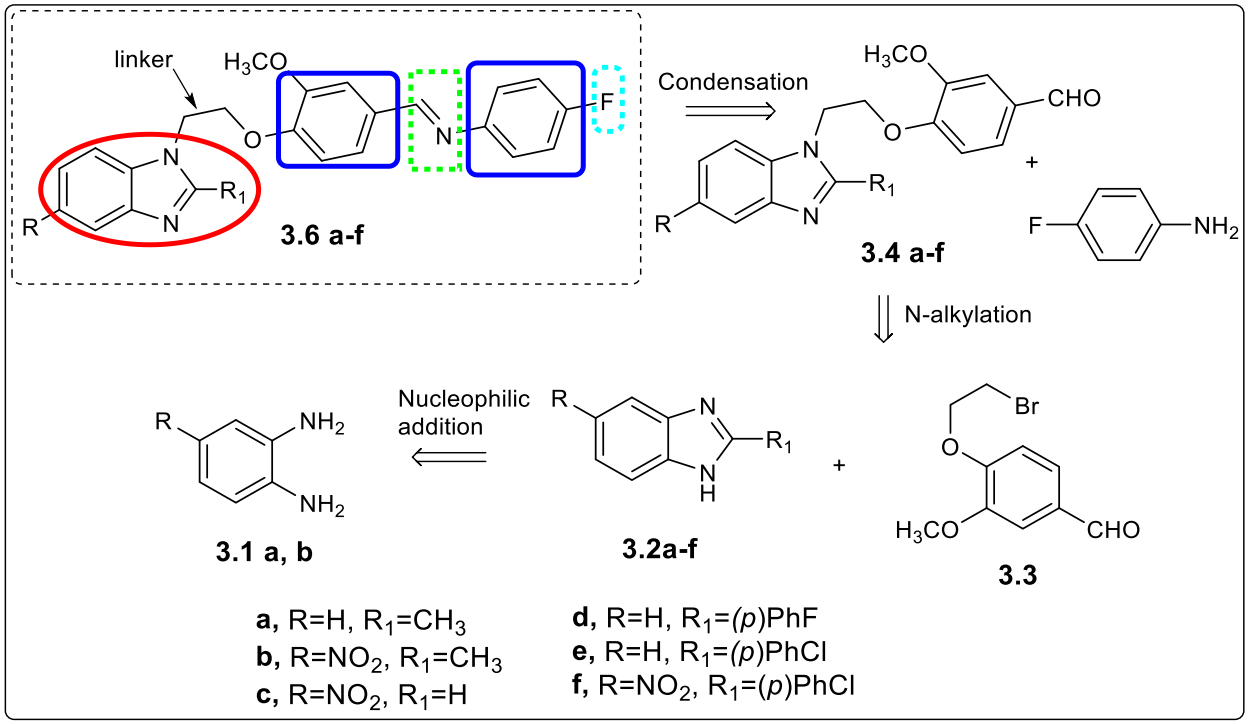

Scheme 3.4: Retrosynthesis of the proposed benzimidazole derivatives

3.8 Reverse Docking and Molecular Similarity as Computational Molecular Docking Strategies

Phenotypic high-throughput screening is referred to as chemical genetic or *in vivo* drug screening used to determine the ability individual compounds to inhibit a particular enzyme in living cells or intact organisms.[169] Phenotypic high throughput screening has been found useful in drug discovery.[170]

Optimization of compounds from initial phenotypic screening projects requires extensive structural activity relationship (SAR) analysis because the potential targets of such compounds

screened phenotypically are unknown.[171] Knowledge of the targets for the phenotypically screened compounds (ligand-target binding) will allow the application of structured based drug design strategies that will improve the specificity of the compounds.[172] It will also give insight into the potential mechanism of actions of the compounds[173] and identify potential off-targets for such compounds.[174] Hence, the mining ligand-target binding is a vital part of the drug discovery process.[175]

Different techniques have been applied to determine target profiles for ligands, including molecular similarity searching, data mining and machine learning, analysis of bioactivity spectra, protein structure-based, and reverse/inverse docking methods.[176] Reverse docking is a powerful tool for target prediction, drug repositioning, and drug rescue. It involves docking a small-molecule ligand in the potential binding cavities of a set of clinically relevant macromolecular targets. The process can potentially identify novel molecular targets for the drug/ligand, which may be suitable for its mechanism of action and side effect profile. Reverse docking has potential application in the lead discovery and optimization stages of the drug discovery cycle. Molecular similarity searching is another strategy that is used to predict target profiles for ligands. Molecular similarity searching is based on the Similar Property Principle and has been used to find molecules that are likely to have similar bioactivity, physicochemical target binding profiles to a reference molecule. The Similar Property Principle states that structurally similar molecules like an active molecule are also expected to be active. Thus, finding molecules that are structurally like a molecule with a known target binding profile is one of the keys to successful target prediction and elucidation of such molecules' mechanism of action(s).

3.8.1 Molecular Similarity Searching of Target Compounds for Target Prediction

In this study, reverse docking and molecular similarity searching were used to establish the *in-silico* breast cancer target profiles for a set of benzimidazole analogues, by docking them against breast cancer targets and search a database of known ligand-target binding profiles.

We used a web-based platform, Swiss Target Prediction, to implement the molecular similarity searching for ligand-target profiling. Swiss Target Prediction accurately predicts bioactive molecules' targets based on a combination of 2D and 3D similarity measures with known ligands. The “smiles” formats of the 12 benzimidazole analogues were imported into Swiss Target Prediction to predict their putative targets of action. The predicted putative target was limited to *Homo sapiens*. In order to improve the reliability of the prediction goal, only high-probability targets were selected. All predicted putative targets identified were searched on Uniprot Database to verify the gene ontology and biological functions of these predicted putative targets.

3.8.2 Molecular Docking for Ligand-Target Binding of Target Benzimidazoles, 3.4a-3.6f, using Estrogen Receptor Alpha (ER) in Breast Cancer as a Suitable Target

Estradiol is one of the anti-estrogens that bind and inhibit estrogen receptor alpha (ER) proliferation in breast cancer. Estradiol such as 17b-estradiol has been found useful in the treatment of breast cancer.[177] Therefore, a crystal structure of human estrogen receptor alpha ligand-binding domain in complex with estradiol was downloaded from protein data bank pdb.[178]

Recent reports have demonstrated 2-substituted benzimidazole derivatives to possess anticancer properties.[158,144,125]. Based on the previous reports, molecular docking studies were performed on benzimidazole derivatives using the crystal structure of human estrogen receptor

(ER) alpha ligand-binding domain in complex with estradiol as the active site. The binding modes of the proposed benzimidazoles in the enzyme active site of human estrogen receptor (ER) alpha were represented in Figure 3.12. The scoring functions and hydrogen bonds formed with the neighboring amino acids are used to predict their binding modes, their binding affinities , and orientation of the target benzimidazoles at the enzyme active site of the human estrogen receptor (ER) alpha (pdb code: 2OCF).[178] A smaller docking score signifies a higher binding affinity of the ligand for the receptor. Obtained docking scores results are summarized in Table 3.1, below.

Table 3.1: Docking scores of targets, 2-substituted benzimidazoles

Compound code	***Docked score**
3.4a	-8,29
3.6a	-8,42
3.4b	-9,16
3.6b	-8,96
3.4c	-8,81
3.6c	-8,95
3.4d	-8,21
3.6d	-7,96
3.4e	-8,38
3.6e	-7,99
3.4f	-7,95
3.6f	-8,71

*Docking scores of 2-substituted benzimidazoles-based target molecules and intermediates.

The most probable target molecule was identified as compound **3.4b** with docking scores of -9,16. This target, as mentioned earlier, revealed a bond with Arg 394 and π interactions with Leu387and Leu 525, Figure 3.14. The binding mode and structure analysis showed that some of these benzimidazoles intermediate compounds, such as **3.4a, 3.4b, 3.4c, 3.4e, 3.4f,** only form a bond with an amino acid Arg394, which conforms to the binding mode of human estrogen receptor alpha ligand-binding domain in complex with estradiol, Figure 3.12. At the same time, there was no other bonding with other essential amino acid residues such as His 524, Glu 353 found in the binding mode of estradiol with the ER-ligand binding.

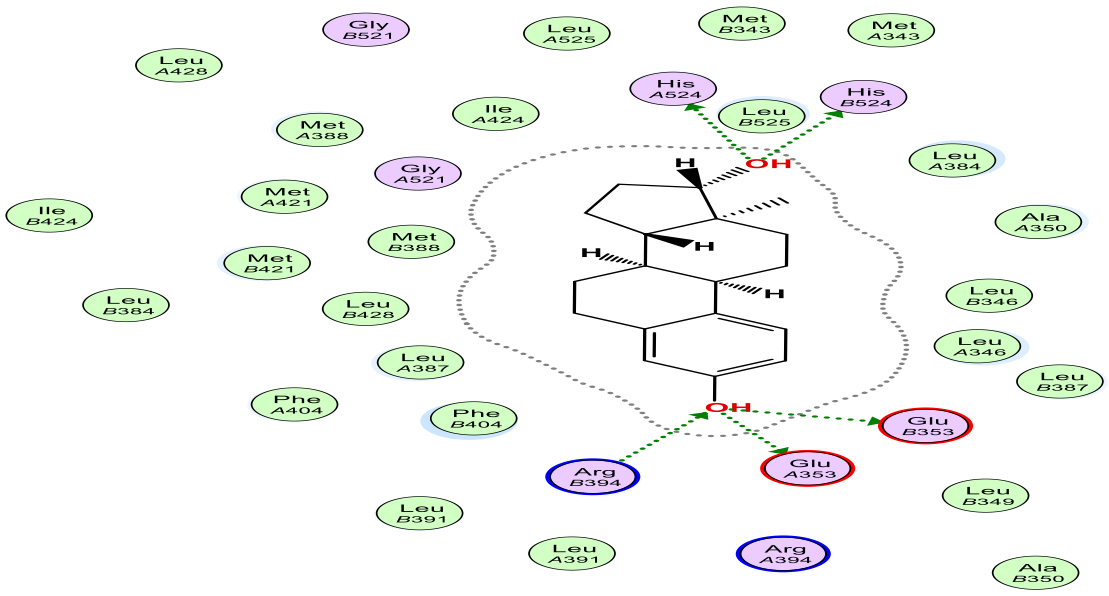

Figure 3.12: The binding mode of estradiol unto the active site of estrogen receptor (ER) alpha

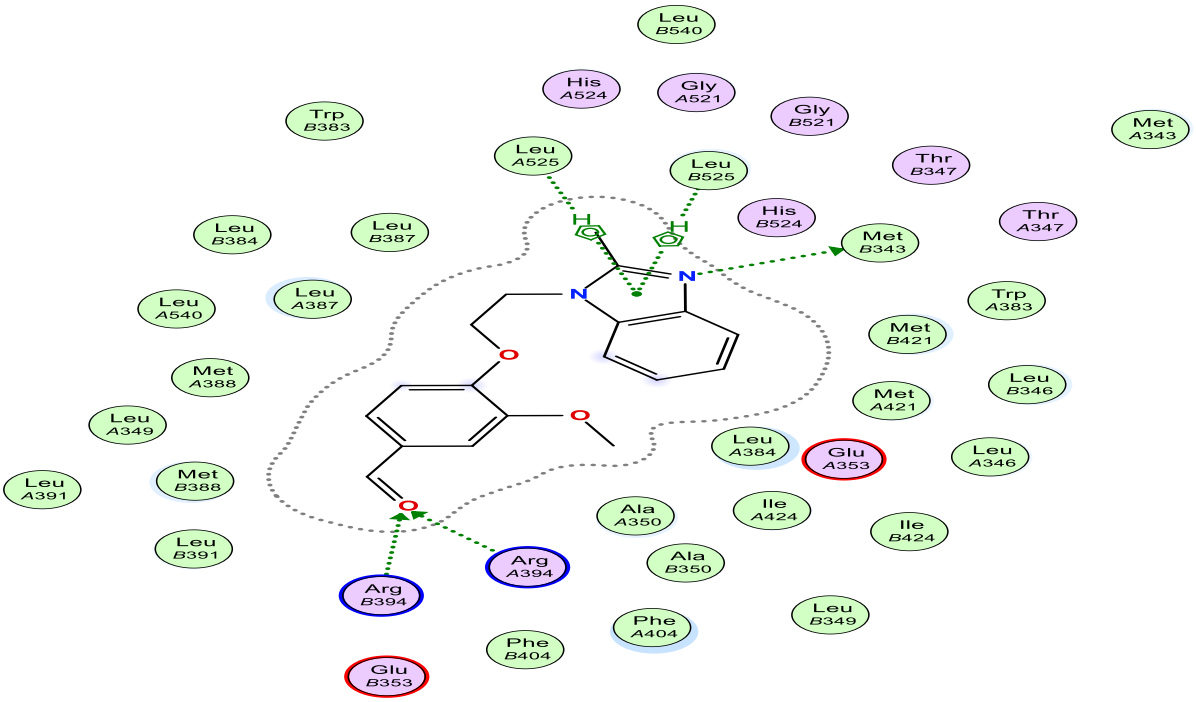

Figure 3.13: The binding mode of the intermediate compound **3.4a** unto the active site of estrogen receptor (ER) alpha.

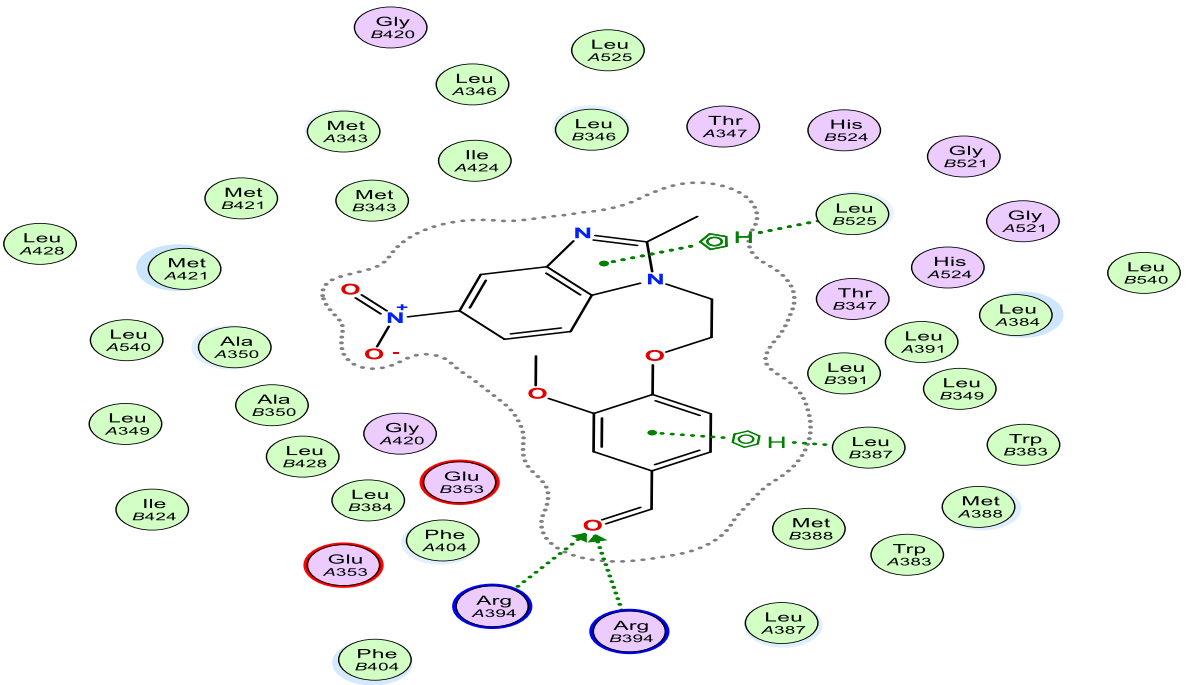

Figure 3.14: The binding mode of the most probable intermediate compound **3.4b** with dock score of -9.16 into the active site of estrogen receptor (ER) alpha.

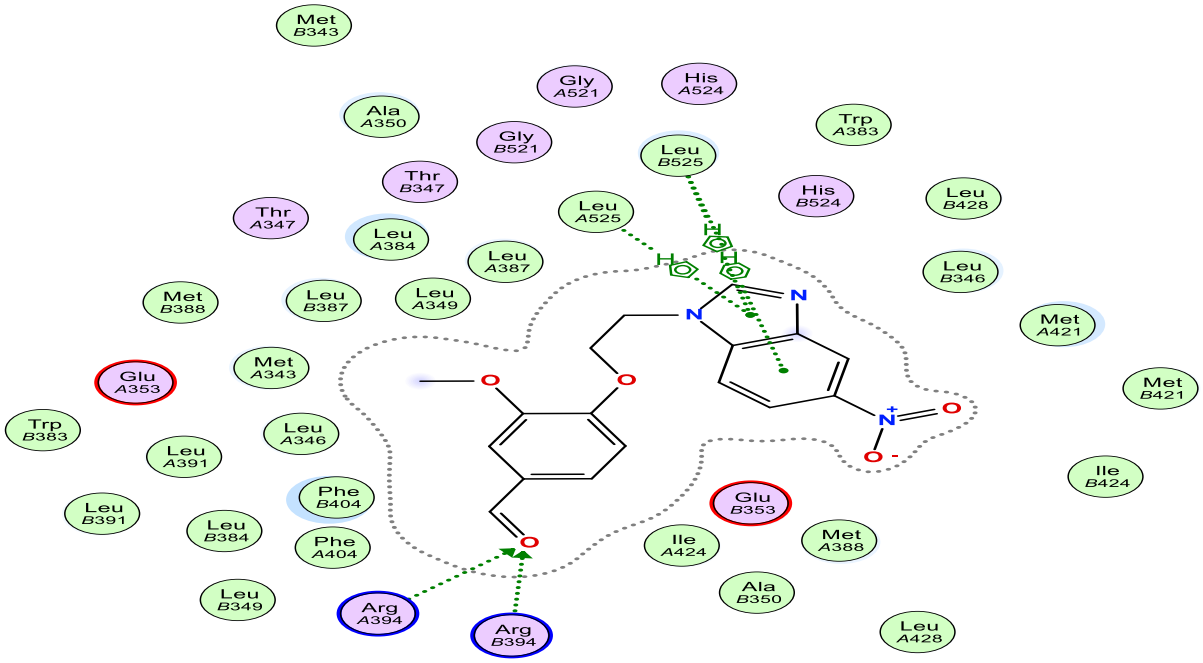

Figure 3.15: The binding mode of the intermediate compound **3.4c** unto the active site of estrogen receptor (ER) alpha.

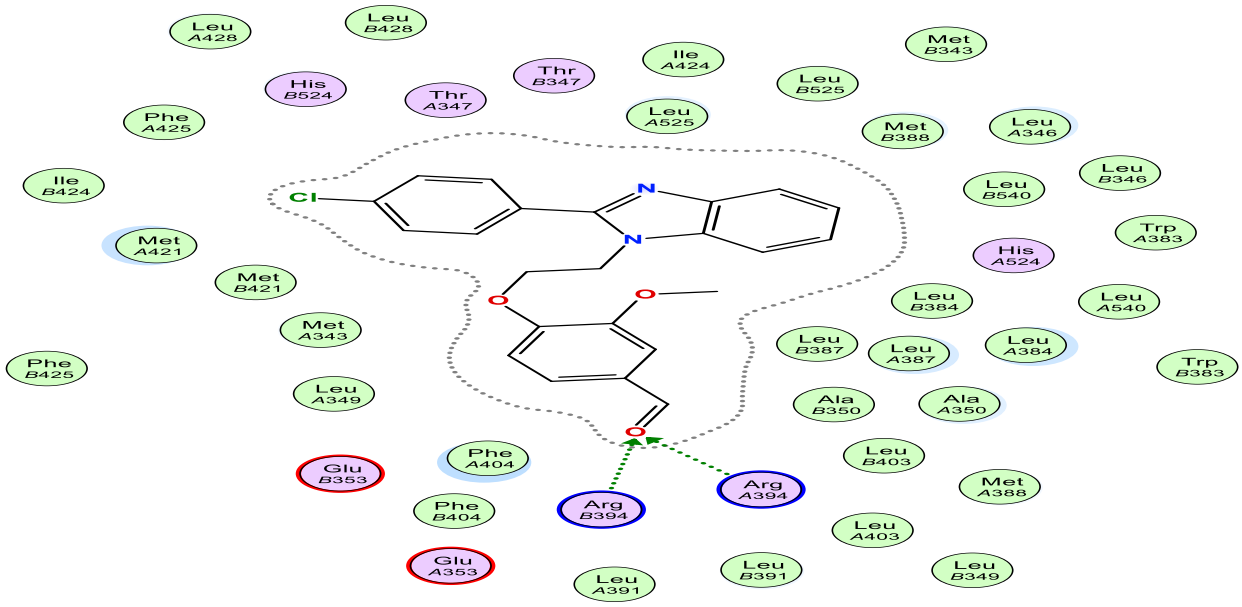

Figure 3.16: The binding mode of the intermediate compound **3.4e** unto the active site of estrogen receptor (ER) alpha.

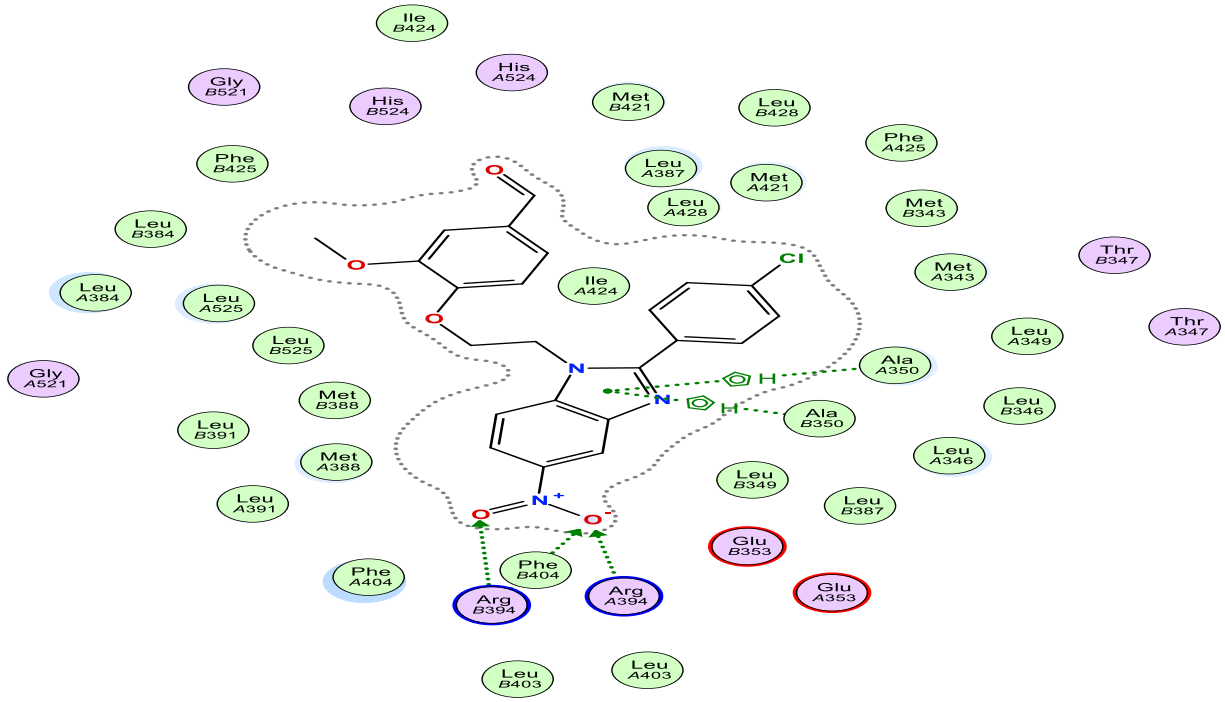

Figure 3.17: The binding mode of the intermediate compound **3.4f** into the active site of estrogen receptor (ER) alpha. Other target benzimidazoles **3.4d, 3.6a-3.6f**, displayed binding interactions with other amino acids that are not comparable with that of estradiol in the active site of estrogen receptor (ER) alpha. The binding modes are depicted in Figure 3.18, below.

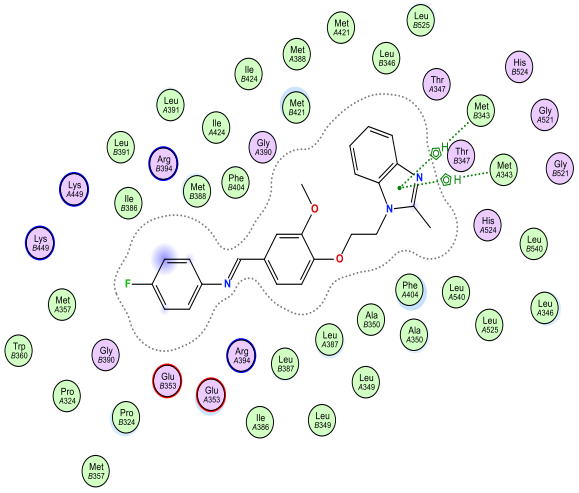

3.6a

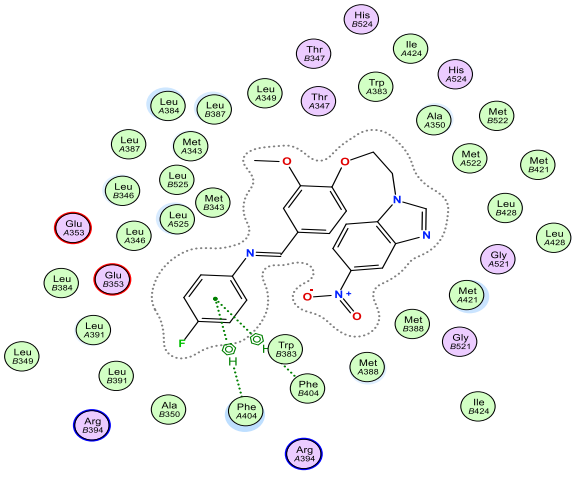

3.6b

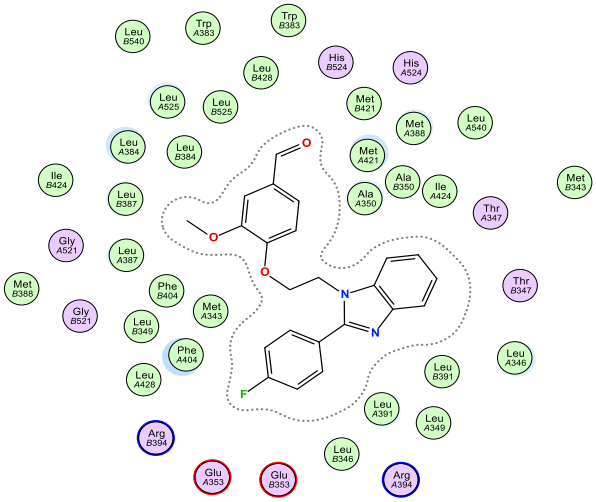

3.6c

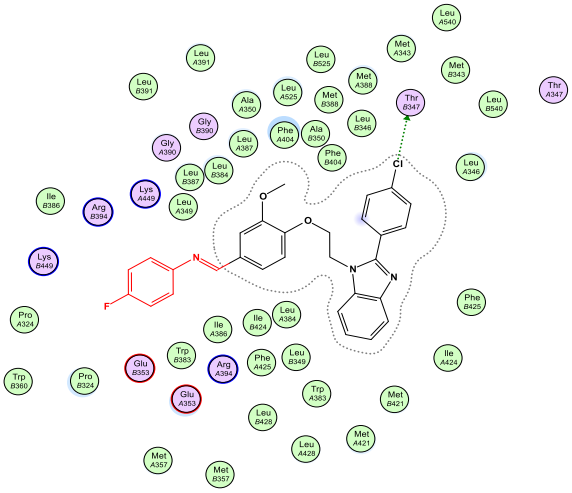

3.6e

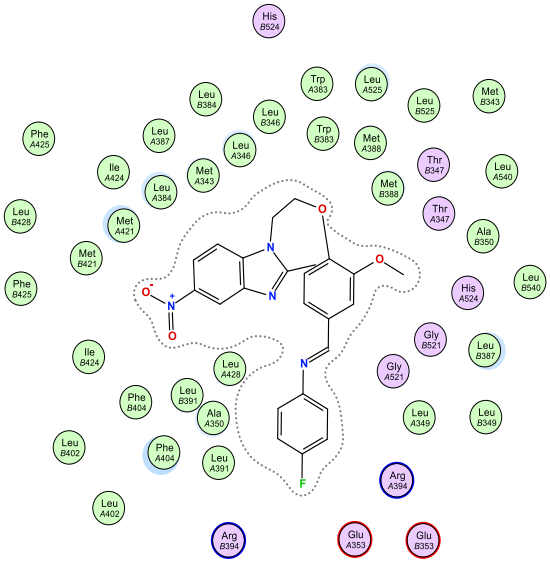

3.6f

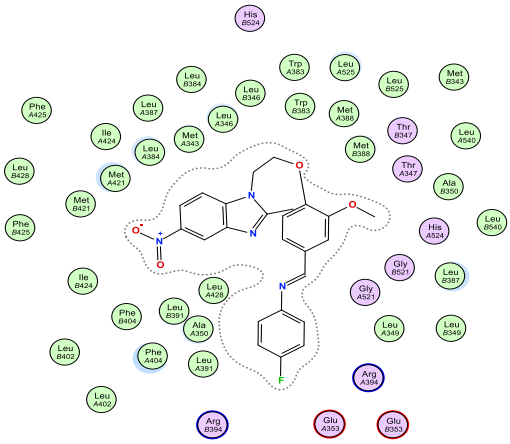

3.4d

Figure 3.18: The binding mode of another target benzimidazoles **3.4d, 3.6a-3.6f,** unto the active site of estrogen receptor (ER) alpha.

3. 9 Synthesis of Derivatives of 2, 5-Disubstituted Benzimidazoles

Despite the undesirable docking scores for most target molecules, we have decided to synthesize all the proposed 2,5-disubstitued benzimidazole derivatives **3.6a-f**, Scheme 3.5, with the view that molecular docking studies are solely a prediction strategy. Also, strongly convinced by the positive feedback from literature reports, [179,180,181], we commenced with the synthesis of the envisaged target compounds, which followed a synthetic pathway as outlined in Scheme 3.5.

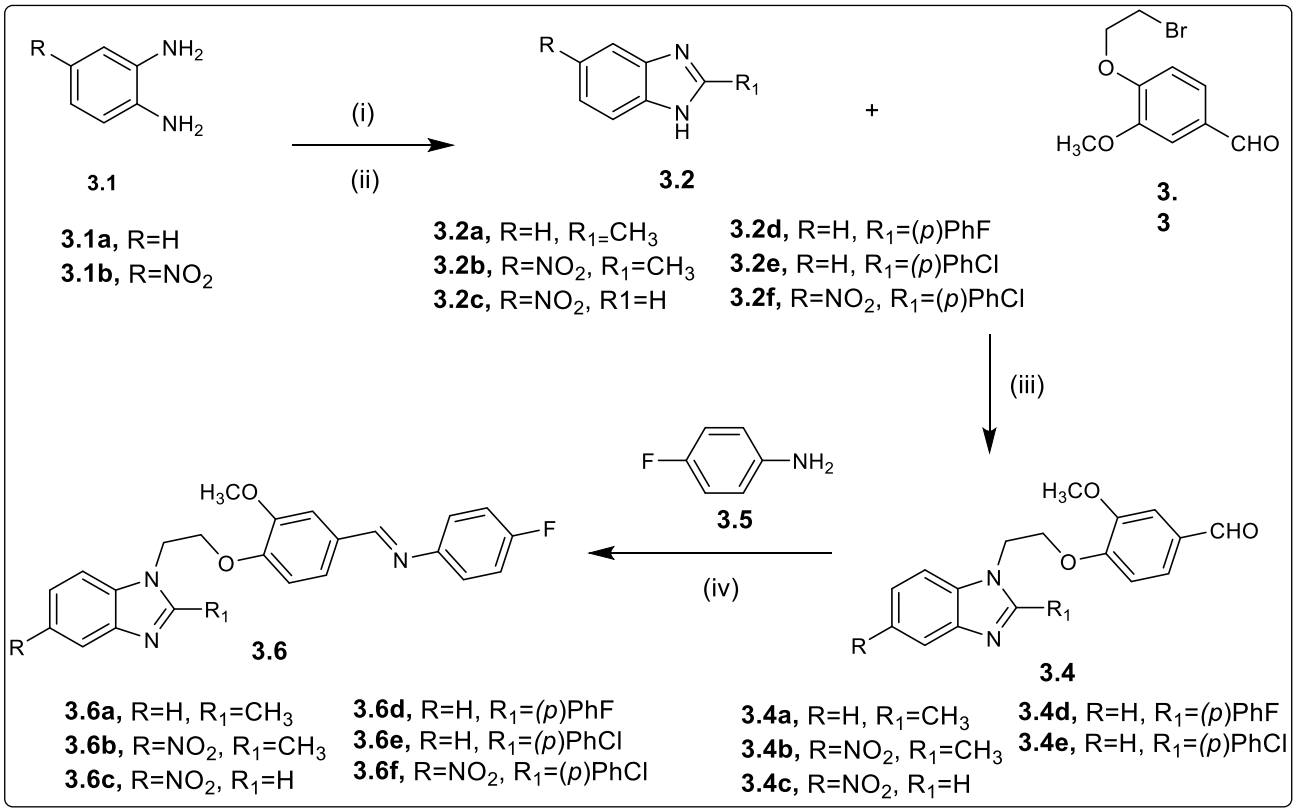

Scheme 3.5: General synthetic pathway towards the target compounds **3.4** and **3.6**. Reagents and reaction conditions: (i) CH_3COOH or HCOOH, 4N HCl, reflux, 2 h (ii) (p)PhXCHO, $Na_2S_2O_5$, EtOH, DMF, refluxed, 120 ^oC; (iii) KOH, DMSO, refluxed, 70 ^oC, 6 h; (iv) DCM, pyrrolidine 60 ^oC, overnight.

3.9.1 Synthesis of 2-(4-Substituted phenyl) Benzimidazoles via a Cyclo-condensation Reaction

To access the proposed target structures, fluorobenzenamine derivatives **3.6a-f**, Scheme 3.4, we began the reaction pathway with a cyclo-condensation reaction. The amino groups of the phenylenediamines **3.1a-b**, were converted to the respective benzimidazole intermediates **3.2a-f**. This was done by employing various carboxylic acids and aldehydes as the amino acceptors. As depicted in Scheme 3.5, two different reaction procedures (i) and (ii) were followed respectively, to afford the desired intermediates **3.2a-f**, in excellent overall yields (39 – 84%), from the precursors, *o*-phenylenediamine **3.1a** and 4-nitro-o-phenylenediamine **3.1b**. The second method was introduced after countless attempts to complete the envisioned **3.2a-f** series had proven unsuccessful. In the first reaction, (i), various carboxylic acid derivatives were used, in the presence of 4N HCl as a catalyst to form the benzimidazole derivatives **3.2a-c** in moderate to excellent yield (39 – 71%); and in the second reaction (ii), (4-substituted phenyl)-5-substituted-1*H*-benzimidazole derivatives **3.2d-f** in moderate to excellent yield (67 - 85%) were synthesized, using a range of aldehyde derivatives with the support of an oxidizing agent, sodium metabisulfite, $Na_2S_2O_5$.

3.9.1.1 Mechanism for the Cyclo-condensation of Benzimidazole

A lone pair of NH_2 attacks the carbonyl of the carboxylic acid by means of an acid catalyst used (HCl). An acid catalyst's protonation of the OH group leads to the formation of oxygen lone pair, then hydroxyl group leaves, thereby removing water. The second lone pair of NH_2 attacks the carbonyl of the carboxylic acid employing acid catalyst used (HCl), which leads to cyclization, then there is a proton transfer. Finally, the benzo-fused aromatic ring is formed,

the lone pair from nitrogen is pushed into the ring then, OH group leaves,which then captures a protonfrom the formed ringirreversibly forming the benzimidazole.[182]

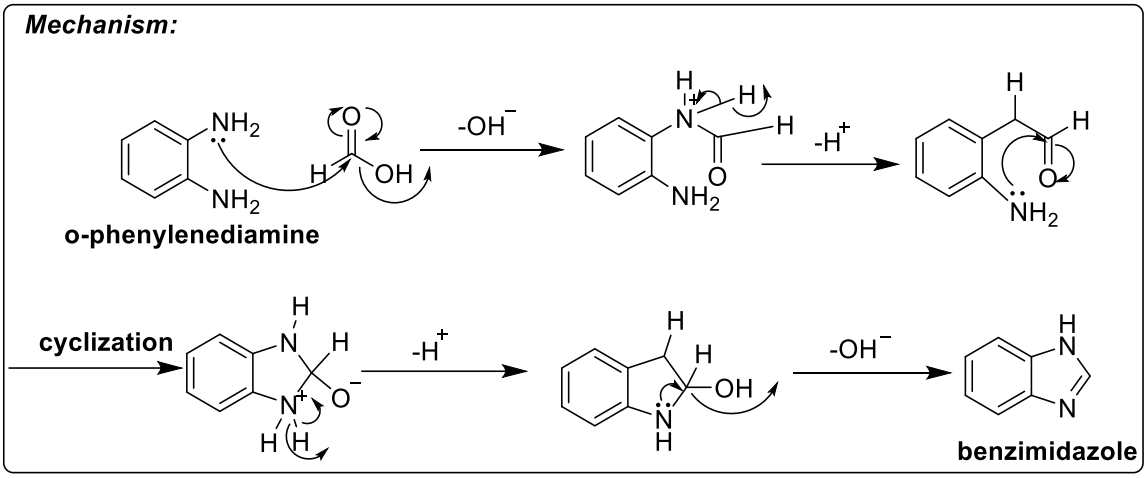

Scheme 3.6: Mechanism for the cyclo-condensation of benzimidazole.

Cyclization of **3.2b** was confirmed with the ^{1}H NMR, which revealed a singlet of imidazole N-H proton, which resonated up-field at 2.09 ppm. Also, a sharp, intense singlet of three protons of n methyl substituent at position 2 of the benzimidazole was noticed at a chemical shift value of 2.51 ppm, Figure 3.19.

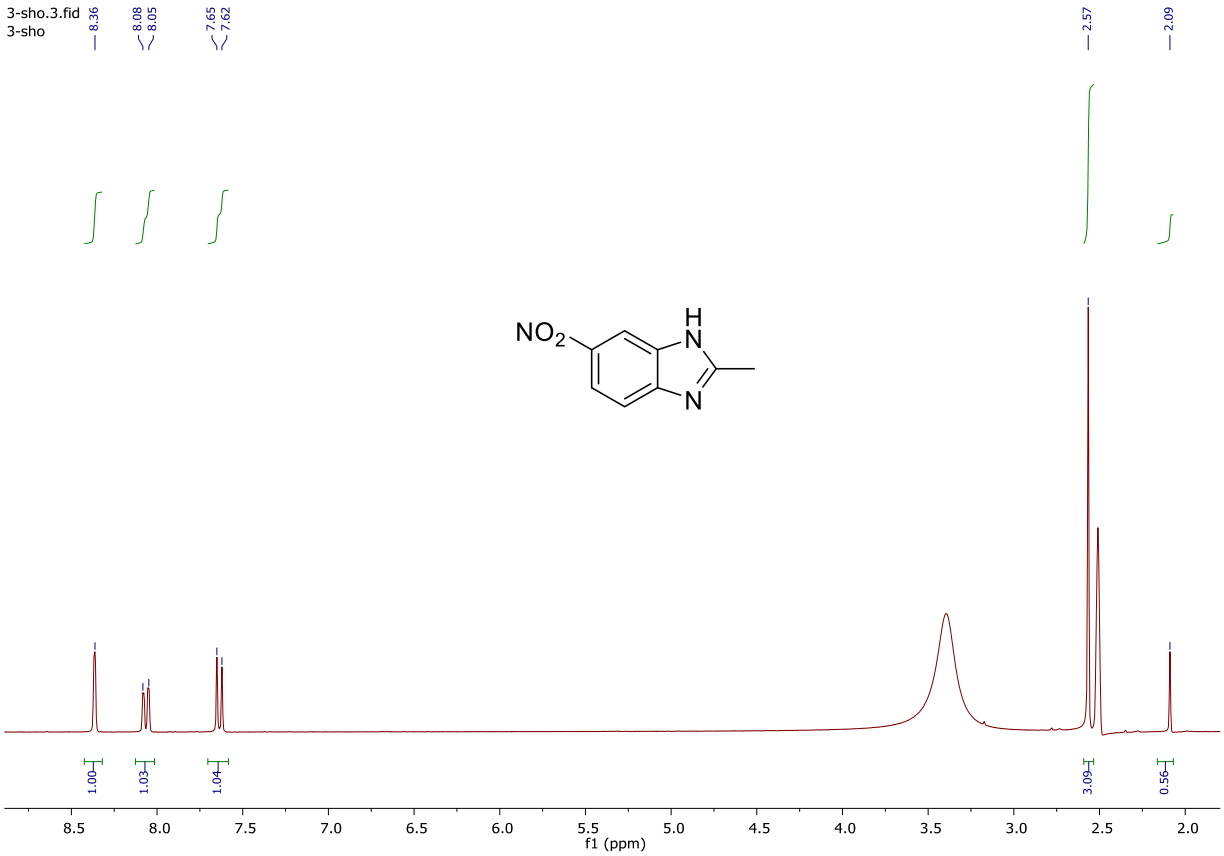

Figure 3.19: ^{1}H NMR (DMSO-d_6, 400 MHz) of compound **3.2b**

3.9.2 Williamson Ether Synthesis of 4-(2-Bromoethoxy)-3-Methoxybenzaldehyde (Vanillin Linker)

With the intention to incorporate the first phenyl group onto the benzimidazole framework, the aryl containing methyll halide **3.3**, Scheme 3.4, was prepared from vanillin by a Williamson ether synthesis reaction. Vanillin was treated with 1,2-dibromoethane in dry acetone at reflux condition of 70°C for 24 h, in the presence of a base, to afford the aldehyde **3.3**, in a moderate yield (41%).

^{1}H NMR of **3.3** revealed two –CH_2 triplets of the ethoxy group seen at δ 3.72 and δ 4.44 ppm, respectively, with a coupling constant of 7.2 Hz. The coupling constants showed that two (CH_2) are neighbors to each other, thereby establishing spin-spin interaction, as shown in Figure 3.20.

The chemical shift value of two protons of CH_2-O is more de-shielded and therefore resonated more downfield (δ 4.44 ppm) than that of the two protons of CH_2-Br, which appeared at δ 3.72 ppm as being a bit more up-field. This is because oxygen is more electronegative than bromine. The IR showed the disappearance of the OH strong absorption band around 3300 -3500 cm^{-1}.

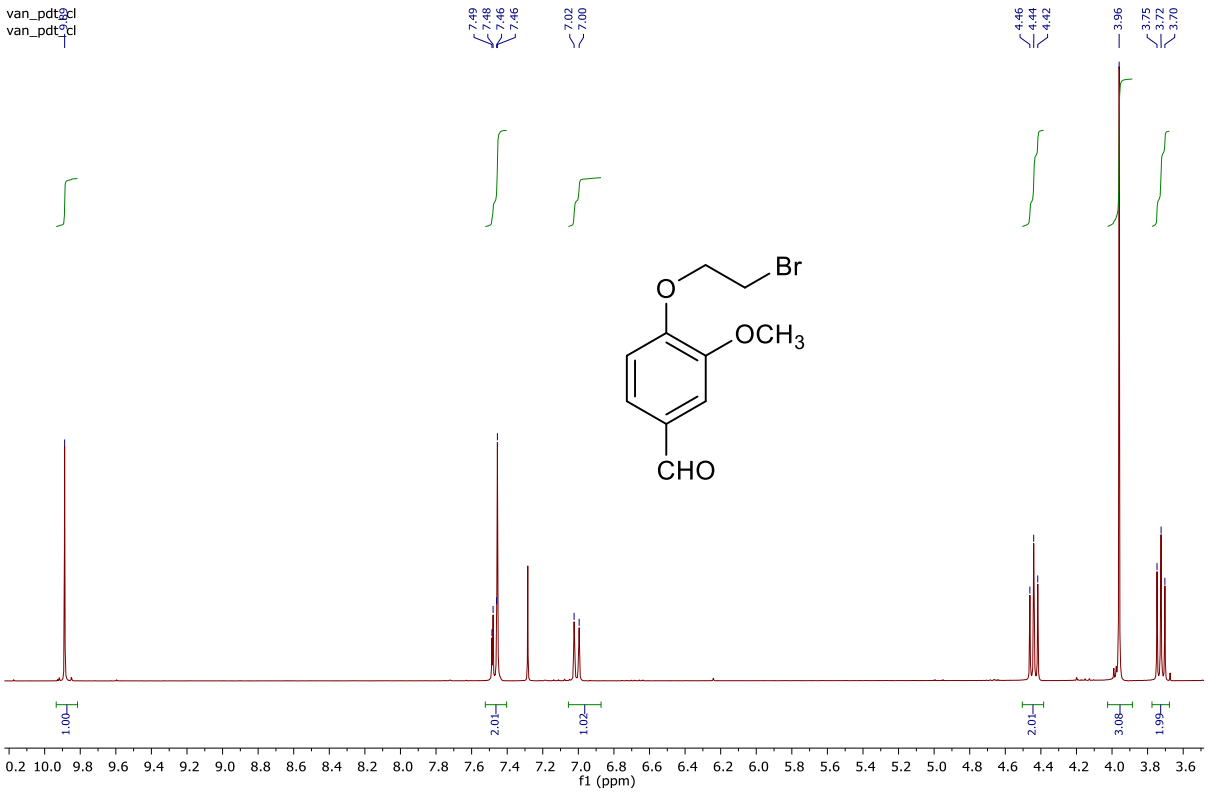

Figure 3.20: ^{1}H NMR of Compound **3.3** (300 MHz, DMSO-d_6)

3.9.3 Synthesis of the N-alkylated benzimidazoles 3.4a-e

The synthesis of the intermediate compounds, which were **3.4a-e**, included an *N*-alkylation reaction, Scheme 3.4, which involved incorporating the prepared vanillin derived linker, and a **3.3** in all the benzimidazole derivatives **3.2a-f** in a single reaction step. In this reaction, it was

found that finely ground KOH and DMSO as the solvent under reflux gave the best results to afford the *N*-alkylation intermediates **3.4a-e** in overall moderate to excellent yields (39 – 81%).

The formation of the aldehydes, **3.4a-e**, was confirmed with the IR absorption spectra, which revealed an absorption band at 2900 cm^{-1} due to stretching vibration frequency aromatic C-H while stretching vibration frequency of the unconjugated weak bands of CH_2 and CH_3 was seen at 2828 and 2661 cm^{-1} respectively. A strong band at 1699 cm^{-1} confirmed the presence of C=O of the aromatic aldehyde. The ^1H NMR spectrum of compound **3.4a** revealed the two intense sharp singlets at δ 2.67 and δ 3.80 ppm, respectively, ascribed to the three methyl protons substituent on the imidazole ring of the benzimidazole moiety and three methoxy protons attached to the vanillin ring. Also, two CH_2 proton triplets of the ethoxy group were observed at δ 4.38 and δ 4.74 ppm with coupling constants of 4.7 Hz. The proton of the aldehyde functional group on the vanillin moiety is seen downfield as a singlet at 9.81 ppm. The other seven peaks, which appeared between δ 7.08-7.61 ppm, were assigned as the aromatic protons found in the benzimidazole and vanillin moieties.

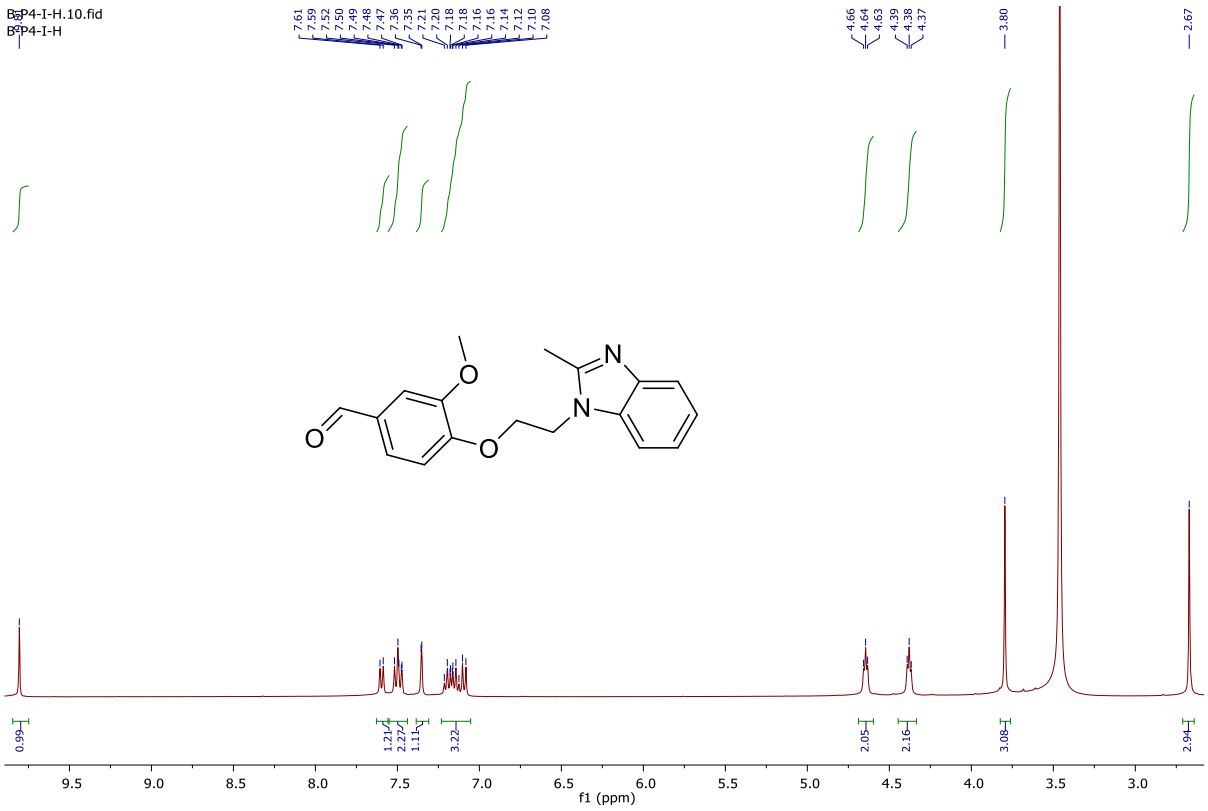

Figure 3.21: ^{1}H NMR of Compound **3.4a** (400 MHz, DMSO-d_6)

The ^{13}C-NMR spectrum of **3.4a** revealed the presence 18 carbon atoms ranging from 13–191 ppm. Out of these, thirteen peaks are found at δ 110–153 ppm, and these include seven tertiary carbons and five quaternary carbons, attributed to the aromatic carbons on the benzimidazole and vanillin moieties. Moreover, the peaks at δ 13. 7 and δ 56.0 ppm accounted for the signals of methyl carbon on the imidazole ring and methoxy carbon on the vanillin ring, respectively Figure 3.22. Furthermore, two carbon atom signals of the two -CH2 of the ethoxy group are seen at 43.1 and 67.5 ppm, respectively Figure 3.22.

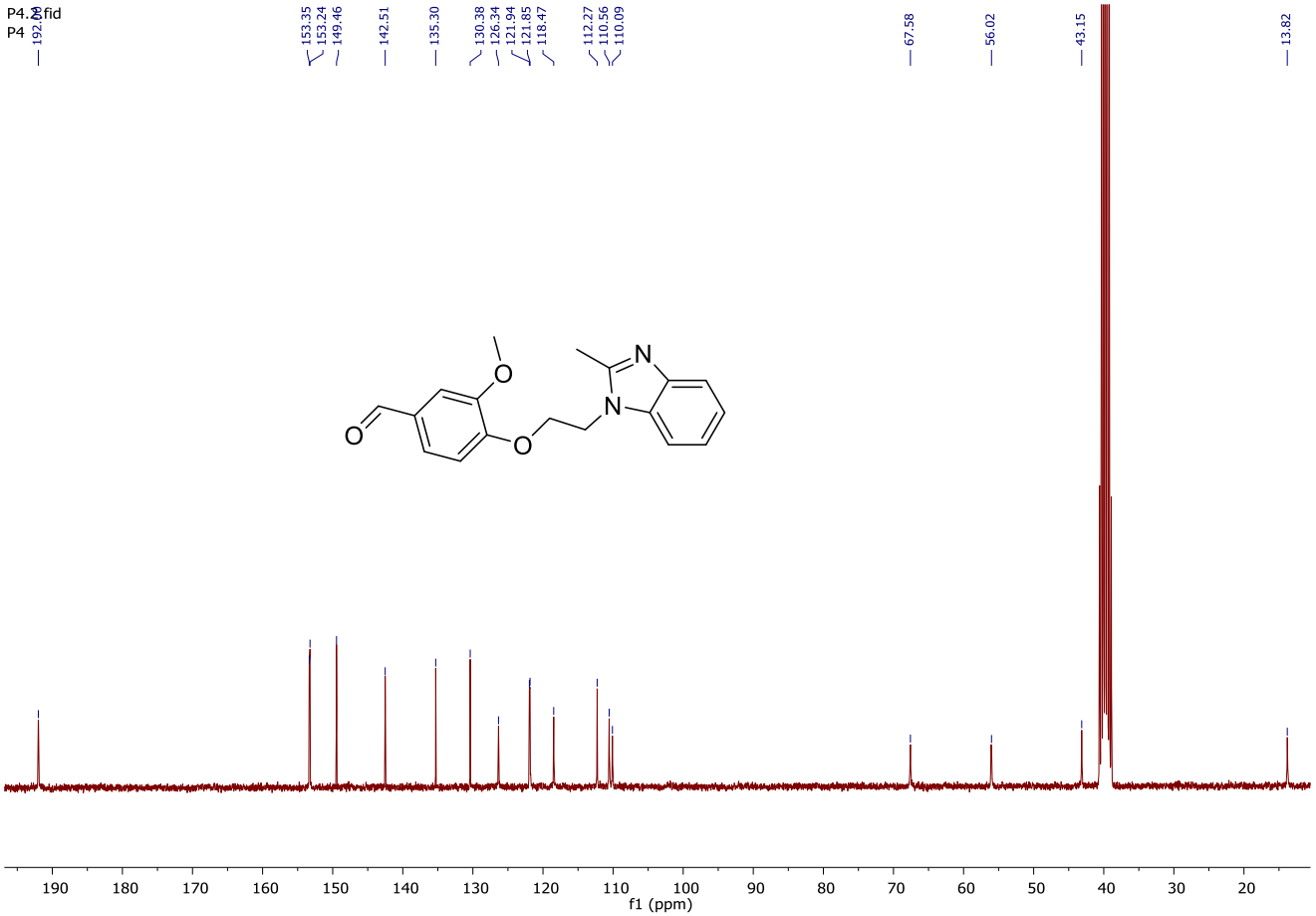

Figure 3.22: ^{13}C NMR of Compound **3.4a** (100 MHz ,DMSO-d_6)

Finally, the mass spectroscopic data of **3.4a** revealed the molecular ion peak at m/z (m+1) 311, which corresponds to the molecular mass of the compound **3.4a** ($C_{18}H_{18}N_2O_3$).

3.9.4 Synthesis of Target Compounds 3.6a-e

The target molecules **3.6a-e** in this chapter are otherwise known as Schiff bases. The reaction to the target compounds proceeded through the nucleophilic addition reaction of aldehydes **3.4a-e**, and 4-fluoroaniline **3.5** in the presence of 10 drops of pyrrolidine, (Scheme 3.4.) The reactions were successful when pyrrolidine was employed as the catalyst, giving moderate-low to excellent yields (33 – 87%) in the absence of harsh acids, metals, and minimum experimental manipulation. However, no product formation was observed when the reaction was done in the

absence of the pyrrolidine catalyst. This essential step in the reaction pathway was only noted after countless failed attempts to synthesize the target molecules.

3.9.4.1 Synthesis of Aldimines or Schiff base via Nucleophilic Catalysis of Pyrrolidine

A nitrogen analog of a ketone or an aldehyde is referred to as a Schiff base. Here, imine (C=N) functionality is used in place of the carbonyl (C=O) group. Under a nucleophilic condition, Schiff bases are prepared from the condensation reaction of aldehyde or ketone and a primary amine. As a result of the effective conjugation, an aryl Schiff base (as in the case with these target compounds **3.6a-f**) tends to be more stable and could easily be made than an aliphatic Schiff base. In this work, as alluded to before, the success of the formation of the products depended on the treatment of the aldehydes **3.4a-e** with the pyrrolidine catalyst, Scheme 3.9. The mechanism is initiated by the interception of pyrrolidine with the aldehydes **3.4a-e** to give rise to the iminium ion, as depicted in Scheme 3.9. Further reaction with the primary amine, 4-fluoroaniline **3.5** with the loss of water, afforded the intermediate aminal, which gave the desired aldimines **3.6a-f**. On completion of the catalytic process, pyrrolidine was liberated to be used again in the process.[181] Then, there is a favorable attack of the primary amine derivative to the electrophilic iminium ion. Thus, aminal is transformed into a four-membered transition state.

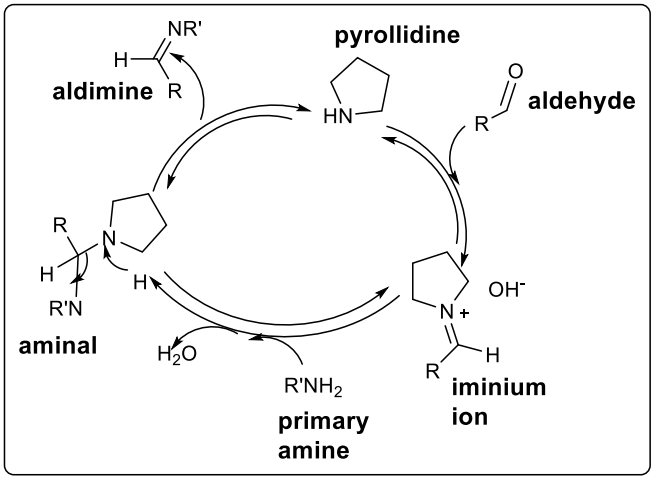

Scheme 3.7: Nucleophilic Catalysis used by Pyrrolidine

The formation of the target compounds **3.6a-e** was further determined by the IR absorption spectrum, which displayed similar characteristic bands to their precursors, except for notable changes which showed the disappearance of the strong band due to the C=O of aldehyde and appearance of the medium band with stretching frequency between 1640 - 1634 cm^{-1} which is characteristic of the C=N stretch, Figure 3.23, and this conforms with the literature.[183] This confirmed the successful conversion of carbonyl (C=O) to imine (C=N) functionality.

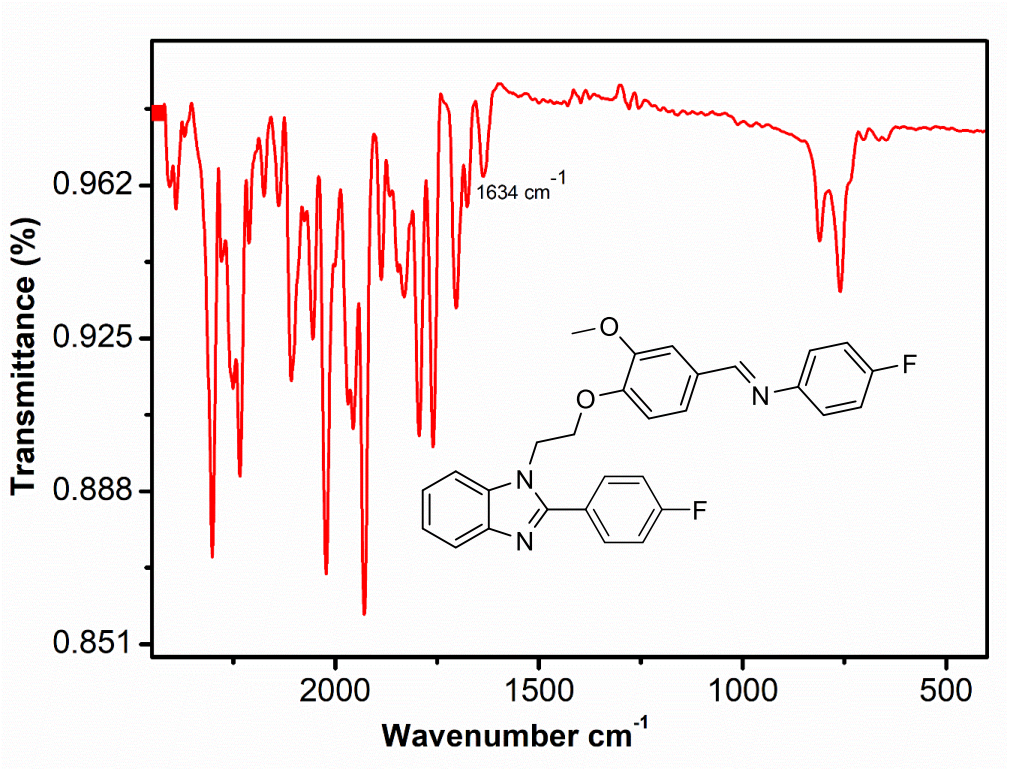

Figure 3.23: Infra-red Spectrum of Compound **3.6d**

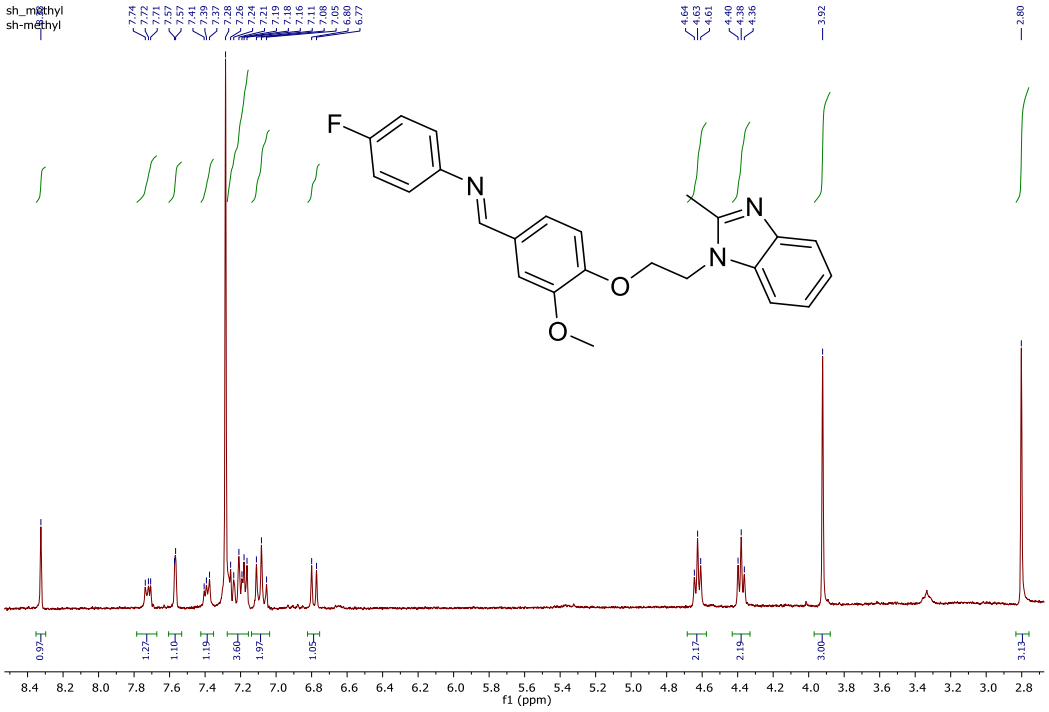

Figure 3.24: ^{1}H NMR of Compound **3.6a** (400 MHz, DMSO-d_6).

In summary, all synthesized **3.1a-b, 3.2a-f,** and target molecules, which were **3.4a-e, 3.6a-e,** were characterized with IR, ^{1}H, and ^{13}C NMR analysis. The ^{1}H NMR spectra of the compounds were run in $CDCl_3$ and DMSO-d_6 at 300 and 400 MHz, respectively, with chemical shift values (δH/C) documented in ppm. Using compound **3.6a** as a reference Figure 3.24, the methyl CH_3 group substituted on position 2 of the 2-methylbenzimidazole ring of **3.2a, 3.4a**, and **3.6a** all resonated up-field at 2.50, 2.67 and 2.70 ppm respectively as 3H singlets while the CH_3 linked on the 2-methyl -5-nitro benzimidazole ring resonated up-field at δ 2.51, 2.76, 2.78 ppm respectively as 3H singlet for compounds **3.2b, 3.4b,** and **3.6b**. The methoxy-linked OCH_3 of compound **3.3** resonated up-field at δ 3.96 ppm, while the aromatic aldehyde was observed downfield at δ 9.89 ppm as singlet and the 2 x (CH_2) of the bromoethylene linker in compound **3.3** were found as 2H triplets at δ 3.72 and 4.44 ppm respectively. The aldehyde signals of compounds **3.4a, 3.4b, 3.4c, 3.4d**, and **3.4e** all appeared downfield between δ 9.80-9.82 ppm as singlets, while their aryl methoxy groups were observed upfield between δ 3.73-3.80 ppm respectively as singlets and their 2 x (CH_2) signals of the ethylene linker in these compounds were all found between 4.11 – 4.82 ppm respectively. All the aryl H signals were noticed downfield of around δ 6.68–8.71 ppm, the NH of the imine functional group in compounds **3.6a, 3.6b, 3.6c, 3.6d, 3.6e**, and **3.6f** appeared downfield as singlets between δ 8.23-8.24 ppm respectively. The ^{13}C NMR spectra were run in $CDCl_3$ and DMSO-d_6 at δ 300 and 400 MHz, respectively, with chemical shift values documented in ppm. In all, the ^{13}C NMR spectra of the structural benzimidazole derivatives range from 13.82 for CH_3 of compound **3.4a** to 192 ppm for the aryl CHO of compound **3.4a**. Unambiguously, the 2-methyl-linked imidazole CH_3 of compounds **3.4a, 3.4b, 3.4d,** and **3.4e** resonated at δ13.87–14.37 ppm. The formation of the ethylene linker on the imidazole ring of compounds **3.4a, 3.4b, 3.4c, 3.4d,** and **3.4e** was validated by the appearance of the CH_2 signals at δ 43.31 - 66.45 ppm, which was absent in the

precursors **2a, 2b, 2c, 2d, 2e, 2f.** The formation of imine in **3.6a, 3.6b, 3.6c, 3.6d, 3.6e, 3.6f** was further confirmed by the presence of C=N signal at δ 160.00- 162.00 ppm as seen in Figure 3.24 for compound **3.6a**, which was not present in the precursors **3.4a, 3.4b, 3.4c, 3.4d,** and **3.4e** respectively from which they were derived.

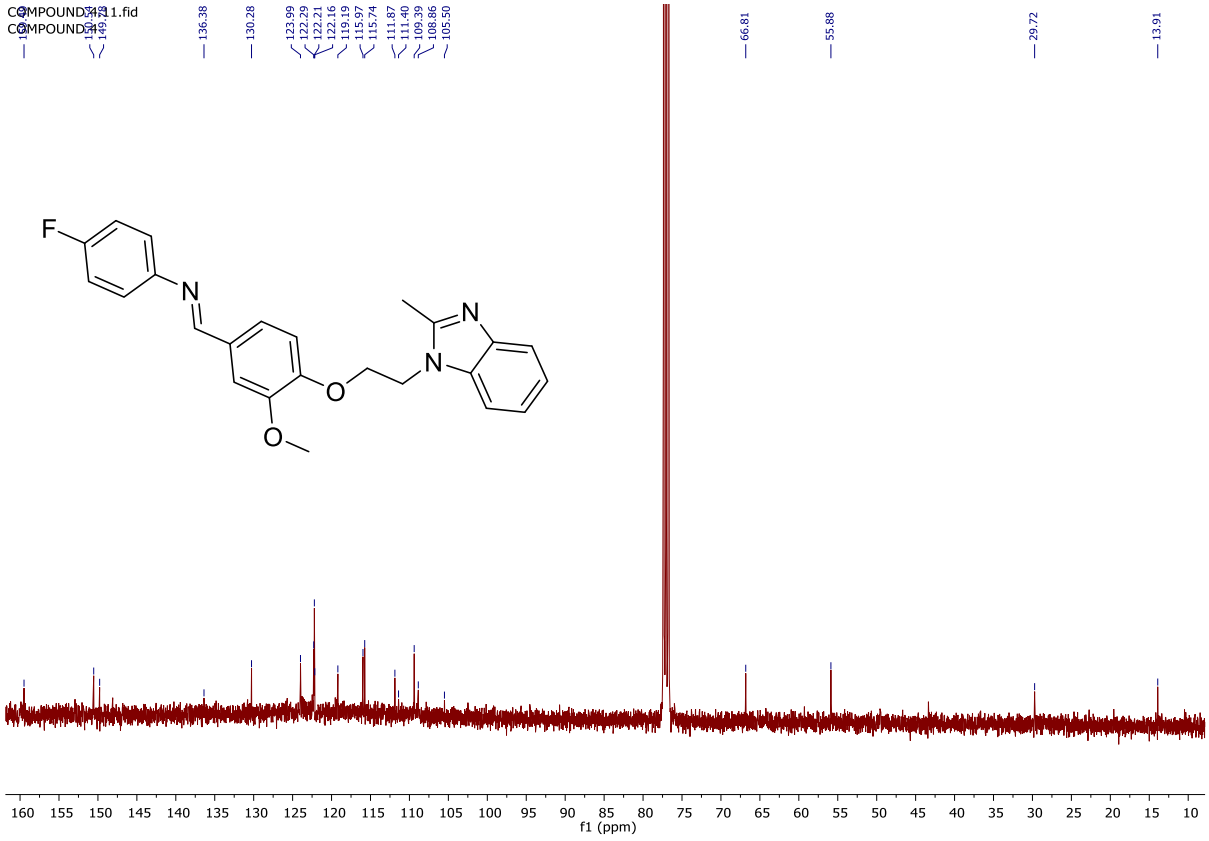

Figure 3.25: ^{13}C NMR of Compound **3.6a** (100 MHz , DMSO-d_6)

The details of the ^{1}H NMR, ^{13}C NMR, and mass spectra are mentioned in the experimental section.

3.10 Cytotoxicity

The preliminary cytotoxicity of target benzimidazoles were accessed by Harshini Mehta at the Department of Biochemistry, Genetics and Microbiology, University of Pretoria. The target compounds **3.4a-d, 3.6b-c, 3.6e-f** were assessed against breast cancer cell line MCF-7, using MTT cell viability assay. The biological screening result is summarized and shown in Figure 3.26. The results revealed that the benzimidazoles derivatives **3.4a-d, 3.6b-3.6f**, even at all concentrations (0.195-100 ug/mL), were unable to induce cell death, nor displayed the cytotoxic effect above 25%, in all cases when compared to the standard, camptothecin which induces cell death at 57% (at 0.08 ug/mL). The absorbance of the plate at 570 nm was measured with a plate-reader. The percentage of cell viability was calculated using the formula below.

$$Percetage\ Cell\ Viability = \left(\frac{Absorbance\ of\ Test\ sample - Absorbance\ of\ Blank}{Absrobance\ of\ Untreated\ sample - Absorbance\ of\ Blank}\right) \times 100$$

Unfortunately, the IC_{50} of the target compounds could not be determined since none of the target compounds gave 50% cell viability or induces cell death at 50%.

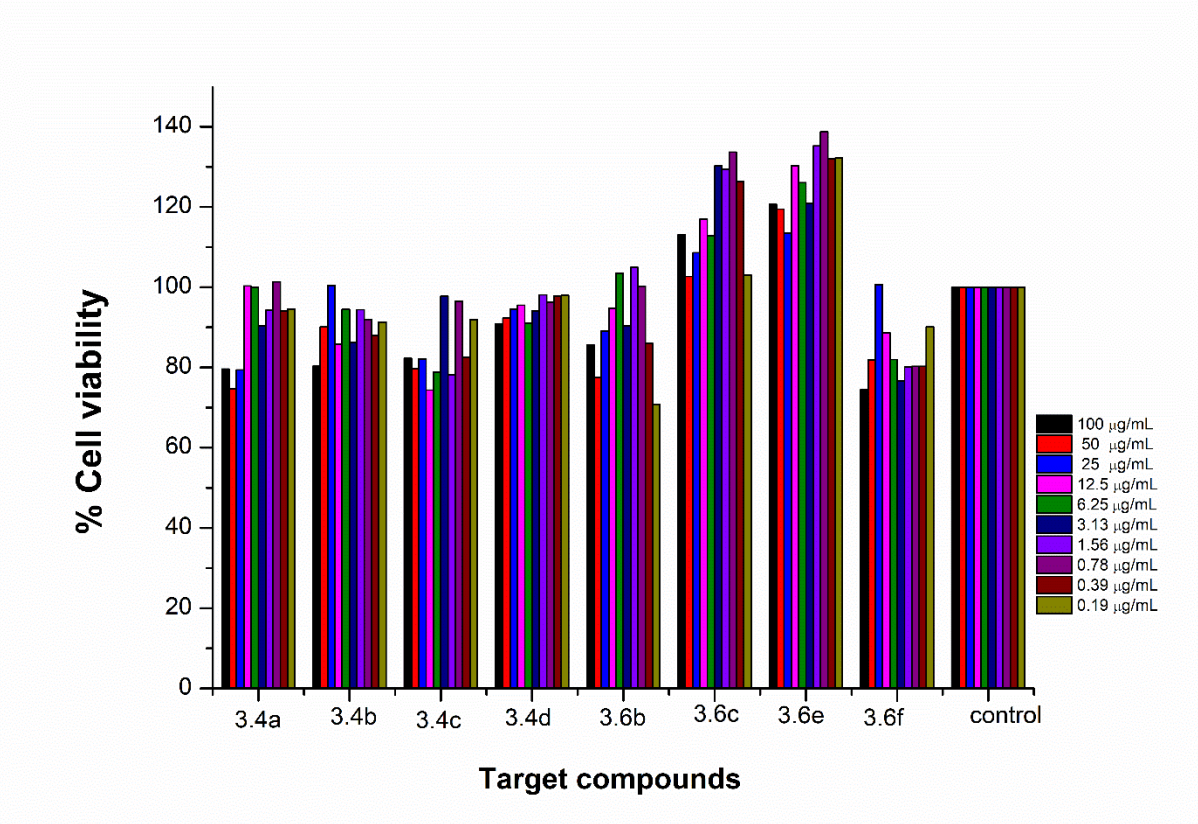

Figure 3.26: Cytotoxicity screening of target compounds

3.11 Conclusion

A library of 2-disubstituted benzimidazole derivatives was successfully synthesized with the use of a pyrrolidine catalyst, which seemed to be the key factor in ensuring the success in the formation of the final products. The target compounds were designed using the reported literature as a guide with respect to their potent anticancer activity and the good docking scores of comparable ligands. Also, in our case the successfully synthesized target compounds were planned to be screened against the breast cancer cell line, MCF-7, as a comparative study. Using a different target as compared to the target used in the prediction molecular docking study, we anticipated that a different outcome in terms of activity could be obtained. Thus, using a reverse docking approach, the target compounds were docked, and the most probable

target is compound **3.4b**, with docking scores of -9,16. This target as mentioned earlier revealed a bond with Arg 394 and π interactions with Leu387and Leu 525. The binding mode and structure analysis showed that some of these benzimidazoles target molecules such as **3.4a, 3.4b, 3.4c, 3.4d, 3.4e, 3.4f, 3.4g,** only form a bond with an amino acid Arg394, which conforms with the binding mode of human estrogen receptor alpha ligand-binding domain in complex with estradiol, while there was no other bonding with other important amino acid residues such as His 524, Glu 353 found in the binding mode of estradiol with the ER-ligand binding. The synthesized compounds were screened for their cytotoxicity activity against MCF-7 cells lines. Still, unfortunately, none of the target compounds, even at all concentration (0.195-100 ug/mL), gave the cytotoxic effect that could be compared to that of the standard drug used, camptothecin which induces cell death at 57% (at 0.08 ug/mL).

The disparity between the molecular docking and bioactivity result could be because some of the target compounds only bind with one amino acid (Arg394) and do not bind with the other two important amino acids (His 524, Glu 353) that estradiol binds to, in the active site of the human estrogen receptor alpha which is responsible for the proliferation of the MCF-7 cells lines. Therefore, in our future work, these target compounds will be modified to be able to bind to the other two amino acids that estradiol binds to, thereby increasing the activities of these target benzimidazoles.

Chapter Four

Synthesis of Quinoxaline-6-Carboxamidine-Urea Based Antimicrobial Compounds

4. Introduction

4.1 The Pathogenic Nature of Microbes

Infectious disease involve the appearance of medical symptoms due to infection, impact, and development of pathogenic biological agents as seen in a specific host organism. Epidemic diseases arise as a result of these pathogenic biological agents.[184] An infectious disease occurs by interaction with microorganisms.[185]

Microbes are also known as micro-organisms, which are either unicellular, multicellular or cell clusters that form the larger part of the earth's ecosystem.[186] Microorganisms do not exist as single species; therefore, they are found in various hosts or environments, which in turn result in microbial interaction with its host or environment.[187] Some microbes exist throughout the human body with essential roles, while some could be harmful to human health.[188] In humans, communities of micro-organisms have complex characteristic mixtures that have co-evolved with their human hosts.[189]

4.1.2 General Characteristics and Classification of Bacteria

Infection is referred to as the arrival, occurrence, and growth of micro-organisms such as bacteria, fungi, and viruses in a human or animal body (and plants), leading to disease.[190] Bacteria are prokaryotic micro-organisms that transmit genetic information in a double-stranded circular molecule of DNA. [191] Bacterial-related diseases are one of the well-known infectious or communicable diseases that can be passed from one person to another by means

of contact with contaminated surfaces, bodily fluids, blood products, insect bites, or through the air. Other examples of communicable diseases are; HIV, hepatitis A, B and C, measles, salmonella, measles, and blood-borne illnesses.[192] Transmission of communicable disease is well known through; faecal-oral, food, sexual intercourse, insect bites, contact with contaminated fomites, droplets, or skin contact. Infectious diseases have been a burden on the world at large.[193] The emergence of infectious disease has impacted the world economies and public health, which is a result of socio-economic, environmental, and ecological factors.[194]

Bacteria are grouped into Gram-positive or Gram-negative based on the features they possess on their cell walls, as seen under a microscope after the administration of stains.[191] The rise in resistant bacteria and the rate at which new and multi-drug resistant species occur is short.[195] To investigate several biologically active compound families against microorganism strains,[196] some methodologies have been established.[197],[198]

4.2 Classification of Antimicrobials and Multi-drug Resistance thereof

Antimicrobials are referred to as any drug agent that possesses the ability to inhibit or eradicate micro-organisms.[199] Also, antibiotic is a word used in place of antimicrobial, and it's otherwise referred to as organic compounds of small molecular weights used in response to some microorganisms.[200] Antibiotic resistance is developed in relation to the presence of DNA in the microorganism and the rate at which DNA is acquired from other microorganisms.[195] This situation has led to a compromised pharmacological activity, thereby affecting the efficacy of antimicrobial drug agents.[199] The increase in prevalent multi-drug resistance microorganisms reported, including *Staphylococcus aureus, Escherichia coli, Staphylococcus epidermidis, Pseudomonas aeruginosa, Enterococcus faecium*, and so on, had been noticed over the years.[201] As a result of the occurrence of multi-drug resistance ravaging globally, there is a

quest for continuous design and discovery of simple new compounds with antimicrobial activities[202]. Therefore, some studies have recently shown the medicinal importance of quinoxaline derivatives through the activity they possess, which include; anticancer,[203] antiviral,[204] antimalarial,[205] antidiabetic,[206] anti-inflammatory,[207] antitubercular,[208] antifungal,[209] and, antimicrobial.[210]

4.3 Chemical Properties and Synthesis of Quinoxalines and their Biological Significance

Quinoxalines are a vital class of nitrogen-containing heterocyclic compounds, otherwise referred to as benzodiazine, or 1, 4-diazanaphthalene. Quinoxalines have two nitrogen heteroatoms at positions 1 and 4 of the benzo-fused diazine nucleus.[211] Quinoxaline **I,** forms isomeric chemical structures with quinazoline **II,** phthalazine **III**, and cinnoline **IV,**[212] as seen in Figure 4.1.

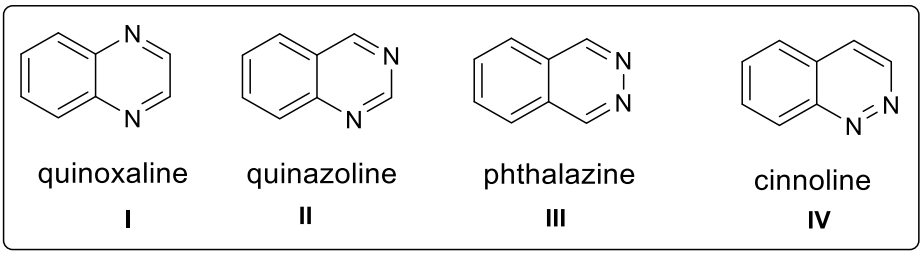

Figure 4.1: Isomeric Chemical Structures of Quinoxalines

Quinoxalines have been found useful and are employed in various fields, which include; agricultural,[213] electroluminescent materials,[214] organic light-emitting devices,[215] organic semiconductor,[215] and indicator dyes,[216] and preparation of azo dyes, fluorescent dyes,[217] pigments,[217] and in medicinal chemistry applications.

Quinoxalines are biologically active compounds that are found in some antibiotics such as; brimonidine, triostin C, varenicline, actinoleutin, and echinomycin, which are generally used in clinical medicine (Figure 4.2).

Echinomycin, also called levomycin, is an antibiotic that prevents the synthesis of microbial RNA through intercalation in double-stranded DNA with the aid of nucleotide sequence selection and act against several transplantable tumors.[218],[219] A number of quinoxaline moieties possess biological activities and are applied in the medical field, which include; anti-inflammatory,[207] anti-diabetic,[206] anti-oxidant,[207] anti-viral,[220] anti-tuberculosis, anti-protozoal,[221] antimalarial[205], anti-depressant, and anti-microbial properties.[201] An increase in allergies and complications of the respiratory system has been traced to the long-lasting use of antimicrobial drugs, which has affected people globally.[222] Therefore, researchers have employed various approaches to design quinoxaline derivatives, including molecular docking tools.

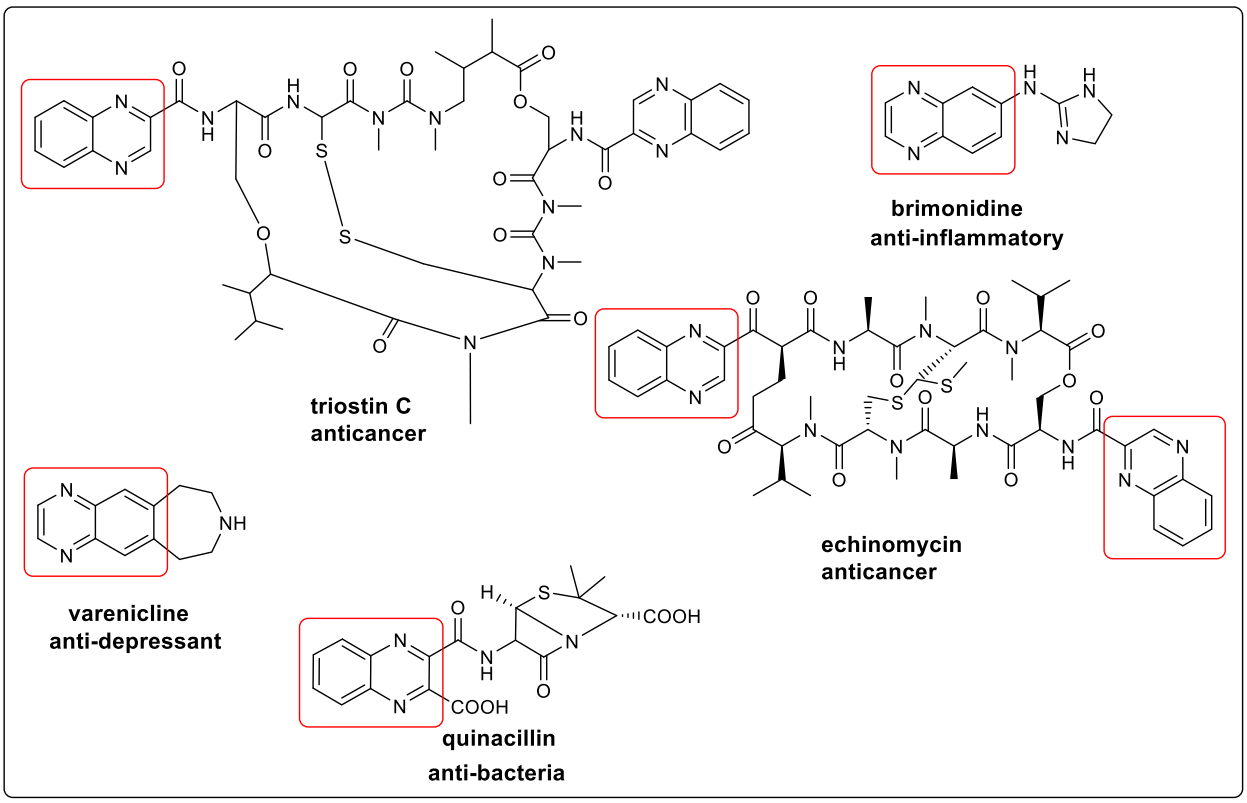

Figure 4.2: Chemical Structures of Some Quinoxaline-based Drugs.[223,224,210]

4.3.1 Some Synthetic Approaches used in the Synthesis of Quinoxaline and its Derivatives

Various synthetic approaches and strategies have been employed in the synthesis of quinoxaline and its derivatives. Ruiz *et al.* [225] investigated the use of recyclable alumina-supported molybdophosphovanadate catalysts to synthesize 2,3-diphenylquinoxaline **III** at room temperature, providing excellent yields Scheme 4.1.[225]

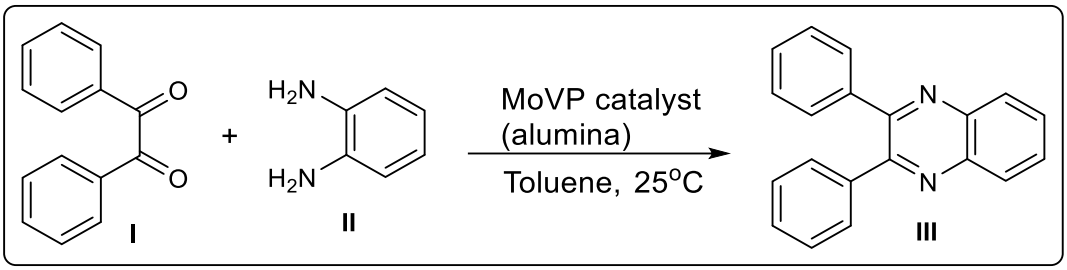

Scheme 4.1: Synthesis of 2,3-diphenylquinoxaline **III**, by means of recyclable alumina-supported molybdophosphovanadates catalysts

Nakhate *et al.* [226] also prepared a series of quinoxaline derivatives via the oxidative coupling of o-phenylenediamines (OPD) with terminal alkynes in the presence of copper-alumina (Cu-Al) catalyst, Scheme 4.2.[226]

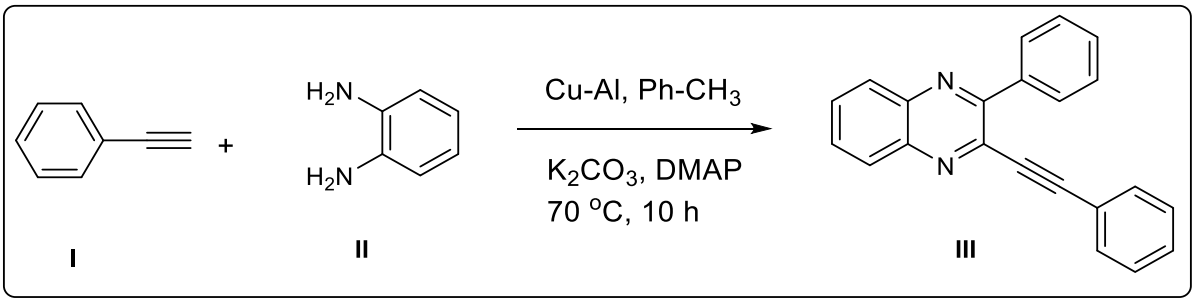

Scheme 4.2: Synthesis of 2-phenyl-3-(2-phenylethynyl) quinoxaline, III via oxidative couplings[226]

One-pot cascade synthetic method was used, which involved the removal of an acidic group of α-aminoxylated dicarbonyl compounds to afford 1,2,3-tricarbonyl compounds, which in-turn underwent condensation reaction with *o*-phenylenediamine to give compound **III**, Scheme 4.3.[227]

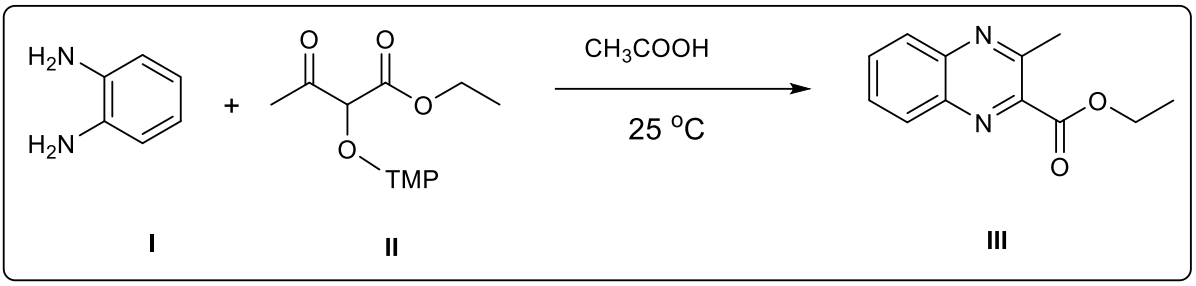

Scheme 4.3: Cascade synthesis of ethyl 3-methylquinoxaline-2-carboxylate, **III**

Rouhani *et al*.,[228] used a reusable catalyst, perlite–SO_3H nanoparticles, to prepare quinoxaline derivatives following a three-component reaction of *o*-phenylenediamine, aromatic aldehydes, and cyclohexyl isocyanide in ethanol under ultrasound irradiation to yield the quinoxaline amine **IV**, Scheme 4.4.

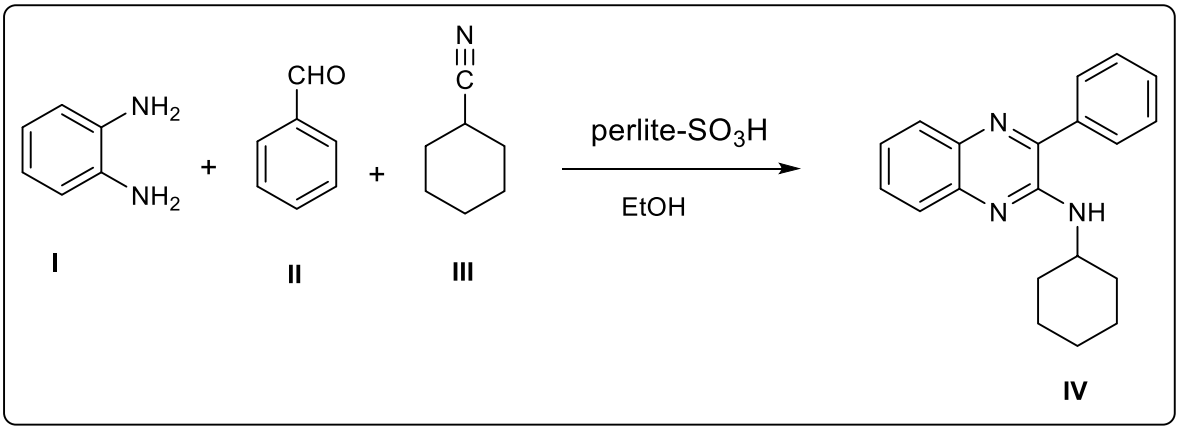

Scheme 4.4: A three-component reaction synthesis of *N*-cyclohexyl-3-phenylquinoxalin-2-amine, **IV**

Quinozaline moieties were synthesized by direct condensation of substituted aromatic 1,2-diamines with 1,2-dicarbonyl in the presence of an eco-friendly re-usable nano-structured nanoparticle, pyrophosphate $Na_2PdP_2O_7$, Scheme 4.5.[229]

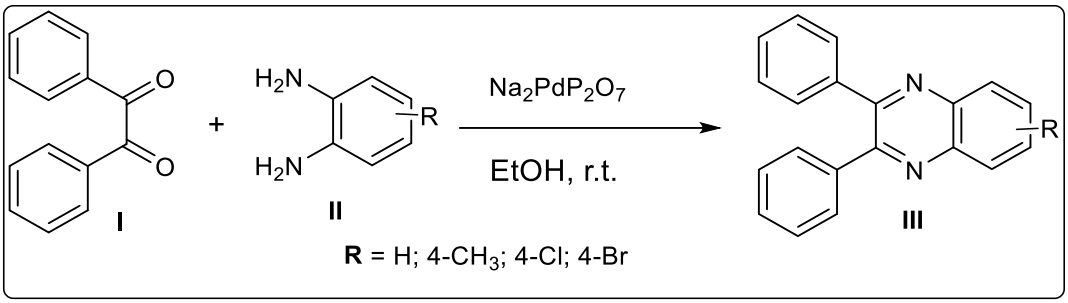

Scheme 4.5: Synthesis of 2,3-diphenylquinoxaline, **III** *via* Pd nanoparticles.[229]

A solvent-free approach was used to prepare quinoxaline derivatives in the presence of Brønsted acidic ionic liquid (BAIL). This method afforded quinoxaline derivative **III** in high yields within a short period (30 mins) Scheme 4.6.[230]

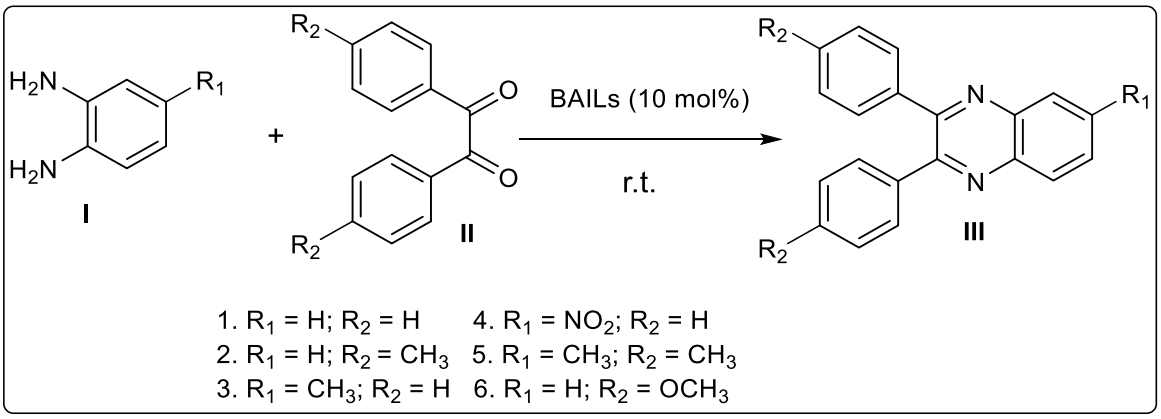

Scheme 4.6: Solvent-free synthesis of quinoxaline, **III.**[230]

4.4 Synthesis of Quinoxaline-6-carboxamidine-urea based Compounds 4.5a-f

In this work, we designed and synthesized a series of quinoxaline-6-carboxamidine-urea based derivatives as an extension of previous findings, which have highlighted their antimicrobial inhibitory significance. Scheme 4.7 depicts the overall synthetic pathway towards the synthesis of the target compounds **4.5a-f**.

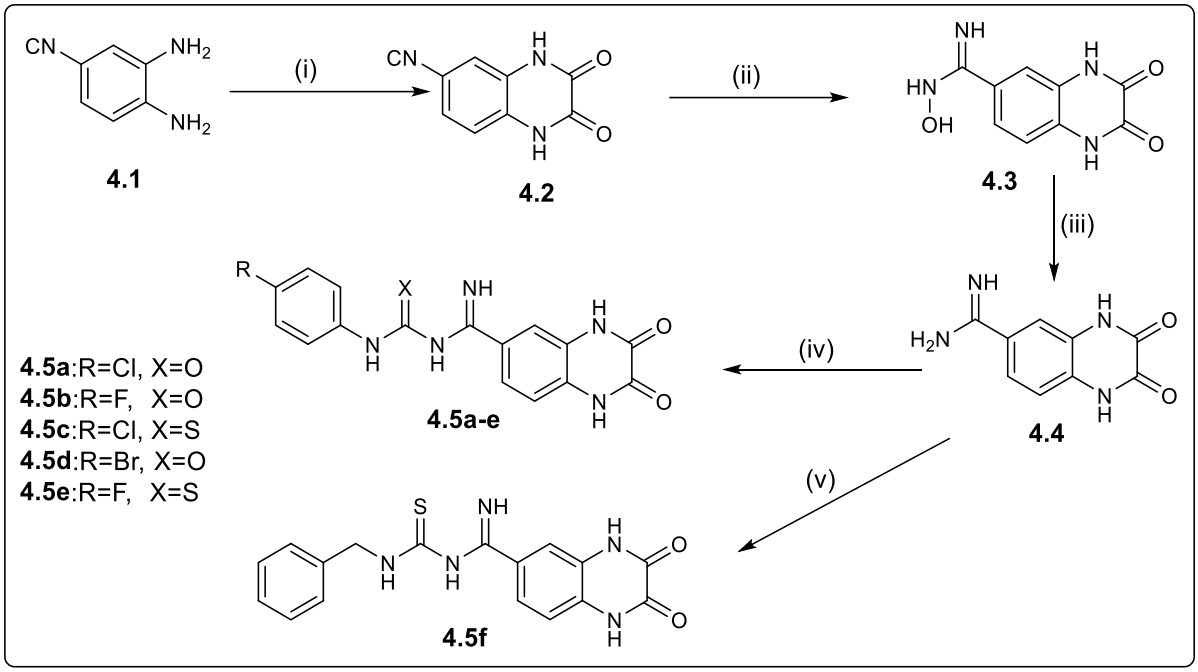

Scheme 4.7: Synthetic path towards target Compounds. Reaction condition (i) oxalic acid, HCl, reflux, 100 ^{o}C, 3 h; (ii) hydroxylamine hydrochloride, KOH, 60 ^{o}C, 16 h; (iii) Pd/C, AcOH, N_2, 120 ^{o}C, 3 h; (iv) arylisocyanate/isothiocyanate, DMSO, Et_3N, 50 ^{o}C, 24 h; (v) benzylisothiocyanate, DMSO, Et_3N, 50 ^{o}C, 24 h.

4.4.1 Synthesis of 6-Isocyanoquinoxaline-2,3(1*H*,4*H*)-dione, 4.2.

Thus, following the synthetic pathway in Scheme 4.7, commercially available 3, 4-diaminobenzonitrile **4.1** underwent a cyclo-condensation reaction with oxalic acid in the presence of aqueous hydrochloric acid to afford the diketone derivative **4.2**.

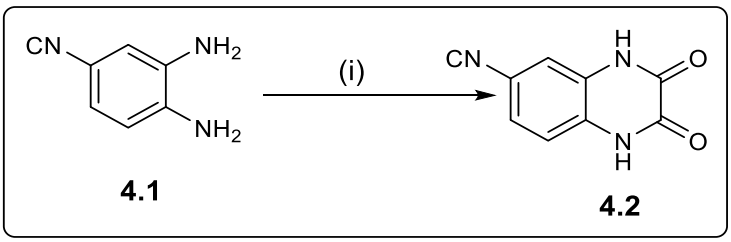

Scheme 4.8: Synthesis of 6-isocyanoquinoxaline-2,3(1*H*, 4*H*)-dione, compound **4.2**. Reaction condition: (i) oxalic acid, HCl, reflux, 100 ^{o}C, 3 h

The formation of compound **4.2** was confirmed with the ^{1}H NMR spectroscopy, which revealed the presence of two singlets corresponding to the two N-H groups of the amide groups of compound **4.2,** resonating at 12.11 and 12.24 ppm, respectively, as seen in Figure 4.3.

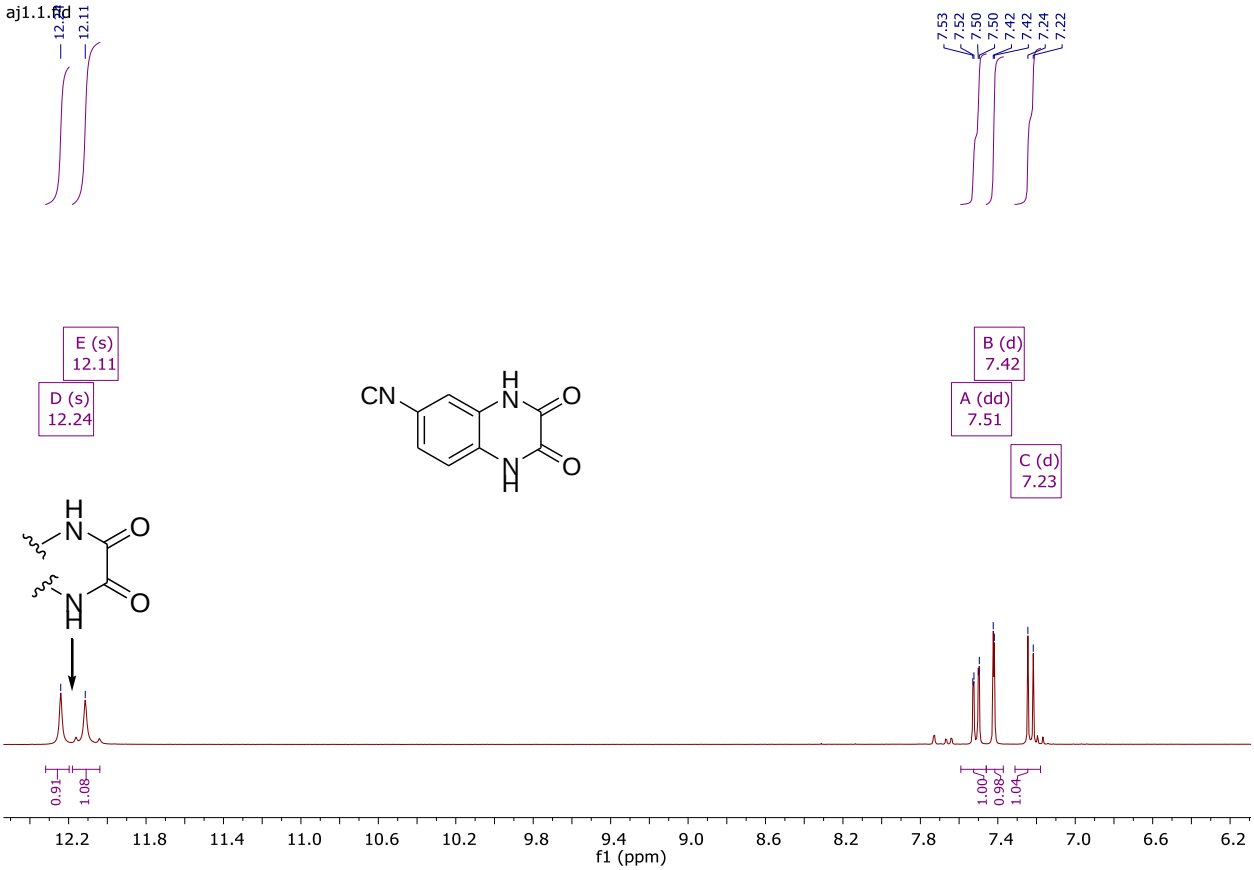

Figure 4.3: ^{1}H NMR of **4.2** (400 MHz, DMSO-d_6)

In addition, further confirmation was provided by ^{13}C NMR spectrum, which revealed the presence of the two C=O of the amide groups, having the highest signals at 155.29 and 155.60 ppm, respectively, as seen in Figure 4.4.

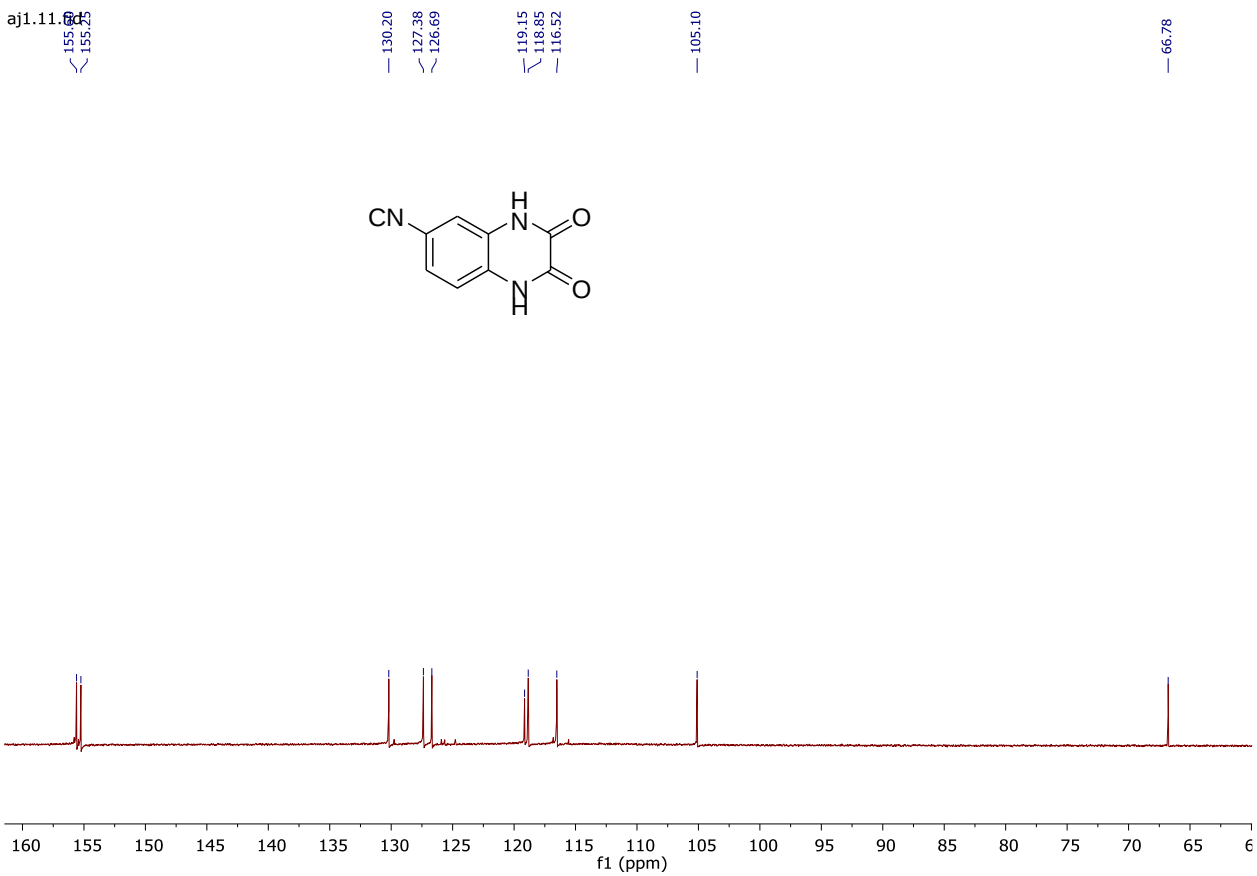

Figure 4.4: ^{13}C NMR of **4.2** (100 MHz, DMSO-d_6)

4.4.2 Synthesis of Amidoxime Derivative, 4.3 of the Quinoxaline-2,3-dione

Amidoximes are molecules containing an amino and hydroxyamino functionality on the same carbon atom, which resembles amides, amidines, and hydroxamic acids.[231] The chemical reaction mechanism involves the nucleophilic attack of the amino group of the hydroxylamine on a nitrile.[232] The nucleophilicity of the nitrogen on the hydroxylamine is increased with the presence of oxygen Scheme 4.9.[233]

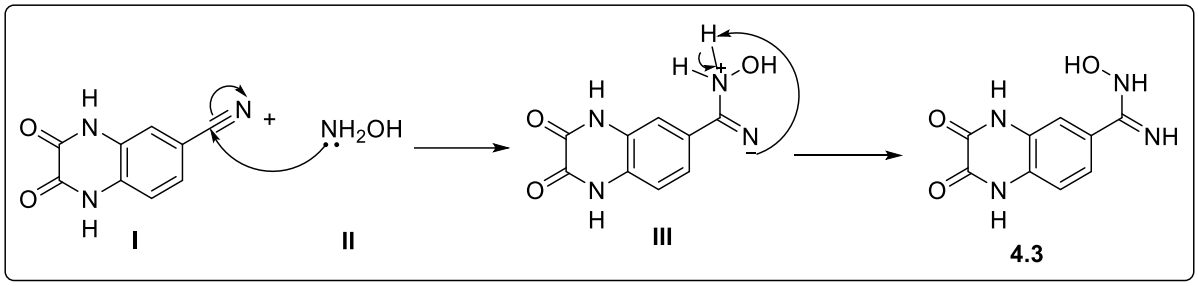

Scheme 4.9: Reaction Mechanism for the formation of 1,2,3,4-tetrahydro-*N*-hydroxy-2,3-dioxoquinoxaline-6-carboxamidine, **4.3**

Subsequently, the quinoxaline-amidoxime derivative was synthesized by treating compound **4.2** with hydroxylamine hydrochloride in the presence of alcoholic KOH.

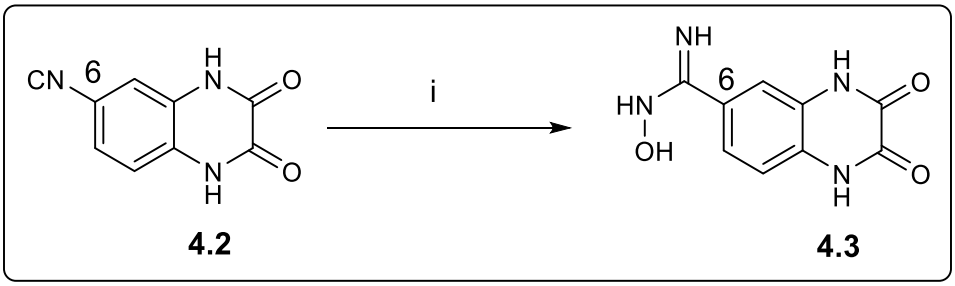

Scheme 4.10: Synthesis of 1,2,3,4-tetrahydro-*N*-hydroxy-2,3- dioxoquinoxaline-6-carboxamidine, compound **4.3**. Reaction condition (i) hydroxylamine hydrochloride, KOH, 60 ^{o}C, 16 h

The formation of compound **4.3** was confirmed with the infrared spectrum, which revealed the conversion of C≡Nat position 6 of the quinoxaline group of compound **4.2** to hydroxyamidine, zwith the disappearance of C≡N which was responsible for the stretching absorption band at 2200 cm^{-1} and appearance of two bands of NH of amidoxime group with stretching frequencies of 3384 and 3495 cm^{-1} respectively. Also, an associated broad bands of the NH/OH functionality are seen at 3183 cm^{-1},[234] Figure 4.5.

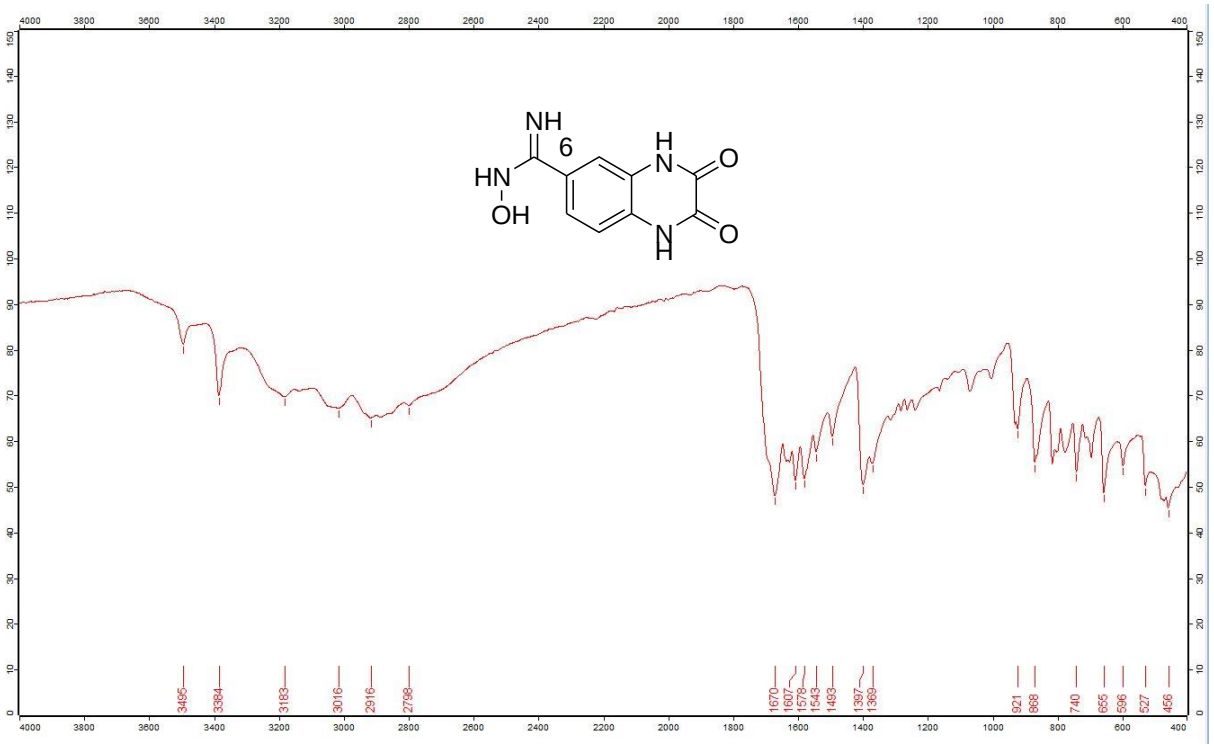

Figure 4.5: Infra-red Spectrum of Compound **4.3**

The ^{1}H NMR also confirmed the formation of compound **4.3**, with the presence of N-hydroxyamidine, attached to the position 6 of the quinoxaline ring. A broad singlet that corresponded to the O-H of the N-hydroxyamidine moiety, was observed at 6.66 ppm, while two additional signals assigned to the two NH's of the amidine group were found to resonate downfield as singlets at 10.05 ppm and upfield at 3.11 ppm TMS scale, respectively, Figure 4.6.

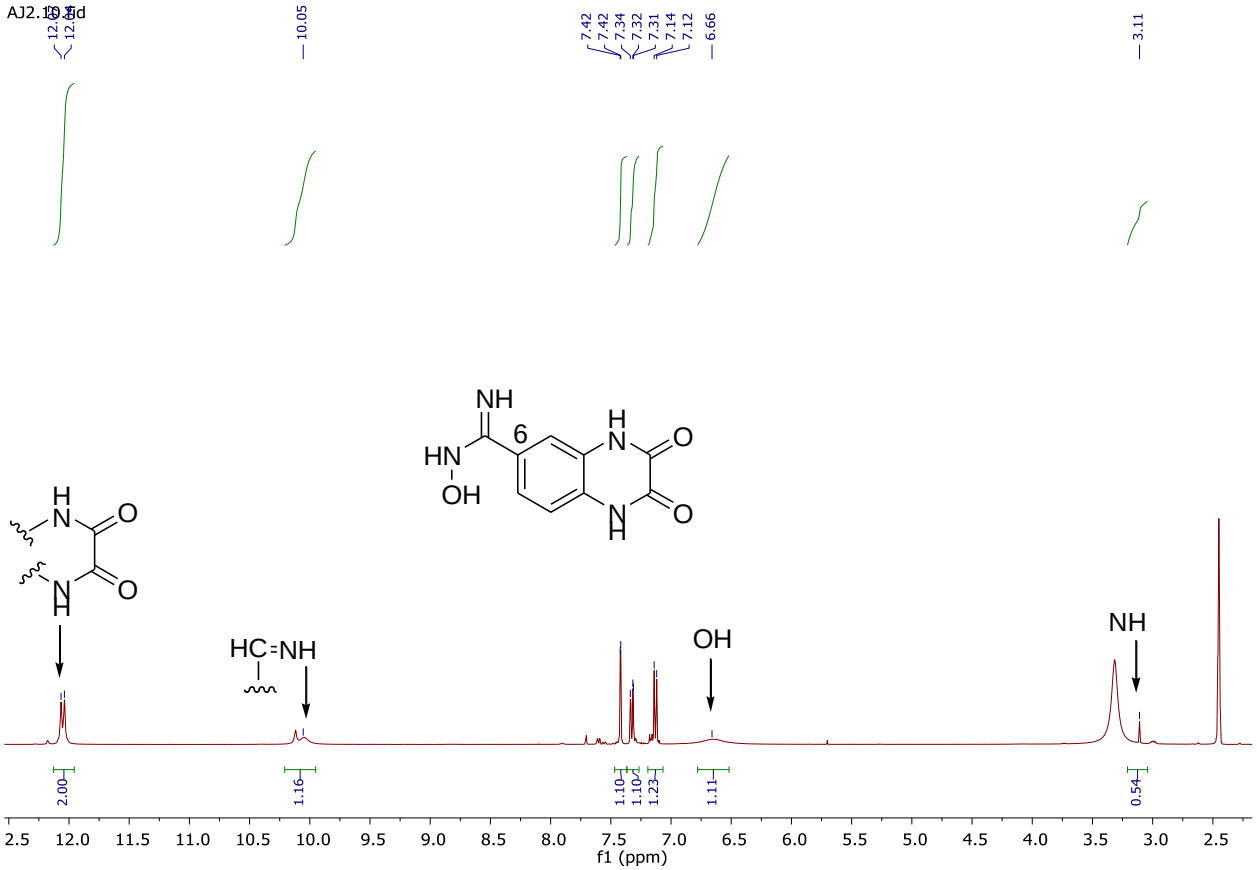

Figure 4.6: ^{1}H NMR of **4.3** (400 MHz, DMSO-d_6)

Furthermore, compound **4.3** was treated with ammonium formate in the presence of palladium on carbon to afford amidine derivative of quinoxaline, **4.4,** Scheme 4.11**.**

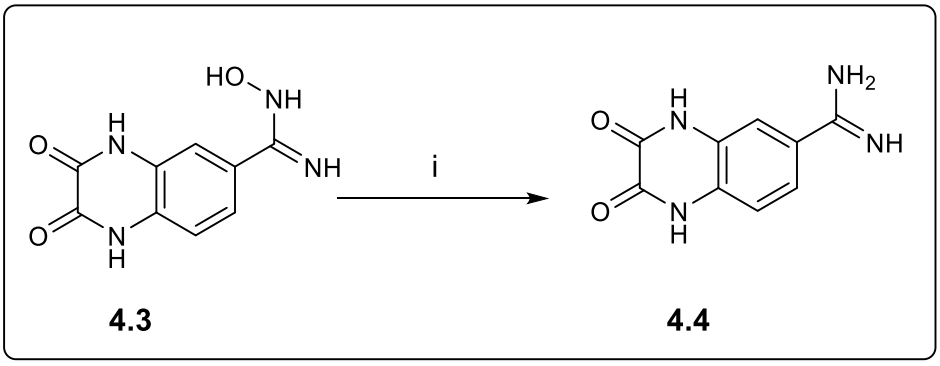

Scheme 4.11: Synthesis of 1,2,3,4-tetrahydro-N-hydroxy-2,3-dioxoquinoxaline-6-carboxamidine, compound **4.4.** Reaction condition: (i) Pd/C, AcOH, N_2, 120 ^{O}C, 3 h

4.4.3 Synthesis of the Target Molecules 4.5a-f *via* Reductive Amination

The synthesis of the target molecules **4.5a-f**, Scheme 4.7, was achieved through a Hofmann and Curtius re-arrangement as the key reaction.[235] The mechanism of this reaction is depicted in Scheme 4.12, which involves a nucleophilic attack of the lone pair of electrons on the nitrogen amine of compound **4.4** on the central electrophilic carbon of the isocyanate **I,** with a subsequent delocalization of a pi-electrons to the nitrogen atom, giving rise to the enolate ion intermediate **II**. Finally, proton transfer, as demonstrated in intermediate **II,** yielded the envisioned compound **4.5**. [236]

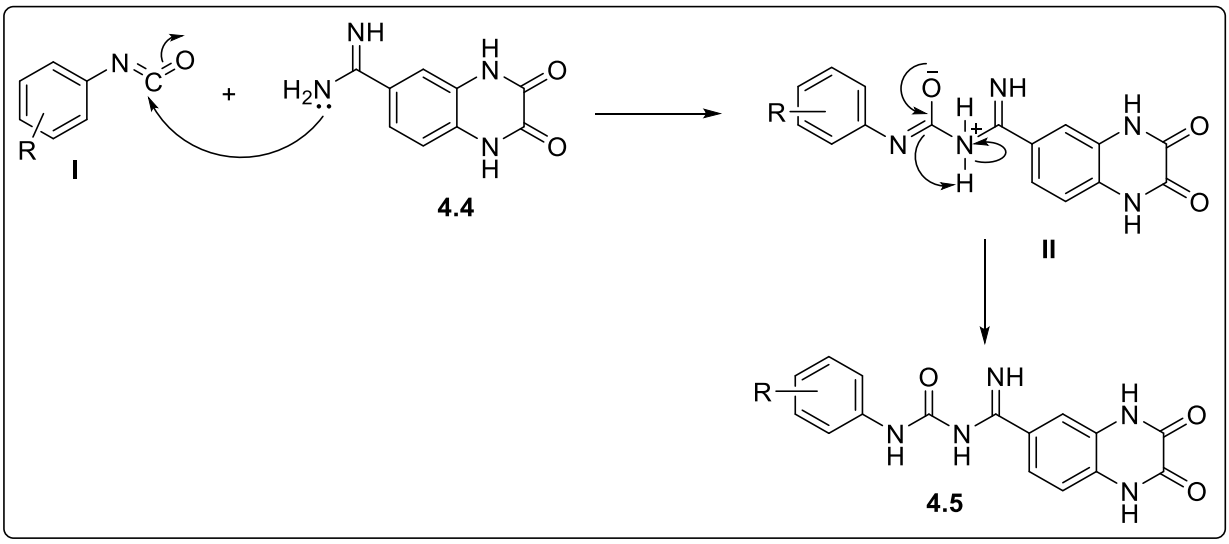

Scheme 4.12: General reaction mechanism for the synthesis of target compounds **4.5a-f**

Compound **4.4** was in turn used to prepare the carboxamidine derivative, **4.5a**, Scheme 4.13. Compound **4.4** underwent reductive amination with series of isocyanates and thiocyanates in the presence of triethylamine to give urea **4.5a**. All the remaining target molecules **4.5b-f** were prepared in a similar manner.

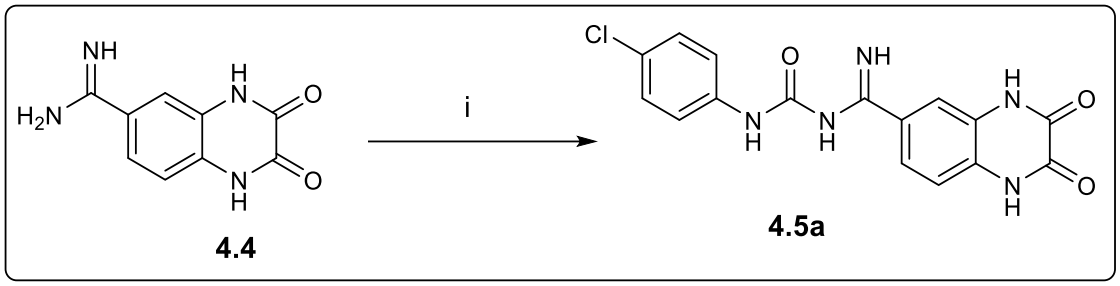

Scheme 4.13: Synthesis of target compound **4.5a**. Reaction condition (i) DMSO, Et_3N, 50 ^oC, 24 h

In general, using compound **4.5a** as a representative spectroscopic study for the target molecules, the infrared spectrum displayed absorption bands due to the stretching vibration frequencies of N–H, C=O, C=C, and C=N at 3471–3294 cm^{-1}, 1712 cm-1, 1590 cm^{-1}, and 1488 cm^{-1}. The absorption bands due to stretching vibration frequencies of CH alkene of the aromatic were seen between 3184-2852 cm^{-1}, Figure 4.7.

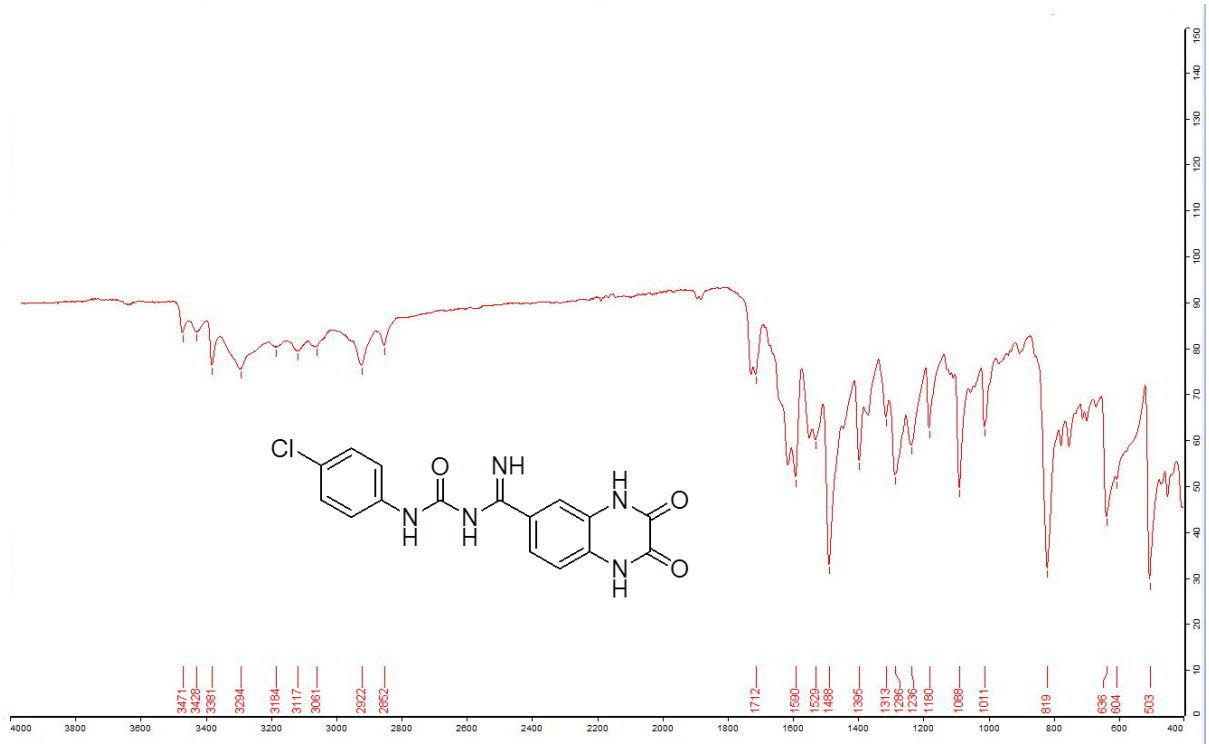

Figure 4.7: Infra-red Spectrum of Compound **4.5a**

Also, the chemical shifts and the multiplicity patterns were consistent with the proposed target compounds. Therefore, the ^{1}H NMR of **4.5a** displayed a singlet corresponding to the two N–H groups of the urea moiety at 5.21 ppm, whereas the two amide N-H groups appeared at 8.31 ppm as an intense singlet, Figure 4.14. Furthermore, a prominent singlet assigned to the N-H of the imidine moiety appeared up-field at 2.55 ppm. Also, the two aromatic rings present in compound **4.5a** were confirmed with the presence of seven aromatic protons seen at 6.55-7.61 ppm downfield TMS scale. The ^{13}C NMR showed sixteen carbons, with C=O of the urea group having the highest signal observed at 168.94 ppm, while the–C=NH of imidine signal was observed at 152.84 ppm, and the other two amides C=O was seen at 148.14 ppm, Figure 4.15. The signals of the remaining fourteen sp^{2} hybridized carbons were found between 115.64 and 139.03 ppm, respectively.

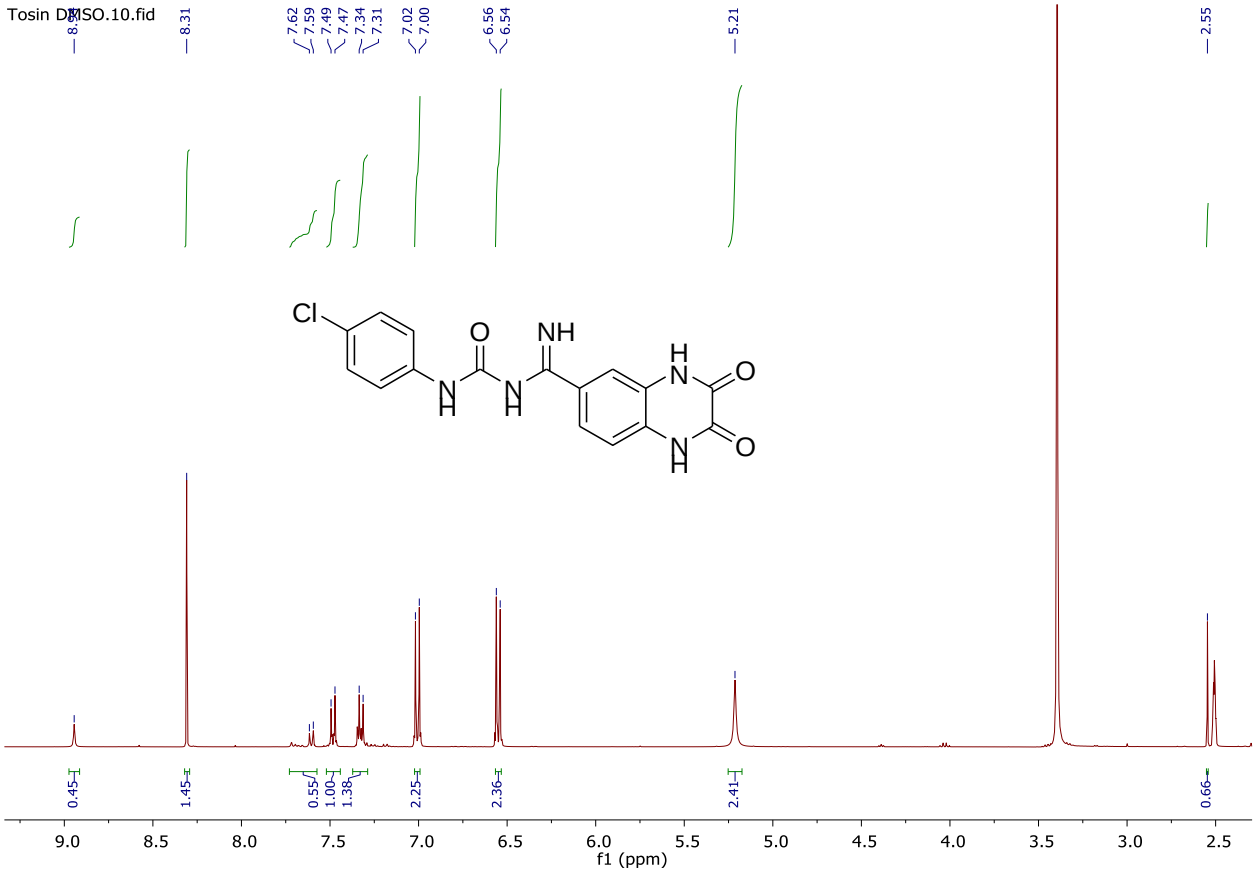

Figure 4.8: ^{1}H NMR of **4.5a** (400 MHz, DMSO-d_6)

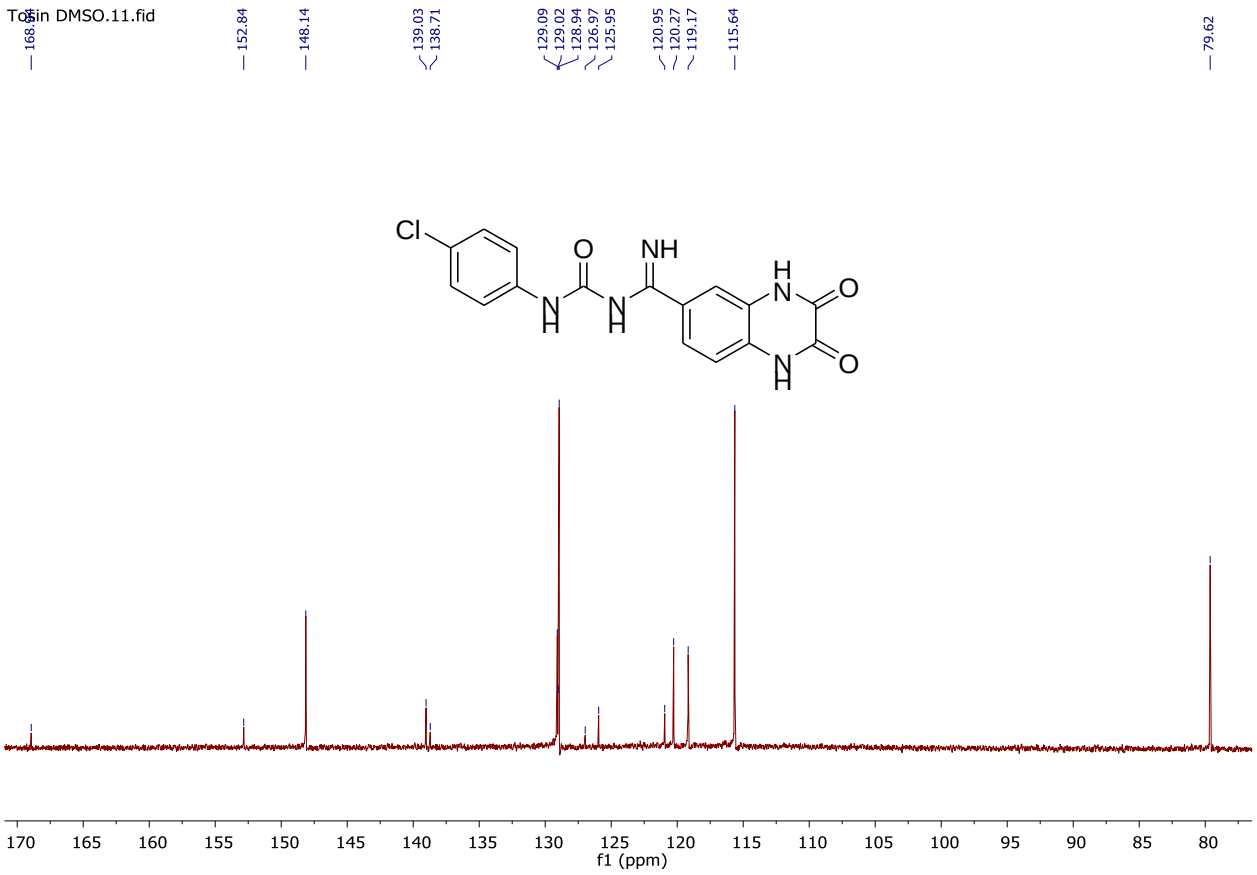

Figure 4.9: ^{13}C NMR of **4.5a** (100 MHz, DMSO-d_6)

4.5 Reported synthesis and molecular docking studies on quinoxaline as antimicrobials

Ammar *et al*. synthesized and screened a series of novel di-substituted sulfonylquinoxaline derivatives against fungi and bacteria. They also studied the binding activities of the series of di-substituted sulfonylquinoxaline **I**, Figure 4.10, to the DNA gyrase binding site. DNA gyrase is the bacterial enzyme that introduces negative supercoils into DNA.[237] The series of di-substituted sulfonylquinoxaline compound I showed potent DNA Gyrase inhibition with IC_{50}= 17 µM bacterial and fungi=10 µM, respectively, which was higher than that of the standard drug Ciprofloxacin (IC_{50} = 26.31 µM). Also, molecular docking of compound **I** displayed an

excellent binding mode and affinity to DNA Gyrase, similar to ciprofloxacin, as seen in Figure 4.10.[210]

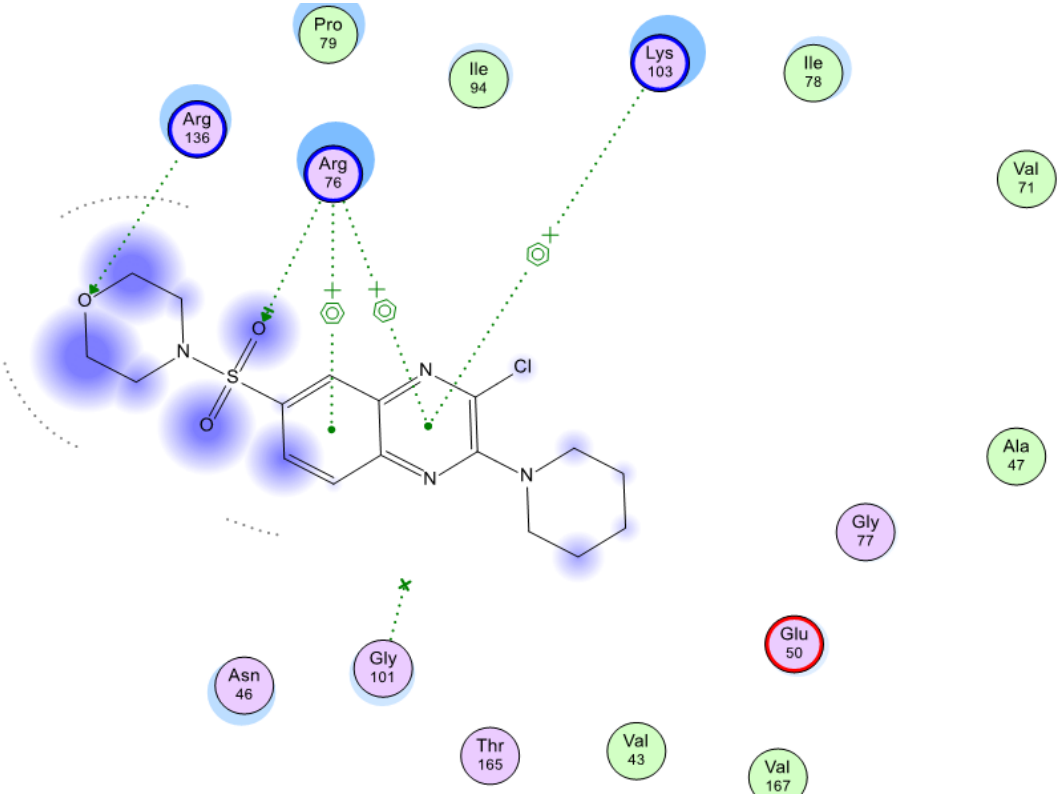

Figure 4.10: Docking of novel di-substituted sulfonylquinoxaline **I** unto DNA gyrase binding site.[210]

Furthermore, Shaaban *et al*.[238] prepared and screened a library of pyrazolo-1,2,4-triazolo[4,3-a]quinoxaline derivatives against microbials, and the most active antimicrobial compounds **I** and **II**, Figure 4.11 out of all the screened compounds were docked against Bacillus anthracis dihydropteroate synthase (DHPS) pterin and *p*-aminobenzoic acid-binding pockets. The docking results showed that these compounds, **I** and **II,** fit into the binding pocket of *Bacillus anthracis* dihydropteroate synthase pterin and p-aminobenzoic acid-binding pockets, Figure 4.11. Furthermore, the docking studies revealed interactions of the hydrogen bonds of these

compounds **I** and **II** with crucial amino acids, such as Asn120, Asp184, Lys220, and Arg254, and hydrophobic interactions with His256.

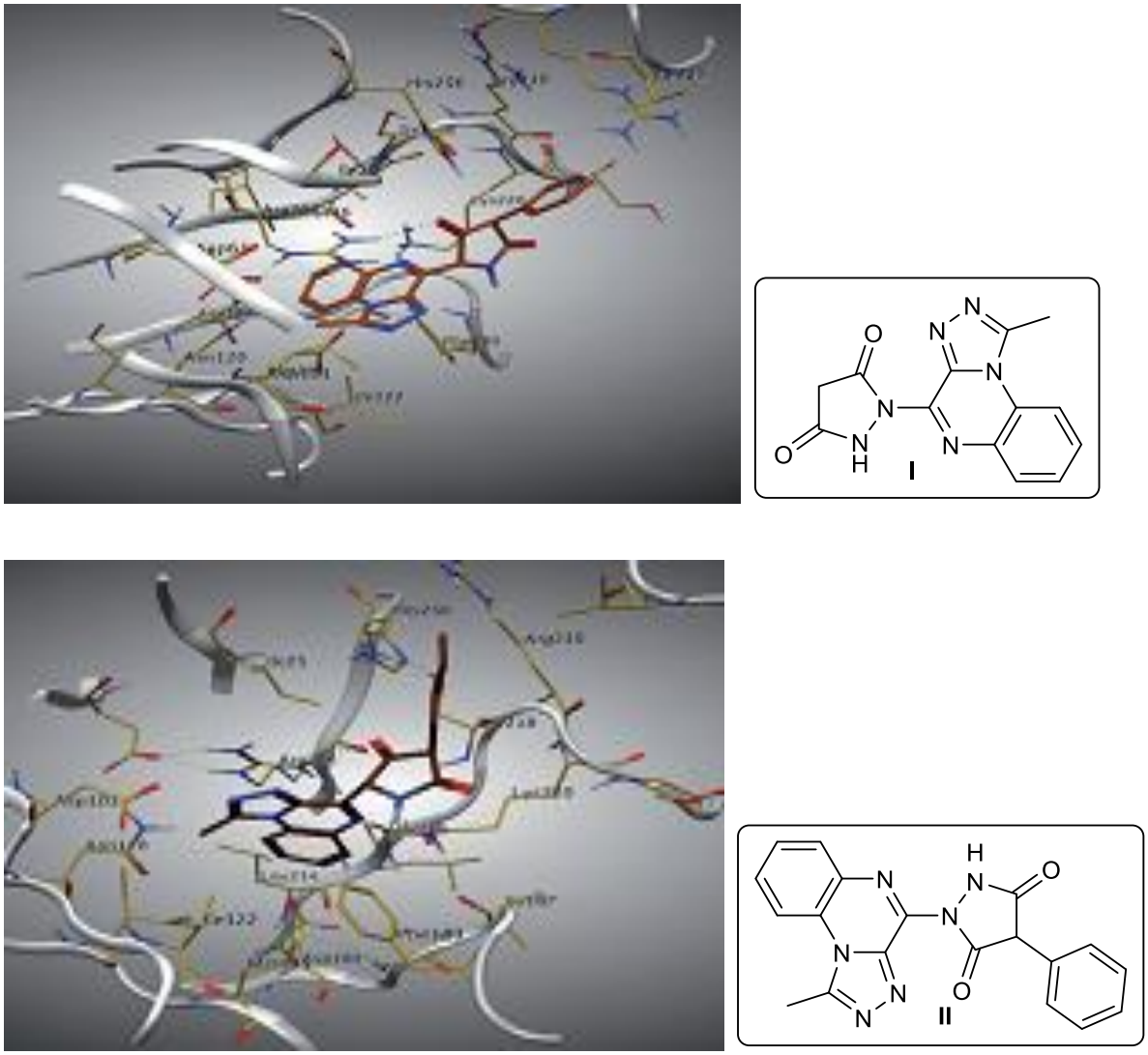

Figure 4.11: Binding of compounds **I** and **II** to BaDHPS in the active site.[238]

Similarly, a report by Sanna and his team showed the antibacterial and antifungal importance of quinoxaline moieties with the substituted electron-withdrawing group at positions 6, Figure 4.12. [210],[239],[240],[241] Notably, the quinoxaline scaffold bearing the chloro-substituent at position 6 exhibited significant antimicrobial activity against *Staphylococcus aureus*. They reported that reasoning for this marked finding may be ascribed to the lipophilicity and the electronic

properties displayed by the substituents, which may have enhanced the biological activities of 5,6-dichloro-3-(trifluoromethyl)quinoxalin-2(1*H*)-one.[210]

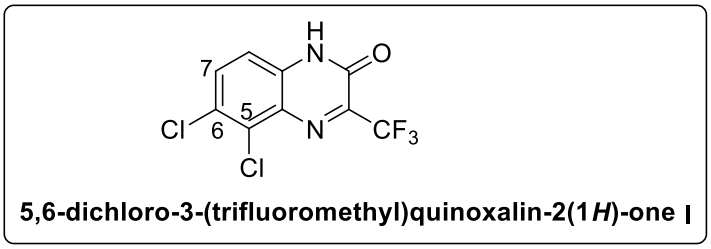

Figure 4.12: Quinoxaline moieties with the substituted electron-withdrawing group at the positions 6

Shintre *et al*., and his group reported the synthesis of thiazolidine–quinoxaline derivatives with amino acid side chains in a four-step reaction by means of microwave irradiation. Some of the synthesized compounds displayed good antimicrobial activity against Gram +ve and Gram -ve bacteria. This notable inhibitory activity was as a result of the presence of 4-fluorophenyl and 4-methoxyphenyl groups along with tyrosine side chains of quinoxaline, Figure 4.13.[206]

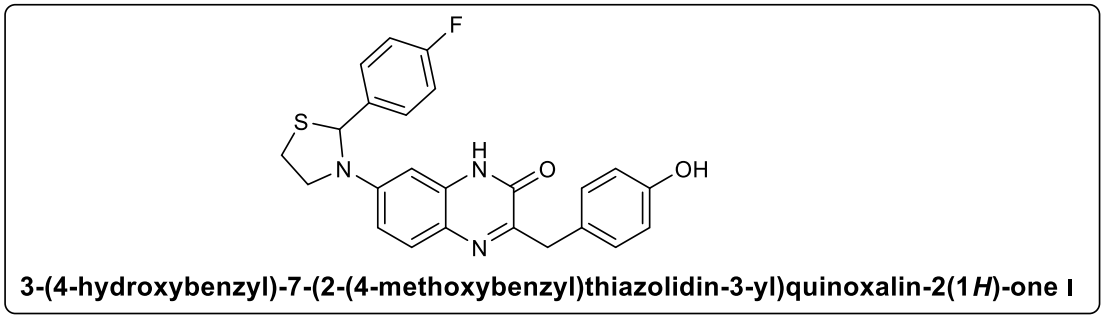

Figure 4.13: Thiazolidine–quinoxaline derivative

4.6 Molecular Docking of Target Molecules 4.5a-f

Molecular docking studies (ligand-protein) were carried out on quinoxaline-6-carboximidine target molecules **4.5a-f** using Schrodinger 2020-3. The target molecules were docked unto six different bacteria proteins namely DNA-gyrase enzyme (PDB code: 1KZN), beta-lactamase (PDB code: 2NZE), *Bacillus anthracis* transpeptidase (PDB code: 3G9K), penicillin-binding protein (PDB code: 3UDI), *Escherichia coli* lytic transglycosylase (PDB code: 2PIC) and *Staphylococcus aureus* dihydrofolate Reductase (PDB code: 4XE6). The molecular docking result with the docking scores is as shown in Table 4.1 below. For these series of target compounds **4.5a-f** when docked unto the active site of each bacteria protein, the most probable targets are *Escherichia coli* lytic transglycosylase (PDB code: 2PICs) and beta-lactamase (PDB code: 2NZE) which gave best docking scores with binding energy ranging between -6,46 and -8,74 respectively. The structural and binding mode analysis displayed hydrogen bond interactions of 4.5b and 4.5f with important amino acids, which include ASP 90, ASN 180, LYS 212, ASP255, GLN 96, and interactions with HIE 88 and LYS 269.

The docking pose of compound **4.5b** displayed hydrogen bond interaction between the nitrogen of primary amine group of the ligand and ASP 90. Also, a water bridge is observed between the oxygen of the urea and ASN 180. There is a pi stacking interaction between the quinoxaline ring and HIE 88.

The docking pose of compound **4.5f** displayed hydrogen bond interaction between the two nitrogens of thiourea group of the ligand and ASP 255. Also, a side chain interaction is seen between the sulphur of the thiourea and GLN 96. A pi stacking interaction is observed between the ligand and LYS 212. Another pi stacking interaction is observed between the ligand and

LYS 269. Also, hydrogen bond interaction is observed between the nitrogen of the quinoxaline ring and LYS 212.

The binding mode of the promising compounds **4.5b** and **4.5f** is as shown in Figure 4.14 and Figure 4.15 respectively.

The result showed that these series of compounds **4.5a-f** would be active against Escherichia coli lytic transglycosylase (PDB code: 2PIC) and beta-lactamase (PDB code: 2NZE), which could be a significant target for the discovery and development of novel antibacterial drug agent.

Table 4.1: Docking scores of quinoxaline-6-carboximidine target molecules **4.5a-f**

ID	1KZN	2NZE	3G9K	3UDI	4XE6	2PIC
4.5a	-4,491	-5,471	-4,208	-3,3	-6,146	-6,87
4.5b	-4,48	-7,863	-4,092	-2,348	-6,454	-6,995
4.5c	-3,555	-5,932	-3,382	-2,394	-7,687	-8,616
4.5d	-4,131	-6,629	-4,648	-2,642	-6,161	-6,456
4.5e	-3,618	-6,283	-2,6	-2,504	-5,514	-8,546
4.5f	-3,738	-6,927	-3,99	-4,994	-6,742	-8,74

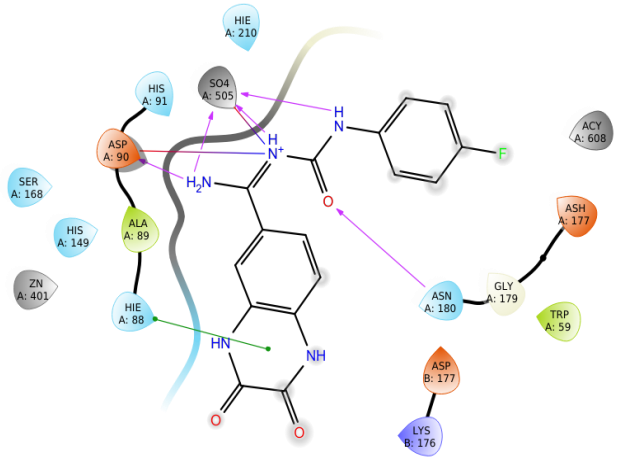

Figure 4.14: The binding mode of **4.5b** unto the active site of Escherichia coli lytic transglycosylase (PDB code: 2PIC)

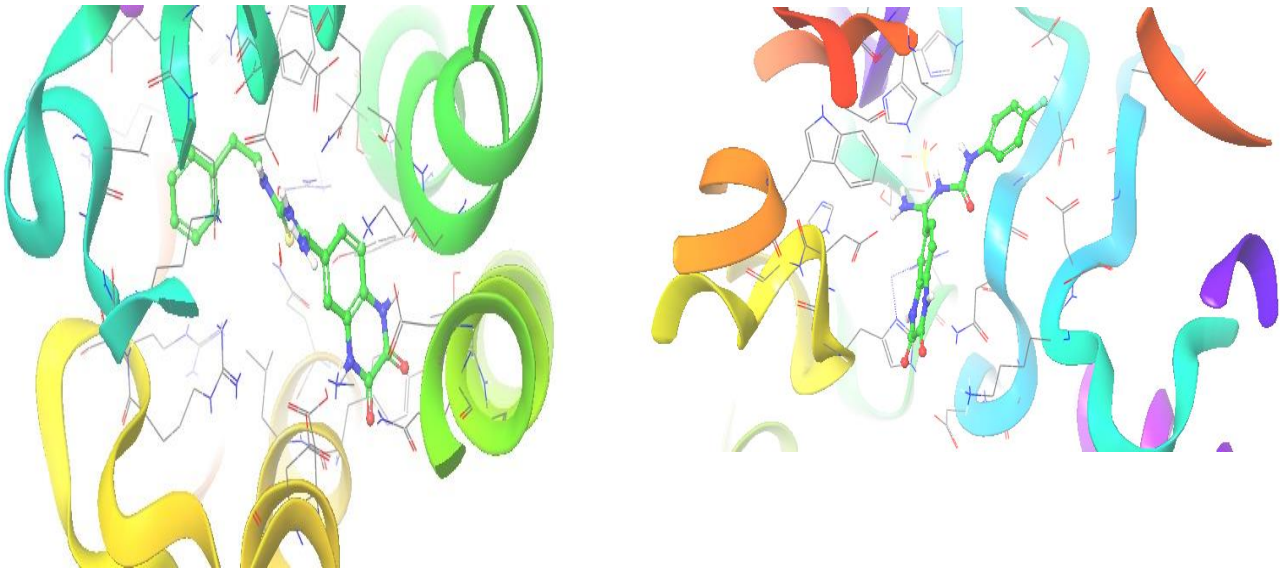

Figure 4.15: The binding mode of **4.5f** unto the active site of beta-lactamase (PDB code: 2NZE)

4.7. Conclusion

The quinoxaline-6-carboximidine target molecules **4.5a-f** were successfully designed and synthesized. Although twelve compounds were designed, only six target compounds were successfully synthesized. The success of these compounds may primarily be due to the presence of an electron-withdrawing substituent on the phenyl ring of the isocyanate. We reasoned that this group seemed to enhance the reactivity of the isocyanate by lowering the electron density of the ring and stabilizing the negative intermediates during the mechanistic pathway, Scheme 4.12. Overall, this finding demonstrates the significance of the presence of an electron-withdrawing group in the isocyanate derivatives towards the reactivity with the amidine **4.4**. However, the reaction failed to occur in isocyanate derivatives without electron-withdrawing substituents, deeming it important reaction criteria. The result of molecular docking and binding of **4.5a-f** to the active sites *Escherichia coli* lytic transglycosylase (PDB code: 2PIC) and beta-lactamase (PDB code: 2NZE), showed that these series of target molecules could be significant targets for the discovery and development of novel antibacterial drug agents.

Chapter Five

Conclusion and Future Work

5.1 Summary and Conclusion

This research work has successfully used molecular hybridization and in-*silico* docking to design antimalarial, anticancer, and antimicrobial agents.

Based on preliminary findings through the *in-silico* studies and previous reports recently carried out on 2,6-dimethyl-4-(1*H*)pyridones, we have successfully synthesized a series of new 4(1*H*)-pyridone-containing intermediates and target molecules by employing, as antimalarial agents. However, only target molecules **2.9a** and **2.9b** were successfully synthesized from the envisaged series, after many failed attempts.

The RTF model-predicted Ki values of compounds **2.9a** and **2.9b**, docked into homology models of *P. falciparum* cytochrome bc1, are 49 nM and 34 nM, respectively. The docked pose of the compound **2.9b** showed a hydrogen bond interaction between the nitrogen of the pyridone and histidine 12. A water bridge is observed between the oxygen of the pyridone and ASP218, Figure 2.9. The pyridone also forms two pi-stacking interactions between HIS192 and PHE210, Figure 2.32. Additional hydrophobic interactions were observed between the ligand and PHE30, VAL34, VAL184, and PHE185, Figure 2.32. Crystallographic evidence from previous findings suggests that strong interactions exist between divalent sulphur atoms, aromatic rings, and sulphur, demonstrating the sulfur-containing linker's importance.[78] The presence of the sulfur-containing linker, together with the additional interactions as shown by the docked compound **2.9b**, may account for the notable low predicted Ki values of compounds **2.9a** and **2.9b**.

Single crystal structures of intermediate compounds **2.4a** and **2.4b** were also determined using X-ray diffraction their unique identities were revealed upon which the side reactions were identified.

Also, new derivatives of 2,6-dimethyl-4H-pyran-4-one compounds **2.15, 2.22-2.26** in Scheme **2.12** were successfully synthesized with moderate to good yields using palladium-catalyzed Suzuki-Miyaura coupling reactions apart from compound **2.26**, which yield was not determined due to its decomposition. SCXRD analysis of the by-products of the reactions forming compounds **2.23 (2.23')** and **2.26 (2.26')** showed that the homocoupling of boronic acids remains to be one of the major side-reactions occurring that lower the yield of the main products.

DFT analysis revealed that the electron density in the HOMO of compounds **2.15, 2.22-2.26** is primarily distributed over the substituted R-groups (resulting biphenyl moiety after C-C coupling), implying a lack of reactivity via either of the pyranone ring's oxygen atoms. TGA analysis confirmed the high rate of instability and thermal decomposition of the selected 2,6-dimethyl-4*H*-pyran-4-one compounds **2.15, 2.22**, and **2.25**, and as a result, we were unable to synthesize the target compounds **2.16, 2.27-2.31**.

Even though all the molecular docking studies were conducted against homology models of *P. falciparum* cytochrome bc_1, due to limited resources, we had no option but to screen the synthesized intermediate and target molecules against the asexual stage of CQ-sensitive (CQS) NF54 and chloroquine-resistance (CQR) K1 *P. falciparum* strains, using CQ as the control.

Out of all the seven newly synthesized compounds **2.9a, 2.9b, 2.10c, 2.11b, 2.11c, 2.12a, 2.12b**, that were screened for antimalarial activities, targets compound **2.9a** and **2.9b** displayed excellent inhibitory activities (96% and 97% at 1 μM, 99% and 98% at 5 μM) against K1 CQ

resistant strain (CQR) and CQ-sensitive (CQS) NF54. Other newly synthesized intermediates **2.10c, 2.11b, 2.11c, 2.12a, 2.12b** gave moderate to low inhibitory *P. falciparum* activities.

Furthermore, the IC_{50}s of the most potent compounds **2.9a** and **2.9b** were determined. Compounds **2.9a** and **2.9b** exhibited remarkable anti-plasmodial activities against K1 CQ resistant strain (CQR) at 0.10 and 0.04, while at 0.13 and 0.05 against *P.falciparum* CQ-sensitive (CQS) NF54.

(ii) Investigation of 2-substituted benzimidazole derived anticancer compounds

Furthermore, a library of 2-disubstituted benzimidazole derivatives was successfully synthesized with the use of a pyrrolidine catalyst, which seemed to be a key factor in ensuring the success in the formation of the final products. The synthesized compounds were screened for their cytotoxicity activity against MCF-7 cells lines, but unfortunately, none of the target compounds, even at all concentration (0.195-100 µg/mL), gave the cytotoxic effect that could be compared to that of the standard drug used, camphothecin, which induces cell death at 57% (at 0.08 µg/mL). Therefore, the target compounds were docked, and the most probable target is compound **3.4b** with docking scores of -9,16. This target described above revealed a bond with Arg 394 and interactions with Leu387and Leu 525. The binding mode and structure analysis showed that oxygen of the carbonyl of the benzimidazoles target molecules such as **3.4a, 3.4a, 3.4b, 3.4c, 3.4e, 3.4f, 3.4g,** only form water bridge with an amino acid Arg394, which conforms with binding mode of human estrogen receptor alpha ligand-binding domain in complex with estradiol, while there was no other bonding with other important amino acid residues such as His 524, Glu 353 found in the binding mode of estradiol with the ER-ligand binding.

The disparity between the molecular docking and bioactivity results of benzimidazole derivatives could be because some of the target compounds only bind to one amino acid (Arg394) and do not bind to the other two important amino acids (His 524, Glu 353) that estradiol binds to, in the active site of the human estrogen receptor alpha which is responsible for the proliferation of the MCF-7 cells lines. Therefore, in our future work, these target compounds will be modified to be able to bind to other two amino acids that estradiol binds unto, thereby increasing the activities of these target benzimidazoles.

(iii) Synthesis of quinoxaline-6-carboxamidine-urea based antimicrobial compounds

Finally, quinoxaline-6-carboximidine target molecules **4.5a-f** were successfully designed and synthesized. Although twelve compounds were designed, only six target compounds were successfully synthesized. The success of these compounds may primarily be as a result of the presence of an electron-withdrawing substituent on the phenyl ring of the isocyanate. We reasoned that this group seemed to enhance the reactivity of the isocyanate, by lowering the electron density of the ring and stabilizing the negatively charged intermediates during the mechanistic pathway, Scheme 4.12.

Overall, this finding demonstrates the significance of the presence of an electron-withdrawing group in the isocyanate derivatives towards the reactivity with the amidine **4.4**. However, the reaction failed to occur in isocyanate derivatives without electron withdrawing substituents, deeming it an important reaction criteria.

The result of molecular docking and binding of **4.5a-f** unto the active sites *Escherichia coli* lytic transglycosylase (PDB code: 2PIC) and beta-lactamase (PDB code: 2NZE), showed that these series of target molecules could be significant targets for the discovery and development of novel antibacterial drug agent.

5.2 Future Work

The following are identified as future work in this research:

1. Further explore the SAR profile of position C5 of the 4-(1*H*)-pyridone scaffold by substitution of a halogen (Br, Cl) to evaluate their plamosdial inhibitory activities and compare the results with **GSK932121** that has halogen substituent on position C5.
2. Bio-evaluate target molecules **2.9a** and **2.9b** against the envisioned *P. falciparum* cytochrome bc_1.
3. Modification of the structures of benzimidazole target molecules so that it can bind to human estrogen receptor alpha which is responsible for the proliferation of the MCF-7 cells lines, thereby increasing the benzimidazole activities.
4. Antimicrobial screening of quinoxaline-6-carboximidamide derivatives against a series of selected microbes.

Chapter Six

Experimental

6.1 General Procedures

All reagents used for this research were purchased commercially from Sigma-Aldrich Chemicals (South Africa) and were used without further purification except otherwise stated. All solvents were purchased from Merck Chemicals South Africa. After reactions were completed, solvents were evaporated under reduced pressure using IKRV 10 Rotary evaporator. The progress and completion of the reaction were monitored by thin-layer chromatography TLC using Merck 60 F254 pre-coated silica gel plates and was visualized under UV light at 254 nm. Column chromatography was performed with Merck silica gel (0.063-0.200 mm) to get a pure compound. Fourier-Transform-Infrared (FT-IR) spectrophotometer was utilized using Bruker Alpha Platinum-ATR spectrometer to obtain infrared data. Melting points were determined with the aid of the Gallenkamp melting point in an open capillary tube and uncorrected. The ^{1}H and ^{13}C Nuclear Magnetic Resonance NMR spectra of synthesized compounds were recorded on either Bruker Avance (DPX-400 spectrometer or a Bruker DRX-300 spectrometer) at 400.21 MHz and 100 MHz or 300 MHz and 75 MHz, using $CDCl_3$, CD_3OD-d_4 or DMSO-d_6. The chemical shifts were reported in part per million with respect to the TMS (internal standard) while the residual solvent peaks were observed thus: ^{1}H NMR signal of $CDCl_3$ at 7.26 ppm and its ^{13}C NMR signal at 77.16 ppm; DMSO-d_6 at 2.50 ppm (^{1}H) and 39.52 ppm (^{13}C). Multiplicities are abbreviated as s = singlet, d = doublet, t = triplet, q = quartet, m = multiplet. Mass analyses were executed on Waters Synapt G2 High-Resolution Mass Spectrometry (HRMS) system through the flow injection analysis (FIA) by means of an electrospray ionization (ESI) probe. The MS data were collected, processed, and analysed on MassLynxTM.

6.2 X-ray Crystallography

Crystalline compounds were analysed for their single-crystal diffraction using Quazar multi-layer optics monochromatic Mo K radiation (K=0.71069) on Bruker D8 venture kappa geometry diffractometer with duo Is sources. All H atoms were placed geometrically in an idealised position and constrained to ride on their parent.

Synthesis of 1-(4-bromophenyl)propan-2-one, 2.3

To a solution of 4-bromophenylacetic acid (10.0 g, 46.50 mmol) in acetic anhydride (21.98 ml, 23.30 mmol) was added 1-methylimidazole (1.9 ml, 23.30 mmol). The resulting mixture was stirred at room temperature for 15 h; then the reaction mixture was poured into 50 ml of cold water and extracted with ethylacetate (150 ml). The organic layer was combined, dried with $MgSO_4$, filtered and concentrated in vacuo. The obtained crude was purified on column chromatography (ethylacetate/n-hexane; 1:6) to obtain a pure product.

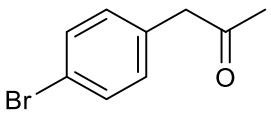

Yellow oil, Yield, 0.1 g, 51%; FT-IR: ν (cm^{-1}) = 3085, 2962 (C*H*); 1671 (C=O); ^{1}H NMR (300 MHz, DMSO-d_6) δ_H 7.50 (d, $^3J_{HH}$ = 8.4 Hz, 2H, Ar*H*), 7.14 (d, $^3J_{HH}$ = 8.4 Hz, 2H, Ar*H*), 3.78 (s, 2H, CH_3), 2.14 (s, 3H, CH_3).

Synthesis of 3-(4-bromophenyl)-2,6-dimethyl-4H-pyran-4-one, 2.4a

Eaton's reagent (5.79 mL, 36.82 mmol) was added to a solution of compound 2.3 (1.5 g, 7.04 mmol) in acetic anhydride (2.42 mL, 28.16 mmol) at room temperature under nitrogen gas. The resulting reaction mixture was refluxed at 95°C for 2 h after which the reaction mixture was cooled to room temperature, pour into ice-water 30 mL, and extracted with toluene. The combined organic layer was collected, washed with saturated sodium hydrogen carbonate

$NaHCO_3$, brine 20 mL, washed with distilled water, dried with anhydrous magnesium sulfate Mg_2SO_4, filtered, and concentrated in vacuo. The crude product was left was separated by colomn chromatography on SiO_2 gel using (ethylacetate/n-hexane; 1:2). The product gave brown crystals.

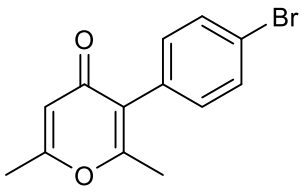

Brown crystals, Yield 61.56%, m.p. 105.9 -107.4°C; FT-IR: ν (cm^{-1}) 3061, 2921, 2852 (CH); 1657 (C=O); ^{1}H NMR (300 MHz, DMSO-d_6) δ_H 7.60 (d, $^3J_{HH}$ = 8.4 Hz, 2H, Ar*H*), 7.18 (d, $^3J_{HH}$ = 8.4 Hz, 2H, Ar*H*), 6.22 (s, 1H, py*H*), 2.28 (s, 3H, CH_3), 2.15 (s, 3H, CH_3). ^{13}C NMR (101 MHz, $CDCl_3$) δ_C 178.2, 164.8, 162.6 (2C), 131.9 (2C) 131.6,131.5, 125.7, 122.1, 113.8, 19.8, 18.6. ESI-HRMS(m/z), Anal. Calcd. 279.

Synthesis of 3-(4-bromophenyl)-2,6-dimethylpyridin-4(1*H*)-one, 2.5:

Solution of compound **2.4** (2 g, 7.2 mmol) and 30% aqueous ammonia (21.11 mL, 54.2 mmol), in ethanol (21.98 ml, 376 mmol), were heated in a sealed pressure tube. The resulting reacting mixture was refluxed at 150°C for 50 hours. The reacting mixture was cooled, poured in ice-water poured (20 mL). The precipitate formed was washed with distilled water (10 mL), ethyl acetate (20 mL), filtered, and dried to afford brown product powder.

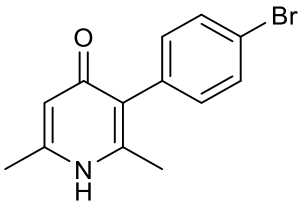

Light brown solid; Yield 0.002 g; FT-IR: ν (cm^{-1}) = 3058, 3016 (C*H*); 1615(C=O); 3265 (N*H*); ^{1}H NMR (300 MHz, $CDCl_3$): δ_H 7.56 (d, $^3J_{HH}$ = 8.4 Hz, 2H, Ar*H*), 7.13 (d, $^3J_{HH}$ = 8.4 Hz, 2H, Ar*H*), 6.22 (s, 1H, py*H*), 2.30 (s, 3H, CH_3), 2.20 (s, 3H, CH_3).

Synthesis of tert-butyl 3-(4-bromophenyl)-2,6-dimethyl-4-oxopyridine-1(4*H*)-carboxylate, 2.6

To a solution of 4-Bromophenyl-2, 6-dimethylpyridin-4(1*H*)-one, **2.5** (0.20 g, 0.72 mmol), in dry acetonitrile, was added di-tert-butyl-bicarbonate (0.34 g, 0.0717 mmol) and DMAP (0.09 g, 1.57 mmol). The reacting mixture was stirred at 40℃ for 14 hours, then the reaction mixture was vacuo under reduced pressure to give a residue. The residue was diluted and extracted with diethyl ether (3, washed with saturated $NaHCO_3$ (3, distilled water (3), brine and dried over magnesium sulphate, Mg_2SO_4. The combined organic layer was concentrated in *vacuo*. The crude product was purified using by colomn chromatography on SiO_2 gel with (diethyl ether /n-hexane; 2:1). The product gave white powder.

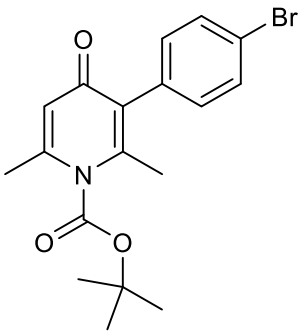

White powder, Yield 0.2 g, 97.3%; FT-IR: ν (cm^{-1}) = 2972, 2922, 2854,(CH); 1716(C=O); ^{1}H NMR (400 MHz, $CDCl_3$) δ_H 7.54 (d, $^3J_{HH}$ = 8.4 Hz, 2H, Ar*H*), 7.12 (d, $^3J_{HH}$ = 8.4 Hz, 2H, Ar*H*), 6.88 (s, 1H, C*H*), 2.56 (s, 3H, CH_3), 2.35 (s, 3H, CH_3), 1.32 (s, 9H, (3 × CH_3)).^{13}C NMR (101 MHz, $CDCl_3$) δ_C 158.9, 157.9, 155.6, 150.4, 133.2, 131.6 (2C), 131.5 (2C), 126.3, 121.9, 114.4, 84.0, 27.3 (3C), 24.4, 23.3.

General procedure for coupling of 4-bromophenylacetic acid to thiols 2.10a-2.10d (2.10a as example):

4-Bromophenylacetic acid, **2.1** (10.0 g, 46.5 mmol), and *N*,*N*-Diisopropylethylamine, DIPEA (12.0 g, 93.0 mmol) were added to dry dioxane (30 mL), evacuated and back filled with argon (3 at a room temperature. To this mixture, were added catalyst, $Pd(dba)_3$ (1.09 g, 1.20 mmol) Xantphos (1.35 g, 2.3 mmol), benzylmercaptan (6.36 g, 51.2 mmol). The whole reacting

mixture was degassed twice more at a room temperature. The reacting mixture was stirred and refluxed at 90$^{\circ C}$for 4 h. The reacting mixture was cooled, filtered to remove precipitate in the mixture and washed with ethyl acetate (500 mL). The reacting mixture was vacuo, under reduced pressure. Then, the mixture was purified by colomn chromatography on SiO_2 gel using (dichloromethane/methanol; 19:1). The product gave yellow powder.

Synthesis of 2-(4-(benzylthio)phenyl)acetic acid, 2.10a:

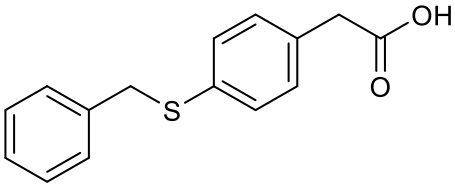

Yellow powder Yield 4.7 g, 41%; FT-IR: ν (cm^{-1}) = 3055, 2917, 2888(C*H*); 1699(C=O); ^{1}H NMR (300 MHz, $CDCl_3$) δ_H 9.95 (s, 1H, O*H*), 7.49 (d, $^3J_{HH}$ = 8.0 Hz, 2H, Ar*H*), 7.29 –7.17 (m, 7H, Ar*H*), 4.08 (s, 2H, CH_2), 3.63 (s, 2H, CH_2). ^{13}C NMR (75 MHz, $CDCl_3$) δ_C 177.4, 137.3, 135.7, 131.3, 129.9 (2C), 129.8 (2C), 128.8 (2C), 128.5 (2C), 127.2, 40.5, 38.9. ESI-HRMS(m/z), Anal. Calcd. for $C_{15}H_{14}O_2S$ (%): C, 69.74; H, 5.46; O, 12.39; S, 12.41; M, 258; Found: C, 69.50; H, 5.41; O, 12.35; S, 12.36; (M+H)+, 259.

Synthesis of 2-(4-(4-chlorobenzylthio)phenyl)acetic acid, 2.10b:

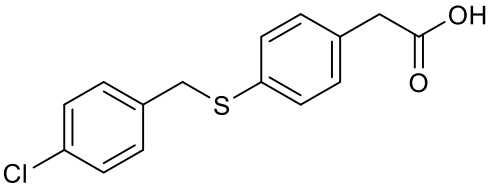

Yellow solid, Yield 3.5 g, 43%; FT-IR: ν (cm^{-1}) = 3020, 2914, 2845 (C*H*); 1699(C=O); ^{1}H NMR (300 MHz, $CDCl_3$) δ_H 10.03 (s, 1H, O*H*), 7.49 (d, $^3J_{HH}$= 8.1 Hz, 2H, Ar*H*), 7.30 – 7.17 (m, 7H, Ar*H*), 4.08 (s, 2H, CH_2), 3.63 (s, 2H, CH_2). ^{13}C NMR (101 MHz, $CDCl_3$) δ_C 177.3, 132.2, 131.8 (4C), 131.1 (4C), 130.3, 130.1, 129.9, 40.5, 38.5. ESI-HRMS(m/z), Anal. Calcd. for $C_{15}H_{13}ClO_2S$ (%): C, 61.86; H, 4.46; O, 11.01; S, 10.99; M, 292; Found: C, 61.64; H, 4.45; O, 10,96; S, 10.95; (M+H) +, 292.

Synthesis of 2-(4-(4-tert-butylbenzylthio)phenyl)acetic acid, 2.10c:

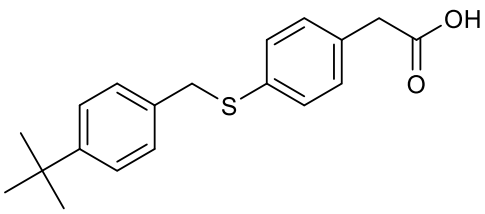

Yellow solid, Yield 5.12 g, 39%; FT-IR: ν (cm^{-1}) = 3021, 2954, 2903(C*H*); 1691(C=O); ^{1}H NMR (400 MHz, $CDCl_3$) δ_H 7.39 – 7.26 (m, 6H, Ar*H*), 7.21 (d, $^{3}J_{HH}$ = 8.3 Hz, 2H, Ar*H*), 4.14 (s, 2H, CH_2), 3.64 (s, 2H, CH_2), 1.34 (s, 9H (3×CH_3)). ^{13}C NMR (101 MHz, $CDCl_3$) δ_C 177.6, 150.2, 136.2, 134.1, 131.0, 129.8 (2C), 129.4 (2C), 128.5 (2C), 125.5(2C), 40.5, 38.4, 34.5, 31.4 (3C). ESI-HRMS(m/z), Anal. Calcd. for $C_{19}H_{22}O_2S$ (%): C, 72.57 H, 7.05; O, 10.18; S, 10.20; M, 314; Found: C, 72.38; H, 7.30; O, 10.16; S, 10.15; (M+H) +, 315.

Synthesis of 2-(4-(4-methoxybenzylthio)phenyl)acetic acid, 2.10d:

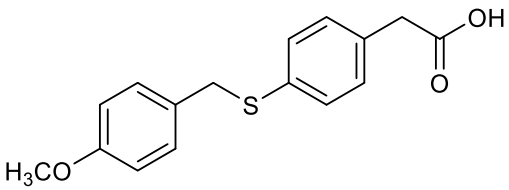

Yellow solid, Yield 5.2 g, 35%; FT-IR: ν (cm^{-1}) = 3016, 2917, 2846(C*H*); 1705(C=O); ^{1}H NMR (300 MHz, DMSO-d_6) δ_C 12.36 (s, 1H, O*H*), 7.33 – 7.14 (m, 6H, Ar*H*), 6.86 (d, $^{3}J_{HH}$ = 8.2 Hz, 2H, Ar*H*), 4.17 (s, 2H, CH_2), 3.72 (s, 3H, OCH_3), 3.53 (s, 2H, CH_2).^{13}C NMR(75 MHz, DMSO-d_6) δC173.1, 158.8, 134.9, 133.1, 130.5 (2C), 130.4 (2C), 129.7 (2C), 128.6 (2C), 114.2 (2C) 55.5, 55.4, 36.6. ESI-HRMS(m/z), Anal. Calcd. for $C_{17}H_{18}O_3S$ (%): C, 67.52 H, 6.01; O, 15.87; S, 10.60; M, 302; Found: C, 67.32; H, 5.94; O, 15.84; S, 10.56; (M+H) +, 303.

Synthesis of 1-(4-(benzylthio)phenyl)propan-2-one, 2.11a:

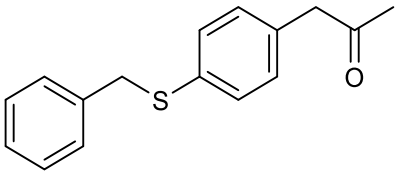

Light-pale yellow powder, Yield 0.8 g, 40%; FT-IR: ν (cm^{-1}) =3054, 2919, 2960(CH); 1700(C=O); ^{1}H NMR MHz, $CDCl_3$) δ_H 7.30 (t, $^{3}J_{HH}$ = 5.7 Hz, 7H, Ar*H*), 7.12 (d, $^{3}J_{HH}$ = 7.9 Hz, 2H, Ar*H*), 4.13 (s, 2H, CH_2), 3.67 (s, 2H, CH_2), 2.17 (s, 3H, CH_3). ^{13}C NMR (101 MHz $CDCl_3$) δ_C 206.2, 158.8, 135.4, 132.3, 130.1 (2C), 129.9 (2C), 129.9 (2C), 129.3, 113.9 (2C), 60.4, 55.3, 50.3, 38.5; Anal. Calcd. for $C_{16}H_{16}OS$ (%):C, 75.0; H, 6.25 O, 6.25; S, 12.49; M, 256; Found: C, 74.6; H, 6.29 O, 6.24; S, 12.51; (M+H) +, 257

Synthesis of 1-(4-(4-chlorobenzylthio)phenyl)propan-2-one, 2.11b:

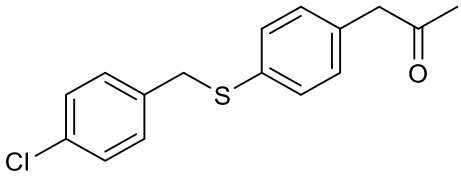

Yellow oil, 1.5 g, 50%; FT-IR: ν (cm^{-1}) = 3088, 2959, 2850(CH); 1674(C=O); ^{1}H NMR (300 MHz, $CDCl_3$) δ_H 7.55 – 7.17 (m, 8H, Ar*H*), 4.08 (s, 2H, CH_2), 3.63 (s, 2H, CH_2). ^{13}C NMR (101 MHz, $CDCl_3$) δ_C 206.1, 134.5, 132.8, 131.7, 130.6 (2C), 130.2, 130.1 (2C), 130.0 (2C), 128.6 (2C), 62.3, 50.4, 38.6. ESI-HRMS(m/z), Anal. Calcd. for $C_{16}H_{15}OClS$ (%): C, 66.08; H, 5.20; Cl, 12.19; O,5.50; S, 11.03 M, 290; Found: C, 65.97; H, 5.15; Cl, 12.19; O,5.49; S, 10.99; (M+H) +, 291.

Synthesis of 1-(4-(4-tert-butylbenzylthio)phenyl)propan-2-one, 2.11c:

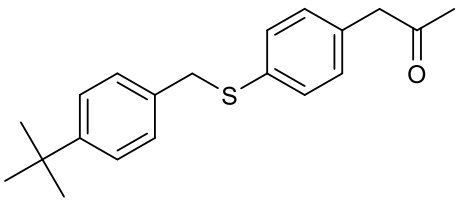

Yellow solid, Yield 2.37 g, 59%; FT-IR: ν (cm^{-1}) = 3054, 2959, 2869(C*H*); 1790(C=O); ^{1}H NMR (300 MHz, $CDCl_3$) δ_H 7.39 – 7.25 (m, 6H, Ar*H*), 7.13(d, $^{3}J_{HH}$ = 7.9 Hz, 2H, Ar*H*), 4.14 (s, 2H, CH_2), 3.68 (s, 2H, CH_2), 2.17 (s, 3H, CH_3), 1.34 (s, 9H, (3×CH_3)). ^{13}C NMR (75 MHz, $CDCl_3$) δ_C 206.2, 150.2, 135.7, 134.1, 132.1, 129.9 (2C), 129.7 (2C), 128.5 (2C), 125.5 (2C), 50.5, 38.5, 34.5,31.4 (3C) ESI-HRMS(m/z), Anal. Calcd. for $C_2OH_{24}OS$

(%): C, 78.88; H, 7.74; O, 5.12; S, 10.26 M, 312; Found: C, 76.78; H, 7.68; O, 5.11; S, 10.22; (M+H) +, 313.

Synthesis of 1-(4-(4-methoxybenzylthio)phenyl)propan-2-one, 2.11d:

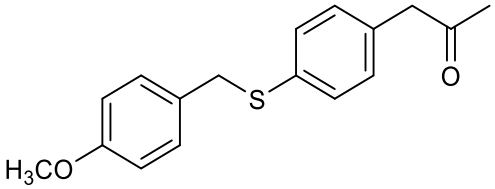

Yellow powder, Yield 3.8 g, 80%; FT-IR: ν (cm-1) = 3002, 2958, 2837(C*H*); 1790(C=O); ^{1}H NMR (400 MHz, $CDCl_3$) δ_H 7.32 – 7.26 (m, 2H, Ar*H*), 7.23 (d, $^{3}J_{HH}$ = 8.6 Hz, 2H, Ar*H*), 7.11 (d, $^{3}J_{HH}$ = 8.2 Hz, 2H, Ar*H*), 6.84 (d, $^{3}J_{HH}$ = 8.7 Hz, 2H), 4.09 (s, 2H, CH_2), 3.80 (s, 3H, OCH_3), 3.67 (s, 2H, CH_2), 2.16 (s, 3H, CH_3). ^{13}C NMR (101 MHz, $CDCl_3$) δ_C 206.2, 158.8, 135.4, 132.3, 130.0 (2C), 129.9 (2C), 129.9 (2C), 129.3 113.9 (2C), 60.4, 55.3, 50.5, 38.5; Anal. Calcd. for $C_{17}H_{18}O_2S$ (%): C, 71.30; H, 6.34; O, 11.17; S, 11.20 M, 286; Found: C, 71.08; H, 6.27 O, 11.13; S, 11.15; $(M+H)^+$, 287.

Synthesis of 3-(4-(benzylthio)phenyl)-2,6-dimethyl-4*H*-pyran-4-one, 2.12a

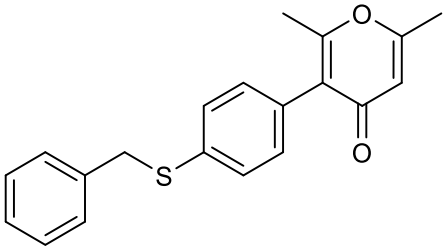

Yellow powder, Yield 0.04 g, 4.8%; FT-IR: ν (cm^{-1}) = 3088, 3041, 2959, 2850(C*H*); 1674(C=O); ^{1}H NMR (300 MHz, $CDCl_3$) δ_H 7.41 – 7.25 (m, 7H, Ar*H*), 7.18 – 7.09 (m, 2H, Ar*H*), 6.22 (s, 1H, C*H*), 4.17 (s, 2H, CH_2), 2.30 (s, 3H, CH_3), 2.19 (s, 3H, CH_3). 13C NMR (101 MHz, Methanol-d_4) δ_C 177.4, 165.5, 162.9, 137.8, 136.2, 132.9, 132.5, 131.4., 131.2, 130.5, 129.3, 128.9, 128.8, 127.5, 121.3, 113.4, 113.3, 36.7, 19.5, 18.8. ESI-HRMS(m/z), Anal. Calcd. for $C_{20}H_{18}O_2S$ (%): C, 74.50; H, 5.63; O, 9.96; S, 9.95; O, 4.50; M, 322; Found: C, 74.27; H, 5.88; O, 9.90; S, 9.90; $(M+H)^+$, 323

Synthesis of 3-(4-(4-chlorobenzylthio)phenyl)-2,6-dimethyl-4*H*-pyran-4-one, 2.12b:

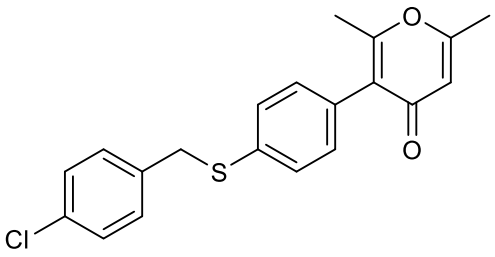

Brownish crystals, Yield 0.38 g, 26%; FT-IR: ν (cm^{-1}) = 3078, 3044, 2921, 2852(CH); 1699(C=O); 1H NMR (300 MHz, $CDCl_3$) δ_H 7.37 – 7.27(m, 6H), 7.19 – 7.12 (m, 2H), 6.22 (s, 1H), 4.12 (s, 2H, C*H*2), 2.30 (s, 3H), 2.19 (s, 3H, C*H*$_3$). ^{13}C NMR (75 MHz, $CDCl_3$) δ_C 207.1, 178.4, 164.7, 162.7, 135.9, 133.0, 130.7 (2C), 130.1 (2C), 129.4 (2C), 128.6 (2C), 125.9, 113.7, 77.47, 38.1, 19.8, 18.6. ESI-HRMS(m/z), Anal. Calcd. for $C_{20}H_{17}ClO_2S$ (%): C, 67.31; H, 4.80; Cl, 9.93; O, 8.97; S, 8.99; M, 356; Found: C, 67.22; H, 4.76; Cl, 9.94; O, 8.96; S, 8.96; (M+H) +, 357.

Synthesis of 3-(4-(benzylthio)phenyl)-2,6-dimethylpyridin-4(1*H*)-one, 2.9a:

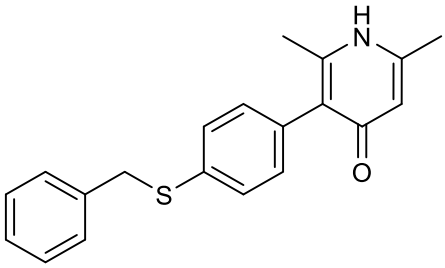

Brown powder, Yield 0.13 g, 28%; FT-IR: ν (cm^{-1}) = 3289(NH); 3056, 3026, 2918, 2850(C*H*); 1708(C=O); ^{1}H NMR (300 MHz, DMSO-d_6) δ_H 11.19 (s, 1H, N*H*), 7.44 – 7.19 (m, 7H, Ar*H*), 7.09 (d, $^3J_{HH}$ = 8.3 Hz, 2H, Ar*H*), 5.95 (s, 1H, py*H*), 4.26 (s, 2H, C*H*$_2$), 2.20(s, 3H, C*H*$_3$), 2.05 (s, 3H, C*H*$_3$). ^{13}C NMR (101 MHz, Methanol-d_4) δ 178.9, 147.8, 146.1, 137.7, 135.6, 132.8, 130.6, 129.2 (2C), 128.5 (2C), 128.0 (2C), 126.7 (2C), 78.0, 37.9, 17.3, 16.7. ESI-HRMS(m/z), Anal. Calcd. for $C_{20}H_{19}NOS$ (%): C, 74.73; H, 5.96; N, 4.36; O, 4.98; S, 9.98; M, 321; Found: C, 74.51; H, 6.21; N, 4.35; O, 4.97; S, 9.93; $(M+H)^+$, 322.

Synthesis of 3-(4-(4-chlorobenzylthio)phenyl)-2,6-dimethylpyridin-4(1*H*)-one, 2.9b

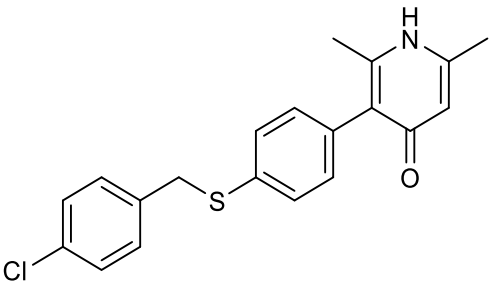

Brown powder, Yield 0.04 g, 9.4%; FT-IR: ν (cm^{-1}) = 3286 (N*H*); 3077, 3041, 2956, 2876(C*H*); 1689(C=O); ^{1}H NMR (300 MHz, DMSO-d_6) δ_H 11.11 (s, 1H, N*H*), 7.44 – 7.26 (m, 6H, Ar*H*), 7.09 (d, $^{3}J_{HH}$ = 8.3 Hz, 2H, Ar*H*), 5.92 (s, 1H, py*H*), 4.26 (s, 2H, CH_2), 2.19 (s, 3H, CH_3), 2.04 (s, 3H, CH_3). ^{13}C NMR (75 MHz, DMSO-d_6) δ_C 178.9, 160.9, 147.7, 147.2, 137.2, 134.3, 133.7, 132.0, 131.6 (2C), 131.1 (2C), 128.8 (2C), 128.2 (2C), 79.6, 33.9, 18.2, 16.1. ESI-HRMS(m/z), Anal. Calcd. for $C_{20}H_{18}ClNOS$ (%): C, 67.50; H, 5.10; Cl, 9.96; N, 3.94; O, 4.50; S, 9.01; M, 355; Found: C, 67.79; H, 4.80; Cl, 10.03; N, 3.95; O, 9.04; S, 9.03; (M-H) +,354.

Synthesis of 4,4,5,5-tetramethyl-2-(4-styrylphenyl)-1,3,2-dioxaborolane 2.14

To a stirring solution of 4-bromostilbene (518.5 mg, 2.00 mmol), bis(pinacolate)diboron (661 mg, 2.60 mmol) in dry 1,4-dioxane (8 mL) at room temperature under nitrogen condition, was added $PdCl_2$(dppf) (163.2 mg, 0.2 mmol) and KOAc (589.1 mg, 6.00 mmol) successively. The reacting mixture was stirred and was heated at 120℃ for 5 h under nitrogen condition. The reaction mixture was cooled to room temperature, diluted with EtOAc and filtered through celite. The filtrate was extracted with EtOAc (320 mL), washed with water (310 mL), brine(25 mL), and the organic layer was collected, dried with $MgSO_4$, and concentrated with *in vacuo*.

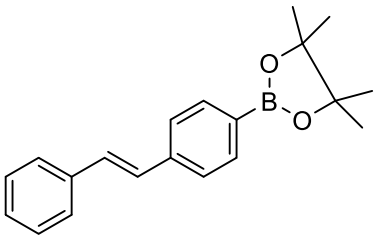

White powder, Yield 62.4%; m.p. 116-120℃; FT-IR: ν (cm^{-1}) = 2978, 2923, 2854(C*H*); 1602(C=C); 1300(C-O); ^{1}H NMR (400 MHz, $CDCl_3$) δ_H 7.78 – 7.70 (m, 2H), 7.50 – 7.39 (m, 4H), 7.29(t, $^{3}J_{HH}$ = 7.5 Hz, 2H, ArH), 7.22 – 7.15 (m, 1H, ArH), 7.07

(d, J = 12.1 Hz, 2H), 1.28 (s, 12H, 4×CH_3). ^{13}C NMR (75 MHz, $CDCl_3$) δ_C 140.0, 137.1, 135.2 (2C), 129.6, 128.7 (2C), 128.6, 127.8 (2C), 126.6 (2C), 125.8 (2C), 83.8 (2C), 24.8 (4C).

General Procedure for the synthesis of 4-(*E*)-1,2-diphenylethene)-2,6-dimethyl-3-phenyl-4*H*-pyran-4-one derivatives, 2.15, 2.22-2.25

To a solution of 4,4,5,5-tetramethyl-2-(4-styrylphenyl)-1,3,2-dioxaborolane, in dry 1,4- were added 3-(4-bromophenyl)-2,6-dimethyl-4H-pyran-4-one, $PdCl_2(PPh_3)_2$ (61.7 mg, 0.0879 mmol), K_2CO_3 (364.9 mg,2.64 mmol) dissolved in minimum amount of water, under Nitrogen gas. The reacting mixture was stirred, heated to 80℃ for 3 h.

Synthesis of 4-(*E*)-1,2-diphenylethene-2,6-dimethyl-3-phenyl-4*H*-pyran-4-one 2.15:

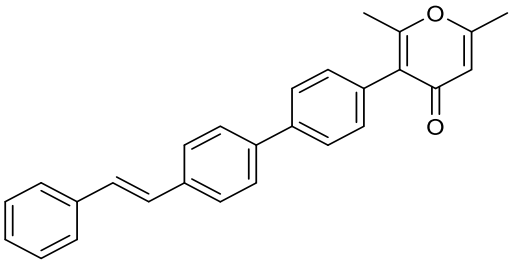

Yellow powder, Yield 38.5%; m.p. 261- 262℃; FT-IR: ν (cm^{-1}) = 2952, 2921, 2855(C*H*); 1700(C=O); ^{1}H NMR (400 MHz, $CDCl_3$) δ_H 7.58 (t, $^3J_{HH}$= 6.9 Hz, 1H, Ar*H*), 7.53 (t, $^3J_{HH}$ = 6.3 Hz, 3H, Ar*H*), 7.47 (d, $^3J_{HH}$ = 7.7 Hz, 2H, Ar*H*), 7.30 (t, $^3J_{HH}$ = 7.6 Hz, 2H, Ar*H*),7.23 (dd, $^3J_{HH}$ = 14.7, $^3J_{HH}$ = 7.8 Hz, 3H, Ar*H*), 7.19 (s, 2H, Ar*H*), 7.09 (s, 2H), *H*-C=C-*H*) 6.17 (s, 1H, -C=C-*H*), 2.23 (s, 3H, CH_3), 2.18 (s, 3H, CH3). ^{13}C NMR (101 MHz, $CDCl_3$) δ_C 186.82, 178.61, 164.66, 162.67, 140.14, 140.01, 137.34, 136.47, 131.65, 130.62 (2C), 128.80(2C), 128.21(2C), 127.67, 127.37(2C), 126.97(2C), 126.95(2C), 126.55(2C), 126.31, 22.71, 18.75.

Synthesis of 2,6-dimethyl-3-(4-styrylphenyl)-4*H*-pyran-4-one, 2.22:

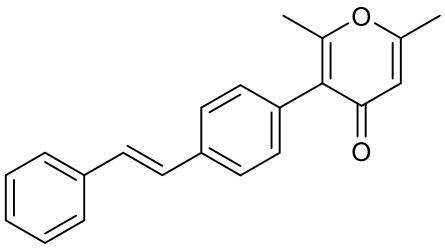

White solid, Yield 58.9%; m.p.185.3-186.8°C; FT-IR: ν (cm^{-1}) = 3036, 2922, 2822(CH); 1650 (C=O); 1608 (C=C); ^{1}H NMR (400 MHz, $CDCl_3$) δ_H 7.46 (dd, $^{3}J_{HH}$ = 6.4, $^{3}J_{HH}$ = 4.0 Hz, 1H), 7.18 (m, 5H, Ar*H*), 7.05(dd, *J* = 14.4, $^{3}J_{HH}$ = 8.0 Hz, 3H, Ar*H*) 6.16 (s, 1H, -C=C*H*), 2.86 (s, 4H, H_2C=CH_2), 2.22 (s, 3H, CH_3), 2.11(s, 3H, CH_3). ^{13}C NMR (101 MHz, $CDCl_3$) δ_C 178.8, 164.6, 162.7, 141.8, 141.4, 131.9, 131.6, 130.1(2C), 128.5(2C), 128.4.(2C), 128.4(2C), 125.9, 113.7, 37.8, 29.7, 19.9, 18.7.

Synthesis of 2,6-dimethyl-3-(4-phenethylphenyl)-4*H*-pyran-4-one, 2.2:

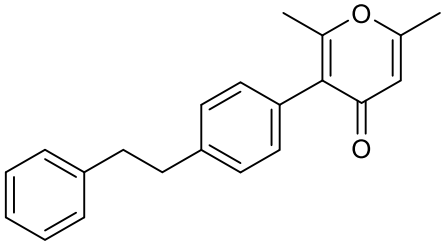

Yellow-green solid, Yield 55.4%; m.p. 112 - 113°C; FT-IR: ν (cm^{-1}) = 3035, 2923, 2853(CH); 1659(C=O); 1608 (C=C); ^{1}H NMR (400 MHz, $CDCl_3$) δ_H 7.51 – 6.99 (m, 9H, Ar*H*), 6.16 (s, 1H, C*H*), 2.86 (s, 4H, (2×CH_2), 2.21 (s, 3H, CH_3), 2.11 (s, 3H, CH_3).^{13}C NMR (101 MHz, $CDCl_3$) δ_C 178.5, 164.6, 162.6, 137.2, 136.9, 131.8, 130.5(2C), 129.0, 128.7(2C), 128.3, 127.7, 126.7(2C), 126.5(2C), 126.3, 113.8, 19.8, 18.7.

Synthesis of 2,6-dimethyl-3-(4-(naphthalen-3-yl)phenyl)-4*H*-pyran-4-one, 2.24

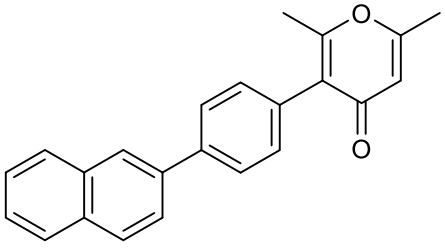

Spike-like golden yellow solid, Yield 75.4%; m.p. 253–255 ^{o}C; FT-IR: ν (cm^{-1}) = 3042, 2922, 2852(C*H*); 1657(C=O); ^{1}H NMR (400 MHz, $CDCl_3$) δ_H 7.98 (s, 1H, ArH), 7.81 (dt, $^{3}J_{HH}$ = 9.0, $^{3}J_{HH}$ = 5.2 Hz, 3H, Ar*H*),7.69 (d, $^{3}J_{HH}$ = 8.3 Hz, 3H, Ar*H*), 7.47 – 7.36 (m, 2H, Ar*H*), 7.28 (d, $^{3}J_{HH}$ = 8.3 Hz, 2H, Ar*H*), 6.16 (s, 1H, C=CH), 2.21 (s, 3H, CH_3), 2.17 (s, 3H, CH3). ^{13}C NMR (101 MHz, $CDCl_3$) δ_C 178.6,

164.6,162.7, 140.6, 138.2, 133.7, 132.7, 131.7, 130.7(2C), 128.5, 128.2, 127.7, 127.4(2C), 126.30(2C), 125.9, 125.8, 125.6, 113.8, 19.8, 18.8.

Synthesis of (*E*)-3-(4-(4-fluorostyryl)phenyl)-2,6-dimethyl-4*H*-pyran-4-one, 2.25:

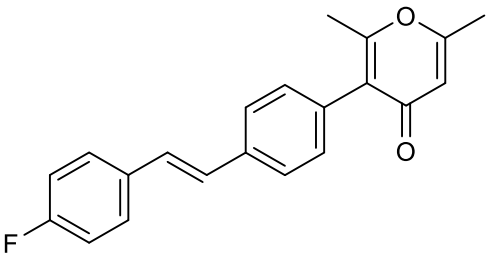

Yellow-white flaky crystals, Yield 0.527 g, 54.7%. ^{1}H NMR (300 MHz, $CDCl_3$) δ_H 7.60 – 7.45 (m, 4H, Ar*H*), 7.29 – 7.23 (dd, $^{3}J_{HH}$ =11.2, $^{3}J_{HH}$ = 5.2 Hz, 2H, *H*C=C*H*), 7.13 – 7.03 (m, 4H, Ar*H*), 6.23 (s, 1H, -C=C*H*), 2.31 (s, 3H, CH_3), 2.24 (s, 3H, CH_3). ^{13}C NMR (75 MHz, CDCl3) δ_C 178.5, 164.6, 163.9, 162.6, 160.7, 136.7, 133.5, 133.4, 131.9, 130.5, 128.1, 127.9, 127.8, 126.4, 126.3, 115.8, 115.5, 113.8, 113.8, 19.7, 18.7.

General Procedure for the Synthesis of 2-substituted benzimidazoles using 3.2c as an example

A solution of 4-nitro-o-phenylenediamine 1a (3.0 g, 19.59 mmoles) in 4N HCl was allowed to stir at an ambient temperature for 10 min. To this stirred solution was added the formic acid

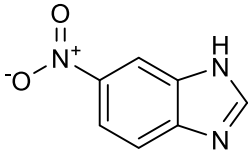

(1.11 mL, 29.39 mmol) was added. The reaction mixture was further heated under reflux at 95o C for 2 hrs. The completion of the reaction was then monitored by TLC. The product mixture was allowed to cool to ambient temperature and basified with 20% sodium hydroxide (pH=10-14) which was allowed to cool on an ice/water bath. The resulting precipitate was filtered, washed with water, and allowed to dry, to afford 6-nitro-1H-benzo[d]imidazole, **3.2c**.

Grey powder, (3.4 g, 70.90%); ^{1}H NMR (300 MHz, DMSO-d$_6$) δ_H 8.14 (dd, 1H, $^{3}J_{HH}$ = 8.4, 5.6 Hz, Ar*H*), 7.59 (s, 1H, N*H*), 7.37 (t, 1H, $^{3}J_{HH}$ = 8.7 Hz, Ar*H*), 7.22 (dd, 1H, $^{3}J_{HH}$ = 5.9, 3.1 Hz, Ar*H*) 2.09 (s, 1H, N*H*).[242]

Synthesis of 2-methyl-1*H*-benzo[d]imidazole, 3.2a:

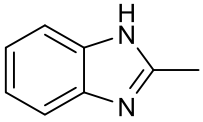

Grey powder, (1.40 g, 39%); ^{1}H NMR (300 MHz, DMSO-d$_6$) δ_H 7.63 – 7.27 (m, 2H, Ar*H*), 7.20 – 6.96 (m, 2H, Ar*H*), 2.50 (s, 3H, C*H*$_3$).[243]

Synthesis of 2-methyl-6-nitro-1*H*-benzo[d]imidazole, 3.2b:

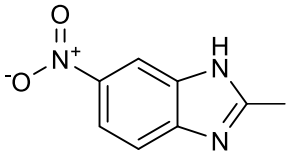

Grey powder, (1.91 g, 54.6%), ^{1}H NMR (300 MHz, DMSO-d$_6$) δ_H 8.36 (s, 1H, Ar*H*), 8.13 – 8.00 (m, 1H, Ar*H*), 7.64 (d, 1H, $^{3}J_{HH}$ = 8.8 Hz, Ar*H*), 2.51 (s, 3H, C*H*$_3$), 2.09 (s, 1H, N*H*).

General Procedure for the synthesis of 2-(4-substitutedphenyl) benzimidazoles, (3.2f as an example):

To a stirred solution of sodium metabisulphite (2.48 g, 13.06 mmol) in distilled water (10 ml), 4-Chlorobenzaldehyde (3.67 g, 26.12 mmol) was added, followed by the addition ethanol (50 ml). The resultant reaction mixture could stir for 30 min at ambient temperature. On cooling the mixture on ice, the precipitate was deposited, filtered, washed with ethanol, and dried. In a separate round bottom flask, the pretreated aldehyde was added to a stirred solution of 4-Nitro-o-phenylenediamine (2.0 g, 13.06 mmol) in anhydrous DMF. The resultant reaction mixture was stirred under reflux at 120℃ for 4 h under an inert atmosphere; TLC confirmed the completion of the reaction. The final mixture was basified with 20% sodium hydroxide solution

(pH=10-14) to yield precipitate, which was filtered, washed with water, and dried to afford clean, 2-(4-Chlorophenyl)-5-nitrobenzimidazole, **3f**, without further purification [244].

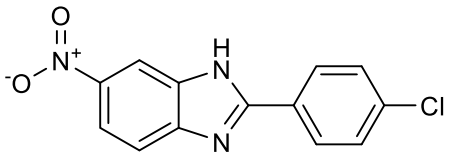

Yellow powder, (2.39 g, 67.4%); 1H NMR (300 MHz, DMSO-d6) δ_H 8.22 (d, 2H, $^3J_{HH}$ = 8.6 Hz, Ar*H*), 8.16 (s, 1H), 7.76 (d, 1H, J = 8.2 Hz, Ar*H*), 7.67 (d, 2H, $^3J_{HH}$ = 8.6 Hz, ArH), 7.62 (dd, 1H, $^3J_{HH}$ = 8.3, 1.5 Hz, Ar*H*), 2.09 (s, 1H, N*H*).

Synthesis of 2-(4-fluorophenyl)-6-nitro-1*H*-benzo[d]imidazole 3.2d;

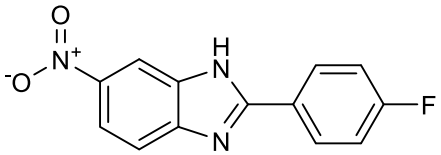

White powder, (4.98 g, 84.6%) ^{1}H NMR (300 MHz, DMSO-d_6) δ_H 8.14 (d, 1H, $^3J_{HH}$ = 46.7 Hz), 7.75 (dd, 3H, $^3J_{HH}$ = 23.2, 7.8 Hz), 7.62 (d, 1H, $^3J_{HH}$ = 7.9 Hz, Ar*H*),7.57 – 7.41 (m, 1H), 7.13 (ddd, 1H, $^3J_{HH}$ = 8.3, 2.6, 1.0 Hz, Ar*H*), 2.09 (s, 1H, N*H*).

Synthesis of 2-(4-chlorophenyl)-1*H*-benzo[d]imidazole 3.2e

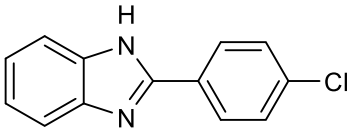

^{1}H NMR (300 MHz, DMSO-d_6) δ_H 8.14 (dd, J = 8.6, 5.4 Hz, 2H), 7.60 (s, 2H), 7.37 (t, J = 8.7 Hz, 2H), 7.22 (dd, J = 6.1, 3.2 Hz, 2H), 2.06(s, 1H).[245]

Synthesis of 4-(2-bromoethoxy)-3-methoxybenzaldehyde 3.3

To a solution of vanillin (5.00 g, 32.86 mmol) in anhydrous acetone (20 mL), K_2CO_3 (13.60 g, 98.58 mmol, 3 eq.) was added. This mixture was allowed to stir for 5 min under N_2 atmosphere, followed by the addition of dibromoethane (8.50 mL, 98.58 mmol). This reaction mixture was refluxed at 75℃ for 15 h. The excess solvent was evaporated *in vacuo* under reduced pressure, and residue was taken up in water and was extracted with DCM. The resulting organic layer was combined, dried with $MgSO_4$, and evaporated *in vacuo*. Then, the crude product was

purified with flash column chromatography using 100% DCM. The product gave white crystals.

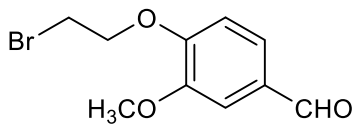

White crystals (3.6 g, 40.5%); FT-IR: ν (cm^{-1}) = 3081, 3000, 2960, 2850 (CH), 1676 cm^{-1}, (C=O) 1585 (C=C), 1262, 1229 (C-O); ^{1}H NMR (300 MHz, $CDCl_3$) δ_H 9.89 (s, 1H, C*H*O), 7.47 (d, $^{3}J_{HH}$ = 7.3 Hz, 2H, Ar*H*), 7.01 (d, $^{3}J_{HH}$ = 8.5 Hz, 1H, Ar*H*), 4.54 – 4.34 (m, 2H, CH_2), 3.96 (s, 3H, OCH_3), 3.81 – 3.66 (m, 2H, CH_2). [246]

Synthesis of 4-(2-(2-substituted-1*H*-benzo[d]imidazol-1-yl)ethoxy)-3-methoxybenzaldehyde, 3.4a-e, (using compound 3.4a as example):

To a solution of benzimidazole **3.2a** (0.3g, 2.27 mmol) in DMSO (11 mL) was added, finely ground KOH (0.127 g, 2.27 mmol). The reacting mixture was then allowed to stir for 15 min at 35°C, followed by the addition of 4-(2-bromoethoxy)-3-methoxybenzaldehyde, 3.3 (0.612 g, 2.49 mmol). The temperature was further increased to 75°C and refluxed for 6 h. The completion of the reaction was monitored by TLC. The product mixture was allowed to cool to room temperature. On dropwise addition of distilled water, the precipitate formed was filtered, washed with water, and 5% solution of KOH. The product was allowed to dry, and a portion was used for the next reaction without further purification.

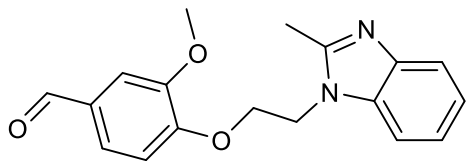

Grey solid, Yield 0.33 g, 39.43%; mp: 167-169°C; FT-IR: ν (cm^{-1}) = 3064, 3000, 2942, 2839 (C*H*), 1669 (C=O), 1589(C=C), 1511 (C=N stretching); 1669 cm^{-1}(C=O) , 1589(C=C), 1511 cm^{-1} (C=N stretching); ^{1}H NMR (300 MHz, DMSO-d_6): δ_H 9.81 (s, 1H, C*H*O), 7.60-7.55 (m, 2H, Ar*H*), 7.50 (t, 2H, $^{3}J_{HH}$ = 9.0 Hz, Ar*H*), 4.64 (t, 2H, $^{3}J_{HH}$ = 4.6 Hz, CH_2)), 4.38 (t, 2H, $^{3}J_{HH}$ = 4.7 Hz, CH_2), 3.80 H_3), 2.67 (s, 3H, CH_3). ^{13}C NMR (75

MHz, DMSO) δ_C 191.9, 153.3, 153.2, 149.4, 142.5, 135.3, 130.3, 126.3, 121.9, 121.8, 118.4, 112.2, 110.5, 110.0, 67.5, 56.0, 43.1, 13.8. ESI-HRMS (m/z) = 311.1449 $(M+H)^+$. Anal. Calcd for $C_{18}H_{18}N_2O_3$: 310.35; C, 69.66; H, 5.85; N, 9.03; O, 15.47% Found: C, 69.42; H, 5.79; N, 8.99; O, 15.43%.

Synthesis of 4-(2-(2-methyl-5-nitro-1*H*-benzo[d]imidazol-1-yl)ethoxy)-3-methoxybenzaldehyde, 3.4b:

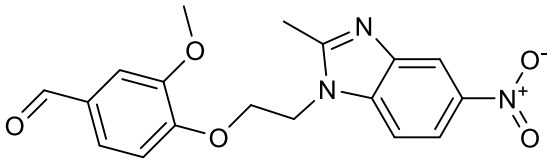

Peach solid, Yield 0.82 g, 80.5%; m.p. 208-210°C; ^{1}H NMR (300 MHz, DMSO-d_6) δ_H 9.80(s, 1H, C*H*O), 8.53 (dd, $^3J_{HH}$ = 109.7, 2.2 Hz, 1H, Ar*H*), 8.12 (ddd, $^3J_{HH}$ = 31.4, 8.9, 2.3 Hz, 1H, Ar*H*), 7.77 (dd, $^3J_{HH}$ = 72.0, 8.9 Hz, 1H, Ar*H*), 7.50 (dd, $^3J_{HH}$ = 8.2, 1.9 Hz, 1H, Ar*H*), 7.34 (dd, $^3J_{HH}$ = 7.2, 1.9 Hz, 1H, Ar*H*), 7.11 (dd, $^3J_{HH}$ = 8.3, 4.5 Hz, 1H, Ar*H*), 4.82 (t, $^3J_{HH}$ = 4.7 Hz, 2H, CH_2), 4.50 (t, $^3J_{HH}$ = 4.8 Hz, 2H, CH_2), 3.79 (s, 3H, CH_3), 2.76 (s, 3H, OCH_3). ^{13}C NMR (101 MHz, DMSO) δ_C 191.88, 159.14, 157.85, 153.10, 149.48, 147.48, 140.28, 135.18, 130.51, 126.29, 118.59, 114.55, 112.42, 108.29, 67.63, 56.05, 43.76, 14.32.ESI-HRMS (m/z) = 356.1246 $(M+H)^+$ Anal. Calcd for $C_{18}H_{17}N_3O_5$: 355.34; C, 60.84; H, 4.82; N, 11.83; O, 22.51% Found.: C, 60.65; H, 4.74; N, 11.79; O, 22.46%.

Synthesis of 4-(2-(5-nitro-1*H*-benzo[d]imidazol-1-yl)ethoxy)-3-methoxybenzaldehyde, 3.4c:

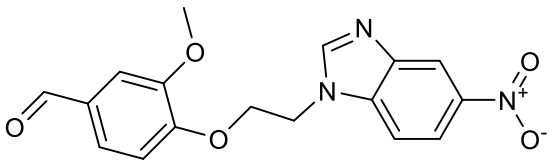

Orange solid, Yield 0.48 g, 76.5%; mp: 180-182°C; FT-IR: ν (cm^{-1}) = 3105, 3016, 2966, 2891, 2847(C*H*), 1740 (C=O), 1592(C=C),1499 (C=N); ^{1}H NMR (300 MHz, DMSO-d_6) δ_H 9.82 (s, 1H, C*H*O), 8.71 – 8.49 (m, 2H, Ar*H*), 8.29 – 7.95 (m, 1H, Ar*H*), 7.83 (d, 1H, $^{3}J_{HH}$ = 8.9 Hz, Ar*H*), 7.51 (d, 1H, $^{3}J_{HH}$ = 8.2 Hz, Ar*H*), 7.35 (s, 1H, Ar*H*), 7.15 (d, 1H, *J* = 8.2 Hz, Ar*H*), 4.82 (t, 2H, $^{3}J_{HH}$ = 4.6 Hz, CH_2), 4.48 (t, 2H, $^{3}J_{HH}$ = 4.7 Hz, CH_2), 3.80 (s, 3H, OCH_3). ^{13}C NMR (101 MHz, $CDCl_3$) δ_C 196.81, 157.84, 154.40, 152.87, 148.07, 143.86, 138.89, 135.30, 130.98, 124.77, 123.01, 122.39, 117.51, 114.94, 73.15, 60.86, 49.47.ESI-HRMS (m/z) = 342.1090 $(M+H)^+$ Anal. Calcd. for $C_{17}H_{15}N_3O_5$: 341.32; C, 59.82; H, 4.43; N, 12.31; O, 23.44% Found.: C, 59.63; H, 4.68; N, 12.27; O, 23.38%.

Synthesis of 4-(2-(2-(4-fluorophenyl)-5-nitro-1*H*-benzo[d]imidazol-1-yl)ethoxy)-3-methoxybenzaldehyde, 3.4d:

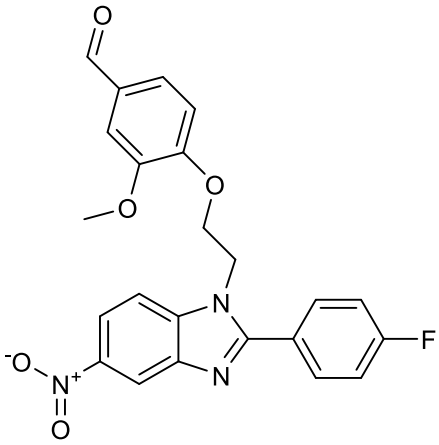

Orange solid, Yield 0.84 g, 49.6%; m.p. 91-93°C; FT-IR: ν (cm^{-1}) =3061, 3003, 2956, 2951, 28547(C-H), 1679 (C=O), 1596(C=C), 1433(C=N); ^{1}H NMR (400 MHz, DMSO-d_6) δ_H 9.82 (s, 1H, C*H*O), 8.04 (s, 1H, Ar*H*), 7.83 (d, 1H, $^{3}J_{HH}$ = 8.1 Hz, Ar*H*), 7.69 (d, 1H, $^{3}J_{HH}$ = 7.7 Hz, Ar*H*), 7.49 – 7.26 (m, 6H, Ar*H*), 7.11 (d, 1H, $^{3}J_{HH}$ = 8.3 Hz, Ar*H*), 4.69 (t, 2H, $^{3}J_{HH}$ = 4.9 Hz, CH_2), 4.53 (t, 2H, $^{3}J_{HH}$ = 4.9 Hz, CH_2), 3.80 (s, 3H, OCH_3). ^{13}C NMR (101 MHz, DMSO) δ_C 207.06, 191.88, 153.53, 152.95, 149.47, 147.98, 143.03, 135.82, 132.89, 132.71, 130.46, 126.22, 122.97, 122.71, 119.56, 116.04, 115.83, 112.30, 111.92, 110.02, 66.96, 56.01, 44.37. ESI-HRMS (m/z) = 437.1953; Anal. Calcd. for $C_{23}H_{18}FN_3O_5$: 435.4045; C, 63.45; H, 4.17; F, 4.36; N, 9.65; O, 18.37% Found: C, 63.12; H, 4.12; F, 4.35; N, 9.61; O, 18.29%.

4-(2-(2-(4-chlorophenyl)-1*H*-benzo[d]imidazol-1-yl)ethoxy)-3-methoxybenzaldehyde, 3.4e:

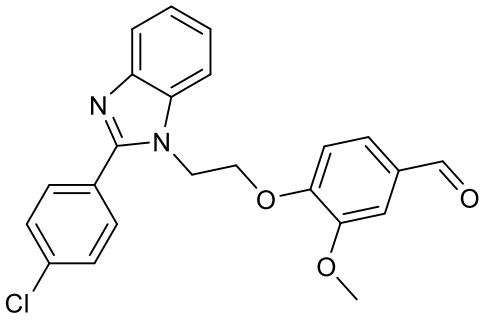

Yellow solid, Yield 0.33 g, 61.5%; mp: 153-155°C; FT-IR: ν (cm^{-1}) =3062, 3003, 2975, 2930, 2875, 2829(C-H), 1689(C=O), 1590(C=C), 1507(C=N). ^{1}H NMR (300 MHz, DMSO-d_6) δ_H 9.82 (s, 1H, C*H*O), 8.24 – 8.13 (m, 1H, Ar*H*), 7.96 (d, 2H, $^{3}J_{HH}$ = 8.6 Hz, Ar*H*), 7.87 – 7.81 (m, 1H, Ar*H*), 7.75 – 7.68 (m, 1H, Ar*H*), 7.63 – 7.56 (m, 2H, ArH), 7.47 (dd, 1H, $^{3}J_{HH}$ = 8.3 and 1.8 Hz, Ar*H*), 7.37 – 7.27 (m, 2H, Ar*H*), 4.71 (t, 2H, $^{3}J_{HH}$ = 4.9 Hz, CH_2), 4.52 (t, 2H, $^{3}J_{HH}$ = 4.8 Hz, CH_2), 3.79 (s, 3H, OCH_3). ^{13}C NMR (75 MHz, DMSO) δ_C 192.4,162.2, 161.0, 153.3, 152.9, 149.4, 143.1, 135.1, 132.1, 130.4, 129.5, 128.6, 126.9, 126.2, 123.1, 122.8, 119.6, 119.3, 111.9, 111.3, 66.9, 55.9, 44.29; ESI-HRMS (m/z) = 407.1167 $(M+H)^+$ Anal. Calcd. for $C_{23}H_{19}ClN_2O_3$:406.11; C, 67.90; H, 4.71; Cl, 8.71; N, 6.89; O, 11.80% Found: C, 67.79; H,4.67 ; Cl, 8.72 N, 6.88 ; O, 11.79%.

General Procedure for the Synthesis of (*E*)-N-((3-(2-(2,6-disubstituted-1*H*-benzo[d]imidazol-1-yl)ethoxy)-5-methoxyphenyl)methylene)-4-fluorobenzenamines 3.6a-e (3.6c a example):

4-Fluoroaniline (0.13mL, 1.42 mmol) was added to a solution of 3-(2-(2,5-disubstituted-1H-benzo[d]imidazol-1-yl)ethoxy)-5-methoxybenzaldehyde (0.48 g, 1.42 mmol) in dichloromethane (20 mL).The mixture was stirred for 5min at room temperature, and 10 drops of pyrollidine was added. The reacting mixture was heated up to 60 °Cwith a Dean Stark and a condenser set up overnight. The reaction mixture was cooled, concentrated under reduced

pressure. The crude product was crystallized from ethanol, filtered, and air-dried to afford a clean product.

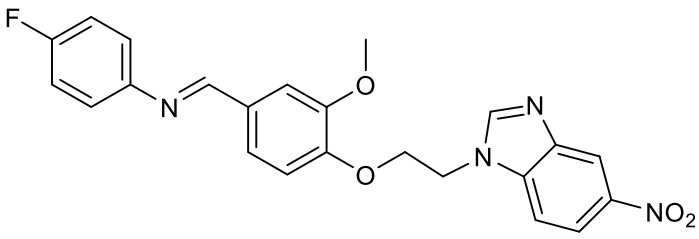

White powder, Yield 0.53 g, 86.9%; m.p. 123-125°C; FT-IR: ν (cm^{-1}) = 3068, 2938, 2875(C*H*), 1588 (C=C) 1502(C=N); ^{1}H NMR (400 MHz, $CDCl_3$) δ_H 8.58 (d, *J* = 55.2 Hz, 1H, Ar*H*), 8.28 (s, 1H, C*H*), 8.24 (s, 1H, C*H*)), 8.17 (d, *J* = 13.0 Hz, 1H, Ar*H*), 7.85 – 7.44 (m, 2H, ArH), 7.22 – 6.93 (m, 5H, ArH), 6.76 (dd, *J* = 8.2, 3.3 Hz, 1H, ArH), 4.69 – 4.54 (m, 2H, CH_2),), 4.39 – 4.29 (m, 2H,CH_2) 3.85 (s, 3H, OCH_3).^{13}C NMR (75 MHz, $CDCl_3$) δ_C 162.75, 159.26, 149.98, 147.20, 143.97, 130.70, 123.80, 122.32, 120.49, 118.77, 118.13, 117.14, 116.03, 112.50, 110.15, 109.55, 107.36, 67.61, 55.93, 45.06; ESI-HRMS (m/z) = 435.1469; Anal. Calcd. for $C_{23}H_{19}FN_4O_4$: 434.139; C, 63.59; H, 4.72; F, 4.37; N, 12.90; O, 14.73% Found: $C_{23}H_{19}FN_4O_4$: 435.1469; C, 63.43; H, 4.59; F, 4.37; N, 12.87; O, 14.71%.

Synthesis of (*E*)-*N*-((4-(2-(2-methyl-1*H*-benzo[d]imidazol-1-yl)ethoxy)-3-methoxyphenyl)methylene)-4-fluorobenzenamine 3.6a:

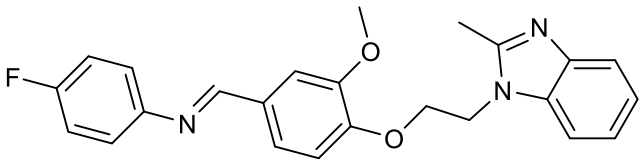

Grey Powder, Yield 0.19 g, 43.9%; m.p. 148-150°C; ^{1}H NMR (400 MHz, $CDCl_3$) δ_H 8.23 (s, 1H), 7.66 – 7.58 (m, 1H), 7.47 (s, 1H), 7.32 – 7.25 (m, 1H), 7.19 – 7.16 (m, 2H), 7.15 – 7.06 (m, 3H), 6.99 (t, J = 8.6 Hz, 2H), 6.69 (d, J = 8.2 Hz, 1H), 4.52 (t, J = 5.3 Hz, 2H), 4.28 (t, J = 5.3 Hz, 2H), 3.82 (s, 3H), 2.70 (s, 3H); ^{13}C NMR (101 MHz, $CDCl_3$) δ_C 159.46, 152.73, 150.52, 149.79, 148.10, 134.73, 130.32, 123.96, 122.29, 122.20, 119.11, 115.96, 115.74, 111.92, 108.90, 66.81, 55.88, 43.39, 13.86;

ESI-HDMS (m/z) = 404.1276 $(M+H)^+$; Anal. Calcd. for $C_{24}H_{22}FN_3O_2$: 403.45; C, 71.45; H, 5.50; F, 4.71; N, 10.42; O, 7.93% Found.: C, 86.11; H, 5.44; F, 4.70; N, 10.3; O, 7.92%.

Synthesis of (*E*)-*N*-((4-(2-(2-methyl-5-nitro-1*H*-benzo[d]imidazol-1-yl)ethoxy)-3-methoxyphenyl)methylene)-4-fluorobenzenamine 3.6b:

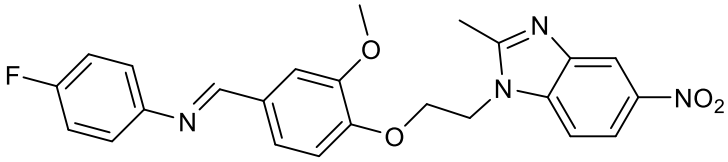

Orange powder; Yield: (0.42. g, 57.2%); m.p, 179-183°C; FT-IR: (cm^{-1}) = 3038, 2992, 2952(C-H), 1591(C=C) 1512(C=N); ^{1}H NMR (400 MHz, $CDCl_3$) δ_H 8.43 (dd, J = 68.0, 2.2 Hz, 1H, Ar*H*), 8.23 (s, 1H, C*H*), 8.13 (td, J = 9.0, 2.2 Hz, 1H, Ar*H*), 7.75 – 7.34 (m, 2H, Ar*H*), 7.16 – 6.94 (m, 5H, Ar*H*), 6.72 (dd, J = 8.2, 6.9 Hz, 1H, Ar*H*), 4.68 – 4.52 (m, 2H, CH_2), 4.37 – 4.23 (m, 2H, CH_2), 3.80 (s, 3H, OCH_3), 2.76 (s, 3H, CH_3). ^{13}C NMR (101 MHz, $CDCl_3$) δ_C 159.29, 150.24, 149.79, 143.20, 130.56, 126.18, 123.89, 122.30, 118.99, 118.24, 115.99, 115.76, 112.07, 111.86, 109.50, 109.20, 106.37, 66.99, 55.80, 44.01, 14.37; ESI-HDMS (m/z) = 449.1580 $(M+H)^+$; Anal. Calcd. for $C_{24}H_{21}FN_4O_4$: 448.45; C, 64.28; H, 4.72; F, 4.24; N, 12.49; O, 14.27%. Found: C, 64.22; H, 4.68; F, 4.23; N, 12.49; O, 14.27%.

Synthesis of (*E*)-*N*-((4-(2-(2-(4-fluorophenyl)-1*H*-benzo[d]imidazol-1-yl)ethoxy)-3-methoxyphenyl)methylene)-4-fluorobenzenamine, 3.6d.

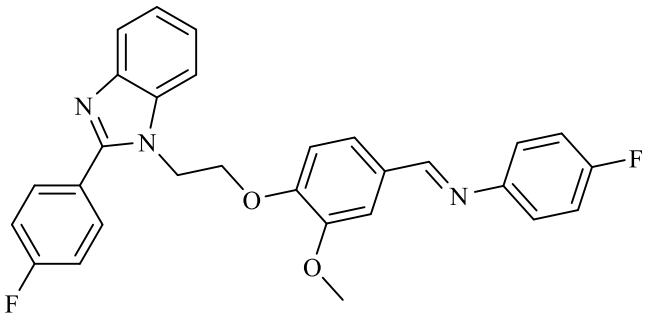

Brown powder, Yield 0.19 g, 40%; m.p. 145-147°C; FT-IR: ν (cm^{-1}) = 3053, 3007, 2958, 2926, 2854 (C-H), 1591(C=C), 1507 (C=N); ^{1}H NMR (400 MHz, $CDCl_3$) δ_H 8.24 (s, 1H, CH), 7.93 (dd, J = 8.6, 5.5 Hz, 2H, Ar*H*), 7.79 – 7.72 (m, 1H, Ar*H*), 7.48 (d, J = 1.8 Hz, 2H, Ar*H*), 7.30

– 7.22 (m, 2H, Ar*H*), 7.18 – 7.06 (m, 5H, Ar*H*), 6.99 (t, J = 8.6 Hz, 2H, Ar*H*), 6.69 (d, J = 8.2 Hz, 1H, Ar*H*), 4.61 (t, J = 5.4 Hz, 2H, CH_2), 4.40 (t, J = 5.5 Hz, 2H, CH_2), 3.82 (s, 3H, OCH_3).^{13}C NMR (101 MHz, $CDCl_3$) δC 158.36, 152.49, 149.39, 148.77, 142.08, 134.51, 131.22, 129.32, 122.90, 122.00, 121.79, 121.25, 121.17, 119.12, 114.93, 114.87, 114.71, 114.66, 110.84, 109.09, 108.34, 65.46, 54.81, 43.30. ESI-HRMS (m/z) = 484.1833 $(M+H)^+$; Anal. Calcd. for $C_{29}H_{23}F_2N_3O_2$: 483.51; C, 72.04; H, 4.79; F, 7.86; N, 8.69; O, 6.62% Found.: C, 71.87; H, 4.75; F, 7.85; N, 8.67; O, 6.61%.

Synthesis of (*E*)-*N*-((4-(2-(2-(4-chlorophenyl)-1*H*-benzo[d]imidazol-1-yl)ethoxy)-3-methoxyphenyl)methylene)-4-fluorobenzenamine 3.6e:

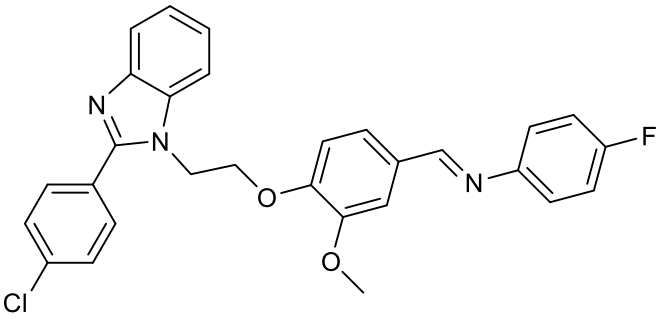

White powder, Yield 0.199 g, 49.4%: m.p. 177-178°C; FT-IR: ν (cm^{-1}) =3084, 3057, 3004, 2922 (C-H), 1587(C=C), 1507(C=N); ^{1}H NMR (400 MHz, $CDCl_3$) δ_H 8.24 (s, 1H), 7.88 (d, J = 8.5 Hz, 2H), 7.80 – 7.73 (m, 1H), 7.51 – 7.41 (m, 4H), 7.33 – 7.23 (m, 2H), 7.16 – 7.05 (m, 3H), 6.99 (t, J = 8.6 Hz, 2H), 6.68 (d, J = 8.2 Hz, 1H), 4.61 (t, J = 5.3 Hz, 2H), 4.40 (t, J = 5.4 Hz, 2H), 3.82 (s, 3H). ^{13}C NMR (101 MHz, $CDCl_3$) δ_C 161.28, 158.85, 158.37, 152.30, 149.33, 148.75, 142.12, 135.14, 134.54, 130.44(2C), 129.32, 127.90(2C), 127.60, 122.89, 122.12, 121.86, 121.25, 121.17, 119.19, 114.93, 114.71, 110.79, 109.11, 108.31, 65.41, 54.81, 43.31.ESI-HRMS (m/z) = 500.1541; Anal. Calcd. for $C_{29}H_{23}ClFN_3O_2$: 499.15; C, 69.67; H, 4.64; Cl, 7.09; F, 3.80; N, 8.40; O, 6.40% Found.: C, 69.12; H, 4.79; Cl, 7.09, F, 3.79; N, 8.39; O, 6.39%.

Synthesis of (*E*)-*N*-((4-(2-(2-(4-chlorophenyl)-5-nitro-1*H*-benzo[d]imidazol-1-yl)ethoxy)-3-methoxyphenyl)methylene)-4-fluorobenzenamine

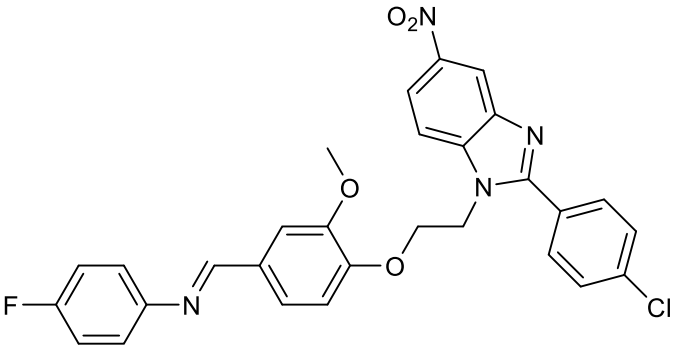

Light-brown powder; (0.19 g, 33.3%), m.p. 200-205°C; FT-IR: ν (cm^{-1}) =3093, 3008, 2965, 2922, 2850 (C-H), 1587(C=C), 1512(C=N); ^{1}H NMR (400 MHz, $CDCl_3$) δ_H 8.60 (dd, J = 38.7, 2.2 Hz, 1H), 8.24 (s, 1H), 8.20 (dd, J = 8.5, 2.1 Hz, 1H), 7.94 – 7.77 (m, 3H), 7.66 (d, J = 9.0 Hz, 1H), 7.49 (d, J = 10.1 Hz, 3H), 7.18 – 6.95 (m, 5H), 6.80 – 6.68 (m, 1H), 4.62 (t, J = 4.7 Hz, 2H), 4.44 (t, $^{3}J_{HH}$ = 4.8 Hz, 2H), 3.80 (s, 3H). ^{13}C NMR (75 MHz, $CDCl_3$) δ_C 162.8, 159.3, 152.5, 150.1, 149.9, 147.8, 147.2, 143.9, 143.8, 133.5, 131.2, 130.7, 123.8, 122.3, 122.2, 120.5, 118.8, 118.1, 117.1, 116.0, 115.7, 112.7, 112.5, 110.2, 109.6, 107.4, 67.6, 55.9, 45.1. ESI-HRMS (m/z) = 545.1392 $(M+H)^+$; Anal. Calcd. for $C_{29}H_{22}ClFN_4O_4$: 544.96; C, 63.91; H, 4.07; Cl, 6.51; F, 3.49; N, 10.28; O, 11.74% Found.: C, 63.84; H, 4.22; Cl, 6.51, F, 3.49; N, 10.27; O, 11.74%.

Synthesis of 6-isocyanoquinoxaline-2,3-(1*H*,4*H*)-dione, 4.2

To a solution of oxalic acid (0.19 g, 2.18 mmol) in aqueous Hydrochloric acid (10 mL, 4 M) was added 3,4-diabenzonitrile (0.2 g, 1.50 mmol). The reaction mixture was refluxed at 100°C for 3 h. The completion of the reaction was confirmed by thin-layer chromatography using 100% ethyl acetate. The reaction mixture was cooled to an ambient temperature, filtered, washed with water, and dried with toluene to afford solid black product. The product was used for the next reaction without any further purification.

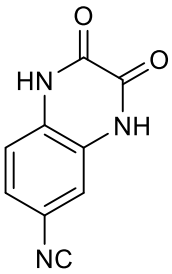

Black powder, Yield 0.18 g, 91.0%; FT-IR: ν (cm^{-1}) = 3379(N-H), 2200(C≡N), 1684(C=O), ^{1}H NMR (300 MHz, DMSO-d_6) δ_H 12.24 (s, 1H, N*H*), 12.11 (s, 1H, N*H*), 7.51 (dd, $^{3}J_{HH}$ = 8.3, 1.8 Hz, 1H, Ar*H*), 7.42 (d, $^{3}J_{HH}$ = 1.7 Hz, 1H, Ar*H*), 7.23 (d, $^{3}J_{HH}$ = 8.3 Hz, 1H, Ar*H*). ^{13}C NMR (101 MHz, DMSO-d_6) δ_C 167.1(CN) 155.6(C=O), 155.2(C=O), 130.3, 127.3, 126.8, 119.2, 118.7, 116.5.

Synthesis of 1,2,3,4-tetrahydro-*N*-hydroxy-2,3-dioxoquinoxaline-6-carboxamidine, 4.3

1 M of KOH (0.060 g, 1.08 mmol) solution in methanol (1.08 mL) was added to a solution of hydroxylamine hydrochloride (75.12 mg, 1.08mmol) in methanol (1.09 mL), at an ambient temperature. The mixture was stirred for 30 mins at room temperature. There was formation of potassium chloride salt, which was filtered and left with the filtrate. To the resulting filtrate in a separate flask, were added 1,2,3,4-tetrahydro-2,3-dioxoquinoxaline-6-carbonitrile (100 mg, 0.540 mmol, 1 eq.) and methanol (10 mL), stirred and heated at 60°C for 16 hours. The reacting mixture was concentrated under to afford a clean brown powder product which was used for the next reaction, without further purification.

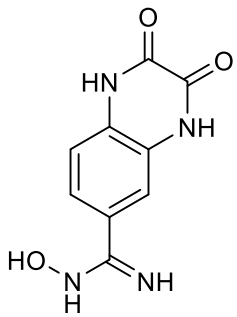

Brown powder, Yield 0.075 g, 74.4%; FT-IR: ν (cm^{-1}) = 3495, 3384(N-H), 1670(C=O), ^{1}H NMR (300 MHz, DMSO-d_6) δ_H 10.88 (s, 1H, OH), 9.63 (s, 1H, N*H*), 7.48 (d, $^{3}J_{HH}$ = 1.8 Hz, 1H), 7.42 – 7.32 (m, 1H, ArH), 7.13 (d, $^{3}J_{HH}$ = 8.4 Hz, 1H, Ar*H*), 5.77 (s, 2H, N*H*), 3.17 (s, 1H, N*H*). ^{13}C NMR (101 MHz, DMSO-d_6) δ_C 167.1(C=NH), 155.6(2C=O), 127.8, 125.9(2C), 121.6, 115.5, 113.6.

Synthesis of 1,2,3,4-tetrahydro-2,3-dioxoquinoxaline-6-carboxamidine, 4.4

To a solution of 1,2,3,4-tetrahydro-N-hydroxy-2,3-dioxoquinoxaline-6-carboxamidine (0.2 g, 0.961 mmol) in acetic acid (6 ml) were added slowly ammonium formate (0.30 g, 4.04 mmol) and 10% Palladium on Carbon (143.15 mg, 1.350 mmol, 1.45 eq.) respectively. The reaction mixture was stirred and refluxed at 120°C for 3 h under nitrogen condition. The mixture was cooled, precipitates formed were filtered through celite and washed with acetic acid. Filtrate was concentrated under reduced pressure. The residue was basified with 1 M NaOH until the precipitate crushed out of the solution at a pH of 6. The precipitate was filtered, wash with distilled water and air dried to afford a brown powder product, which was used for the next reaction without further purification.

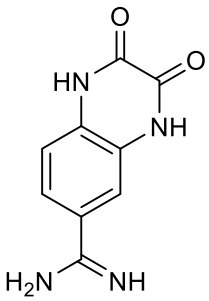

White powder, Yield 0.19 g, 82.4%; FT-IR: ν (cm^{-1}) = 3374, 3300(N-H), 1684(C=O), ^{1}H NMR (400 MHz, DMSO-d_6) δ_H 7.49 (s, 1H, Ar*H*), 7.42 (d, $^{3}J_{HH}$ = 8.4 Hz, 1H, Ar*H*), 7.19 (d, $^{3}J_{HH}$ = 8.3 Hz, 1H, Ar*H*), 1.72 (s, 4H, 4(N*H*).

General procedure for the synthesis of target compounds (4.5a-f) using 4.5f as an example

Triethylamine (O.67 mL, 4.16 mmol) was added to a solution of benzimidamide hydrochloride (0.2 g, 1.04 mmol) and benzylisothiocyanate (0.310 mL, 2.08 mmol) in DMSO (10 mL).The resulting mixture was stirred at 60°C for 24 h. The mixture was poured into distilled water and precipitate formed was filtered, air dried to give a clean yellow solid.

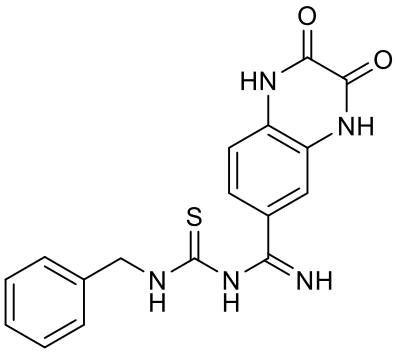

Yellow solid, Yield 0.21 g, 51.9%; FT-IR: ν (cm^{-1}) = 3284 (N-H), 3061, 3030(CH), 1453, 737 (C=S); ^{1}H NMR (400 MHz, Acetone-d6) δ_H 7.42 – 6.97 (m, 8H), 4.21 (d, J = 6.0 Hz, 2H), 2.77 (s, 1H), 1.78 (s, 2H). ^{13}C NMR (101 MHz, Acetone-d_6) δ_C 205.36, 128.29, 128.27, 128.22, 127.46, 127.19, 126.92, 126.78, 42.65.

_N_-((4-chlorophenyl)carbamoyl)-2,3-dioxo-1,2,3,4-tetrahydroquinoxaline-6-carboximidamide, 4.5a:

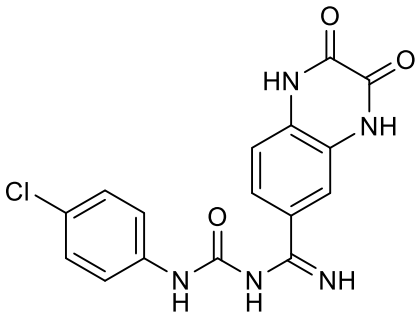

Light-brown solid, 0.26 g, 81.5%; FT-IR: ν (cm^{-1}) = 3381, 3294 (NH), 1712(C=O); ^{1}H NMR (400 MHz, DMSO-d_6) δ_H 8.31 (s, 1H, Ar*H*), 7.77 – 7.17 (m, 3H, Ar*H*), 7.07 – 6.93(m, 2H, Ar*H*), 6.63 – 6.46 (m, 2H, Ar*H*), 5.21 (s, 2H, N*H*), 2.55 (s, 1H, N*H*). ^{13}C NMR (101 MHz, DMSO-d_6) δ_C 168.9(C=NH), 152.8(C=O), 148.1(2C=O), 139.0, 138.7, 129.1, 129.0, 128.9(2C), 125.9, 120.95, 120.27, 119.2, 115.6(2C).

_N_-((4-fluorophenyl)carbamoyl)-2,3-dioxo-1,2,3,4-tetrahydroquinoxaline-6-carboximidamide, 4.5b:

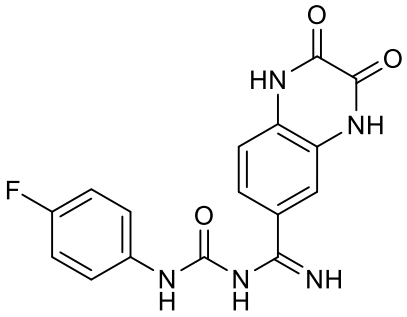

Light-yellow powder, Yield 0.28 g, 47.7%; ^{1}H NMR (400 MHz, DMSO-d_6) δ_H 8.70 (s, 2H, N*H*), 7.54 – 7.39 (m, 4H, Ar*H*), 7.22 – 7.00 (m, 3H, ArH). ^{13}C NMR (101 MHz, DMSO-d_6) δ_C 159.00(C=NH), 156.63(C=O), 153.21(2C=O), 136.49, 136.47, 120.53(2C), 120.45(4C), 115.83(2C), 115.61(2C).

***N*-((4-chlorophenyl)carbamothioyl)-2,3-dioxo-1,2,3,4-tetrahydroquinoxaline-6-carboximidamide, 4c:**

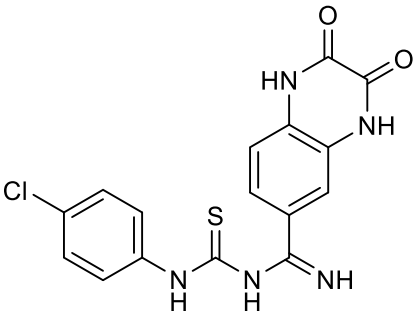

Brown powder, Yield 0.17 g, 46.5% ; ^{1}H NMR (400 MHz, DMSO-d$_6$) δ_H 10.06 (s, 1H, N*H*), 9.97 (s, 1H, NH), 7.64 – 7.48 (m, 3H, Ar*H*), 7.46 – 7.28 (m, 4H, Ar*H*), 2.55 (s, 1H, N*H*), 2.04 (s, 2H, Ar*H*). ^{13}C NMR (101 MHz, DMSO-d$_6$) δ_C 180.1(C=S), 168.9(C=N*H*), 167.8(2C=O), 138.9, 138.7, 129.0(2C), 128.8(2C), 126.94, 125.8(2C), 120.9(2C), 115.6.

***N*-((4-bromophenyl)carbamoyl)-2,3-dioxo-1,2,3,4-tetrahydroquinoxaline-6-carboximidamide 4.5d:**

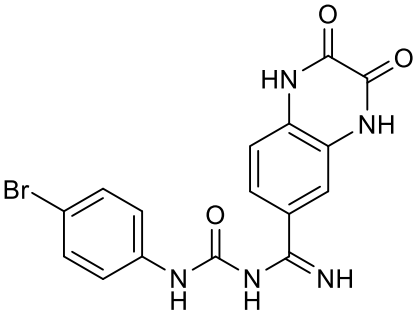

Brown powder, Yield 0.39 g, 86.7%; FT-IR: ν (cm-1) = 3465, 3296 (N-H), 1633(C=O); ^{1}H NMR (400 MHz, DMSO-d$_6$) δ_H 9.61 (s, 1H, N*H*), 9.53 (s, 1H, Ar*H*), 7.77 – 7.38 (m, 5H, Ar*H*), 7.08 (d, $^{3}J_{HH}$ = 8.4 Hz, 1H, Ar*H*), 2.55 (s, 1H, N*H*). ^{13}C NMR (101 MHz, DMSO-d$_6$) δ_C 165.56 (C=N*H*), 164.03(C=O), 153.04(2)(C=O), 140.48, 139.77, 131.90(3C), 131.64, 120.75(4C), 113.63, 113.52.

6.3 Procedures for Biological Activities

Antimalarial Activity of 4(1*H*)-pyridone

Pyridones compounds were measured using a Malaria SYBR Green I based assay. This assay is used to track the drug susceptibility of the malaria parasites and to give account for the

compound's different mode of action.[247] SYBR Green I is a dye that fluoresce brightly when it comes into contact with Plasmodium DNA.[248]

Procedure for Antimalarial Activity of 4(1*H*)-pyridone

Human erythrocytes (O+ /A+) were suspended in complete culture medium [RPMI 1640 medium (Sigma-Aldrich) laced with 25 mM HEPES (Sigma-Aldrich), 20 mM D-glucose (Sigma-Aldrich), 200 µM hypoxanthine (Sigma-Aldrich), 0.2% sodium bicarbonate, 24 µg/ml Gentamicin (Sigma-Aldrich) and 0.5% AlbuMAX II] in a gaseous environment (90% N2, 5% O2, and 5% CO2) [249] while P. falciparum parasites were maintained at 37 ℃. Ring-stage (intra-erythrocytic) NF54 P. falciparum parasite cultures (200 µl at 1% haematocrit, 1% parasitaemia) were treated with the compounds. Chloroquine diphosphate (1 Mm) and complete RPMI media were used as positive and negative controls respectively. These controls were incubated under a gas mixture (90% N_2, 5% O_2, and 5% CO_2) for 96 h at 37℃ in 96-well plates. At the end of the 96 h period, P. falciparum parasite cultures of equal volumes (100 µl each) were aliquoted and mixed with SYBR Green I lysis buffer (0.2 µl/ml 10 000x SYBR Green I, Invitrogen; 20 mM Tris, pH 7.5; 5 mM EDTA; 0.008% (w/v) saponin; 0.08% (v/v) Triton X-100) at room temperature. The samples were incubated for 1 h; afterward fluorescence was measured by means of a GloMax®-Explorer Detection System with Instinct® Software (Promega, excitation at 485 nm and emission at 538 nm). The 'background' fluorescence (i.e. the fluorescence measured in the samples derived from chloroquine-treated infected erythrocytes in which parasite proliferation was completely inhibited) was subtracted from the total fluorescence measured for each sample to measure parasite proliferation. Data obtained were analyzed in Excel, and graphs plotted using GraphPad 7. All experiments were done in triplicate (n=3).

MTT Assay for cytotoxity of 2-disubstituted benzimidazoles

Cancer cells at a seeding density of 10 000 cells well per a 96-well were suspended into tissue culture plates. The plates were incubated in a humified chamber at 37°C with 5% CO2 supply for 24 hours to allow cells to attach. The following day 2 µL of the benzimidazoles was added to each well, at different concentrations. The plates were incubated in a humified chamber at 37°C with 5% CO2 supply for 24 hours. The following day fresh MTT solution at 5 mg/mL in 1X PBS was prepared, and 20 µL of MTT solution was added to all the wells, without removing the media. The plates were incubated in a humified chamber at 37°C with 5% CO2 supply for 4 hours to allow for MTT to metabolize into formazan without removing the media, and 20 µL of MTT solution was added to all the wells. All media were removed from the wells after incubation. All experiments were done in triplicate (n=3).The absorbance of the plate at 570 nm was measured using a plate-reader to identify the number of survival cells and the percentage of viability was calculated using the formula below:

$$Percetage\ Cell\ Viability = \left(\frac{Absorbance\ of\ Test\ sample - Absorbance\ of\ Blank}{Absrobance\ of\ Untreated\ sample - Absorbance\ of\ Blank}\right) \times 100$$

6.4 Molecular Modelling Procedure

The X-ray structure of mitochondrial cyt bc1 from Saccharomyces cerevisiae with atovaquone bound in the catalytic Qo site (RSCB PDB ID: 4PD4 in Figure 2.32) was used the protein target on to which compound 5, compound 6 and atovaquone were docked. The protein used for the docking was prepared using protein Schrodinger Maestro preparation wizard (Schrödinger Release 2021-3: Maestro, Schrödinger, LLC, New York, NY, 2021.). The preparation steps include the assignment of the hydrogen bonds, bond orders, addition of hydrogens, optimization, minimization of the proteins, and deletion of waters beyond 5Å from the het

group. Protein receptor grid was generated (using the co-crystallized ligand to define the binding site for docking) with Glide (Schrödinger Release 2021-3: Glide, Schrödinger, LLC, New York, NY, 2021.) The 3D structures of the three ligands (compound **2.9a**, compound **2.9b** and Atovaquone) were prepared using Schrödinger Maestro software **(**Schrödinger Release 2021-3**:** Maestro, Schrödinger, LLC, New York, NY, 2021**).** Minimization of all ligands was carried out using the OPLS-2005 force field module.[250] The electrostatic potential values were plotted on the surface of ligands using electrostatic potential fitting charge (ESP) atomic charges by OPLS2005 force field, (Figure 2.34). The ligands (compound **2.9a**, compound **2.9b** and Atovaquone) were docked on to the previously defined binding site of the prepared cytochrome bc1 complex (RSCB PDB ID: 4PD4) using glide's ligand docking module (extra-precision). The ligand binding energies and ligand strain energies of the ligand-receptor complex obtained from Glide was calculated with the prime MMGBSA (solvation with VSGB and forcefield defined with OPLS4). Prime MM-GBSA calculates the energy of the optimized free receptors, free ligands, and a complex of the ligands with cytochrome bc1 complex.

References

References

(1) Jones, A. W. Early Drug Discovery and the Rise of Pharmaceutical Chemistry. *Drug Test. Anal.* **2011**, *3* (6), 337–344. https://doi.org/10.1002/dta.301.

(2) Zhou, S. F.; Zhong, W. Z. Drug Design and Discovery: Principles and Applications. *Molecules* **2017**, *22* (2), 1–6. https://doi.org/10.3390/molecules22020279.

(3) Chikhale, H.; Nerkar, A.; Society, G. E. Review on *In-Silico* Techniques An Approach to Drug Discovery. *Current Trends in Pharmacy and Pharmaceutical Chemistry* **2020**, 2(1), 24-32.

(4) Cava, C.; Castiglioni, I. Integration of Molecular Docking and *in vitro* Studies: A Powerful Approach for Drug Discovery in Breast Cancer. *Appl. Sci.* **2020**, *10* (19), 1–18. https://doi.org/10.3390/app10196981.

(5) Wadood, A.; Ahmed, N.; Shah, L.; Ahmad, A.; Hassan, H.; Shams, S. *In-Silico* Drug Design: An Approach Which Revolutionarised the Drug Discovery Process. *OA Drug Des. Deliv.* **2013**, *1* (1), 1-4. https://doi.org/10.13172/2054-4057-1-1-1119.

(6) Pinzi, L.; Rastelli, G. Molecular Docking: Shifting Paradigms in Drug Discovery. *Int. J. Mol. Sci.* **2019**, *20* (18), 1-23. https://doi.org/10.3390/ijms20184331.

(7) Cui, M.; Mihaly, M.; Hong-Xing, Z.; Meng, X.-Y. Molecular Docking: A Powerful Approach for Structure-Based Drug Discovery. *Curr. Comput. Aided. Drug Des.* **2011**, *7* (2), 146–157. https://doi.org/10.2174/157340911795677602.

(8) Dar, A. M.; Mir, S. Molecular Docking: Approaches, Types, Applications and Basic

Challenges. *J. Anal. Bioanal. Tech.* **2017**, *08* (02), 8–10. https://doi.org/10.4172/2155-9872.1000356.

(9) Jorgensen, L. Computational Approaches to Molecular Recognition L Lamb and William. *Model Syst.* **1997**, *1* (1), 449–457.

(10) Ferreira, L. G.; Dos Santos, R. N.; Oliva, G.; Andricopulo, A. D. Molecular Docking and Structure-Based Drug Design Strategies; Molecules **2015**, 20(7), 13384-13421. https://doi.org/10.3390/molecules200713384.

(11) Chen, Y.-C. Beware of Docking! *Trends Pharmacol. Sci.* **2015**, *36* (2), 78–95. https://doi.org/https://doi.org/10.1016/j.tips.2014.12.001.

(12) Joseph Sahayarayan, J.; Soundar Rajan, K.; Nachiappan, M.; Prabhu, D.; Guru Raj Rao, R.; Jeyakanthan, J.; Hossam Mahmoud, A.; Mohammed, O. B.; Morgan, A. M. A. Identification of Potential Drug Target in Malarial Disease Using Molecular Docking Analysis. *Saudi J. Biol. Sci.* **2020**,1-7. https://doi.org/10.1016/j.sjbs.2020.10.019.

(13) Shoichet, B. K.; McGovern, S. L.; Wei, B.; Irwin, J. J. Lead Discovery Using Molecular Docking. *Curr. Opin. Chem. Biol.* **2002**, *6* (4), 439–446. https://doi.org/10.1016/S1367-5931(02)00339-3.

(14) Kitchen, D. B.; Decornez, H.; Furr, J. R.; Bajorath, J. Docking and Scoring in Virtual Screening for Drug Discovery: Methods and Applications. *Nat. Rev. Drug Discov.* **2004**, *3* (11), 935–949. https://doi.org/10.1038/nrd1549.

(15) Timo, G. O.; Reis, R. S. S. V. dos; Melo, A. F. de; Costa, T. V. L.; Magalhães, P. de O.; Homem-de-Mello, M. Predictive Power of *in silico* Approach to Evaluate Chemicals against m. Tuberculosis: A Systematic Review. *Pharmaceuticals* **2019**, *12* (3), 1-23.

https://doi.org/10.3390/ph12030135.

(16) Lionta, E.; Spyrou, G.; Vassilatis, D. K.; Cournia, Z. Send Orders for Reprints to Reprints@benthamscience.Net Structure-Based Virtual Screening for Drug Discovery: Principles, Applications and Recent Advances. *Curr. Top. Med. Chem.* **2014**, *14*, 1923–1938. https://doi.org/10.2174/1568026614666140929124445.

(17) Suresh, P.; Basu, P. K. Improving Pharmaceutical Product Development and Manufacturing: Impact on Cost of Drug Development and Cost of Goods Sold of Pharmaceuticals. *J. Pharm. Innov.* **2008**, *3* (3), 175–187. https://doi.org/10.1007/s12247-008-9043-1.

(18) Kharkar, P. S.; Warrier, S.; Gaud, R. S. Reverse Docking: A Powerful Tool for Drug Repositioning and Drug Rescue. *Future Med. Chem.* **2014**, *6* (3), 333–342. https://doi.org/10.4155/fmc.13.207.

(19) Park, K.; Cho, A. E. Using Reverse Docking to Identify Potential Targets for Ginsenosides. *J. Ginseng Res.* **2017**, *41* (4), 534–539. https://doi.org/10.1016/j.jgr.2016.10.005.

(20) Lee, A.; Lee, K.; Kim, D. Using Reverse Docking for Target Identification and Its Applications for Drug Discovery. *Expert Opin. Drug Discov.* **2016**, *11* (7), 707–715. https://doi.org/10.1080/17460441.2016.1190706.

(21) Stewart, B. W.; Bray, F.; Forman, D.; Ohgaki, H.; Straif, K.; Ullrich, A.; Wild, C. P. Cancer Prevention as Part of Precision Medicine: “Plenty to Be Done.” *Carcinogenesis* **2016**, *37* (1), 2–9. https://doi.org/10.1093/carcin/bgv166.

(22) Temelkovski, D.; Kiss, T.; Terstyanszky, G.; Greenwell, P. Extending Molecular

Docking Desktop Applications with Cloud Computing Support and Analysis of Results. *Futur. Gener. Comput. Syst.* **2019**, *97*, 814–824.

(23) Huang, H.; Zhang, G.; Zhou, Y.; Lin, C.; Chen, S.; Lin, Y.; Mai, S.; Huang, Z. Reverse Screening Methods to Search for the Protein Targets of Chemopreventive Compounds. *Front. Chem.* **2018**, *6* (138), 1-28. https://doi.org/10.3389/fchem.2018.00138.

(24) Viegas-Junior, C.; Danuello, A.; da Silva Bolzani, V.; Barreiro, E. J.; Fraga, C. A. M. Molecular Hybridization: A Useful Tool in the Design of New Drug Prototypes. *Curr. Med. Chem.* **2007**, *14* (17), 1829–1852. https://doi.org/10.2174/092986707781058805.

(25) Rj, S.; Pal, S.; Jayashree, A. Molecular Hybridization - An Emanating Tool in Drug Design. *Med. Chem. (Los. Angeles).* **2019**, *9*, 93–95.

(26) Zhang, S.; Saathoff, J. M.; He, L.,8-Molecular Hybridization: An Emerging Tool for the Design of Novel Therapeutics for Alzheimer's Disease; Decker, M. B. T.-D. of H. M. for D. D., Ed.; Elsevier, **2017**, 219–237. https://doi.org/https://doi.org/10.1016/B978-0-08-101011-2.00008-8.

(27) Tanwar, J.; Das, S.; Fatima, Z.; Hameed, S. Multidrug Resistance : An Emerging Crisis Multidrug Resistance : An Emerging Crisis.*Interdisciplinary Perspective on Infectious Disease* **2014**, 2014, 1-7 https://doi.org/10.1155/2014/541340.

(28) Valavanidis, A. Malaria, a Lethal Human Infectious Disease. Despite the Progress, There Were 228 Million Cases of Malaria Worldwide and 405,000 Deaths in 2018. *Scientific Review* **2020**, *1*, 1–28.

(29) Al-Awadhi, M.; Ahmad, S.; Iqbal, J. Current Status and the Epidemiology of Malaria in the Middle East Region and Beyond. *Microorganisms* **2021**, *9* (2), 338.

(30) Menkin-smith, L.; Winders, W. T. Malaria (Plasmodium Vivax) Pathophysiology. **2019**, 1–9.

(31) Tong, M. X.; Hansen, A.; Hanson-Easey, S.; Cameron, S.; Xiang, J.; Liu, Q.; Liu, X.; Sun, Y.; Weinstein, P.; Han, G.-S. Perceptions of Malaria Control and Prevention in an Era of Climate Change: A Cross-Sectional Survey among CDC Staff in China. *Malar. J.* **2017**, *16* (1), 1–10.

(32) Snow, R. W.; Trape, J. F.; Marsh, K. The Past, Present and Future of Childhood Malaria Mortality in Africa. *Trends Parasitol.* **2001**, *17* (12), 593–597. https://doi.org/10.1016/S1471-4922(01)02031-1.

(33) Bhat, H. R.; Singh, U. P.; Yadav, P. S.; Kumar, V.; Gahtori, P.; Das, A.; Chetia, D.; Prakash, A.; Mahanta, J. Synthesis, Characterization and Antimalarial Activity of Hybrid 4-Aminoquinoline-1,3,5-Triazine Derivatives. *Arab. J. Chem.* **2016**, *9*, 625–631. https://doi.org/10.1016/j.arabjc.2011.07.001.

(34) Sinha, S.; Sarma, P.; Sehgal, R.; Medhi, B. Development in Assay Methods for in Vitro Antimalarial Drug Efficacy Testing: A Systematic Review. *Front. Pharmacol.* **2017**, *8*, 1–14. https://doi.org/10.3389/fphar.2017.00754.

(35) Biamonte, M. A.; Wanner, J.; Le Roch, K. G. Recent Advances in Malaria Drug Discovery. *Bioorganic Med. Chem. Lett.* **2013**, *23* (10), 2829–2843. https://doi.org/10.1016/j.bmcl.2013.03.067.

(36) Tuteja, R. Malaria− an overview. *The FEBS journal*, *274*(18), 4670-4679.

(37) Cox, F. E. History of the Discovery of the Malaria Parasites and Their Vectors. *Parasites and Vectors* **2010**, *3* (1), 1–9. https://doi.org/10.1186/1756-3305-3-5.

(38) Kato, N.; Comer, E.; Sakata-Kato, T.; Sharma, A.; Sharma, M.; Maetani, M.; Bastien, J.; Brancucci, N. M.; Bittker, J. A.; Corey, V.; Clarke, D.; Derbyshire, E. R.; Dornan, G. L.; Duffy, S.; Eckley, S.; Itoe, M. A.; Koolen, K. M. J.; Lewis, T. A.; Lui, P. S.; Lukens, A. K.; Lund, E.; March, S.; Meibalan, E.; Meier, B. C.; McPhail, J. A.; Mitasev, B.; Moss, E. L.; Sayes, M.; Van Gessel, Y.; Wawer, M. J.; Yoshinaga, T.; Zeeman, A. M.; Avery, V. M.; Bhatia, S. N.; Burke, J. E.; Catteruccia, F.; Clardy, J. C.; Clemons, P. A.; Dechering, K. J.; Duvall, J. R.; Foley, M. A.; Gusovsky, F.; Kocken, C. H. M.; Marti, M.; Morningstar, M. L.; Munoz, B.; Neafsey, D. E.; Sharma, A.; Winzeler, E. A.; Wirth, D. F.; Scherer, C. A.; Schreiber, S. L. Diversity-Oriented Synthesis Yields Novel Multistage Antimalarial Inhibitors. *Nature* **2016**, *538* (7625), 344–349. https://doi.org/10.1038/nature19804.

(39) Bloland, P. B. Drug Resistance in Malaria. A Background Document for the WHO Global Strategy for Containment of Antimicrobial Resistance. **2001**, 12.

(40) Teguh, S. C.; Klonis, N.; Duffy, S.; Lucantoni, L.; Avery, V. M.; Hutton, C. A.; Baell, J. B.; Tilley, L. Novel Conjugated Quinoline-Indoles Compromise Plasmodium Falciparum Mitochondrial Function and Show Promising Antimalarial Activity. *J. Med. Chem.* **2013**, *56* (15), 6200–6215. https://doi.org/10.1021/jm400656s.

(41) <p>Prashant Singh, K. K. S. K. A. and R. C. Virtual Screening and Docking Studies of Synthesized Chalcones: Potent Anti-Malarial Drug. *Int. J. Drug Dev. Res.* **2016**, *8* (1), 49–56.

(42) Nqoro, X.; Tobeka, N.; Aderibigbe, B. Quinoline-Based Hybrid Compounds with Antimalarial Activity. *Molecules* **2017**, *22* (12), 2268. https://doi.org/10.3390/molecules22122268.

(43) Unicef. The Global Malaria Burden Malaria Prevention And Treatment. *Prescriber* **2000**, 18, 16.

(44) National Department of Health. National Guidelines for the Treatment of Malaria, South Africa 2018. **2017**.

(45) Petersen, I.; Eastman, R.; Lanzer, M. Drug-Resistant Malaria: Molecular Mechanisms and Implications for Public Health. *FEBS Lett.* **2011**, *585* (11), 1551–1562. https://doi.org/10.1016/j.febslet.2011.04.042.

(46) Deepika, F.; Chaturaka, R.; Senaka, R. Primaquine in Vivax Malaria : An Update and Review on Management Issues. *Malar. J.* **2011**, *10* (1), 351. https://doi.org/10.1186/1475-2875-10-351.

(47) Mishra, M.; Mishra, V. K.; Kashaw, V.; Iyer, A. K.; Kashaw, S. K. Comprehensive Review on Various Strategies for Antimalarial Drug Discovery. *Eur. J. Med. Chem.* **2017**, *125*, 1300–1320. https://doi.org/10.1016/j.ejmech.2016.11.025.

(48) Khera, A., & Mukherjee, R. Arteisinin resistance: cause for worry?. *Journal of Marine Medical Society* **2019**, *21*(1), 4.https://doi.org/10.4103/jmms.jmms.

(49) Capper, M. J.; O'Neill, P. M.; Fisher, N.; Strange, R. W.; Moss, D.; Ward, S. A.; Berry, N. G.; Lawrenson, A. S.; Hasnain, S. S.; Biagini, G. A.; Antonyuk, S. V. Antimalarial 4(1H)-Pyridones Bind to the Q_i Site of Cytochrome Bc_1. *Proc. Natl. Acad. Sci.* **2015**, *112* (3), 755–760. https://doi.org/10.1073/pnas.1416611112.

(50) Nambozi, M.; Tinto, H.; Mwapasa, V.; Tagbor, H.; Kabuya, J.-B. B.; Hachizovu, S.; Traoré, M.; Valea, I.; Tahita, M. C.; Ampofo, G.; Buyze, J.; Ravinetto, R.; Arango, D.; Thriemer, K.; Mulenga, M.; van Geertruyden, J.-P.; D'Alessandro, U. Artemisinin-

Based Combination Therapy during Pregnancy: Outcome of Pregnancy and Infant Mortality: A Cohort Study. *Malar. J.* **2019**, *18* (1), 105. https://doi.org/10.1186/s12936-019-2737-7.

(51) Meyer-Rath, G.; Johnson, L.; Pillay, Y.; Blecher, M.; Brennan, A. T.; Long, L.; Moultrie, H.; Sanne, I.; Fox, M. P.; Rosen, S. Changing the South African national antiretroviral therapy guidelines: the role of cost modelling. *PLoS One* **2017,** 12(10)

(52) Blasco, B.; Leroy, D.; Fidock, D. A. Parasite Biology To the Clinic. *Nat. Med.* **2017**, *23* (8), 917–928. https://doi.org/10.1038/nm.4381.Antimalarial.

(53) Corrêa Soares, J. B. R.; Menezes, D.; Vannier-Santos, M. A.; Ferreira-Pereira, A.; Almeida, G. T.; Venancio, T. M.; Verjovski-Almeida, S.; Zishiri, V. K.; Kuter, D.; Hunter, R.; Egan, T. J.; Oliveira, M. F. Interference with Hemozoin Formation Represents an Important Mechanism of Schistosomicidal Action of Antimalarial Quinoline Methanols. *PLoS Negl. Trop. Dis.* **2009**, *3* (7). https://doi.org/10.1371/journal.pntd.0000477.

(54) Nagaraj, V. A.; Sundaram, B.; Varadarajan, N. M.; Subramani, P. A.; Kalappa, D. M.; Ghosh, S. K.; Padmanaban, G. Malaria Parasite-Synthesized Heme Is Essential in the Mosquito and Liver Stages and Complements Host Heme in the Blood Stages of Infection. *PLoS Pathog.* **2013**, *9* (8), e1003522.

(55) Puri, S. K.; Singh, R. L.; Chauhan, V. S. Hemozoin Formation in Malaria: A Two-Step Process Involving Histidine-Rich Proteins and Lipids. **2003**, *308*, 736–743. https://doi.org/10.1016/S0006-291X(03)01465-7.

(56) Olafson, K. N.; Ketchum, M. A.; Rimer, J. D.; Vekilov, P. G. Mechanisms of Hematin Crystallization and Inhibition by the Antimalarial Drug Chloroquine. *Proc. Natl. Acad. Sci.* **2015**, *112* (16). https://doi.org/10.1073/pnas.1501023112.

(57) Tempera, C.; Franco, R.; Caro, C.; André, V.; Eaton, P.; Burke, P.; Hänscheid, T. Characterization and Optimization of the Haemozoin-like Crystal (HLC) Assay to Determine Hz Inhibiting Effects of Anti-Malarial Compounds. *Malar. J.* **2015**, *14* (1), 1–12. https://doi.org/10.1186/s12936-015-0913-y.

(58) Bloland, Peter B., and World Health Organization. *Drug resistance in malaria*. No. WHO/CDS/CSR/DRS/2001.4. World Health Organization, **2001**.

(59) White, N. J. Review Series Antimalarial Drug Resistance. *Trends Parasitol.* **2004**, *113* (8), 1084–1092. https://doi.org/10.1172/JCI200421682.1084.

(60) Cui, L.; Mharakurwa, S.; Ndiaye, D.; Rathod, P. K.; Rosenthal, P. J. Antimalarial Drug Resistance: Literature Review and Activities and Findings of the ICEMR Network. *Am. J. Trop. Med. Hyg.* **2015**, *93* (Suppl 3), 57–68. https://doi.org/10.4269/ajtmh.15-0007.

(61) Grimberg, B. T.; Mehlotra, R. K. Expanding the Antimalarial Drug Arsenal-Now, but How? *Pharmaceuticals* **2011**, *4* (5), 681–712. https://doi.org/10.3390/ph4050681.

(62) Vallières, C.; Avery, S. V. The Candidate Antimalarial Drug Mmv665909 Causes Oxygen-Dependent MRNA Mistranslation and Synergizes with Quinoline-Derived Antimalarials. *Antimicrob. Agents Chemother.* **2017**, *61* (9). https://doi.org/10.1128/AAC.00459-17.

(63) Tse, E. G.; Korsik, M.; Todd, M. H. The Past, Present and Future of Anti-Malarial Medicines. *Malar. J.* **2019**, *18* (1), 1–21. https://doi.org/10.1186/s12936-019-2724-z.

(64) Monastyrskyi, A.; Kyle, D. E.; Manetsch, R. 4(1H)-Pyridone and 4(1H)-Quinolone Derivatives as Antimalarials with Erythrocytic, Exoerythrocytic, and Transmission Blocking Activities. *Curr. Top. Med. Chem.* **2014**, *14* (14), 1693–1705.

https://doi.org/10.2174/1568026614666140808124638.

(65) Yeates, C. L.; Batchelor, J. F.; Capon, E. C.; Cheesman, N. J.; Fry, M.; Hudson, A. T.; Trimming, H.; Woolven, J.; Bueno, J. M.; Chicharro, J.; Fernández, E.; M, J.; Gargallo-viola, D.; Gómez, F.; Heras, D.; Herreros, E.; León, M. L.; Pudney, M. Synthesis and Structure – Activity Relationships of 4-Pyridones as Potential Antimalarials Synthesis and Structure – Activity Relationships of 4-Pyridones as Potential Antimalarials. *J. Med. Chem.* **2008**, No. Scheme 1, 2845–2852. https://doi.org/10.1021/jm0705760.

(66) Barton, V.; Fisher, N.; Biagini, G. A.; Ward, S. A.; O'Neill, P. M. Inhibiting Plasmodium Cytochrome Bc1: A Complex Issue. *Curr. Opin. Chem. Biol.* **2010**, *14* (4), 440–446. https://doi.org/10.1016/j.cbpa.2010.05.005.

(67) Bueno, J. M.; Manzano, P.; Garc??a, M. C.; Chicharro, J.; Puente, M.; Lorenzo, M.; Garc??a, A.; Ferrer, S.; G??mez, R. M.; Fraile, M. T.; Lavandera, J. L.; Fiandor, J. M.; Vidal, J.; Herreros, E.; Gargallo-Viola, D. Potent Antimalarial 4-Pyridones with Improved Physico-Chemical Properties. *Bioorganic Med. Chem. Lett.* **2011**, *21* (18), 5214–5218. https://doi.org/10.1016/j.bmcl.2011.07.044.

(68) Flores-Sumoza, M.; Alcázar, J. J.; Márquez, E.; Mora, J. R.; Lezama, J.; Puello, E. Classical QSAR and Docking Simulation of 4-Pyridone Derivatives for Their Antimalarial Activity. *Molecules* **2018**, *23* (12), 1–12. https://doi.org/10.3390/molecules23123166.

(69) Brockmeyer, F.; Manetsch, R. Progress in the Optimization of 4(1 H)-Quinolone Derivatives as Antimalarials Targeting the Erythrocytic, the Exoerythrocytic and the Transmitting Stages of the Malaria Parasite . *Chim. Int. J. Chem.* **2017**, *71* (4), 213–219. https://doi.org/10.2533/chimia.2017.213.

(70) Rosa, J. C. De; Beatriz, D.; Fiandor, J. M.; Fraile, T.; Garc, M.; Herreros, E. Synthesis and Structure − Activity Relationships of the Novel Antimalarials 5 - Pyridinyl-4(1 H) - Pyridones. **2018**, *4* (Figure 1). https://doi.org/10.1021/acs.jmedchem.7b01256.

(71) Fan, J. Pharmacokinetics Pharmacokinetics. **2017**, No. October. https://doi.org/10.1016/j.bcp.2013.09.007.

(72) White, N. J. Pharmacokinetic and Pharmacodynamic Considerations in Antimalarial Dose Optimization. **2013**, *57* (12), 5792–5807. https://doi.org/10.1128/AAC.00287-13.

(73) Bueno, J. M.; Calderon, F.; Chicharro, J.; De La Rosa, J. C.; Díaz, B.; Fernández, J.; Fiandor, J. M.; Fraile, M. T.; García, M.; Herreros, E.; García-Pérez, A.; Lorenzo, M.; Mallo, A.; Puente, M.; Saadeddin, A.; Ferrer, S.; Angulo-Barturen, I.; Burrows, J. N.; León, M. L. Synthesis and Structure-Activity Relationships of the Novel Antimalarials 5-Pyridinyl-4(1 H)-Pyridones. *J. Med. Chem.* **2018**, *61* (8), 3422–3435. https://doi.org/10.1021/acs.jmedchem.7b01256.

(74) Bueno, J. M.; Herreros, E.; Angulo-Barturen, I.; Ferrer, S.; Fiandor, J. M.; Gamo, F. J.; Gargallo-Viola, D.; Derimanov, G. Exploration of 4(1H)-Pyridones as a Novel Family of Potent Antimalarial Inhibitors of the Plasmodial Cytochrome Bc1. *Future Med. Chem.* **2012**, *4* (18), 2311–2323. https://doi.org/10.4155/fmc.12.177.

(75) Esvan, Y. J.; Zeinyeh, W.; Boibessot, T.; Nauton, L.; Meijer, L.; Giraud, F.; Moreau, P. European Journal of Medicinal Chemistry Discovery of Pyrido [3 , 4- g] Quinazoline Derivatives as CMGC Family Protein Kinase Inhibitors : Design , Synthesis , Inhibitory Potency and X-Ray Co e Crystal Structure. **2016**, *118*, 170–177. https://doi.org/10.1016/j.ejmech.2016.04.004.

(76) Gamo, F.-J.; Sanz, L. M.; Vidal, J.; de Cozar, C.; Alvarez, E.; Lavandera, J.-L.; Vanderwall, D. E.; Green, D. V. S.; Kumar, V.; Hasan, S.; Brown, J. R.; Peishoff, C. E.; Cardon, L. R.; Garcia-Bustos, J. F. Thousands of Chemical Starting Points for Antimalarial Lead Identification. *Nature* **2010**, *465* (7296), 305–310. https://doi.org/10.1038/nature09107.

(77) Dunbar, K. L.; Scharf, D. H.; Litomska, A.; Hertweck, C. Enzymatic Carbon–Sulfur Bond Formation in Natural Product Biosynthesis. *Chem. Rev.* **2017**, *117* (8), 5521–5577.

(78) Zauhar, R. J.; Colbert, C. L.; Morgan, R. S.; Welsh, W. J. Evidence for a Strong Sulfur–Aromatic Interaction Derived from Crystallographic Data. *Biopolym. Orig. Res. Biomol.* **2000**, *53* (3), 233–248.

(79) Amyes, T. L.; Richard, J. P. Rational Design of Transition-State Analogues as Potent Enzyme Inhibitors with Therapeutic Applications. *ACS Chem. Biol.* **2007**, *2* (11), 711–714.

(80) Fernández, J.; Chicharro, J.; Bueno, J. M.; Lorenzo, M. Isoxazole Mediated Synthesis of 4-(1H)Pyridones: Improved Preparation of Antimalarial Candidate GSK932121. *Chem. Commun.* **2016**, *52* (66), 10190–10192. https://doi.org/10.1039/C6CC05277K.

(81) Dalla Vechia, L.; de Souza, R. O. M. A.; de Mariz e Miranda, L. S. The Dakin-West Reaction: Past, Present and Future. *Tetrahedron* **2018**, *74* (33), 4359–4371. https://doi.org/10.1016/j.tet.2018.07.010.

(82) Application, E. P. Tepzz 46¥ 9a_t (11). **2010**, *1* (19).

(83) Tran, K.; Bickar, D. Dakin - West Synthesis of -Aryl Ketones. **2006**, No. 13, 6640–6643.

(84) Itoh, T.; Mase, T. A General Palladium-Catalyzed Coupling of Aryl Bromides/Triflates

and Thiols. *Org. Lett.* **2004**, *6* (24), 4587–4590. https://doi.org/10.1021/ol047996t.

(85) Fujita, Y., Yonehara, M., Kitahara, K., Shimokawa, J., Hashimoto, Y., & Ishikawa, M. Confirmation of molecular planarity disruption effect on aqueous solubility improvement of β-naphthoflavone analogs. *Heterocycles* **2011**, *83* (11), 2563–2575. https://doi.org/10.3987/COM-11-12352.

(86) Foris, A. On NH NMR Chemical Shifts , Part II : Porphyrins , Porphyrinoids , and Related Compounds, 1-70.

(87) Darnbrough, S.; Mervic, M.; Condon, S. M.; Burns, C. J. An Improved Synthesis of N-Boc Protected Aryl Amines. *Synth. Commun.* **2001**, *31* (21), 3273–3280. https://doi.org/10.1081/SCC-100106036.

(88) Ll, P. A.; Cata, A. D. I. U. M.-; Ed, L. Y. Z.; Cou, C.; Ngs, P. L. I. Palladium-Catalyzed Cross Couplings in Organic Synthesis. **2010**, *50005*, 0–12.

(89) Silva, V. L. M.; Silva, A. M. S. Palladium-Catalysed Synthesis and Transformation of Quinolones. *Molecules* **2019**, *24* (2). https://doi.org/10.3390/molecules24020228.

(90) Barnett, K. L.; Howard, J. R.; Treager, C. J.; Shipley, A. T.; Stullich, R. M.; Qu, F.; Gerlach, D. L.; Shaughnessy, K. H. Air-Stable [(R3P)PdCl2]2 Complexes of Neopentylphosphines as Cross-Coupling Precatalysts: Catalytic Application and Mechanism of Catalyst Activation and Deactivation. *Organometallics* **2018**, *37* (9), 1410–1424. https://doi.org/10.1021/acs.organomet.8b00082.

(91) Miyaura, N., & Suzuki, A. Palladium-catalyzed cross-coupling reactions of organoboron compounds. *Chemical reviews* **1995**, *95*(7), 2457-2483.

(92) Itoh, T.; Mase, T. A General Palladium-Catalyzed Coupling of Aryl Bromides/Triflates

and Thiols. *Org. Lett.* **2004**, *6* (24), 4587–4590. https://doi.org/10.1021/ol047996t.

(93) Gunther, F. A. Nuclear Magnetic Resonance: Applications to Organic Chemistry. *J. Agric. Food Chem.* **1959**, *7* (11), 796. https://doi.org/10.1021/jf60105a607.

(94) Coates, J. Interpretation of Infrared Spectra, a Practical Approach. Citeseer 2000.

(95) Serratice, M.; Bertrand, B.; Janssen, E. F. J.; Hemelt, E.; Zucca, A.; Cocco, F.; Cinellu, M. A.; Casini, A. Gold (I) Compounds with Lansoprazole-Type Ligands: Synthesis, Characterization and Anticancer Properties in Vitro. *Medchemcomm* **2014**, *5* (9), 1418–1422.

(96) Chemler, S. R.; Trauner, D.; Danishefsky, S. J. The B -Alkyl Suzuki - Miyaura Cross-Coupling Reaction : A Versatile C - C Bond-Forming Tool REVIEWS The B -Alkyl Suzuki - Miyaura Cross-Coupling Reaction : Development , Mechanistic Study , and Applications in Natural Product Synthesis **. *Angew. Chem. Int. Ed* **2001**, *40*, 4544–4568.

(97) Ding, S.; Xu, L.; Miao, Z. Unsymmetrical Diboron Reagents: Application in Borylation Reactions of Unsaturated Bonds. *Molecules* **2019**, *24* (7). https://doi.org/10.3390/molecules24071325.

(98) Defrancesco, H.; Dudley, J.; Coca, A. Boron Chemistry: An Overview. *ACS Symp. Ser.* **2016**, *1236*, 1–25. https://doi.org/10.1021/bk-2016-1236.ch001.

(99) Brown, D. G.; Boström, J. Analysis of Past and Present Synthetic Methodologies on Medicinal Chemistry: Where Have All the New Reactions Gone? *J. Med. Chem.* **2016**, *59* (10), 4443–4458. https://doi.org/10.1021/acs.jmedchem.5b01409.

(100) Buskes, M. J. Discovery and Development. *Genet. Eng. Biotechnol. News* **2014**, *34* (8),

12. https://doi.org/10.1089/gen.34.08.07.

(101) Biajoli, A. F. P.; Schwalm, C. S.; Limberger, J.; Claudino, T. S.; Monteiro, A. L. Recent Progress in the Use of Pd-Catalyzed C-C Cross-Coupling Reactions in the Synthesis of Pharmaceutical Compounds. *J. Braz. Chem. Soc.* **2014**, *25* (12), 2186–2214. https://doi.org/10.5935/0103-5053.20140255.

(102) Nakagawa, S.; Bainbridge, K. A.; Butcher, K.; Ellis, D.; Klute, W.; Ryckmans, T. Application of Barluenga Boronic Coupling (BBC) to the Parallel Synthesis of Drug-like and Drug Fragment-like Molecules. *ChemMedChem* **2012**, *7* (2), 233–236. https://doi.org/10.1002/cmdc.201100339.

(103) Larsen, R. D.; King, A. O.; Chen, C. Y.; Corley, E. G.; Foster, B. S.; Roberts, F. E.; Yang, C.; Lieberman, D. R.; Reamer, R. A.; Tschaen, D. M.; Verhoeven, T. R.; Reider, P. J.; Young, S. Lo; Rossano, L. T.; Brookes, S.; Meloni, D.; Moore, J. R.; Arnett, J. F. Efficient Synthesis of Losartan, A Nonpeptide Angiotensin II Receptor Antagonist. *J. Org. Chem.* **1994**, *59* (21), 6391–6394. https://doi.org/10.1021/jo00100a048.

(104) Crawley, M. L.; Trost, B. M. *Applications of Transition Metal Catalysis in Drug Discovery and Development: An Industrial Perspective*; John Wiley & Sons, **2012**.

(105) Taheri Kal K, A., Heravi, M. M., & Momeni, T. Current applications of Suzuki–Miyaura coupling reaction in the total synthesis of natural products: an update. *Applied Organometallic Chemistry* **2018**, *32*(3), e4210.

(106) Wei, C.; Jiang, Z.; Tian, S.; Zhang, D. Highly Facile Approach to the Formal Total Synthesis of Camptothecin. *Tetrahedron Lett.* **2013**, *54* (34), 4515–4517. https://doi.org/https://doi.org/10.1016/j.tetlet.2013.06.057.

(107) Fortun, S.; Beauclair, P.; Schmitzer, A. Metformin as a Versatile Ligand for Recyclable Palladium-Catalyzed Cross-Coupling Reactions in Neat Water. *RSC Adv.* **2017**, *7*, 21036–21044. https://doi.org/10.1039/C7RA01197K.

(108) Pinter, B.; Fievez, T.; Bickelhaupt, F. M.; Geerlings, P.; De Proft, F. On the Origin of the Steric Effect. *Phys. Chem. Chem. Phys.* **2012**, *14* (28), 9846–9854. https://doi.org/10.1039/c2cp41090g.

(109) Hintermann, L. Comprehensive Organic Name Reactions and Reagents. By Zerong Wang. *Angew. Chemie Int. Ed.* **2010**, *49* (15), 2659–2660. https://doi.org/https://doi.org/10.1002/anie.201000292.

(110) McKeage, K.; Scott, L. Atovaquone/Proguanil: A Review of Its Use for the Prophylaxis of Plasmodium Falciparum Malaria. *Drugs* **2003**, *63* (6), 597–623. https://doi.org/10.2165/00003495-200363060-00006.

(111) Yeates, C. L., Batchelor, J. F., Capon, E. C., Cheesman, N. J., Fry, M., Hudson, A. T., ... & León, M. L. Synthesis and structure–activity relationships of 4-pyridones as potential antimalarials. *Journal of medicinal chemistry* **2008**, *51*(9), 2845-2852.

(112) American Cancer Society. Cancer Facts and Figures 2018. *Am. Cancer Soc.* **2018**, 1–71. https://doi.org/10.1182/blood-2015-12-687814.

(113) Ginsburg, O., Bray, F., Coleman, M. P., Vanderpuye, V., Eniu, A., Kotha, S. R., ... & Conteh, L. The global burden of women's cancers: a grand challenge in global health. *The Lancet* **2017**, *389*(10071), 847-860..

(114) Siegel, R. L.; Miller, K. D.; Jemal, A. Cancer Statistics, 2018. *CA. Cancer J. Clin.* **2018**, *68* (1), 7–30. https://doi.org/10.3322/caac.21442.

(115) World Cancer Research Fund; American Institute for Cancer Research. Recommendations and Public Health and Policy Implications. **2018**.

(116) Section, S.; Epidemic, T. O. Global Cancer Facts & Figures 4 Th Edition. **2018**.

(117) Arruebo, M.; Vilaboa, N.; Sáez-Gutierrez, B.; Lambea, J.; Tres, A.; Valladares, M.; González-Fernández, Á. Assessment of the Evolution of Cancer Treatment Therapies. *Cancers (Basel).* **2011**, *3* (3), 3279–3330.

(118) Shurbaji, Samar H. "The influence of shear stress on nanomaterial's uptake by cancer." Master's thesis, 2020.

(119) Bagnyukova, T. V; Serebriiskii, I. G.; Zhou, Y.; Hopper-Borge, E. A.; Golemis, E. A.; Astsaturov, I. Chemotherapy and Signaling: How Can Targeted Therapies Supercharge Cytotoxic Agents? *Cancer Biol. Ther.* **2010**, *10* (9), 839–853.

(120) Liang, X.-J.; Chen, C.; Zhao, Y.; Wang, P. C. Circumventing Tumor Resistance to Chemotherapy by Nanotechnology. In *Multi-Drug Resistance in Cancer*; Springer, **2010**, 467–488.

(121) Husain, A.; Rashid, M.; Mishra, R.; Parveen, S.; Shin, D. S.; Kumar, D. Benzimidazole Bearing Oxadiazole and Triazolo-Thiadiazoles Nucleus: Design and Synthesis as Anticancer Agents. *Bioorganic Med. Chem. Lett.* **2012**, *22* (17), 5438–5444. https://doi.org/10.1016/j.bmcl.2012.07.038.

(122) Sontakke, V. A.; Ghosh, S.; Lawande, P. P.; Chopade, B. A.; Shinde, V. S. A Simple , Efficient Synthesis of 2-Aryl Benzimidazoles Using Silica Supported Periodic Acid Catalyst and Evaluaton of Anticancer Activity. **2013**, *2013*, 3–10.

(123) Tan, Y. J., Lee, Y. T., Yeong, K. Y., Petersen, S. H., Kono, K., Tan, S. C., & Oon, C. E.

Anticancer activities of a benzimidazole compound through sirtuin inhibition in colorectal cancer. *Future medicinal chemistry* **2018**, *10*(17), 2039-2057.

(124) Kapoor, A.; Dhiman, N. Anticancer Evaluation of 2-Aryl Substituted Benzimidazole Derivatives Bearing. **2016**, *8* (12), 149–156.

(125) Shrivastava, N.; Naim, M. J.; Alam, M. J.; Nawaz, F.; Ahmed, S.; Alam, O. Benzimidazole Scaffold as Anticancer Agent: Synthetic Approaches and Structure–Activity Relationship. *Archiv der Pharmazie*. 2017., *350*(6), e201700040. https://doi.org/10.1002/ardp.201700040.

(126) Salahuddin; Shaharyar, M.; Mazumder, A. Benzimidazoles: A Biologically Active Compounds. *Arab. J. Chem.* **2017**, *10*, 157–173. https://doi.org/10.1016/j.arabjc.2012.07.017.

(127) Ahmad, T.; Devision, B.; Ray, S. K.; Rahman, S. Synthesis of Benzimidazole Derivatives Containing Schiff Base Exhibiting Antimicrobial Activities. *Int. J. Res. Stud. Biosci.* **2017**, *5* (7). https://doi.org/10.20431/2349-0365.0507003.

(128) Ajani, O. O.; Tolu-bolaji, O. O.; Olorunshola, S. J.; Zhao, Y.; Aderohunmu, D. V. Disubstituted Benzimidazole Derivatives and Their in Vitro Antibacterial Efficacy. *J. Adv. Res.* **2017**, *8* (6), 703–712. https://doi.org/10.1016/j.jare.2017.09.003.

(129) Enumula, S.; Pangal, A.; Gazge, M.; Shaikh, J. A.; Ahmed, K. Diverse Pharmacological Aspects of Benzimidazole Derivatives : A Review. **2014**, *4* (4), 78–88.

(130) Anand, K.; Wakode, S. Development of Drugs Based on Benzimidazole Heterocycle: Recent Advancement and Insights. *350 ~ Int. J. Chem. Stud.* **2017**, *5* (2), 350–362.

(131) Ali, I.; Lone, M. N.; Aboul-Enein, H. Y. Imidazoles as Potential Anticancer Agents.

Medchemcomm **2017**, *8* (9), 1742–1773. https://doi.org/10.1039/c7md00067g.

(132) Gaba, M.; Mohan, C. *Development of Drugs Based on Imidazole and Benzimidazole Bioactive Heterocycles: Recent Advances and Future Directions*; Springer US, 2016; Vol. 25. https://doi.org/10.1007/s00044-015-1495-5.

(133) Singh, N.; Pandurangan, A.; Rana, K.; Anand, P.; Ahamad, A.; Tiwari, A. K. Benzimidazole: A Short Review of Their Antimicrobial Activities. *Int. Curr. Pharm. J.* **2012**, *1* (5), 119–127. https://doi.org/10.3329/icpj.v1i5.10284.

(134) Shaharyar, M.; Mazumder, A. Synthesis , Characterization and Antimicrobial Activity of 1 , 3 , 4-Oxadiazole Bearing 1H-Benzimidazole Derivatives. *Arab. J. Chem.* **2017**, *10*, S503–S508. https://doi.org/10.1016/j.arabjc.2012.10.010.

(135) Desai, N. C.; Shihory, N. R.; Kotadiya, G. M.; Desai, P. Synthesis, Antibacterial and Antitubercular Activities of Benzimidazole Bearing Substituted 2-Pyridone Motifs. *Eur. J. Med. Chem.* **2014**, *82*, 480–489. https://doi.org/10.1016/j.ejmech.2014.06.004.

(136) Sharma, K.; Shrivastava, A.; Mehra, R. N.; Deora, G. S.; Alam, M. M.; Zaman, M. S.; Akhter, M. Synthesis of Novel Benzimidazole Acrylonitriles for Inhibition of Plasmodium Falciparum Growth by Dual Target Inhibition. *Arch. Pharm. (Weinheim).* **2018**, *351* (1). https://doi.org/10.1002/ardp.201700251.

(137) Camacho, J.; Barazarte, A.; Gamboa, N.; Rodrigues, J.; Rojas, R.; Vaisberg, A.; Gilman, R.; Charris, J. Synthesis and Biological Evaluation of Benzimidazole-5-Carbohydrazide Derivatives as Antimalarial, Cytotoxic and Antitubercular Agents. *Bioorganic Med. Chem.* **2011**, *19* (6), 2023–2029. https://doi.org/10.1016/j.bmc.2011.01.050.

(138) Peter, M.; Jo, S.; Kim, H.; Kim, S.; Kim, K.; Kong, S.; Jeong, H.; Ahn, S.; No, Z.; Yeon,

J. European Journal of Medicinal Chemistry Discovery of 2-Iminobenzimidazoles as Potent Hepatitis C Virus Inhibitors with a Novel Mechanism of Action. *Eur. J. Med. Chem.* **2014**, *78*, 35–42. https://doi.org/10.1016/j.ejmech.2014.03.030.

(139) Vitale, G.; Corona, P.; Loriga, M.; Carta, A.; Paglietti, G.; Giliberti, G.; Sanna, G.; Farci, P.; Marongiu, M. E.; La Colla, P. 5-Acetyl-2-Arylbenzimidazoles as Antiviral Agents. Part 4. *Eur. J. Med. Chem.* **2012**, *53*, 83–97. https://doi.org/10.1016/j.ejmech.2012.03.038.

(140) Gaba, M.; Singh, S.; Mohan, C. Benzimidazole: An Emerging Scaffold for Analgesic and Anti-Inflammatory Agents. *European Journal of Medicinal Chemistry*. 2014. https://doi.org/10.1016/j.ejmech.2014.01.030.

(141) Tantray, M. A.; Khan, I.; Hamid, H.; Sarwar, M.; Dhulap, A. Bioorganic Chemistry GSK-3 b Inhibitors with in Vivo Antidepressant Activity. *Bioorg. Chem.* **2018**, *77*, 393–401. https://doi.org/10.1016/j.bioorg.2018.01.040.

(142) Al-Mudaris, Z. A.; Majid, A. S. A.; Ji, D.; Al-Mudarris, B. A.; Chen, S. H.; Liang, P. H.; Osman, H.; Jamal Din, S. K. K.; Abdul Majid, A. M. S. Conjugation of Benzylvanillin and Benzimidazole Structure Improves DNA Binding with Enhanced Antileukemic Properties. *PLoS One* **2013**, *8* (11), 1–11. https://doi.org/10.1371/journal.pone.0080983.

(143) Ibrahim, H. A.; Refaat, H. M. Versatile Mechanisms of 2-Substituted Benzimidazoles in Targeted Cancer Therapy. **2020**, *8*.

(144) Çevik, U. A.; Sağlık, B. N.; Osmaniye, D.; Çavuşoğlu, B. K.; Karaduman, A. B.; Atlı, Ö.; Özkay, Y.; Kaplancıklı, Z. A. Synthesis , Anticancer Evaluation and Molecular

Docking Studies of New Benzimidazole- 1 , 3 , 4- Oxadiazole Derivatives as Human Topoisomerase Types I Poison. *J. Enzyme Inhib. Med. Chem.* **2020**, *35* (1), 1657–1673. https://doi.org/10.1080/14756366.2020.1806831.

(145) Vijayakumar, K.; Sountharrajan, S.; Suganya, E. Synthesis , Characterization , and Evaluation of Cancer Prevention Activity of Novel Modified Heterocyclic Compounds. **2018**, *19*, 247–252. https://doi.org/10.22034/APJCP.2018.19.1.247.

(146) Yadav, S.; Narasimhan, B.; kaur, H. Perspectives of Benzimidazole Derivatives as Anticancer Agents in the New Era. *Anticancer. Agents Med. Chem.* **2016**, *16* (11), 1403–1425. https://doi.org/10.2174/1871520616666151103113412.

(147) Karaaslan, C.; Bakar, F.; Goker, H. Antiproliferative Activity of Synthesized Some New Benzimidazole Carboxamidines against MCF-7 Breast Carcinoma Cells. *Zeitschrift fur Naturforsch. - Sect. C J. Biosci.* **2018**, *73* (3–4), 137–145. https://doi.org/10.1515/znc-2017-0067.

(148) Alpan, A. S.; Zencir, S.; Zupkó, I.; Coban, G.; Rthy, B.; Gunes, H. S.; Topcu, Z. Biological Activity of Bis-Benzimidazole Derivatives on DNA Topoisomerase i and HeLa, MCF7 and A431 Cells. *J. Enzyme Inhib. Med. Chem.* **2009**, *24* (3), 844–849. https://doi.org/10.1080/14756360802420831.

(149) Jiang, Y.; Chen, K.; Shen, Z.; Sun, Q.; Li, B.; Chu, B.; Li, L.; Liu, F.; Gao, C. New Benzimidazole Acridine Derivative Induces Human Colon Cancer Cell Apoptosis in Vitro via the ROS-JNK Signaling Pathway. *Acta Pharmacol. Sin.* **2015**, *36* (9), 1074–1084. https://doi.org/10.1038/aps.2015.44.

(150) Omar, M. A.; Shaker, Y. M.; Galal, S. A.; Ali, M. M.; Kerwin, S. M.; Li, J.; Tokuda,

H.; Ramadan, R. A.; El, H. I. Bioorganic & Medicinal Chemistry Synthesis and Docking Studies of Novel Antitumor Benzimidazoles. *Bioorg. Med. Chem.* **2012**, *20* (24), 6989–7001. https://doi.org/10.1016/j.bmc.2012.10.010.

(151) Magd-El-Din, A. A., Mousa, H. A., Labib, A. A., Hassan, A. S., Abd El-All, A. S., Ali, M. M., El-Desoky, A. H. Benzimidazole–Schiff bases and their complexes: synthesis, anticancer activity and molecular modeling as Aurora kinase inhibitor. *Zeitschrift für Naturforschung C* **2018**., *73*(11-12), 465-478.

(152) Li, Y.; Tan, C.; Gao, C.; Zhang, C.; Luan, X.; Chen, X.; Liu, H.; Chen, Y.; Jiang, Y. Bioorganic & Medicinal Chemistry Discovery of Benzimidazole Derivatives as Novel Multi-Target EGFR , VEGFR-2 and PDGFR Kinase Inhibitors. *Bioorg. Med. Chem.* **2011**, *19* (15), 4529–4535. https://doi.org/10.1016/j.bmc.2011.06.022.

(153) Bezerra, D. P.; Soares, A. K. N.; De Sousa, D. P. Overview of the Role of Vanillin on Redox Status and Cancer Development. *Oxid. Med. Cell. Longev.* **2016**, *2016*. https://doi.org/10.1155/2016/9734816.

(154) Elsherbiny, N. M.; Younis, N. N.; Shaheen, M. A.; Elseweidy, M. M. The Synergistic Effect between Vanillin and Doxorubicin in Ehrlich Ascites Carcinoma Solid Tumor and MCF-7 Human Breast Cancer Cell Line. *Pathol. Res. Pract.* **2016**, *212* (9), 767–777. https://doi.org/10.1016/j.prp.2016.06.004.

(155) Tahlan, S.; Kumar, S.; Ramasamy, K.; Lim, S. M.; Adnan, S.; Shah, A. In - Silico Molecular Design of Heterocyclic Benzimidazole Scaffolds as Prospective Anticancer Agents. *BMC Chem.* **2019**, 1–22. https://doi.org/10.1186/s13065-019-0608-5.

(156) Oduselu, G. O.; Ajani, O. O.; Ajamma, Y. U.; Brors, B.; Adebiyi, E. Homology

Modelling and Molecular Docking Studies of Selected Substituted Benzo [d] Imidazol-1-Yl) Methyl) Benzimidamide Scaffolds on Plasmodium Falciparum Adenylosuccinate Lyase Receptor. *Bioinformatics and biology insights* **2019,** *13*, 1177932219865533. https://doi.org/10.1177/1177932219865533.

(157) Viana, J. D. O.; Félix, M. B.; Maia, S.; Serafim, V. D. L.; Scotti, L.; Scotti, M. T. Drug Discovery and Computational Strategies in the Multitarget Drugs Era. *Brazilian Journal of Pharmaceutical Sciences*, **2018**, 54, 1–25.

(158) Mohamed, A. A. B.; Badria, F. A.; Maarouf, A. R.; Abdel-aziz, N. I.; Elsenduny, F. Synthesis , Antitumor Evaluation and Molecular Modeling Study of Novel Benzimidazoles and Pyrazinobenzimidazoles. *J Appl Pharm Sci*, **2017**, *7* (6), 206–214. https://doi.org/10.7324/JAPS.2017.70631.

(159) Kurkinen, S. T.; Niinivehmas, S.; Ahinko, M.; Lätti, S.; Pentikäinen, O. T.; Postila, P. A. Improving Docking Performance Using Negative Image-Based Rescoring . *Frontiers in Pharmacology* . 2018, p 260.

(160) Chu, B.; Liu, F.; Li, L.; Ding, C.; Chen, K.; Sun, Q.; Shen, Z.; Tan, Y.; Tan, C.; Jiang, Y. A Benzimidazole Derivative Exhibiting Antitumor Activity Blocks EGFR and HER2 Activity and Upregulates DR5 in Breast Cancer Cells. *Cell Death Dis.* **2015**, *6*, e1686. https://doi.org/10.1038/cddis.2015.25.

(161) Li, Y.; Meng, Q.; Yang, M.; Liu, D.; Hou, X.; Tang, L.; Wang, X.; Lyu, Y.; Chen, X.; Liu, K.; Yu, A.-M.; Zuo, Z.; Bi, H. Current Trends in Drug Metabolism and Pharmacokinetics. *Acta Pharm. Sin. B* **2019**, *9* (6), 1113–1144. https://doi.org/10.1016/j.apsb.2019.10.001.

(162) Guan, L.; Yang, H.; Cai, Y.; Sun, L.; Di, P.; Li, W.; Liu, G.; Tang, Y. ADMET-Score - a Comprehensive Scoring Function for Evaluation of Chemical Drug-Likeness. *Medchemcomm* **2018**, *10* (1), 148–157. https://doi.org/10.1039/c8md00472b.

(163) Vyas, V. K.; Ghate, M.; Chintha, C.; Patel, P. 3D QSAR Studies on Substituted Benzimidazole Derivatives as Angiotensin II-AT1 Receptor Antagonist. *Curr. Comput. Aided. Drug Des.* **2013**, *9* (3), 433–445. https://doi.org/10.2174/15734099113099990028.

(164) Al-Warhi, T.; Said, M. A.; El Hassab, M. A.; Aljaeed, N.; Ghabour, H. A.; Almahli, H.; Eldehna, W. M.; Abdel-Aziz, H. A. Unexpected Synthesis, Single-Crystal X-Ray Structure, Anticancer Activity, and Molecular Docking Studies of Certain 2–((Imidazole/Benzimidazol–2–Yl)Thio)–1–Arylethanones. *Crystals* **2020**, 10(6), 446 https://doi.org/10.3390/cryst10060446.

(165) Mathew, B.; Mathew, G. E.; Suresh, J.; Usman, D.; Safna, P. N. S. S. and K. F. Ligand Based Drug Design of New Heterocyclic Imines of GABA Analogues: A Molecular Docking Approach for the Discovery of New GABA-AT Inhibitors. *Central Nervous System Agents in Medicinal Chemistry* **2017**, *17*(1), 58–63. https://doi.org/http://dx.doi.org/10.2174/1871524916666160104143108.

(166) Ibrahim, H. A.; Refaat, H. M. Versatile Mechanisms of 2-Substituted Benzimidazoles in Targeted Cancer Therapy. *Futur. J. Pharm. Sci.* **2020**, *6*(1), 41. https://doi.org/10.1186/s43094-020-00048-8.

(167) Purser, S.; Moore, P. R.; Swallow, S.; Gouverneur, V. Fluorine in Medicinal Chemistry. *Chem. Soc. Rev.* **2008**, *37* (2), 320–330. https://doi.org/10.1039/B610213C.

(168) Shah, P., Westwell, A. D.The role of fluorine in medicinal chemistry. *Journal of enzyme inhibition and medicinal chemistry* ***2007***, *22*(5), 527-540. https://doi.org/10.1080/14756360701425014.

(169) Etzion, Y.; Muslin, A. J. The Application of Phenotypic High-Throughput Screening Techniques to Cardiovascular Research. *Trends Cardiovasc. Med.* **2009**, *19* (6), 207–212. https://doi.org/10.1016/j.tcm.2009.12.006.

(170) MacArron, R.; Banks, M. N.; Bojanic, D.; Burns, D. J.; Cirovic, D. A.; Garyantes, T.; Green, D. V. S.; Hertzberg, R. P.; Janzen, W. P.; Paslay, J. W.; Schopfer, U.; Sittampalam, G. S. Impact of High-Throughput Screening in Biomedical Research. *Nat. Rev. Drug Discov.* **2011**, *10* (3), 188–195. https://doi.org/10.1038/nrd3368.

(171) Vogels and Abbott. Published in Final Edited Form as: Nat Neurosci. 2009 April ; 12(4): 483–491. Doi:10.1038/Nn.2276. **2009**, *18*(0), 1067–1073. https://doi.org/10.1016/j.drudis.2013.07.001.Phenotypic.

(172) Moffat, J. G.; Vincent, F.; Lee, J. A.; Eder, J.; Prunotto, M. Opportunities and Challenges in Phenotypic Drug Discovery: An Industry Perspective. *Nat. Rev. Drug Discov.* **2017**, *16* (8), 531–543. https://doi.org/10.1038/nrd.2017.111.

(173) Davis, R. L. Mechanism of Action and Target Identification: A Matter of Timing in Drug Discovery. *iScience* **2020**, *23*(9), 101487. https://doi.org/10.1016/j.isci.2020.101487.

(174) Van Vleet, T. R.; Liguori, M. J.; Lynch, J. J.; Rao, M.; Warder, S. Screening Strategies and Methods for Better Off-Target Liability Prediction and Identification of Small-Molecule Pharmaceuticals. *SLAS Discov.* **2019**, *24* (1), 1–24.

https://doi.org/10.1177/2472555218799713.

(175) Guo, D.; Heitman, L. H.; Ijzerman, A. P. The Role of Target Binding Kinetics in Drug Discovery. *ChemMedChem* **2015**, *10* (11), 1793–1796. https://doi.org/10.1002/cmdc.201500310.

(176) Cereto-Massagué, A.; Ojeda, M. J.; Valls, C.; Mulero, M.; Pujadas, G.; Garcia-Vallve, S. Tools for in Silico Target Fishing. *Methods* **2015**, *71* (C), 98–103. https://doi.org/10.1016/j.ymeth.2014.09.006.

(177) Traphagen, N. A.; Hosford, S. R.; Jiang, A.; Marotti, J. D.; Brauer, B. L.; Demidenko, E.; Miller, T. W. High Estrogen Receptor Alpha Activation Confers Resistance to Estrogen Deprivation and Is Required for Therapeutic Response to Estrogen in Breast Cancer. *Oncogene* **2021,** *40*(19), 3408-3421.https://doi.org/10.1038/s41388-021-01782

(178) Koide, A.; Abbatiello, S.; Rothgery, L.; Koide, S. Probing Protein Conformational Changes in Living Cells by Using Designer Binding Proteins: Application to the Estrogen Receptor. *Proc. Natl. Acad. Sci. U. S. A.* **2002**, *99*(3), 1253–1258. https://doi.org/10.1073/pnas.032665299.

(179) Rao, B. A.; Sarasija, M.; Kiran, K.; Rao, A. S.; Ashok, D. Synthesis, Characterisation, and Antibacterial Activity of Some Novel Vanillin Related Hydrazone Derivatives Bearing 1,2,3-Triazole Ring. *Russ. J. Gen. Chem.* **2017**, *87* (6), 1288–1294. https://doi.org/10.1134/s1070363217060251.

(180) Divaeva, L. N.; Klimenko, A. I.; Morkovnik, A. S.; Fetisov, L. N.; Kuz, T. A.; Zubenko, A. A.; Bodryakova, M. A.; Bodryakov, A. N. SYNTHESIS AND ANTIMICROBIAL AND PROTISTOCIDAL ACTIVITY OF 1- (2-ARYLOXYETHYL- AND 2-

HALOBENZYL) -3-. **2015**, *49* (2), 91–95. https://doi.org/10.1007/s11094-015-1228-6.

(181) Morales, S.; Guijarro, F. G.; García Ruano, J. L.; Cid, M. B. A General Aminocatalytic Method for the Synthesis of Aldimines. *J. Am. Chem. Soc.* **2014**, *136* (3), 1082–1089. https://doi.org/10.1021/ja4111418.

(182) Roeder, C. H.; Day, A. R. Benzimidazole Studies. I. The Mechanism Of Benzimidazole Formation From O-Phenylenediamine. *J. Org. Chem.* **1941**, *06*(1), 25–35. https://doi.org/10.1021/jo01201a002.

(183) Namli, H.; Turhan, O. Background Defining during the Imine Formation Reaction in FT-IR Liquid Cell. **2006**, *64*, 93–100. https://doi.org/10.1016/j.saa.2005.07.020.

(184) Overview, A. N.; Infectious, O. N. Indian Journal of Pharmaceutical Science & Research. **2012**, *2* (2), 63–75.

(185) Smith, H. The Role of Microbial Interactions in Infectious Disease. *Philos. Trans. R. Soc. Lond. B. Biol. Sci.* **1982**, *297*(1088), 551–561. https://doi.org/10.1098/rstb.1982.0060.

(186) O'Malley, M. A., *Philosophy of microbiology*. **2014**, Cambridge University Press.1–269. https://doi.org/10.1017/CBO9781139162524. O'Malley, M. (2014).

(187) Braga, R. M.; Dourado, M. N.; Araújo, W. L. Microbial Interactions: Ecology in a Molecular Perspective. *Brazilian J. Microbiol.* **2016**, *47*, 86–98. https://doi.org/10.1016/j.bjm.2016.10.005.

(188) Kumar, A.; Chordia, N. Role of Microbes in Human Health. *Appl. Microbiol. Open Access* **2017**, *03* (02), 2–4. https://doi.org/10.4172/2471-9315.1000131.

(189) Dethlefsen, L.; McFall-Ngai, M.; Relman, D. A. An Ecological and Evolutionary Perspective on Human–Microbe Mutualism and Disease. *Nature* **2007**, *449* (7164), 811–818. https://doi.org/10.1038/nature06245.

(190) Barreto, M. L.; Teixeira, M. G.; Carmo, E. H. Infectious Diseases Epidemiology. *J. Epidemiol. Community Health* **2006**, *60* (3), 192–195. https://doi.org/10.1136/jech.2003.011593.

(191) Lewis, P. F. Bacterial Infections. *Pediatrics* **2005**, 1, 839–847. https://doi.org/10.1016/B978-0-323-01199-0.50123-7.

(192) Edemekong, P. F.; Huang, B. Epidemiology of Prevention of Communicable Diseases. **2021**.

(193) Murray, C. J. .; Lopez, A. D. Global Burden of Disease and Injur Y Series the Global Burden of Disease. *Oms* **1996**, 1–46.

(194) Jones, K. E.; Patel, N. G.; Levy, M. A.; Storeygard, A.; Balk, D.; Gittleman, J. L.; Daszak, P. Global Trends in Emerging Infectious Diseases. *Nature* **2008**, *451* (7181), 990–993. https://doi.org/10.1038/nature06536.

(195) Alanis, A. J. Resistance to Antibiotics : Are We in the Post-Antibiotic Era ? **2005**, *36*, 697–705. https://doi.org/10.1016/j.arcmed.2005.06.009.

(196) Bisen, P. S.; Debnath, M.; Prasad, G. B. K. S. MICROBES: Concepts and Applications. **2012**, No. September.

(197) Gradelski, E.; Kolek, B.; Bonner, D. P.; Valera, L.; Minassian, B.; Fung-Tomc, J. Activity of Gatifloxacin and Ciprofloxacin in Combination with Other Antimicrobial Agents. *Int. J. Antimicrob. Agents* **2001**, *17*(2), 103–107. https://doi.org/10.1016/S0924-

8579(00)00317-4.

(198) Quinn, P. J.; Markey, B. K.; Leonard, F. C.; Hartigan, P.; Fanning, S.; Fitzpatrick, Es. *Veterinary Microbiology and Microbial Disease*; John Wiley & Sons, 2011.

(199) Fernandes, R.; Amador, P.; Prudêncio, C. β-Lactams: Chemical Structure, Mode of Action and Mechanisms of Resistance. *Rev. Med. Microbiol.* **2013**, *24* (1), 7–17. https://doi.org/10.1097/MRM.0b013e3283587727.

(200) Davies, J. Are Antibiotics Naturally Antibiotics? *J. Ind. Microbiol. Biotechnol.* **2006**, *33* (7), 496–499. https://doi.org/10.1007/s10295-006-0112-5.

(201) Ajani, O. O.; Obafemi, C. A.; Nwinyi, O. C.; Akinpelu, D. A. Bioorganic & Medicinal Chemistry Microwave Assisted Synthesis and Antimicrobial Activity of 2-Quinoxalinone-3-Hydrazone Derivatives. *Bioorg. Med. Chem.* **2010**, *18* (1), 214–221. https://doi.org/10.1016/j.bmc.2009.10.064.

(202) Obafemi, C. A.; Akinpelu, D. A. Synthesis and Antimicrobial Activity of Some 2(1H)-Quinoxalinone-6-Sulfonyl Derivatives. *Phosphorus, Sulfur Silicon Relat. Elem.* **2005**, *180* (8), 1795–1807. https://doi.org/10.1080/104265090889396.

(203) Ahmed, E. A.; Mohamed, M. F. A.; Omran, A.; Salah, H. Synthesis, EGFR-TK Inhibition and Anticancer Activity of New Quinoxaline Derivatives. *Synth. Commun.* **2020**, *50* (19), 2924–2940. https://doi.org/10.1080/00397911.2020.1787448.

(204) Montana, M.; Montero, V.; Khoumeri, O.; Vanelle, P. Quinoxaline Derivatives as Antiviral Agents: A Systematic Review. *Molecules* **2020**, *25*(12). https://doi.org/10.3390/molecules25122784.

(205) Guillon, J.; Grellier, P.; Labaied, M.; Sonnet, P.; Léger, J. M.; Déprez-Poulain, R.;

Forfar-Bares, I.; Dallemagne, P.; Lemaître, N.; Péhourcq, F.; Rochette, J.; Sergheraert, C.; Jarry, C. Synthesis, Antimalarial Activity, and Molecular Modeling of New Pyrrolo[1,2-a]Quinoxalines, Bispyrrolo[1,2-a]Quinoxalines, Bispyrido[3,2-e]Pyrrolo[1,2-a]Pyrazines, and Bispyrrolo[1,2-a]Thieno[3,2-e]Pyrazines. *J. Med. Chem.* **2004**, *47*(8), 1997–2009. https://doi.org/10.1021/jm0310840.

(206) Shintre, S. A.; Ramjugernath, D.; Islam, M. S.; Mopuri, R.; Mocktar, C.; Koorbanally, N. A. Synthesis, in Vitro Antimicrobial, Antioxidant, and Antidiabetic Activities of Thiazolidine–Quinoxaline Derivatives with Amino Acid Side Chains. *Med. Chem. Res.* **2017**, *26* (9), 2141–2151. https://doi.org/10.1007/s00044-017-1922-x.

(207) Burguete, A.; Pontiki, E.; Hadjipavlou-Litina, D.; Ancizu, S.; Villar, R.; Solano, B.; Moreno, E.; Torres, E.; Pérez, S.; Aldana, I.; Monge, A. Synthesis and Biological Evaluation of New Quinoxaline Derivatives as Antioxidant and Anti-Inflammatory Agents. *Chem. Biol. Drug Des.* **2011**, *77*(4), 255–267. https://doi.org/10.1111/j.1747-0285.2011.01076.x.

(208) Puratchikody, A.; Natarajan, R.; Jayapal, M.; Doble, M. Synthesis, in Vitro Antitubercular Activity and 3D-QSAR of Novel Quinoxaline Derivatives. *Chem. Biol. Drug Des.* **2011**, *78*(6), 988–998. https://doi.org/10.1111/j.1747-0285.2011.01246.x.

(209) Zhang, H.; Zhang, J.; Qu, W.; Xie, S.; Huang, L.; Chen, D.; Tao, Y.; Liu, Z.; Pan, Y.; Yuan, Z. Design, Synthesis, and Biological Evaluation of Novel Thiazolidinone-Containing Quinoxaline-1,4-Di-N-Oxides as Antimycobacterial and Antifungal Agents. *Front. Chem.* **2020**, *8*, 1–15. https://doi.org/10.3389/fchem.2020.00598.

(210) Ammar, Y. A.; Farag, A. A.; Ali, A. M.; Ragab, A.; Askar, A. A.; Elsisi, D. M.; Belal, A. Design, Synthesis, Antimicrobial Activity and Molecular Docking Studies of Some

Novel Di-Substituted Sulfonylquinoxaline Derivatives. *Bioorg. Chem.* **2020**, *104*, 104164. https://doi.org/10.1016/j.bioorg.2020.104164.

(211) Ajani, O. O.; Nlebemuo, M. T.; Adekoya, J. A.; Ogunniran, K. O.; Siyanbola, T. O.; Ajanaku, C. O. Chemistry and Pharmacological Diversity of Quinoxaline Motifs as Anticancer Agents. **2019**, *69*, 177–196.

(212) Husain, A.; Madhesia, D. Available Online through Recent Advances in Pharmacological Activities of Quinoxaline Derivatives. **2011**, *4* (3), 924–929.

(213) Mahadik, P.; Jagwani, D.; Joshi, R. A Greener Chemistry Approach for Synthesis of 2 , 3-Diphenyl Quinoxaline. **2014**, *1*(6), 482–490.

(214) Kulkarni, A. P.; Zhu, Y.; Jenekhe, S. A. Quinoxaline-Containing Polyfluorenes: Synthesis, Photophysics, and Stable Blue Electroluminescence. *Macromolecules* **2005**, *38*(5), 1553–1563. https://doi.org/10.1021/ma048118d.

(215) Dailey, S.; Feast, W. J.; Peace, R. J.; Sage, I. C.; Till, S.; Wood, E. L. Synthesis and Device Characterisation of Side-Chain Polymer Electron Transport Materials for Organic Semiconductor Applications. *J. Mater. Chem.* **2001**, *11*(9), 2239–2244. https://doi.org/10.1039/b104674h.

(216) Luo, X.; Lim, L. T. Cinnamil- And Quinoxaline-Derivative Indicator Dyes for Detecting Volatile Amines in Fish Spoilage. *Molecules* **2019**, *24* (20), 8–10. https://doi.org/10.3390/molecules24203673.

(217) Inflammatory, A.; Of, A.; New, S.; Quinoxaline, D. O. F. Available Online Http://Www.Ijddr.in Covered in Official Product of Elsevier , The Netherlands Anti Inflammatory Activity Of Some New Thio-Ether. **2010**, *2* (4), 810–815.

(218) El-atawy, M. A.; Hamed, E. A.; Alhadi, M.; Omar, A. Z. Synthesis and Antimicrobial Activity of Some New Substituted Quinoxalines. *Molecules* **2019**, *24*(22), 4198.

(219) Nakhate, K.; Mishra, A. Design , Synthesis , and Characterization of Quinoxaline Derivatives as a Potent Antimicrobial Agent. *Journal of Heterocyclic Chemistry* **2018** , *56*(2), 566-578.https://doi.org/10.1002/jhet.3431.

(220) Amin, M. A.; Youssef, M. M. Use of Modern Technique for Synthesis of Quinoxaline Derivatives as Potential Anti-Virus Compounds Use of Modern Technique for Synthesis of Quinoxaline Derivatives as Potential Anti-Virus Compounds. Der Pharma Chemica, **2012**, 4 (3), 1323-1329

(221) Guillon, J.; Cohen, A.; Boudot, C.; Valle, A.; Milano, V.; Das, R. N.; Guédin, A.; Moreau, S.; Ronga, L.; Savrimoutou, S.; Demourgues, M.; Reviriego, E.; Rubio, S.; Ferriez, S.; Agnamey, P.; Pauc, C.; Moukha, S.; Dozolme, P.; Nascimento, S. Da; Laumaillé, P.; Bouchut, A.; Azas, N.; Mergny, J. L.; Mullié, C.; Sonnet, P.; Courtioux, B. Design, Synthesis, and Antiprotozoal Evaluation of New 2,4-Bis[(Substituted-Aminomethyl)Phenyl]Quinoline, 1,3-Bis[(Substituted-Aminomethyl)Phenyl]Isoquinoline and 2,4-Bis[(Substituted-Aminomethyl)Phenyl]Quinazoline Derivatives. *J. Enzyme Inhib. Med. Chem.* **2020**, *35* (1), 432–459. https://doi.org/10.1080/14756366.2019.1706502.

(222) Vieira, M.; Pinheiro, C.; Fernandes, R.; Paulo, J. Antimicrobial Activity of Quinoxaline 1 , 4-Dioxide with 2- and 3-Substituted Derivatives ☪. *Microbiol. Res.* **2014**, *169* (4), 287–293. https://doi.org/10.1016/j.micres.2013.06.015.

(223) Chen, Q.; Bryant, V. C.; Lopez, H.; Kelly, D. L.; Luo, X.; Natarajan, A. 2,3-Substituted Quinoxalin-6-Amine Analogs as Antiproliferatives: A Structure-Activity Relationship

Study. *Bioorganic Med. Chem. Lett.* **2011**, *21* (7), 1929–1932. https://doi.org/10.1016/j.bmcl.2011.02.055.

(224) Bertino, B.; Blanchet-Réthoré, S.; Thibaut de Ménonville, S.; Reynier, P.; Méhul, B.; Bogouch, A.; Gamboa, B.; Dugaret, A. S.; Zugaj, D.; Petit, L. Brimonidine Displays Anti-inflammatory Properties in the Skin through the Modulation of the Vascular Barrier Function. *Exp. Dermatol.* **2018**, *27* (12), 1378–1387.

(225) Ruiz, D. M.; Autino, J. C.; Quaranta, N.; Vázquez, P. G.; Romanelli, G. P. An Efficient Protocol for the Synthesis of Quinoxaline Derivatives at Room Temperature Using Recyclable Alumina-Supported Heteropolyoxometalates. *Sci. World J.* **2012**, *2012* (Iii). https://doi.org/10.1100/2012/174784.

(226) Nakhate, A. V; Rasal, K. B.; Deshmukh, G. P.; Gupta, S. S. R.; Mannepalli, L. K. Synthesis of Quinoxaline Derivatives from Terminal Alkynes and O-Phenylenediamines by Using Copper Alumina Catalyst. *J. Chem. Sci.* **2017**, *129* (11), 1761–1769. https://doi.org/10.1007/s12039-017-1393-0.

(227) Yan, J.; Xu, Y.; Zhuang, F.; Tian, J.; Zhang, G. Highly Efficient Synthesis of Quinoxaline Derivatives from Compounds. *Mol. Divers.* **2016**, *20* (2), 567–573. https://doi.org/10.1007/s11030-016-9657-z.

(228) Rouhani, M.; Ramazani, A. Perlite–SO3H Nanoparticles: Very Efficient and Reusable Catalyst for Three-Component Synthesis of N-Cyclohexyl-3-Aryl-Quinoxaline-2-Amine Derivatives under Ultrasound Irradiation. *J. Iran. Chem. Soc.* **2018**, *15*(10), 2375–2382. https://doi.org/10.1007/s13738-018-1426-8.

(229) Dânoun, KarimEco-friendly approach to access of quinoxaline derivatives using

nanostructured pyrophosphate Na2PdP2O7as a new, efficient and reusable heterogeneous catalyst; Essamlali, Y.; Amadine, O.; Mahi, H.; Zahouily, M. Eco-Friendly Approach to Access of Quinoxaline Derivatives Using Nanostructured Pyrophosphate Na2PdP2O7as a New, Efficient and Reusable Heterogeneous Catalyst. *BMC Chem.* **2020**, *14* (1), 1–13. https://doi.org/10.1186/s13065-020-0662-z.

(230) Zyryanov, G. Synthesis of Quinoxaline Derivatives Catalyzed By Brønsted Acidic Ionic Liquid Under Solvent-Free Conditions. *Современные Синтетические Методологии Для Создания Лекарственных Препаратов И Функциональных Материалов (Mosm2019). — Екатеринбург, 2019* **2019**, *050012* (October), 195–195.

(231) Adamczyk-Woźniak, A.; Borys, K. M.; Sporzyński, A. Recent Developments in the Chemistry and Biological Applications of Benzoxaboroles. *Chem. Rev.* **2015**, *115*(11), 5224–5247. https://doi.org/10.1021/cr500642d.

(232) Kölmel, D. K.; Kool, E. T. Oximes and Hydrazones in Bioconjugation: Mechanism and Catalysis. *Chem. Rev.* **2017**, *117*(15), 10358–10376. https://doi.org/10.1021/acs.chemrev.7b00090.

(233) Rosenberg, S.; Silver, S. M.; Sayer, J. M.; Jencks, W. P. Evidence for Two Concurrent Mechanisms and a Kinetically Significant Proton Transfer Process in Acid-Catalyzed O-Methyloxime Formation. *J. Am. Chem. Soc.* **1974**, *96* (26), 7986–7998.

(234) Sahyoun, T.; Arrault, A.; Schneider, R. Amidoximes and Oximes: Synthesis, Structure, and Their Key Role as No Donors. *Molecules* **2019**, *24*(13). https://doi.org/10.3390/molecules24132470.

(235) Rearrangement, T. C.; Insight, M.; Applications, R.; Syntheses, N. P. HHS Public

Access. **2019**, *16*(12), 2006–2027. https://doi.org/10.1039/c8ob00138c.The.

(236) Baker, J. W.; Gaunt, J. 4. The Mechanism of the Reaction of Aryl Iso Cyanates with Alcohols and Amines. Part III. The "Spontaneous" Reaction of Phenyl Iso Cyanate with Various Alcohols. Further Evidence Relating to the Anomalous Effect of Dialkylanilines in the Base-Catalysed Re. *J. Chem. Soc.* **1949**, 19–24.

(237) Drlica, K.; Zhao, X. DNA Gyrase, Topoisomerase IV, and the 4-Quinolones. *Microbiol. Mol. Biol. Rev.* **1997**, *61* (3), 377–392. https://doi.org/10.1128/.61.3.377-392.1997.

(238) El-attar, M. A. Z.; Elbayaa, R. Y.; Shaaban, O. G.; Habib, N. S. Synthesis of Antimicrobial Agents with Potential Inhibition of DHPS Enzyme. *Future Medicinal Chemistry* **2018**, *10*(18), 2155-2175.

(239) Sanna, P.; Carta, A.; Loriga, M.; Zanetti, S.; Sechi, L. Synthesis of Substituted 2-Ethoxycarbonyl-and 2-Carboxyquinoxalin-3-Ones for Evaluation of Antimicrobial and Anticancer Activity. *Farm.* **1998**, *53*(7), 455–461.

(240) Sanna, P.; Carta, A.; Loriga, M.; Zanetti, S.; Sechi, L. Synthesis of 3, 6, 7-Substituted-Quinoxalin-2-Ones for Evaluation of Antimicrobial and Anticancer Activity. Part 2. *Farm.* **1999**, *54*(3), 161–168.

(241) Sanna, P.; Carta, A.; Loriga, M.; Zanetti, S.; Sechi, L. Preparation and Biological Evaluation of 6/7-Trifluoromethyl (Nitro)-, 6, 7-Difluoro-3-Alkyl (Aryl)-Substituted-Quinoxalin-2-Ones. Part 3. *Farm.* **1999**, *54*(3), 169–177.

(242) Lakshmi, P. C.; Esther, R. V; Spoorthy, Y. N.; Ravindranath, L. K. Synthesis Characterization and Antimicrobial Activity of 6-Nitro-1H-Benzo [d] Imidazole-2-Yl) Methyl)-6-Oxido-4, 8-Dihydro1H-[1, 3, 2] Dioxaphosphepino [5, 6-c] Pyrazole-6-Yl)

Ureas/Carboxamides-Mannich Bases. *J. Chem. Pharma ceutical Res.* **2013**, *5*, 280.

(243) Rathee, P. S.; Dhankar, R.; Bhardwaj, S.; Gupta, M.; Kumar, R. Synthesis and Antimicrobial Studies of Novel Benzimidazole Derivatives. *J. Appl. Pharm. Sci.* **2011**, *1*(4), 127.

(244) Shaukat, A.; Mirza, H. M.; Ansari, A. H.; Yasinzai, M.; Zaidi, S. Z.; Dilshad, S.; Ansari, F. L. Benzimidazole Derivatives: Synthesis, Leishmanicidal Effectiveness, and Molecular Docking Studies. *Med. Chem. Res.* **2013**, *22*(8), 3606–3620. https://doi.org/10.1007/s00044-012-0375-5.

(245) Jian, F.-F.; Yu, H.-Q.; Qiao, Y.-B.; Zhao, P.-S.; Xiao, H.-L. 2-(4-Chlorophenyl)-1H-Benzimidazole. *Acta Crystallogr. Sect. E Struct. Reports Online* **2006**, *62*(11), 5194–5195.

(246) Sum, T. H.; Sum, T. J.; Galloway, W. R. J. D.; Collins, S.; Twigg, D. G.; Hollfelder, F.; Spring, D. R. Combinatorial Synthesis of Structurally Diverse Triazole-Bridged Flavonoid Dimers and Trimers. *Molecules* **2016**, *21*(9). https://doi.org/10.3390/molecules21091230.

(247) Leidenberger, M.; Voigtländer, C.; Simon, N.; Kappes, B. SYBR® Green I-Based Fluorescence Assay to Assess Cell Viability of Malaria Parasites for Routine Use in Compound Screening BT - Cell Viability Assays: Methods and Protocols; Gilbert, D. F., Friedrich, O., Eds.; Springer New York: New York, NY, 2017; 97–110. https://doi.org/10.1007/978-1-4939-6960-9_9.

(248) Smilkstein, M.; Sriwilaijaroen, N.; Kelly, J. X.; Wilairat, P.; Riscoe, M. Simple and Inexpensive Fluorescence-Based Technique for High-Throughput Antimalarial Drug

Screening. *Antimicrob. Agents Chemother.* **2004**, *48*(5), 1803–1806. https://doi.org/10.1128/AAC.48.5.1803-1806.2004.

(249) Distefano, M. D. Discovery of Novel Alkylated (Bis)Urea and (Bis)Thiourea Polyamine Analogues with Potent Antimalarial Activities. **2015**, *54*(5), 213–223. https://doi.org/10.1007/978-1-62703-673-3.

(250) Harder, E.; Damm, W.; Maple, J.; Wu, C.; Reboul, M.; Xiang, J.; Wang, L.; Lupyan, D.; Dahlgren, M.; Knight, J.; Kaus, J.; Cerutti, D.; Krilov, G.; Jorgensen, W.; Abel, R.; Friesner, R. OPLS3: A Force Field Providing Broad Coverage of Drug-like Small Molecules and Proteins. *J. Chem. Theory Comput.* **2016**, *2016*, 12(1), 281-296.

8 Appendix

1. Copies of Selected Spectra
2. Crystallographic Data of some of the Crystal Structures
3. Publication

FIGURE S1: ^{1}H NMR Spectrum of **2.3**

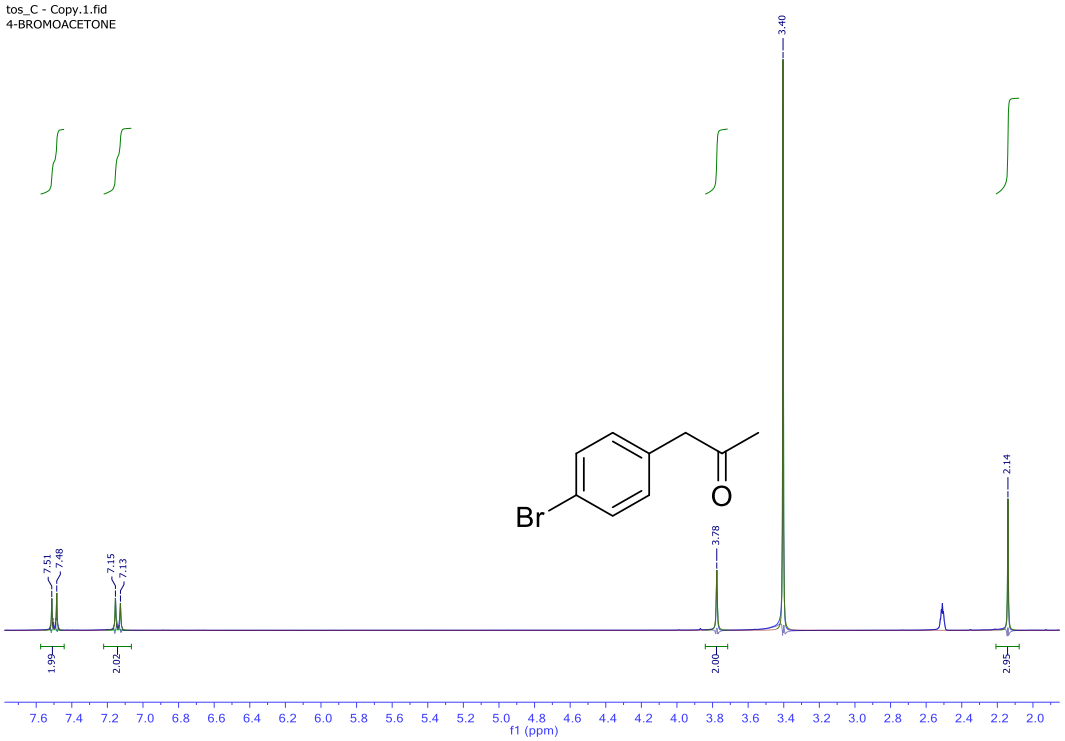

FIGURE S2: ^{1}H NMR Spectrum of **2.4a**

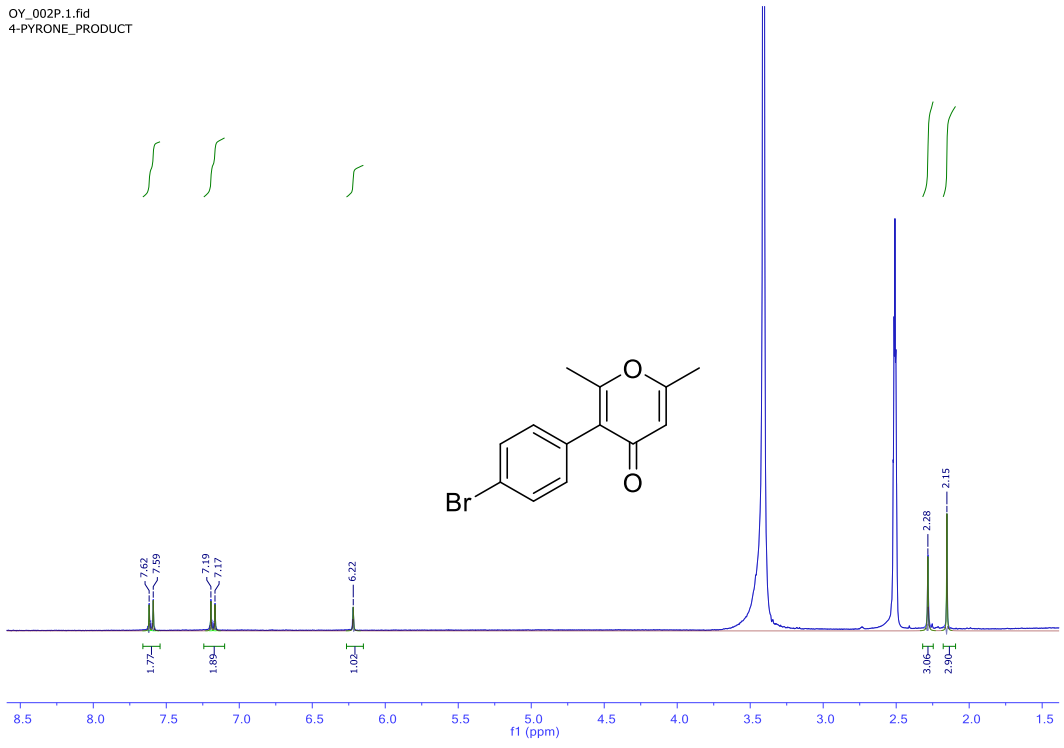

FIGURE S3: ^{13}C NMR Spectrum of **2.4a**

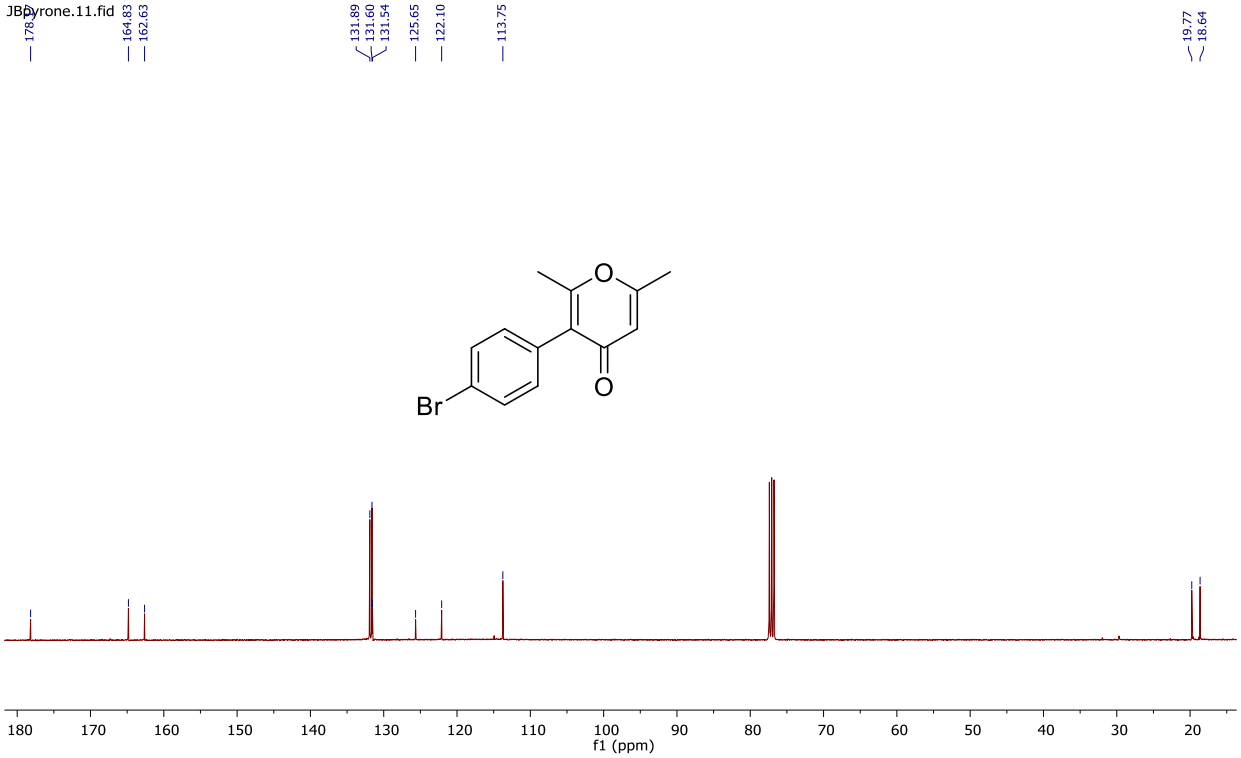

FIGURE S4: ^{1}H NMR Spectrum of **2.5**

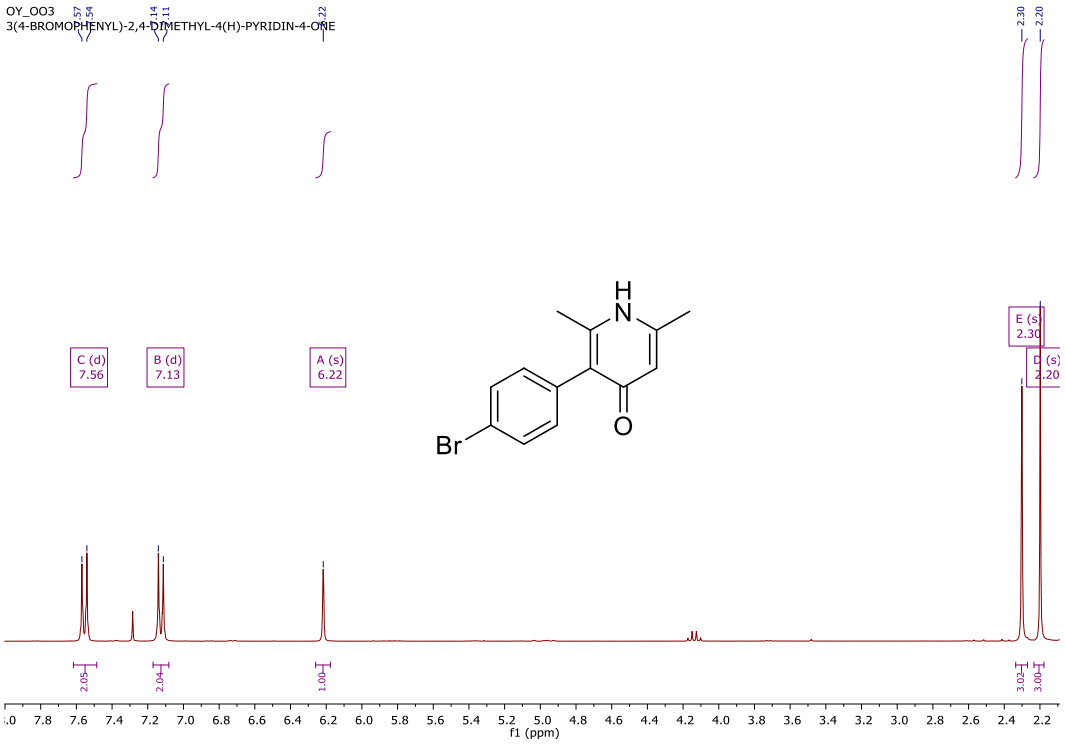

FIGURE S5: ^{1}H NMR Spectrum of **2.10a**

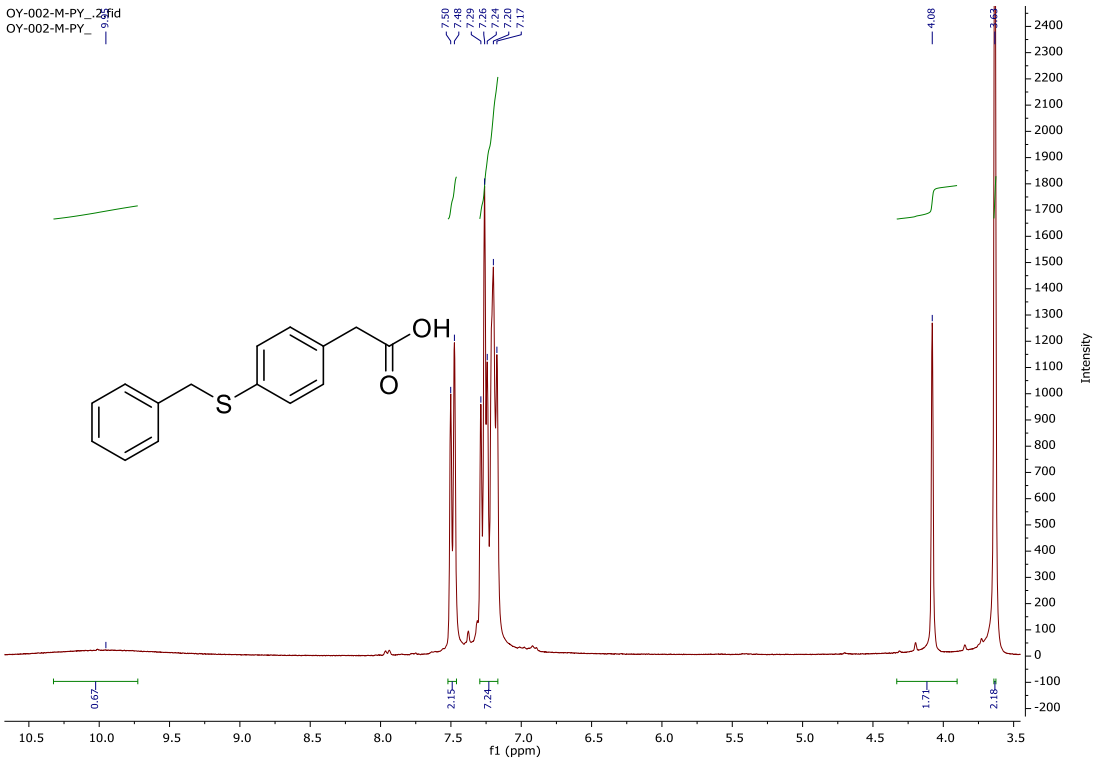

FIGURE S6: ^{13}C NMR Spectrum of **2.10a**

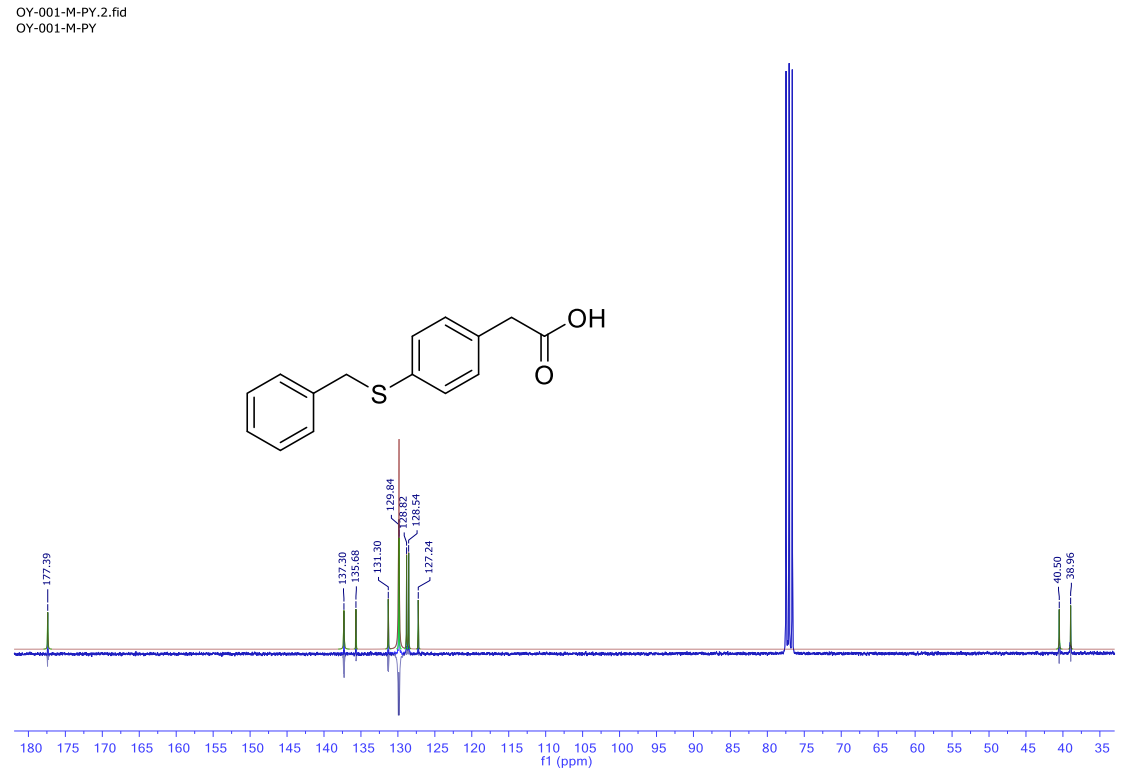

FIGURE S7: ^{1}H NMR Spectrum of **2.10c**

FIGURE S8: ^{13}C NMR Spectrum of **2.10c**

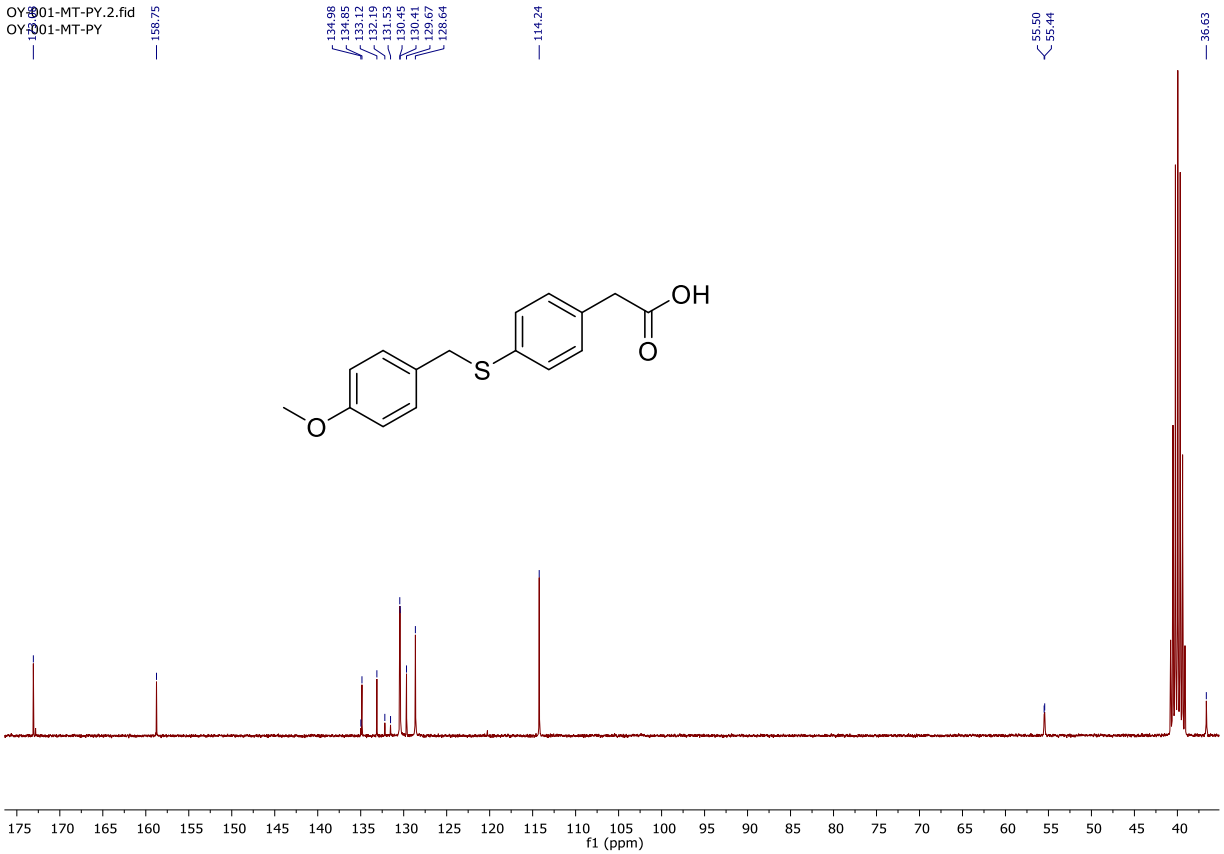

FIGURE S9: ^{1}H NMR Spectrum of **2.11a**

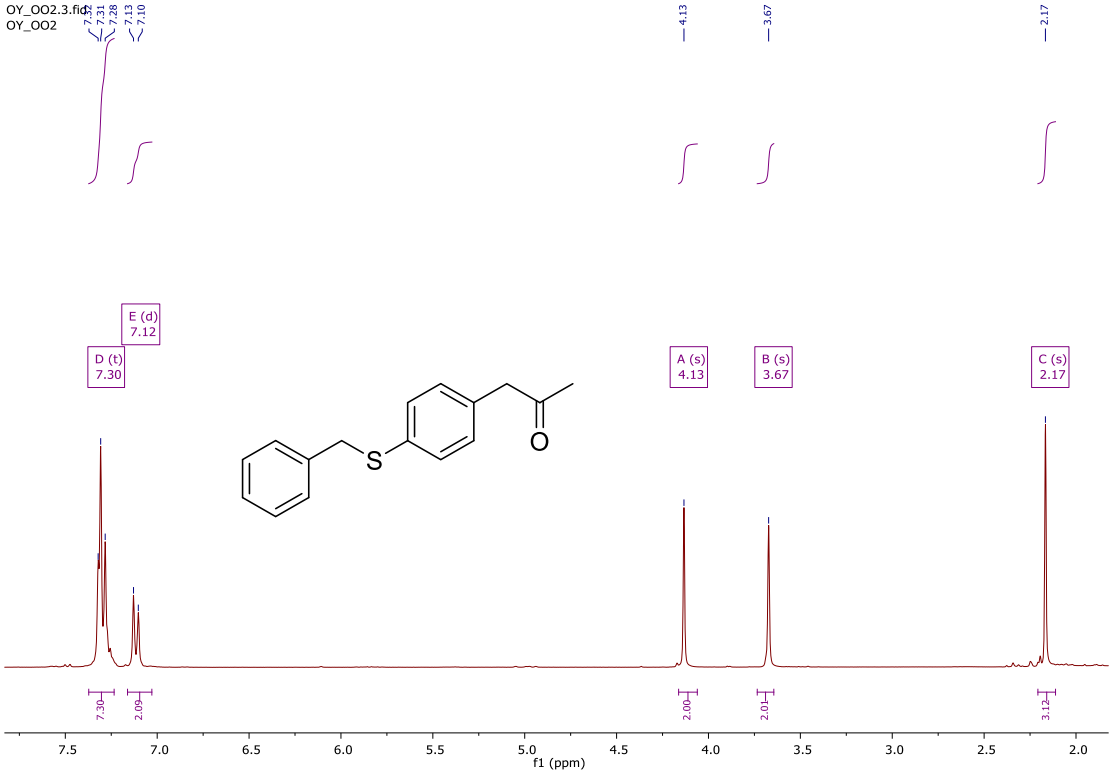

FIGURE S10: ^{13}C NMR Spectrum of **2.11a**

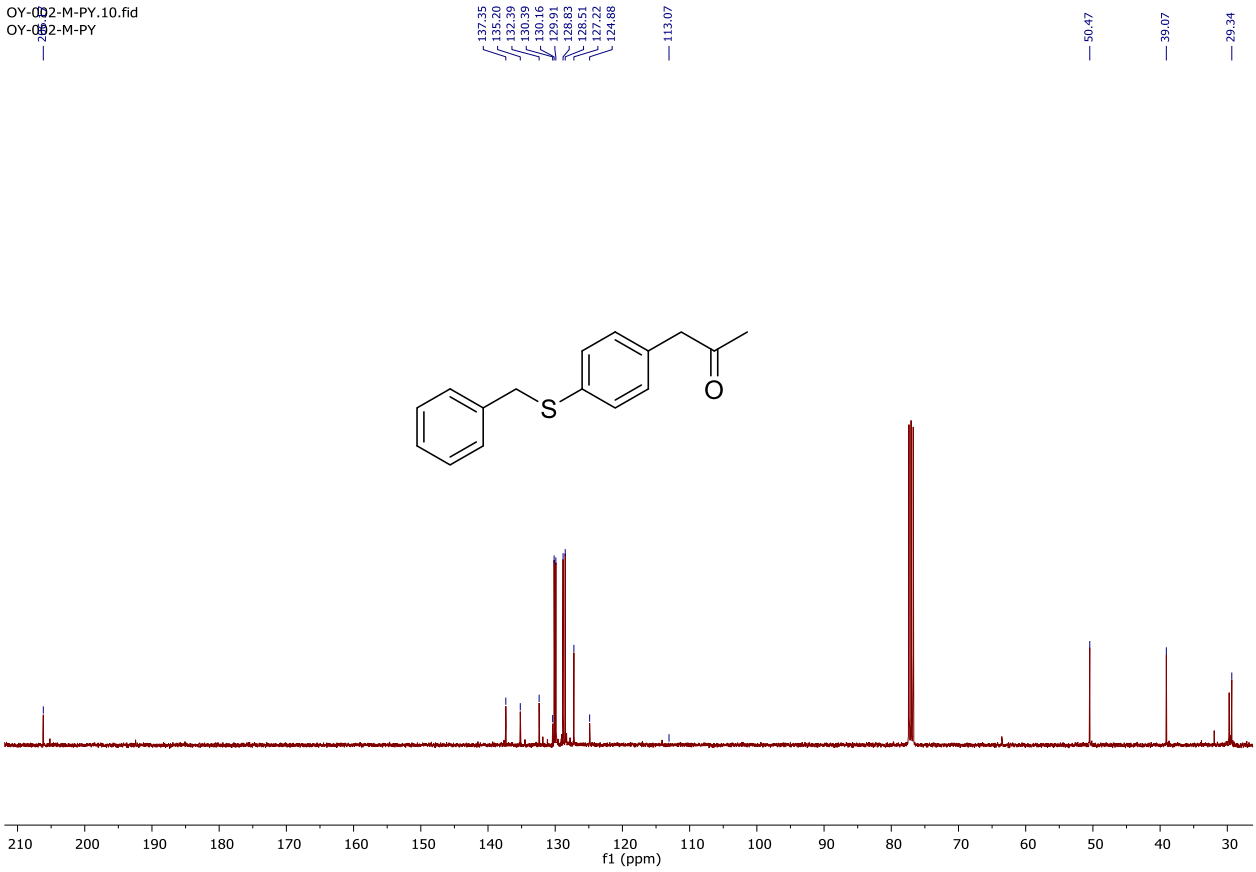

FIGURE S11: ^{1}H NMR Spectrum of **2.11c**

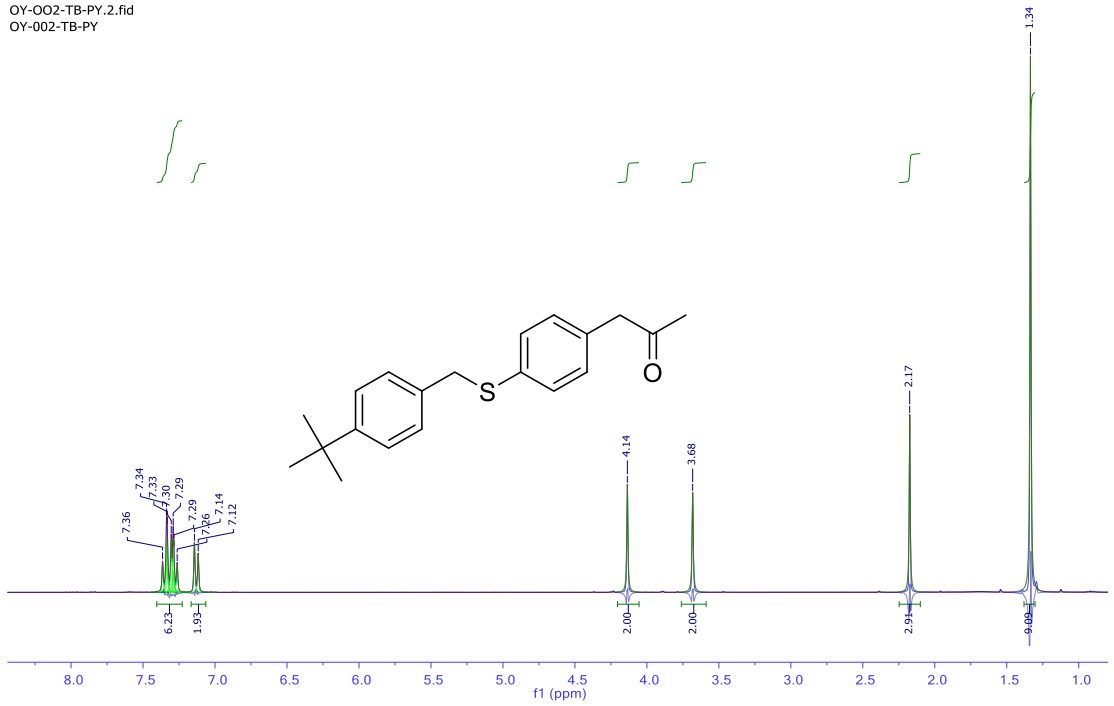

FIGURE S12: ^{13}C NMR Spectrum of **2.11c**

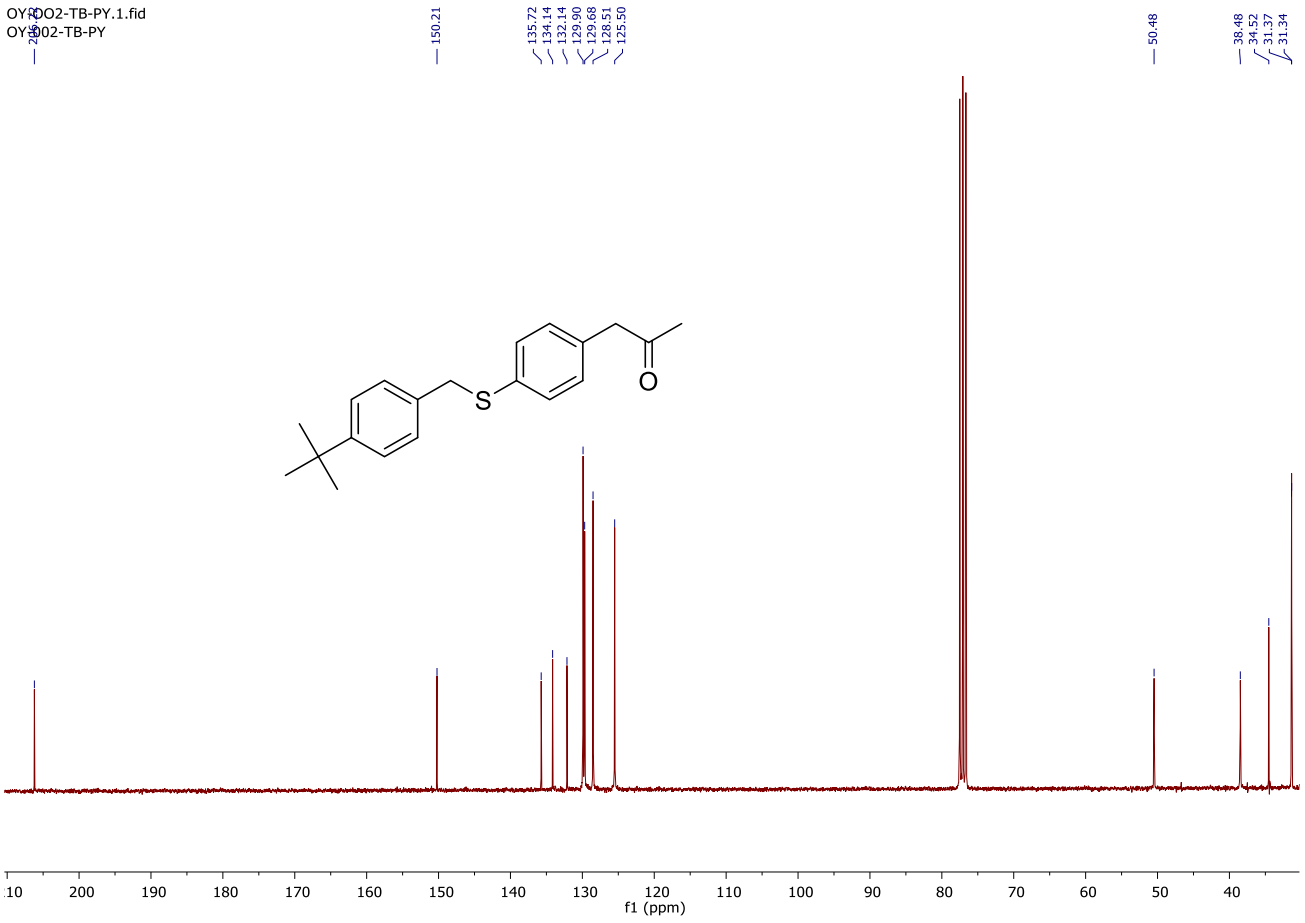

FIGURE S13: ^{1}H NMR Spectrum of **2.12b**

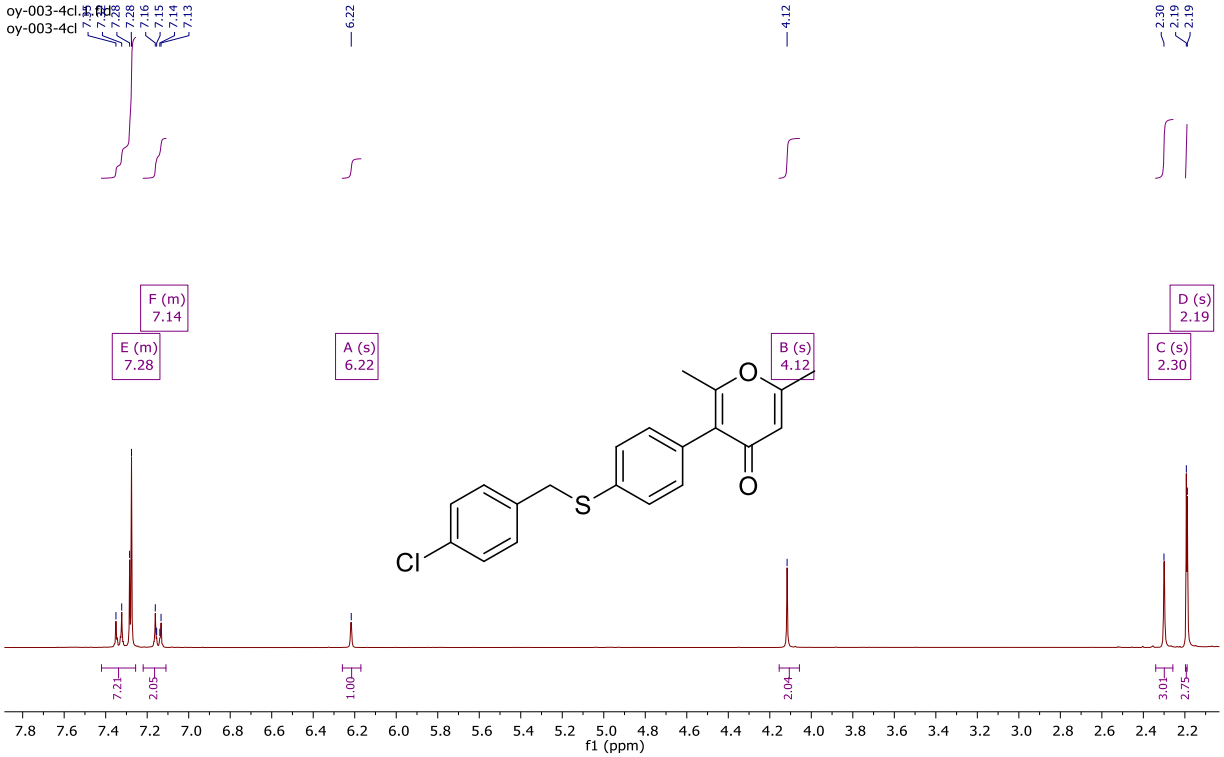

FIGURE S14: ^{13}C NMR Spectrum of **2.12b**

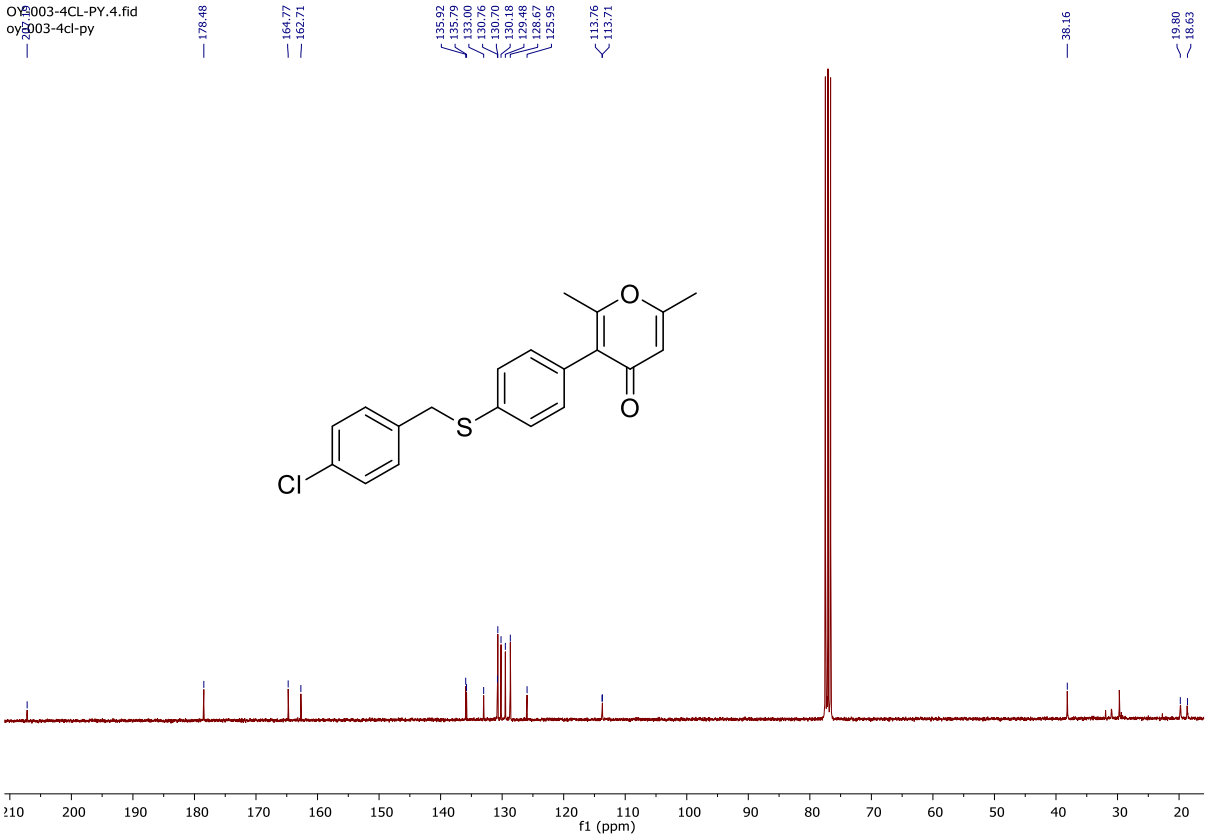

FIGURE S15: ^{13}H NMR Spectrum of **2.9a**

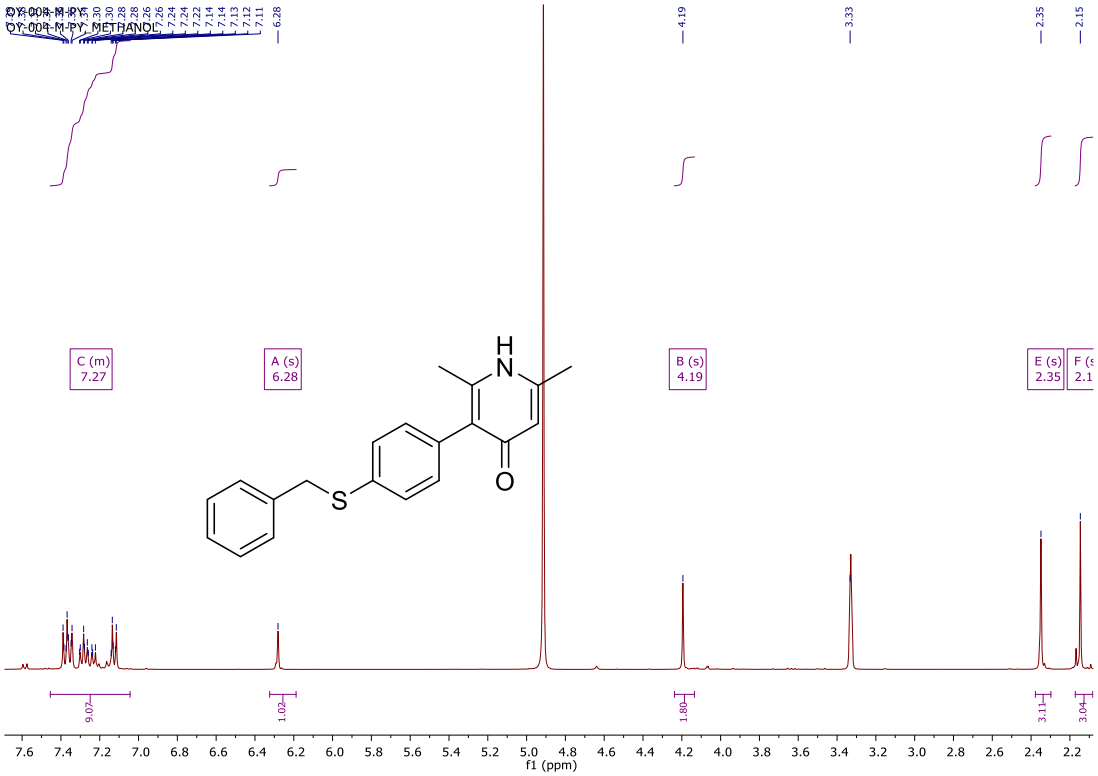

FIGURE S15: ^{13}C NMR Spectrum of **2.9a**

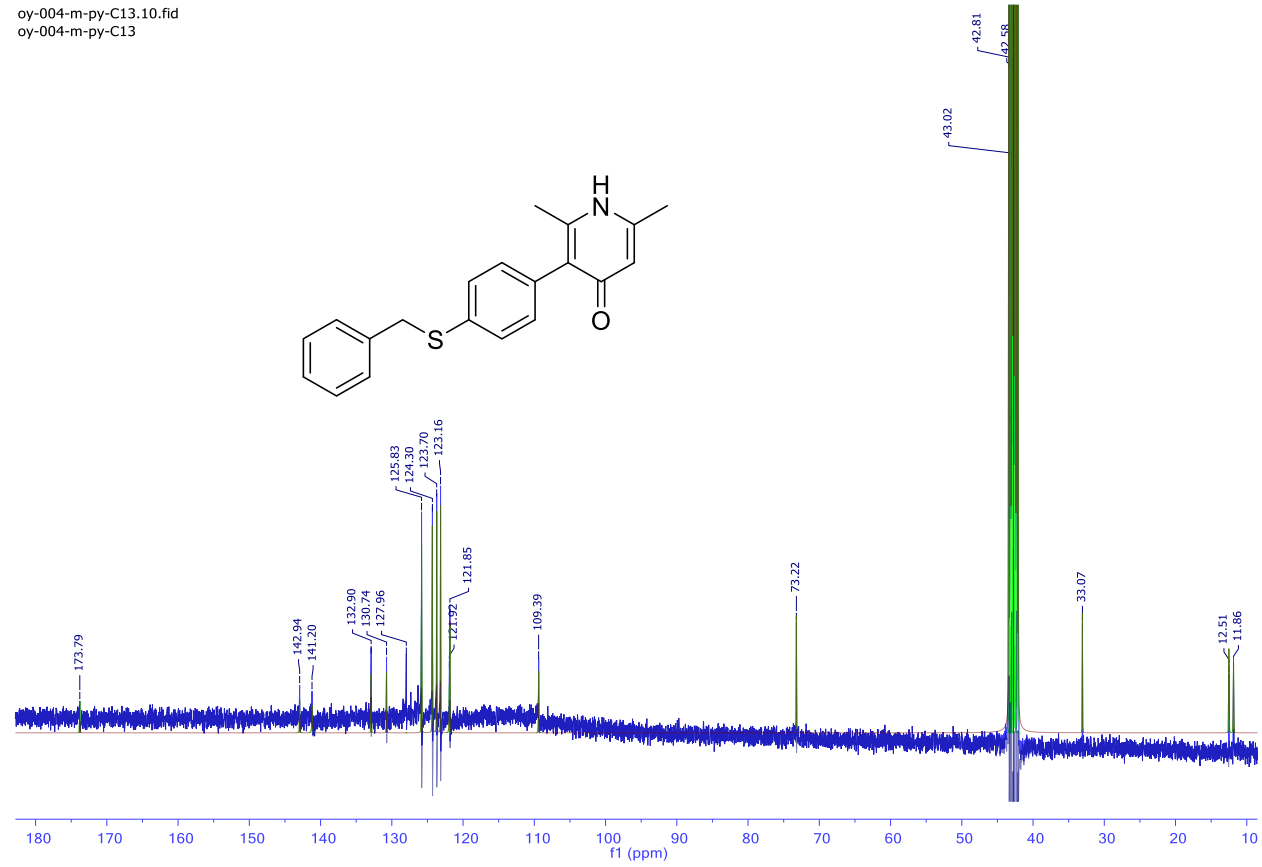

FIGURE S16: H NMR Spectrum of **2.14**

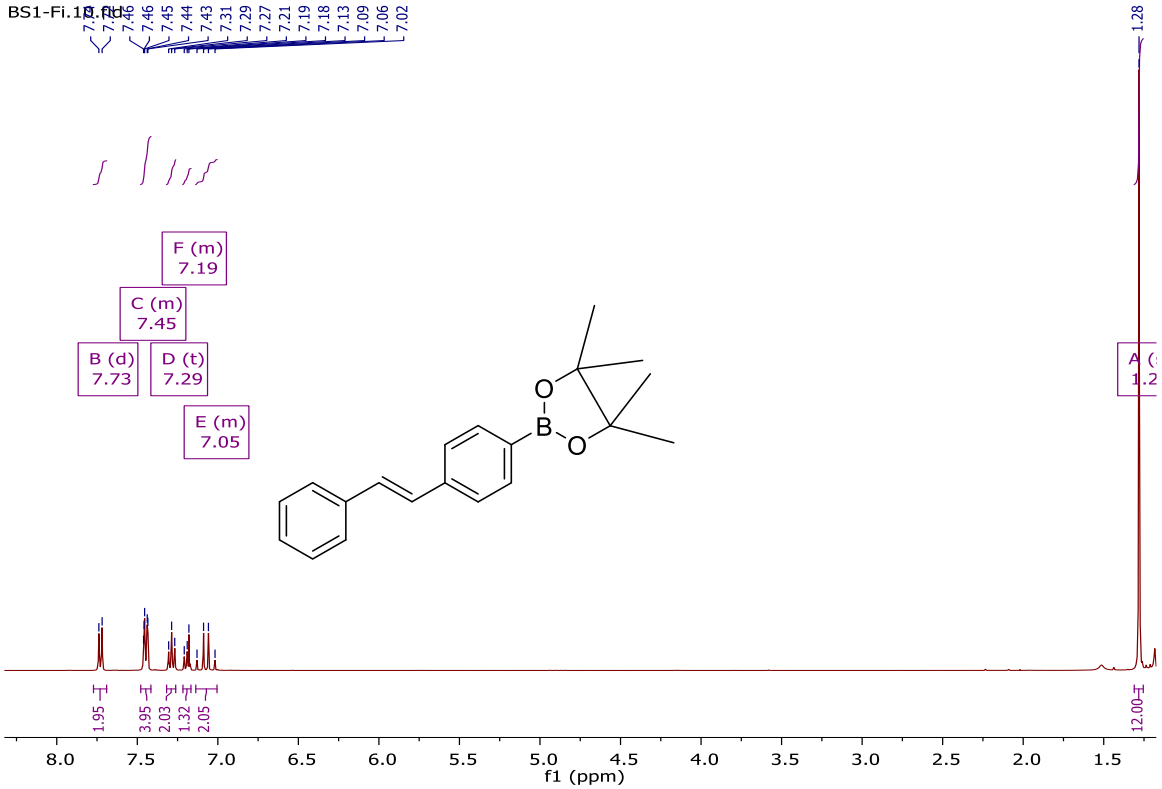

FIGURE S17: ^{1}C NMR Spectrum of **2.14**

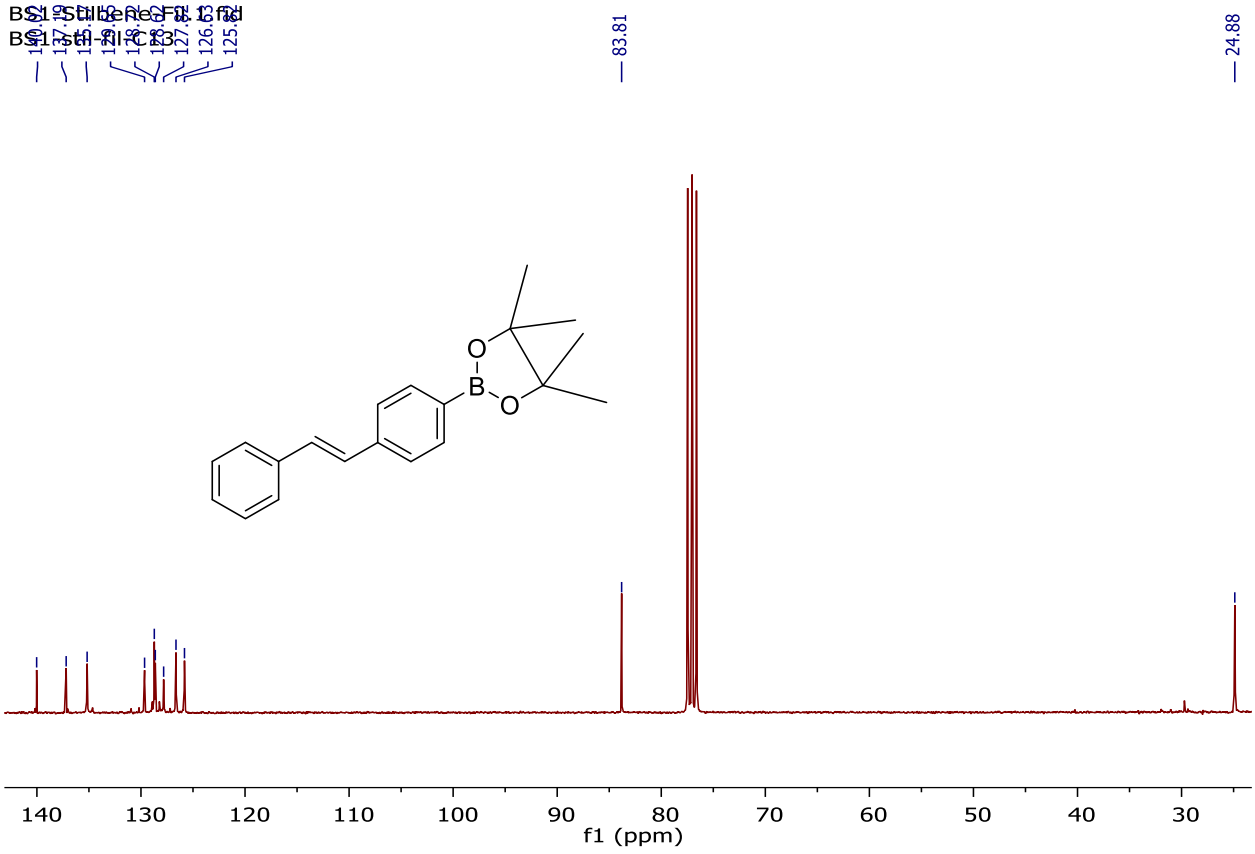

FIGURE S18: ^{1}H NMR Spectrum of **2.15**

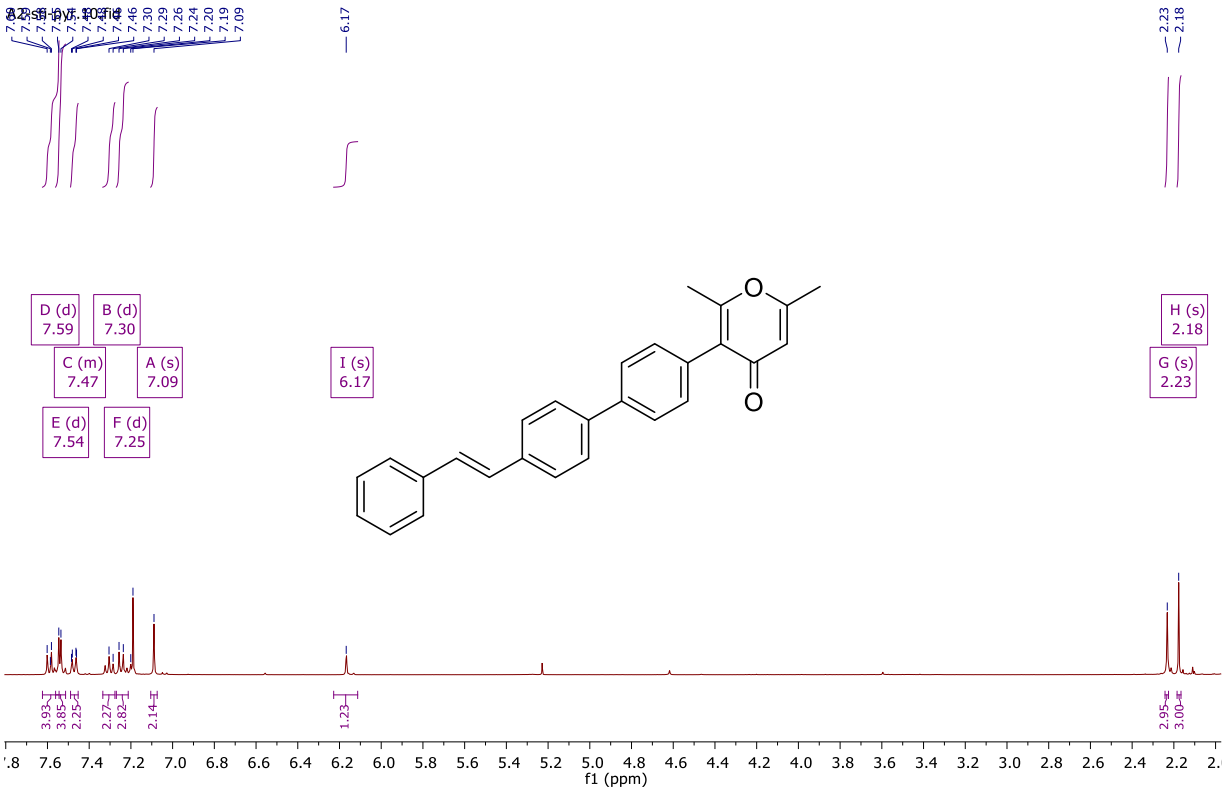

FIGURE S19: ^{1}H NMR Spectrum of **2.24**

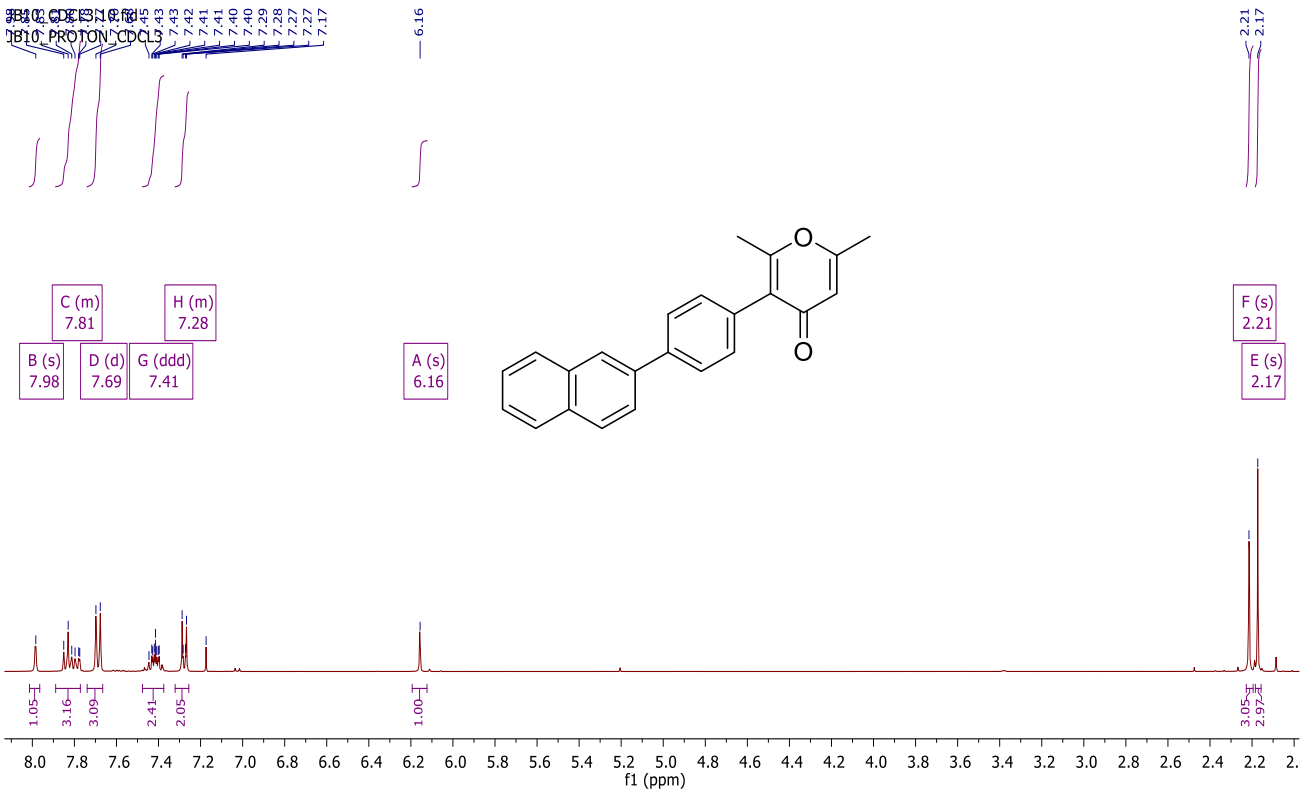

FIGURE S20: ^{1}C NMR Spectrum of **2.24**

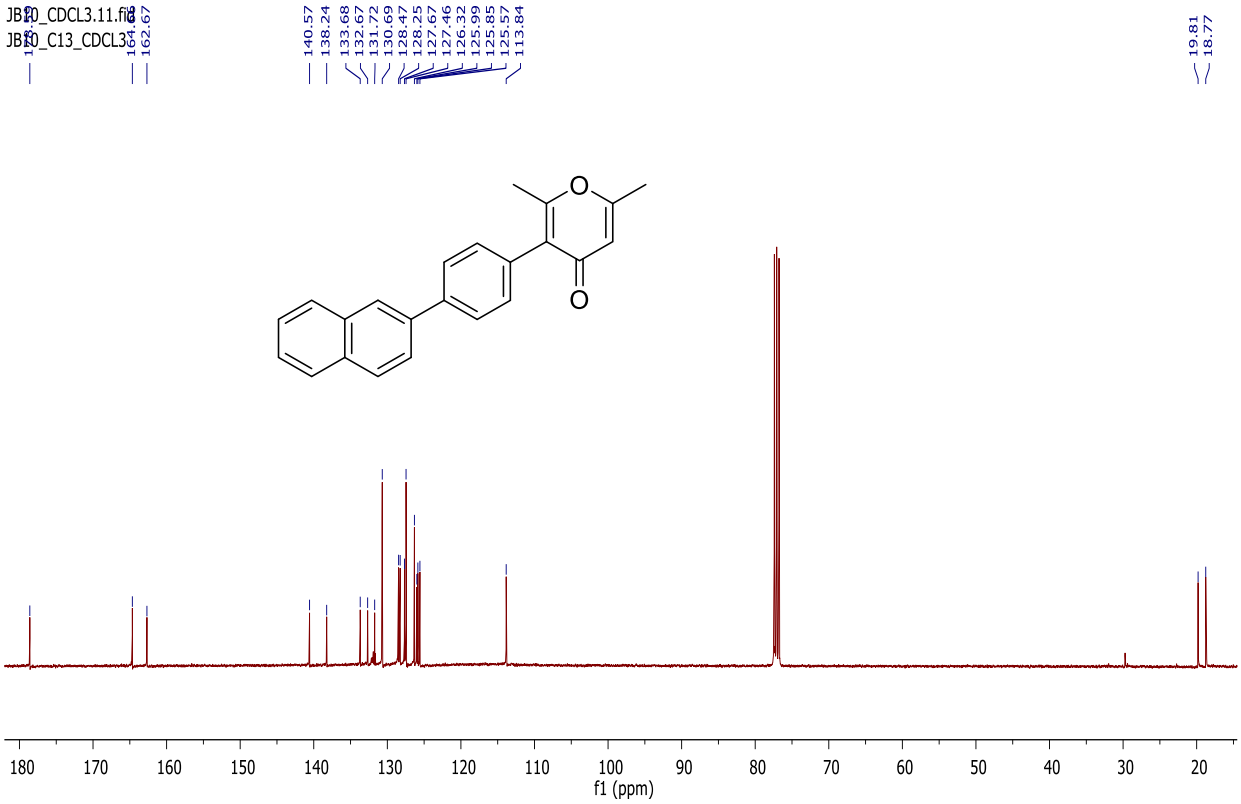

FIGURE S21: ^{1}H NMR Spectrum of **2.24**

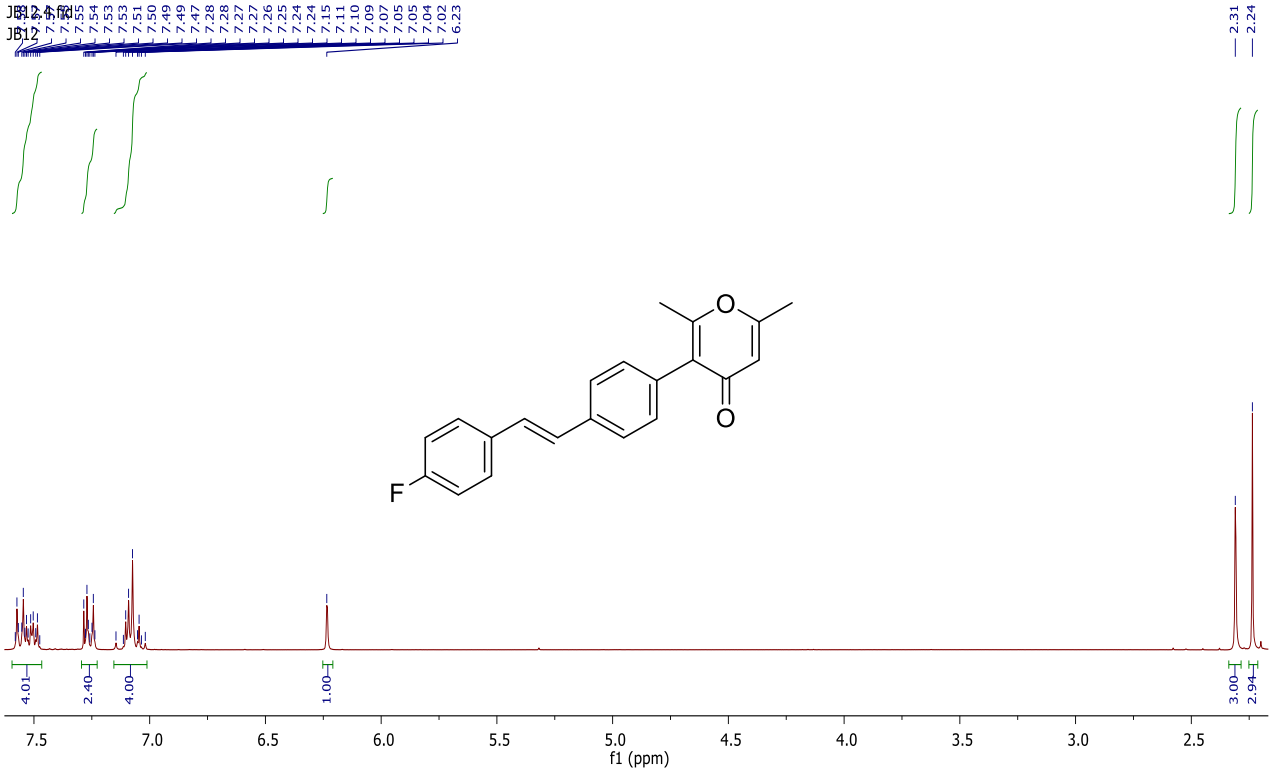

FIGURE S22: ^{1}C NMR Spectrum of **2.25**

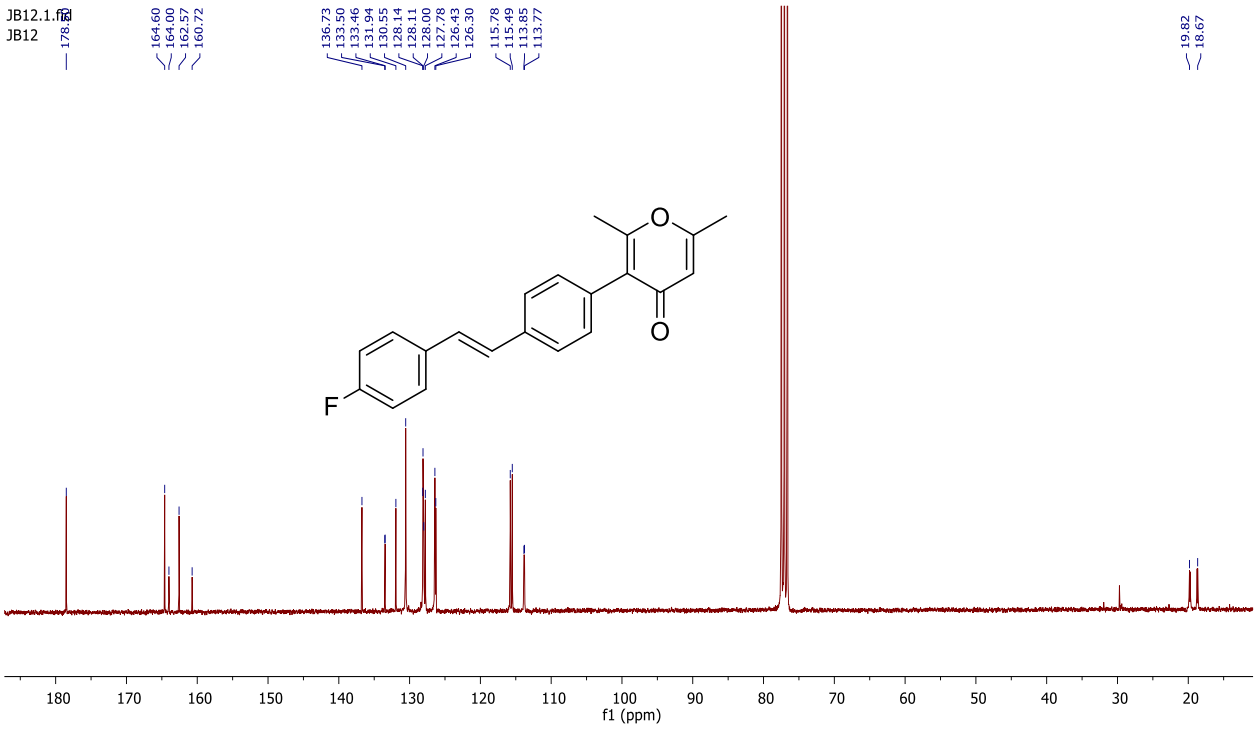

FIGURE S23: ^{1}H NMR Spectrum of **3.2b**

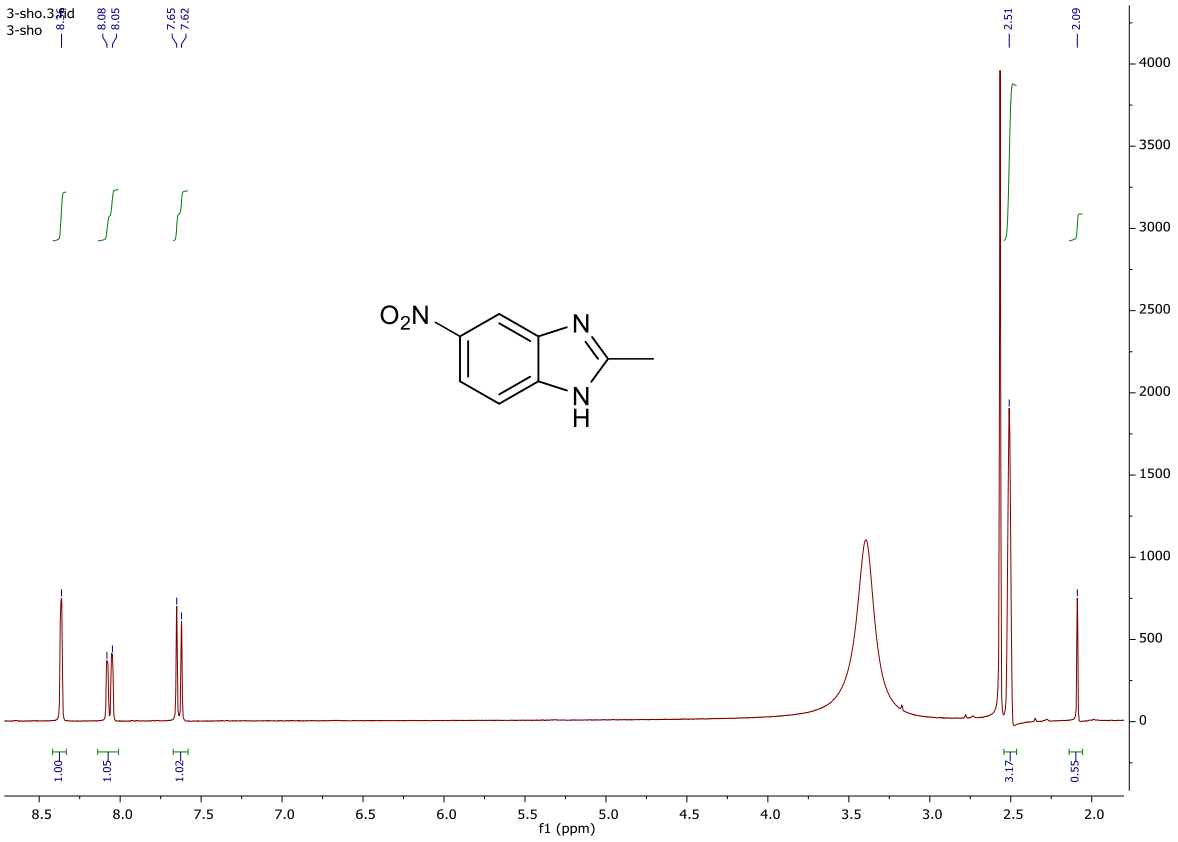

FIGURE S24: ^{1}H NMR Spectrum of **3.2d**

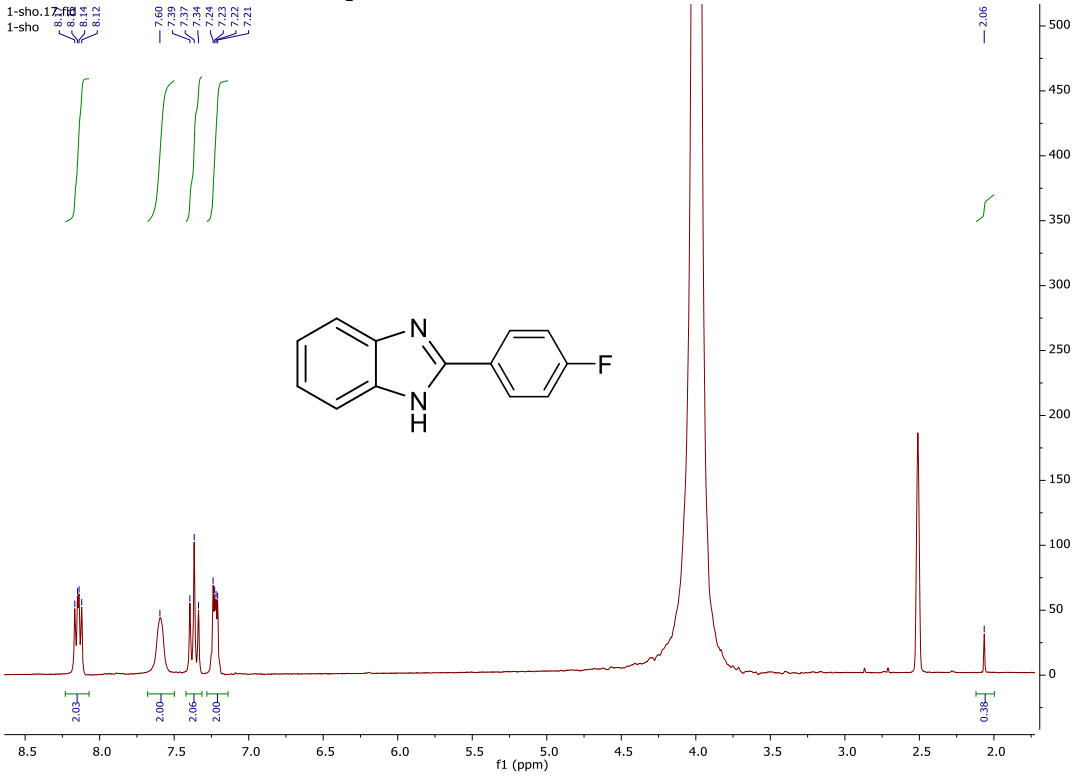

FIGURE S25: ^{1}H NMR Spectrum of **3.3**

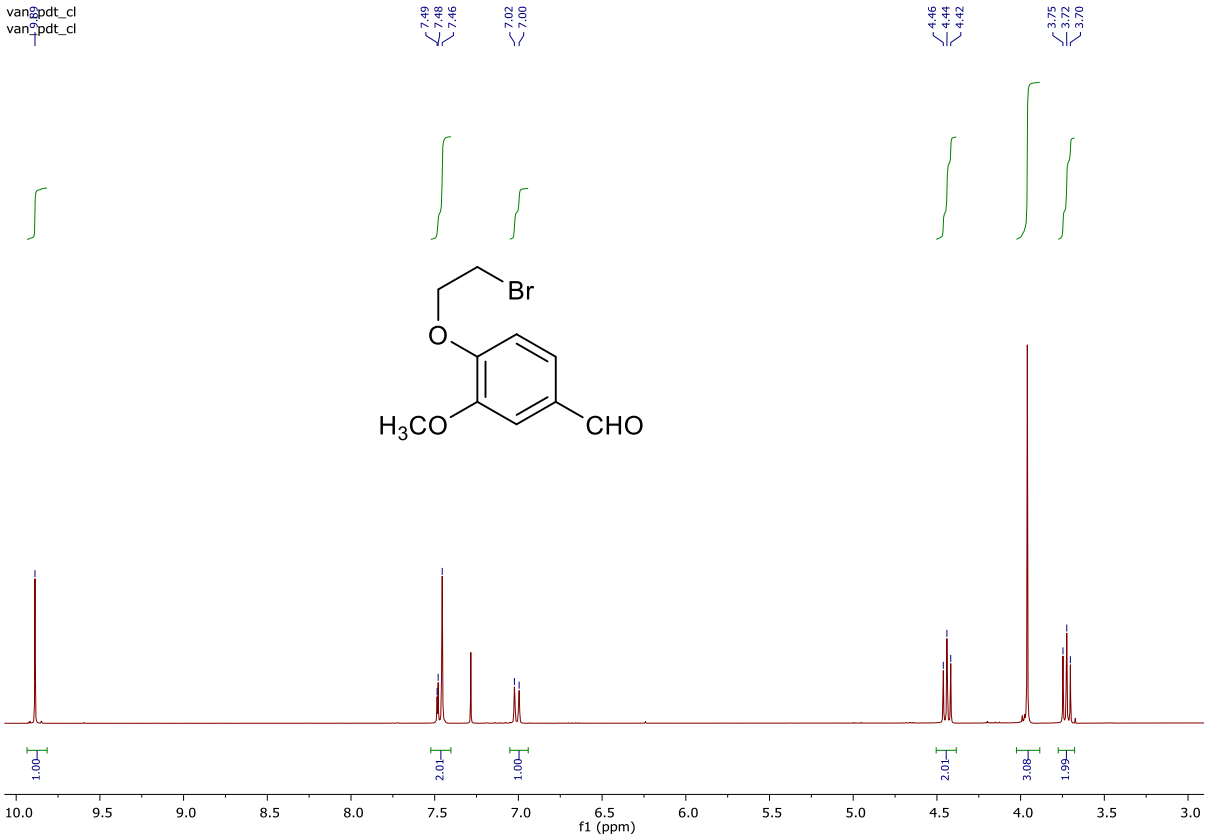

FIGURE S26: ^{1}H NMR Spectrum of **3.4a**

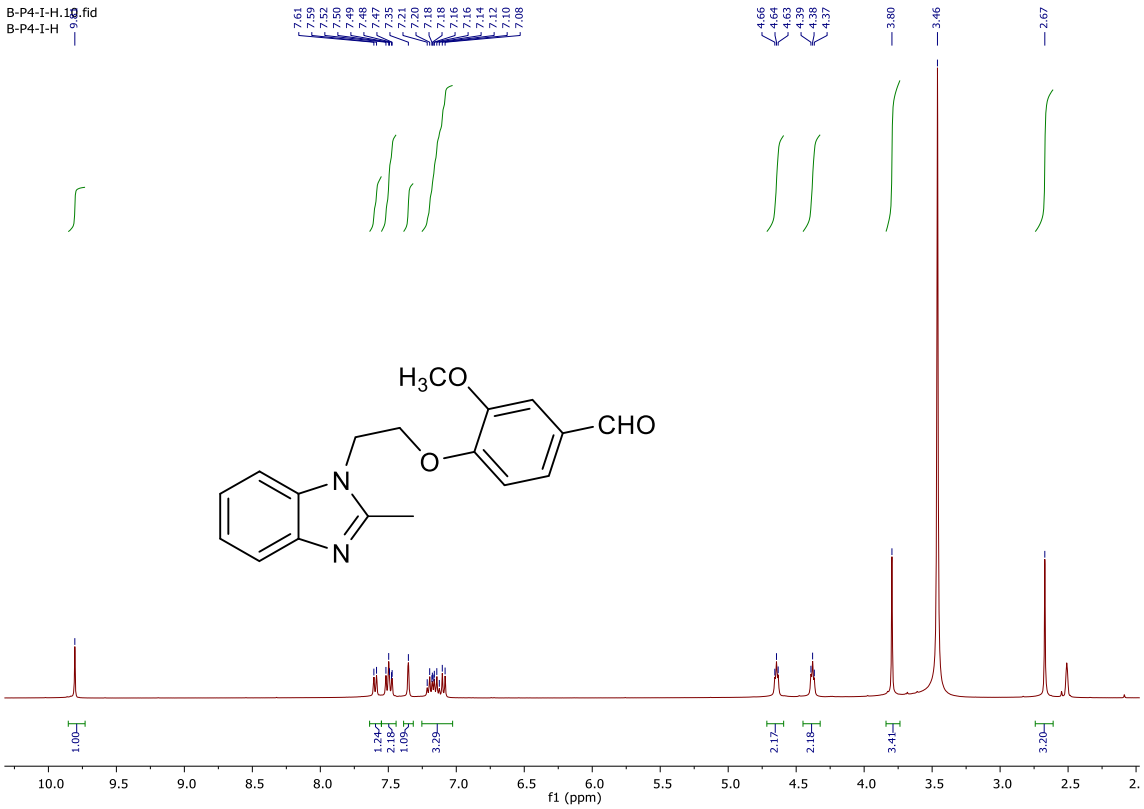

FIGURE S27: ^{13}C NMR Spectrum of **3.4a**

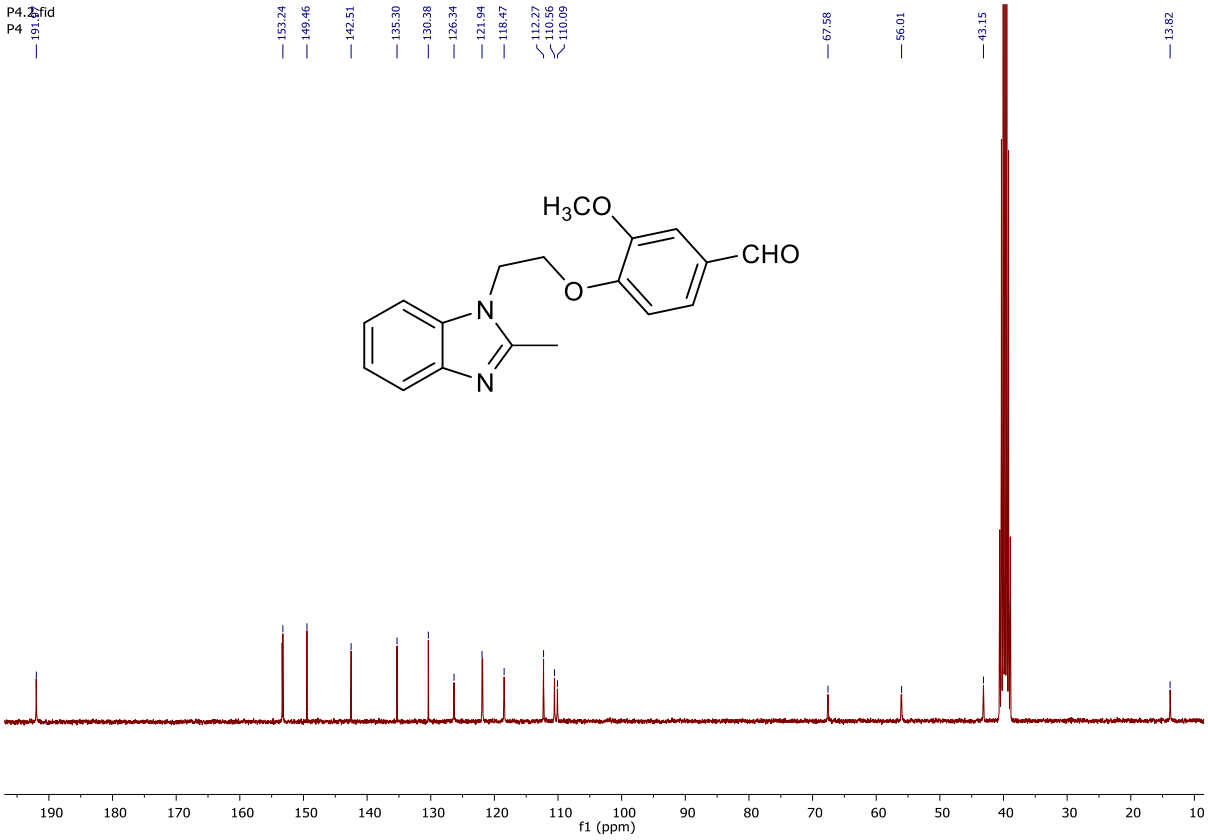

FIGURE S28: ^{1}H NMR Spectrum of **3.4e**

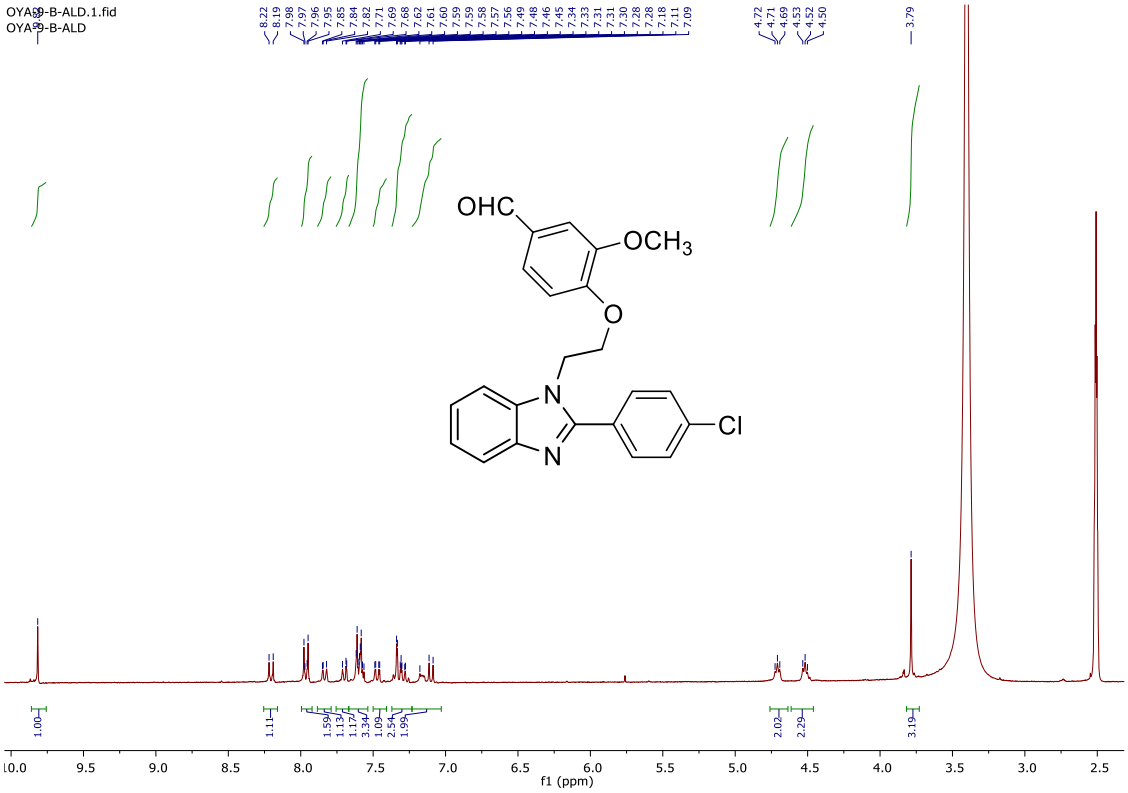

FIGURE S28: ^{13}C NMR Spectrum of **3.4e**

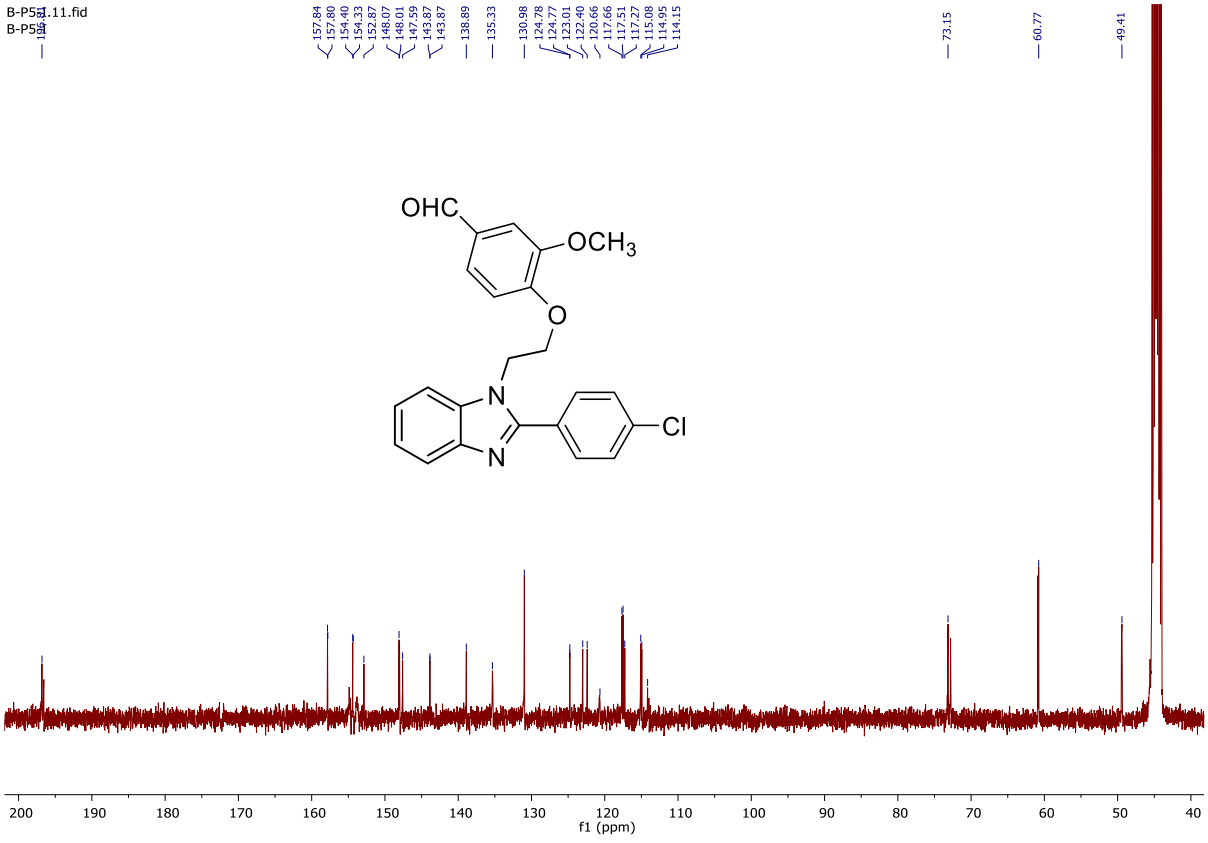

FIGURE S29: ^{13}H NMR Spectrum of **3.6d**

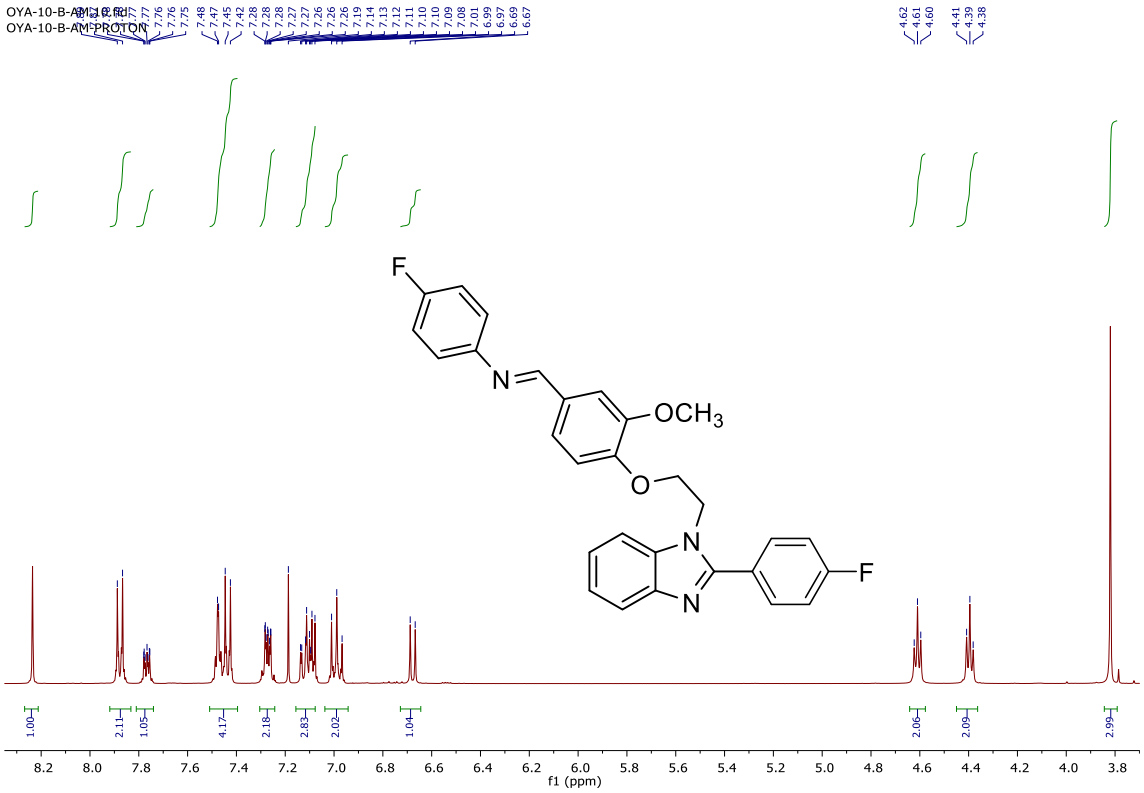

FIGURE S30: ^{13}C NMR Spectrum of **3.6d**

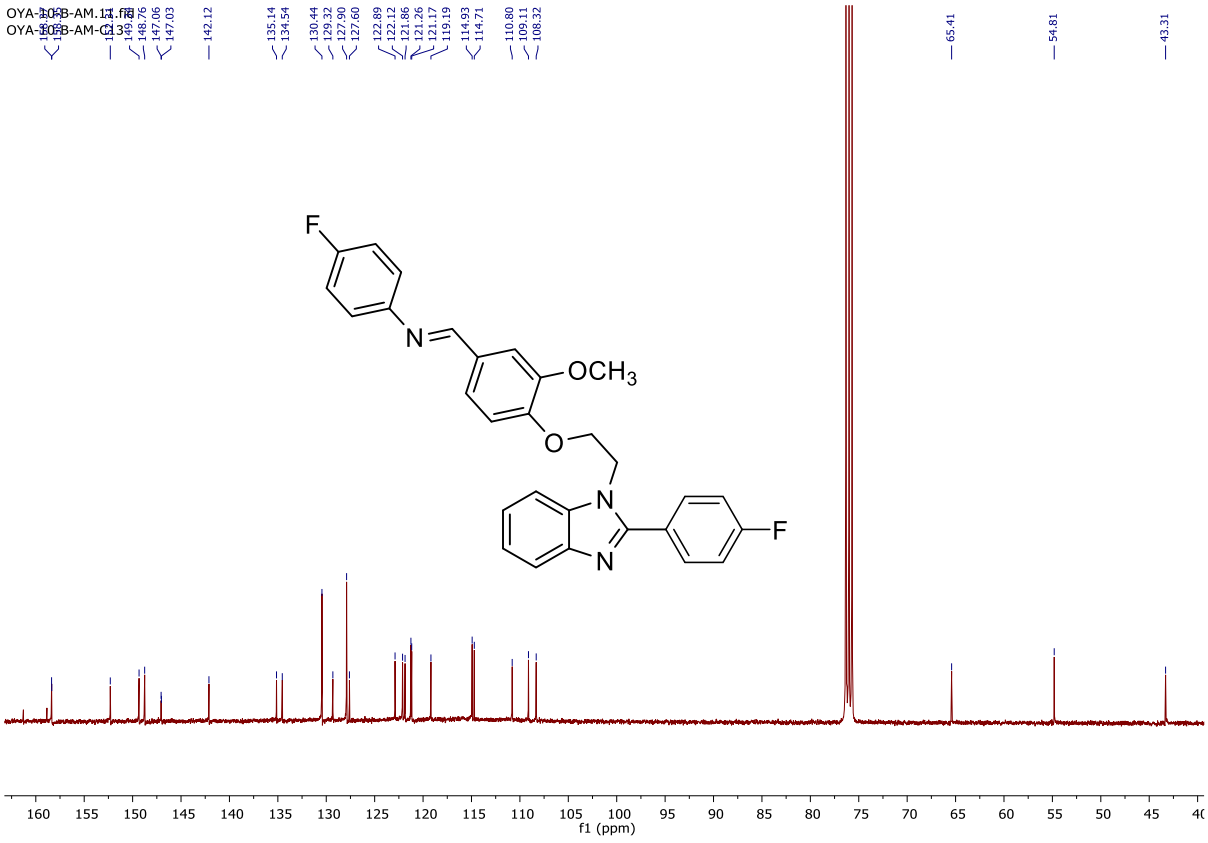

FIGURE S31: ^{1}H NMR Spectrum of **4.5c**

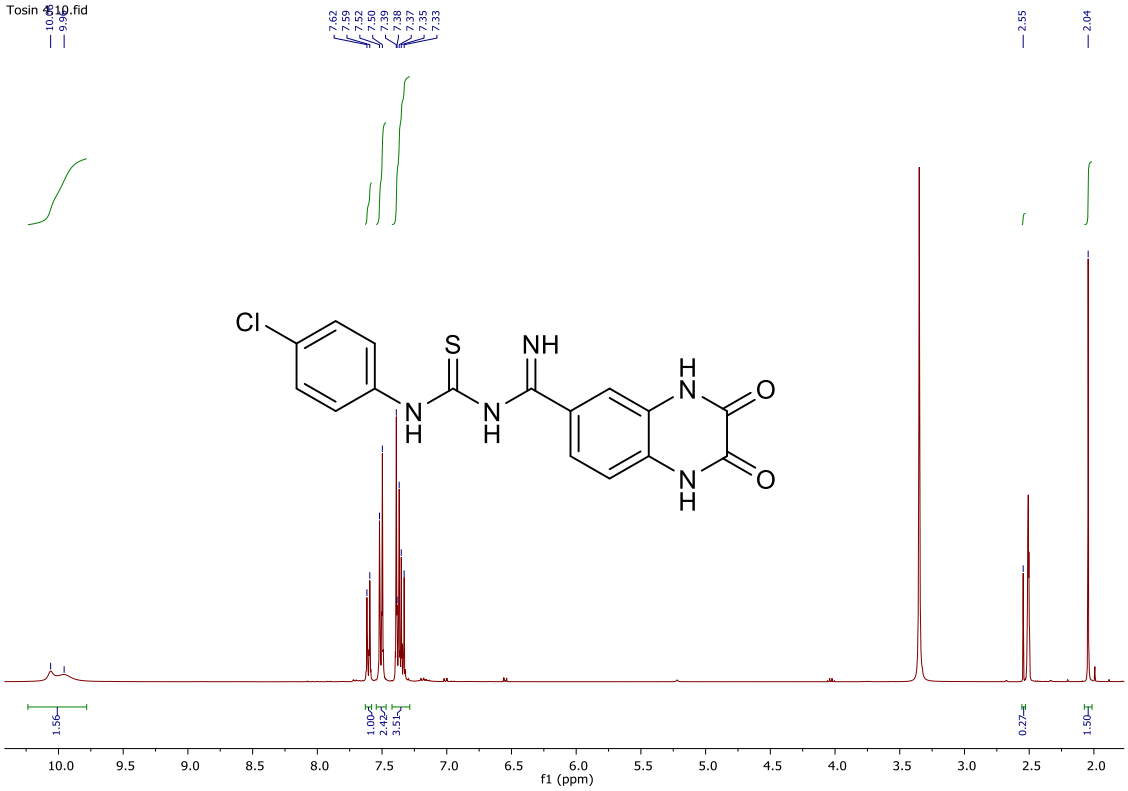

FIGURE S32: ^{13}C NMR Spectrum of **4.5c**

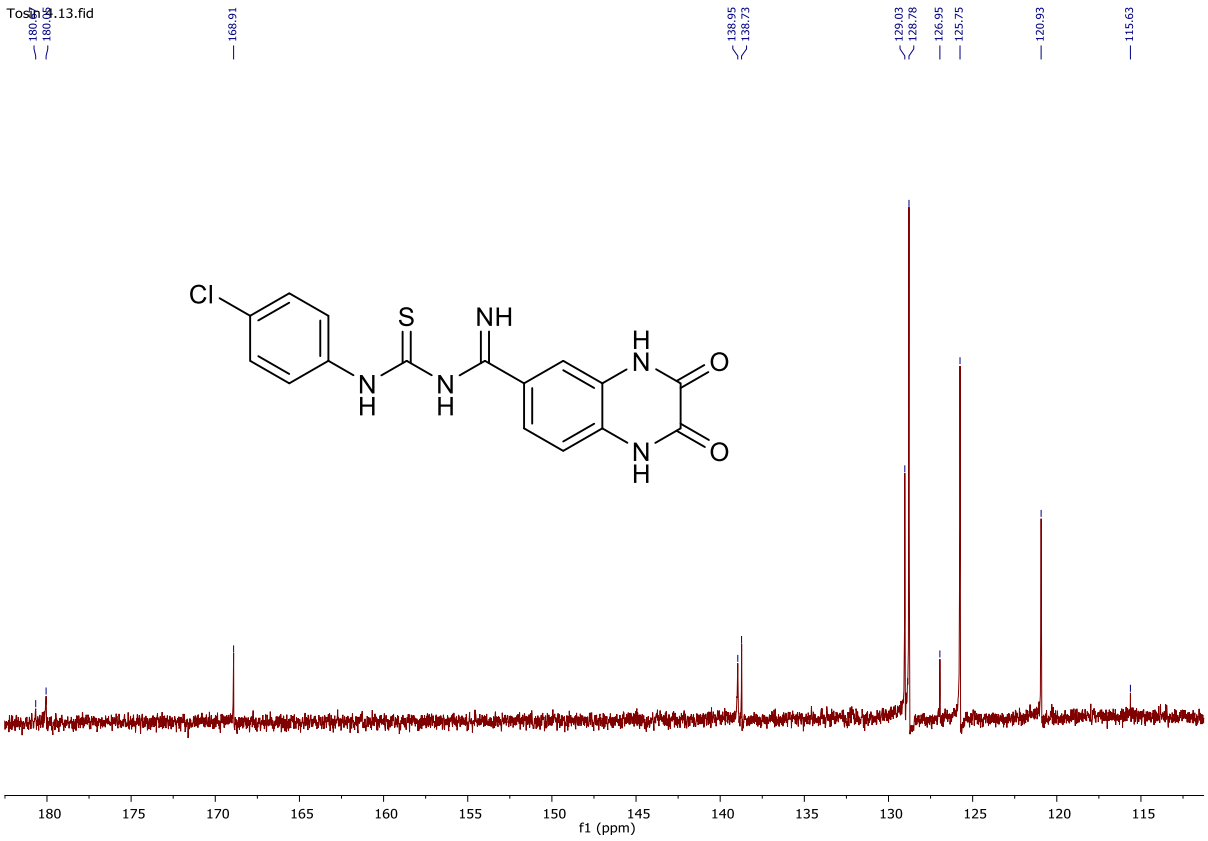

Table S1: Crystal data and structure refinement for **2.4a** and **2.4b**

Complex	**2.4a**	**2.4b**
Emp. formula	$C_{13}H_{11}BrO_2$	$C_{19}H_{14}Br_2O_2$
CCDC Identifier	2069544	2069545
Form. weight (g.mol^{-1})	279.13	434.12
Crystal system	monoclinic	orthorhombic
Space group	$P2_1/c$	$P2_12_12_1$
Crystal description	pale yellow block	pale yellow block
a (Å)	6.93170(10)	5.97640(10)
b (Å)	21.7480(3)	11.4680(2)
c (Å)	7.7775(2)	24.4564(3)
α (°)	90	90
β (°)	103.417(2)	90
γ (°)	90	90
Volume (Å^3)	1140.46(4)	1676.18(5)
Z	4	4
Abs. coeff. (m.mm^{-1})	4.764	6.187
F(000)	560	856
Independent refl.	2255	3307
Completeness (%)	100	100
Data/Restr/Para	2255/0/148	3307/0/211
Goodness of fit on F^2	1.093	1.090
Final R_1 indexes	0.0639	0.0679
wR_2 indices (all data)	0.1755	0.1853
Largest diffr. peak and hole (e.Å^{-3})	1.26/-1.71	1.19/-1.09

Table S2: Selected bond lengths and angles for **2.4a** and **2.4b**

Description	**2.4a**	**2.4b**
O6-C1	1.363(4)	1.370(10)
O6-C5	1.368(4)	1.361(10)
C3-O14	1.246(5)	1.238(10)
C10-Br13	1.902(3)	1.910(8)
C20-Br23	-	1.894(9)
C1-O6-C5	120.0(3)	120.5(7)
C2-C3-O14	121.8(3)	122.2(7)
C3-C4-C7	118.5(3)	119.5(7)
C3-C2-C17	-	119.2(7)
O14-C3-C4-C7	-5.1(5)	2.0(12)
O14-C3-C2-C17	-	-7.0(12)
C3-C2-C17-C18	-	119.7(8)
C3-C4-C7-C8	49.1(5)	-67.9(11)
C4-C5-O6-C1	178.0(3)	-4.5(13)
O14-C3-C2-C1	-178.9(3)	176.8(8)

SCXRD molecular structure of the byproduct of **9d** and **9f** (**9d'** and **9f'**, respectively) (**Figures S33** and **S44**).

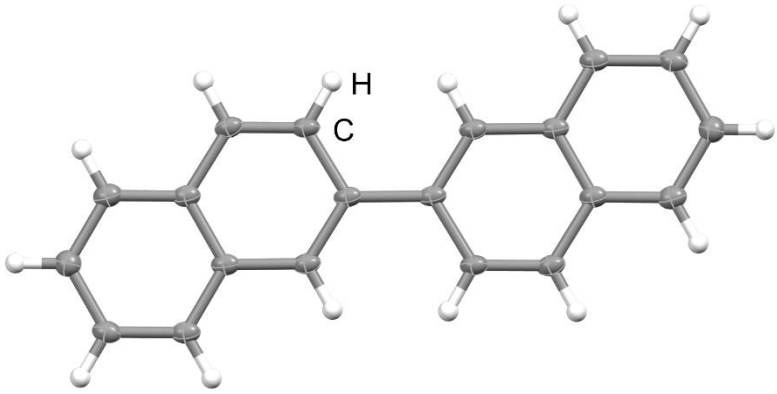

Figure S33: Molecular structure of the byproduct of **9d** (**9d'**). Thermal ellipsoids are drawn at 50% probability level.

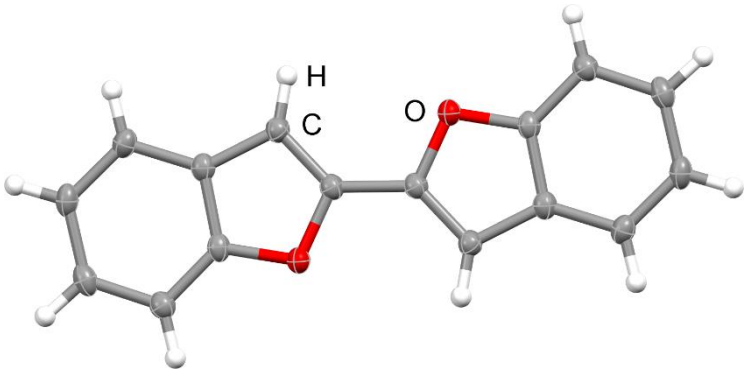

Figure S34. Molecular structure of the byproduct of **9f** (**9f'**). Thermal ellipsoids are drawn at 50% probability level.